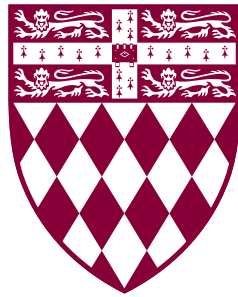




# Stationary Anti-de Sitter Black Hole Solutions in and out of Equilibrium



**William D. Biggs**

Supervisor: Prof. Jorge E. Santos

Department of Applied Mathematics and Theoretical Physics  
University of Cambridge

This dissertation is submitted for the degree of  
*Doctor of Philosophy*

Fitzwilliam College

August 2024



## Declaration

This thesis is the result of my own work and includes nothing which is the outcome of work done in collaboration except as declared in the preface and specified in the text. It is not substantially the same as any work that has already been submitted, or, is being concurrently submitted, for any degree, diploma or other qualification at the University of Cambridge or any other University or similar institution except as declared in the preface and specified in the text. It does not exceed the prescribed word limit for the relevant Degree Committee.

William D. Biggs  
August 2024



I would like to dedicate this thesis to my parents ...



## Acknowledgements

Firstly, I would like to thank my supervisor, Jorge. I think the extent to which one enjoys and excels during a PhD is very much (perhaps too much) dependent upon one's relationship with their supervisor, and I feel extremely lucky to have had Jorge as mine. For each project, he provided key insights and ideas in each of our discussions, not to mention the wealth of numerical code that he had previously developed for other projects, which proved to be absolutely indispensable. His excitement when things were going well and his understanding and support in the times when I struggled kept me going and made my PhD a truly fantastic experience.

I am also thankful to all the friends who have supported me throughout my PhD — those who I met in my time in Cambridge, both through the department and through my college, as well as older friends who have been with me for so long. There are too many of you to name but I am so thankful for each and every one of you.

I am quite sure that I would not have been able to achieve this without the love and support that my family have given me. My grandparents, Colin and Carol, taught me what it means to be graceful and kind. As for my siblings, James and Anna, I am so proud of the people that they have become and I hope they share that pride in me — they are and always have been the best friends I could ask for. Most of all, I'd like to thank my parents, David and Katie, who have given me everything and have always been there for me, through thick and thin. I can never thank you enough.



# Abstract

Stationary solutions are perhaps the most fundamental objects in any physical theory. In this thesis we numerically obtain a number of stationary black hole solutions to the Einstein-Maxwell equations with a negative cosmological constant. The AdS/CFT correspondence has caused an upsurge in studying anti-de Sitter (AdS) space, and under this duality, the study of classical black holes corresponds to studying thermal states of very strongly coupled conformal field theories (CFTs) — an extremely challenging feat without the aid of holography.

Firstly, we consider a braneworld scenario, which is a string theory-inspired mechanism for extra dimensions in our Universe. We present such rotating braneworld black hole solutions, which closely resemble standard Kerr black holes at large scales, supporting the phenomenological viability of the braneworld model. We shall discuss how these solutions are also dual to a four-dimensional black hole solution whose geometry is corrected by the coupling to a strongly coupled CFT with a UV cutoff.

Next, we consider a CFT living on a fixed black hole background with a positive cosmological constant. There are two classes of bulk solutions in this case, distinguished by their horizon structure, and corresponding to two different phases of the CFT on the boundary black hole background. One possible bulk solution is static and contains two disconnected Killing horizons, whilst the other is only stationary and contains only a single horizon which is not Killing.

We then consider the effect of deforming a CFT by the addition of a background electric field. The dual solution also has a non-Killing horizon, but due to the fact that the flow is generated by the Joule effect rather than a difference in temperatures, we find subtle differences in the horizon structure to other flowing solutions previously obtained. From the dual solution, we compute the conductivity of the field theory.

Finally, we present the first examples of static, charged binary black hole solutions. These are held in dynamic equilibrium due to the presence of a background electric field. The solutions run over a surprisingly large parameter space, and some of these parameters do not have clear interpretations in terms of the boundary theory. Indeed,

the solutions represent a continuous non-uniqueness for given boundary charges of asymptotically anti-de Sitter black hole solutions in Einstein-Maxwell theory.

A common theme will be the ways in which these solutions succeed and fail to be in equilibrium. Many of the solutions possess non-Killing horizons which have classical flow along them, which has a profound impact on the horizon structure. Others possess multiple horizons which may have distinct temperatures or electrostatic potentials. In either case, these features prevent the solutions from being in thermodynamic equilibrium, despite the solutions being stationary.

Chapter 1 provides a literature review, whilst Chapter 2 describes the numerical methods used to obtain the solutions of the thesis, many of which are standard. The original work of the thesis is presented in Chapters 3-6, which are each based on a paper (Refs. [1-4], respectively) written in collaboration with Jorge E. Santos.

# Table of contents

<b>Declaration</b>	<b>iii</b>
<b>Acknowledgements</b>	<b>vii</b>
<b>Abstract</b>	<b>ix</b>
<b>List of figures</b>	<b>xv</b>
<b>Notation</b>	<b>xvii</b>
<b>1 Introduction</b>	<b>1</b>
1.1 General Relativity . . . . .	2
1.2 Stationary, asymptotically flat black holes . . . . .	4
1.2.1 Uniqueness theorems . . . . .	7
1.2.2 Black hole thermodynamics . . . . .	9
1.2.3 Higher dimensions . . . . .	12
1.3 Anti-de Sitter space . . . . .	13
1.3.1 The geometry of anti-de Sitter space . . . . .	13
1.3.2 The AdS/CFT correspondence . . . . .	17
1.3.3 Holographic renormalization . . . . .	20
1.3.4 Asymptotically AdS black holes . . . . .	23
1.4 Black droplets and funnels . . . . .	27
1.4.1 The gravitational duals to a CFT on Schwarzschild . . . . .	28
1.4.2 Global black droplets and funnels . . . . .	30
1.5 The Randall-Sundrum model . . . . .	30
1.5.1 The RSI model . . . . .	31
1.5.2 The RSII model . . . . .	32
1.5.3 The connection between the RSII model and AdS/CFT . . . . .	35
1.5.4 Static RSII black holes . . . . .	39

---

1.6	The black hole solutions of this thesis . . . . .	41
<b>2</b>	<b>Numerical methods for finding stationary black holes solutions</b>	<b>44</b>
2.1	The DeTurck method . . . . .	46
2.1.1	Including a Maxwell field . . . . .	47
2.2	Bondi-Sachs gauge . . . . .	48
2.2.1	Including a Maxwell field . . . . .	51
2.3	The Newton-Raphson method . . . . .	51
2.4	A toolbox of tricks . . . . .	54
2.4.1	Damping . . . . .	54
2.4.2	Obtaining a good seed . . . . .	55
2.4.3	Patching . . . . .	56
2.4.4	Turning points . . . . .	57
<b>3</b>	<b>Rotating Randall-Sundrum II black holes</b>	<b>59</b>
3.1	Introduction . . . . .	59
3.2	Obtaining braneworld black holes . . . . .	63
3.2.1	The Ansatz . . . . .	63
3.2.2	Boundary conditions . . . . .	67
3.3	Properties of the braneworld black holes . . . . .	69
3.3.1	Entropy of the horizon . . . . .	69
3.3.2	Geometry of the bifurcating Killing horizon . . . . .	70
3.3.3	Orbits . . . . .	71
3.4	Discussion . . . . .	73
<b>4</b>	<b>Black tunnels and hammocks</b>	<b>76</b>
4.1	Introduction . . . . .	76
4.2	Black tunnels . . . . .	80
4.2.1	Ansatz for the black tunnels . . . . .	81
4.2.2	Boundary conditions . . . . .	82
4.2.3	Extracting the holographic stress tensor . . . . .	84
4.3	Black hammocks . . . . .	87
4.3.1	The integration domain for the black hammocks . . . . .	87
4.3.2	Ansatz for the black hammocks . . . . .	88
4.3.3	Boundary conditions . . . . .	90
4.3.4	Extracting the holographic stress tensor . . . . .	92
4.3.5	Properties of the hammock horizon . . . . .	94

---

4.4	Results . . . . .	97
4.4.1	The position of the hammock horizon . . . . .	97
4.4.2	Embeddings of the horizons . . . . .	98
4.4.3	The ergoregion of the hammocks . . . . .	100
4.4.4	Energy . . . . .	101
4.4.5	Flow . . . . .	103
4.4.6	Expansion and shear of the hammock horizon . . . . .	105
4.5	Discussion . . . . .	108
<b>5</b>	<b>Holographic batteries</b>	<b>113</b>
5.1	Introduction . . . . .	113
5.2	Finding the holographic batteries . . . . .	116
5.2.1	Bondi-Sachs gauge . . . . .	118
5.2.2	DeTurck gauge . . . . .	122
5.3	Results . . . . .	124
5.3.1	Stress tensor and conserved current . . . . .	124
5.3.2	Conductivity . . . . .	124
5.3.3	Energy Flow . . . . .	127
5.3.4	Properties of the bulk horizon . . . . .	128
5.3.5	Detuning the temperatures . . . . .	130
5.4	Discussion . . . . .	130
<b>6</b>	<b>Charged static AdS black hole binaries</b>	<b>133</b>
6.1	Introduction . . . . .	133
6.2	The numerical construction of AdS binaries . . . . .	136
6.2.1	The Israel-Khan solution . . . . .	137
6.2.2	Empty global AdS . . . . .	140
6.2.3	The <i>Ansätze</i> . . . . .	140
6.2.4	Coordinate transformations . . . . .	142
6.2.5	Boundary conditions . . . . .	143
6.2.6	The reference metric . . . . .	145
6.2.7	Patching and numerics . . . . .	147
6.2.8	Removing the $\mathbb{Z}_2$ symmetry . . . . .	149
6.2.9	Changing the number of dimensions . . . . .	150
6.2.10	Extracting the holographic quantities . . . . .	151
6.3	Results . . . . .	153
6.3.1	Charges . . . . .	153

---

6.3.2	The parameter space of solutions . . . . .	154
6.3.3	Thermodynamics . . . . .	157
6.4	Discussion . . . . .	158
<b>7</b>	<b>Discussion</b>	<b>160</b>
	<b>References</b>	<b>163</b>
	<b>Appendix A Convergence tests</b>	<b>180</b>
A.1	Convergence properties of the rotating RSII black holes . . . . .	180
A.2	Convergence properties of the black tunnels . . . . .	181
A.3	Convergence properties of the black hammocks . . . . .	182
A.4	Convergence properties of the holographic batteries . . . . .	183
A.5	Convergence properties of the charged AdS binary solutions . . . . .	185
	<b>Appendix B Universal properties of the holographic batteries for small voltage</b>	<b>187</b>
B.1	Conductance for other profiles . . . . .	187
B.2	A proof of the linear behaviour of the conductance . . . . .	188

# List of figures

1.1	The Penrose diagram of $\text{AdS}_3$ . . . . .	16
1.2	The temperature of a AdS-Schwarzschild black hole . . . . .	24
1.3	The phase diagram of the Hawking-Page transition . . . . .	26
1.4	A sketch of a black droplet and a black funnel . . . . .	28
1.5	A sketch of a global black droplet and a global black funnel . . . . .	31
1.6	The Penrose diagram of the Randall-Sundrum II spacetime . . . . .	34
3.1	The coordinate domain of a static RSII black hole. . . . .	64
3.2	Entropy of the rotating RSII black holes . . . . .	70
3.3	The Ricci scalar of the induced geometry of the horizon of the braneworld black holes . . . . .	71
3.4	Inner-most stable circular orbits of the RSII black holes . . . . .	72
4.1	Sketches of a black tunnel and a black hammock . . . . .	79
4.2	The coordinate domain of the black tunnel . . . . .	81
4.3	The coordinate domain of the black hammock . . . . .	87
4.4	The Penrose diagram of the de Sitter-Schwarzschild solution depicting constant time-slices of the ingoing coordinates . . . . .	94
4.5	Embeddings of a black tunnels and a black hammock . . . . .	99
4.6	The ergoregion of the black hammock . . . . .	100
4.7	The energy of the black tunnels and the black hammocks . . . . .	103
4.8	The flow along the black hammocks . . . . .	104
4.9	Properties of the hammock horizon . . . . .	106
4.10	The expansion of the hammock horizon . . . . .	107
4.11	The shear of the hammock horizon . . . . .	109
5.1	A sketch of the boundary geometry and a global funnel . . . . .	114
5.2	The stress tensor of the holographic batteries . . . . .	125
5.3	The conductance, $G$ , of the holographic batteries . . . . .	126

---

5.4	The affine parameter and expansion of the horizon of a holographic battery	129
5.5	The horizon structure of the detuned holographic batteries . . . . .	131
6.1	A sketch of a charged binary solution in AdS . . . . .	135
6.2	The Israel-Khan spacetime . . . . .	139
6.3	The coordinate domain of the binary solutions . . . . .	143
6.4	The patching method used to find $\mathbb{Z}_2$ symmetric binary solutions . . . .	148
6.5	The patching method used to find non- $\mathbb{Z}_2$ symmetric binary solutions .	149
6.6	The proper distance between and the charges of the two horizons of the binary solutions . . . . .	155
6.7	Various thermodynamic quantities of the binary solutions . . . . .	156
A.1	Convergence test for the rotating RSII black holes . . . . .	181
A.2	Convergence test for the black tunnels . . . . .	182
A.3	Convergence test for the black hammocks . . . . .	183
A.4	Convergence test for the holographic batteries in Bondi-Sachs gauge . .	184
A.5	Convergence test for the holographic batteries in DeTurck gauge . . . .	184
A.6	Convergence test for the charged binary solutions . . . . .	185
B.1	The conductance of the holographic batteries for different choices of profile	188

# Notation

We will use natural units with  $c = \hbar = 1$ . For a Lorentzian metric we take a mostly positive signature. We use Einstein summation convention throughout. Different letters for indices have the following meaning:

- Latin indices near the beginning of the alphabet  $a, b, \dots$  refer to all spacetime components of the bulk spacetimes.
- Latin indices from the middle of the alphabet  $i, j, \dots$  refer to spatial components of the bulk spacetimes.
- Greek indices  $\mu, \nu, \dots$  refer to components of the boundary of the spacetimes, which in this thesis is either the conformal boundary or a Randall-Sundrum brane. These run over all of the bulk directions except the radial AdS direction.
- We shall also use upper-case Latin indices, though the precise meaning of these shall be defined in each case individually.

Through we shall use  $d$  to denote the number of bulk spacetime dimensions, whilst  $D = d - 1$  will be the number of boundary dimensions.



# Chapter 1

## Introduction

Einstein’s theory of general relativity [5, 6] is a physical theory famed for both its beauty and its complexity. In his earlier theory of special relativity [7], Einstein had revolutionised our understanding of space and time by exploring the implications of a curious empirical observation — that the speed of light in a vacuum is the same in any inertial frame. Minkowski later reinterpreted special relativity by unifying space and time into a single four-dimensional entity called *spacetime* [8]. The essence of general relativity is that spacetime is itself also a dynamical field, bending and warping due to the presence of energy and matter, and that this curvature of spacetime is the cause of the force we recognise as gravity.

This idea is quantified by one of the most famous equations in all of physics, the *Einstein equation*, given by

$$R_{ab} - \frac{1}{2}Rg_{ab} + \Lambda g_{ab} = 2T_{ab}. \quad (1.1)$$

Roughly speaking (we will go into far more detail momentarily), the left hand side describes the curvature of spacetime itself, whilst the right hand side describes the energy, momentum and stress of the matter residing on this curved spacetime. From this equation, we see how general relativity is intrinsically, and intricately, a dynamical theory. In the words of John Wheeler: “Space tells matter how to move. Matter tells space how to curve”.

This thesis, however, is not concerned with dynamical solutions of the Einstein equation, but, rather, with stationary solutions, *i.e.* those that do not vary over time. Time-independent solutions are perhaps the most fundamental objects in any physical theory, often providing insight into the general behaviour of the theory once dynamics are included. Indeed, the study of stationary black holes within general relativity has

been a rich source of progress in understanding gravity over the past century and has led to some of the most pressing open questions in theoretical physics.

Until fairly recently, relatively few stationary solutions were known. One reason for this is the difficulty involved with solving the Einstein equation, which generally yields a set of coupled, non-linear partial differential equations (PDEs). Only in a few special cases can these equations be solved exactly, though many methods have been developed in the past few decades to solve them numerically. Secondly, in many physically motivated scenarios there are theorems which restrict stationary black holes to be described by a surprisingly small family of exact solutions. However, if one drops some assumptions of these theorems by considering higher dimensional spacetimes or a non-zero cosmological constant, it turns out that there is a myriad of stationary black hole solutions.

Progress in the understanding of string theory and holography has to a large extent motivated further study into such solutions since the turn of the century, particularly those in anti-de Sitter (AdS) space, *i.e.* those which solve Einstein's equation with a negative cosmological constant,  $\Lambda < 0$ . But before coming to these, let us first recount some basic facts about black holes and the theory of general relativity (much more detail can be found in the standard textbooks [9–12]), and discuss anti-de Sitter space and its fascinating properties.

## 1.1 General Relativity

The fundamental object of general relativity (GR) is the *metric*,  $g_{ab}$ , of a Lorentzian manifold,  $\mathcal{M}$ . Throughout this thesis, we will be interested in *Einstein-Maxwell theory* which describes dynamical gravity coupled to a Maxwell field. The *Einstein-Hilbert* action for this theory is given by

$$S = \frac{1}{16\pi G} \int_{\mathcal{M}} d^d x \sqrt{-g} (R - 2\Lambda - F_{ab}F^{ab}), \quad (1.2)$$

where  $g$  and  $R$  are, respectively the determinant and Ricci scalar of the metric,  $G$  is Newton's constant of gravitation,  $\Lambda$  is the cosmological constant, and  $F = dA$  is the field strength tensor of the Maxwell field with vector potential  $A^a$ .

Varying this action with respect to the metric yields the Einstein equation (1.1), where the *stress tensor*,  $T_{ab}$ , is defined in terms of the field strength tensor. It is often useful to substitute the Ricci scalar for the trace of the stress tensor by considering

the trace of (1.1). This yields the Einstein equation written in *trace-reversed form*:

$$R_{ab} - \frac{2\Lambda}{d-2}g_{ab} = 2\tilde{T}_{ab}, \quad (1.3a)$$

where  $\tilde{T}_{ab}$  is the *trace-reversed stress tensor*, which for a Maxwell field is given by

$$\tilde{T}_{ab} = F_a{}^c F_{bc} - \frac{1}{2(d-2)}g_{ab}F_{cd}F^{cd}. \quad (1.3b)$$

Varying the action (1.2) with respect to the vector potential yields the generalisation of the usual Maxwell equation to curved space:

$$\nabla^a F_{ab} = 0. \quad (1.4)$$

One of the most important concepts across all of physics is that of symmetry. In GR, a symmetry can be described by a *Killing vector field* (KVF),  $X^a$ , which preserves the metric:

$$\mathcal{L}_X g = 0 \quad \text{or, equivalently,} \quad \nabla_a X_b + \nabla_b X_a = 0. \quad (1.5)$$

We call a spacetime *stationary* if it possesses a Killing vector field,  $k^a$ , which is causal in the vicinity of the asymptotic boundary.<sup>1</sup> This stationary spacetime is called *static* if there exists a spacelike hypersurface,  $\Sigma$ , which is everywhere orthogonal to orbits of  $k$ . These definitions become a little clearer if one takes coordinates with  $k^a = (\partial/\partial t)^a$ . Then a stationary metric is given by

$$ds^2 = -N^2 dt^2 + h_{ij} (dx^i + N^i dt) (dx^j + N^j dt), \quad (1.6)$$

where  $N$ ,  $N^i$  and  $h_{ij}$  are independent of  $t$ . It is static if there is a choice of the coordinate  $t$  such that  $N^i = 0$ .

We call a spacetime *axisymmetric* if it possesses a spacelike KVF,  $m^a$ , whose orbits form closed curves. In a coordinate basis with  $m^a = (\partial/\partial\phi)^a$ , this definition requires that  $\phi$  is a periodic coordinate.

The simplest metric one can write down is that of Minkowski space:

$$ds^2 = -dt^2 + dr^2 + r^2 d\Omega_{(2)}^2, \quad (1.7)$$

---

<sup>1</sup>The requirement is often that the vector is timelike *everywhere*, though, technically speaking, this would not allow for the existence of ergoregions.

with  $d\Omega_{(2)}^2$  denoting the metric on a unit 2-sphere. This is a solution to the vacuum Einstein equation with zero cosmological constant. Solutions which approach Minkowski space far away from any matter or black holes are called *asymptotically flat*.<sup>2</sup> The inclusion of a cosmological constant has an effect on the spacetime on large scales, and so solutions to the Einstein equation with non-zero cosmological constant will not be asymptotically flat. We will in particular be interested in solutions with a negative cosmological constant which asymptote to a maximally symmetric solution called anti-de Sitter space. Before considering such spacetimes, let us briefly review some results regarding asymptotically flat black holes in four dimensions.

## 1.2 Stationary, asymptotically flat black holes

Exact black hole solutions of general relativity are few and far between. The first such solution was discovered only a few months after Einstein introduced general relativity by Schwarzschild [13] when he was stationed on the Eastern front in the first world war. The Schwarzschild solution describes an asymptotically flat, static, spherically symmetric black hole. The large amount of symmetry in this case means that the vacuum Einstein equation reduces to a single ordinary differential equation (ODE) for one function of the radial coordinate. The solution is given by

$$ds^2 = -f(r) dt^2 + \frac{dr^2}{f(r)} + r^2 d\Omega_{(2)}^2 \quad (1.8a)$$

where

$$f(r) := 1 - \frac{2M}{r}, \quad (1.8b)$$

and with  $d\Omega_{(2)}^2$  denoting the metric on a unit 2-sphere. The parameter,  $M$ , denotes the mass of the black hole. The metric is clearly static with respect to the Killing vector field,  $k^a = (\partial/\partial t)^a$ .

This simple solution already demonstrates some of the interesting, and often mind-boggling, features of black holes. Firstly, the  $(rr)$ -component of the metric diverges at  $r = 2M$ , though this turns out only to be a coordinate singularity, meaning that it is the coordinate system that is breaking down rather than there being any physical singularities leading to infinite tidal forces for observers. It can be cured by instead

---

<sup>2</sup>See standard general relativity textbooks [9–12] for a more rigorous definition of asymptotic flatness.

using *ingoing Eddington-Finkelstein coordinates*, defined by

$$dt = dv - \frac{dr}{f(r)}. \quad (1.9)$$

The metric becomes

$$ds^2 = -f(r) dv^2 + 2 dv dr + r^2 d\Omega_{(2)}^2. \quad (1.10)$$

The metric and inverse metric in these coordinates, as well as their determinants, are regular at  $r = 2M$ . Thus, one can extend the metric through  $r = 2M$  all the way to  $r = 0$ , at which the metric again becomes singular. This time though, the Kretschmann scalar, defined by  $K = R_{abcd}R^{abcd}$ , also diverges. This scalar is a gauge independent quantity associated to the tidal forces that an observer would experience, and hence the singularity at  $r = 0$  is physical and cannot be cured by a change of coordinates.

It can be shown that no signal from an observer at  $r < 2M$  can be sent to an asymptotic observer. This is, in fact, the definition of a *black hole*: a region of spacetime from which no future-directed causal curves extend to infinity. Roughly speaking then, a black hole is a region of spacetime so curved, and hence gravitationally attractive, that not even light is fast enough to escape its influence.

Any future-directed curve starting in the  $r < 2M$  region of the Schwarzschild solution necessarily reaches the singularity at  $r = 0$  in finite affine time. Singularities also arise in Newtonian gravity when spherical symmetry is assumed, but they are cured by including rotation, and thus these Newtonian singularities are not generic but are instead an artifact of the large amount of symmetry. One may wonder if the black hole singularity of the Schwarzschild solution of general relativity is similarly non-generic. However, the singularity theorems of Penrose and Hawking [14–16, 9] show that this is not the case; singularities are generic in general relativity and are present whenever there is a horizon.<sup>3</sup>

The boundary of the black hole region, in this case the  $r = 2M$  hypersurface, is called the *event horizon*. The normal,  $n_a$ , to an event horizon must be a null vector, hence the horizon is an example of a *null hypersurface*. The normal to the horizon of the Schwarzschild solution is given by  $n_a = (dr)_a$  which is indeed null at  $r = 2M$ . Raising the index, we see that  $n^a = (\partial/\partial v)^a$ . We call  $n^a$  a *generator* of the horizon.

---

<sup>3</sup>More precisely, if a spacetime satisfying the Einstein equation with matter satisfying the null energy conditions contains a trapped surface, then there exist future-inextendible geodesics with finite affine length within the trapped region, meaning that the spacetime is geodesically incomplete.

Note that  $(\partial/\partial v)^a$  is a KVF, and hence, the horizon is generated by a Killing vector. Any horizon satisfying this property is named a *Killing horizon*.

We may wonder whether there exist other spherically symmetric solutions of the vacuum Einstein equation, however, this is forbidden by Birkhoff's theorem [17]:

**Theorem 1.1 (Birkhoff)** *Let  $(\mathcal{M}, g)$  be a spherically symmetric,  $C^2$ , solution to the vacuum Einstein equation. Then  $(\mathcal{M}, g)$  is isometric to the Schwarzschild solution.*

Roughly speaking, this means that “spherical symmetry implies staticity”. Moreover, it implies that the spacetime in the exterior of *any* spherically symmetric body of matter is isometric to the Schwarzschild metric, even if the body of matter itself is time-dependent.

The Reissner-Nordström metric [18–21] describes a charged, static, spherically symmetric, asymptotically flat black hole solution of Einstein-Maxwell theory. This solution also possesses an event horizon, and in a very similar manner to above, one can extend through to a black hole region within the horizon using ingoing coordinates. This time though, one reaches an *inner* horizon before reaching a physical singularity. This inner horizon is a Cauchy horizon, meaning that there is no unique analytic extension through it. The strong cosmic censorship conjecture [22], however, posits that the existence of this inner horizon is an artifact of the large amount of the symmetry of the solution and will not arise from generic initial data.

It is a testament to how difficult general relativity becomes whenever any assumptions of symmetry are dropped that there was an almost fifty year interval between the discovery of the Schwarzschild solution and the Kerr solution [23], which is an exact solution describing a rotating, axisymmetric, asymptotically flat, stationary, vacuum black hole.

Unlike for the Schwarzschild and Reissner-Nordström solutions, the stationary Killing vector does not generate the horizon of the black hole. Instead it is generated by  $\xi^a = k^a + \Omega_H m^a$ , where  $k^a$  and  $m^a$  denote the stationary and axisymmetric Killing vectors of the Kerr metric, respectively. The defining equation of a Killing vector is linear, and hence  $\xi^a$  is also a Killing vector, meaning that the horizon of the Kerr black hole is also a Killing horizon.

The horizon is still preserved by the stationary isometry, and so the stationary Killing vector,  $k^a$ , must be tangent to the horizon and thus orthogonal to the null generator  $\xi^a$  at the horizon, meaning that it must be null or spacelike there. However, if it were null, then it would itself be a generator of the horizon. Since this is not the case, the stationary Killing vector field must in fact be spacelike on the horizon of the Kerr black hole. Moreover, since the norm of  $k^a$  is continuous, this means there

is an open subspace of the spacetime around the horizon in which  $k^a$  is spacelike. This region is called the *ergoregion*, and its boundary, where  $k^a$  is null, is called the *ergosurface*. Note that this analysis will hold whenever we have a stationary black hole spacetime whose horizon is not generated by the stationary Killing vector field — such a spacetime must necessarily have an ergoregion.

The presence of the ergoregion leads to interesting phenomena. Firstly, it implies that an observer situated within the ergoregion cannot remain stationary in space relative to an asymptotic observer, *i.e.* an observer cannot follow an orbit of  $k^a$  inside the ergoregion. In the case of Kerr, this can be understood with the concept of *frame-dragging*: the rotating black hole literally drags space around with it as it spins, meaning that all observers are pulled around too in its gravitational whirlpool. From within the ergoregion it is still possible for an observer to escape to infinity (so long as they do not cross the horizon), but they must do so by spinning with the black hole whilst accelerating away from it. Secondly, the ergoregion allows for the possibility of energy extraction from the black hole via the Penrose process [24] or via superradiance [25–27].

Again one can transform to ingoing coordinates in order to extend through the event horizon of the Kerr black hole. Similarly to the Reissner-Nordström case there is a Cauchy horizon in the interior which is expected to be non-generic.

The generalisation of the Kerr solution to Einstein-Maxwell theory, the Kerr-Newman solution [28, 29], was discovered shortly after the Kerr solution. It is an exact solution describing a charged, rotating black hole and depends upon four parameters, the mass  $M$ , the angular momentum  $J$ , the electric charge  $Q$ , and the magnetic charge  $P$ . In Section 1.2.2, we will see that each of these parameters can be defined as charges, *i.e.* as integrals at infinity. All the other four-dimensional, asymptotically flat solutions mentioned above are special cases of the Kerr-Newman solution (Schwarzschild is  $J = Q = P = 0$ , Reissner-Nordström is  $J = 0$ , and Kerr is  $Q = P = 0$ ).

### 1.2.1 Uniqueness theorems

For four-dimensional, asymptotically flat black holes, there are a large number of uniqueness results, as reviewed in [30, 31].

Firstly, Israel showed that a regular, static vacuum black hole spacetime is isometric to the Schwarzschild solution [32]. Bunting and Masood-ul-Alam later provided an alternative proof [33] based on the positive energy theorem [34–36]. Israel also extended this to the electro-vacuum case to show that a charged, static black hole spacetime must be isometric to Reissner-Nordström, under the further assumption that the event horizon

is a connected surface [37]. This extra assumption is necessary due to some famous multi-horizon solutions in Einstein-Maxwell theory called the Majumdar-Papapetrou solutions [38, 39], which are a configuration of extremally charged black holes, in which the gravitational attraction between the black holes is balanced by their electric repulsion. However, the Reissner-Nordström and Majumdar-Papapetrou solutions are the only static, asymptotically flat electro-vacuum black hole spacetimes [40, 41]. Furthermore, it was shown that if the stationary Killing vector field generates the horizons, then the spacetime must be static [42, 43]. These can be combined to give the following:

**Theorem 1.2 (Static Uniqueness Theorem)** *Let  $(\mathcal{M}, g)$  be an asymptotically flat black hole solution of the Einstein-Maxwell equations in four dimensions with stationary Killing vector field,  $k^a$ , and suppose the event horizon is generated by  $k^a$ . Then  $(\mathcal{M}, g)$  is static with respect to  $k^a$ . Furthermore, if the event horizon is connected then  $(\mathcal{M}, g)$  is a member of the Reissner-Nordström family, and if the horizon is disconnected then  $(\mathcal{M}, g)$  is a Majumdar-Papapetrou solution.*

In the case that the black hole is not static or spherically symmetric, the rigidity theorem [44, 9] effectively states that a stationary black hole is axisymmetric and possesses a Killing horizon:

**Theorem 1.3 (Rigidity Theorem)** *Let  $(\mathcal{M}, g)$  be an analytic, asymptotically flat, four-dimensional black hole solution to the Einstein-Maxwell equation which is stationary with respect to a Killing vector field,  $k^a$ . Then the horizon is generated by a Killing vector field  $\xi^a = k^a + \Omega_H m^a$ , where  $\Omega_H$  is a constant, called the angular velocity, and  $m^a$  is a spacelike Killing vector field whose orbits form closed curves, i.e.  $(\mathcal{M}, g)$  is axisymmetric.*

The assumption that the metric is analytic is unphysical, and was later weakened [45–49]. One important ingredient of the proofs of the rigidity theorem is the topology theorems [44, 50, 51] which dictate that for any four-dimensional, asymptotically flat black hole spacetime, the intersection of the event horizon with a Cauchy surface must topologically be a two-sphere.

Finally, under the assumption of stationarity and axisymmetry (or stationarity and analyticity, after appealing to Hawking’s rigidity theorem), Carter [52] and Robinson [53] obtained the uniqueness theorem:

**Theorem 1.4 (Axisymmetric Uniqueness Theorem)** *Let  $(\mathcal{M}, g)$  be a stationary, axisymmetric, regular, asymptotically flat black hole solution to the vacuum Einstein*

equation with a connected, non-degenerate event horizon. Then  $(\mathcal{M}, g)$  is a non-extremal member of the Kerr family which is parameterised by two asymptotic charges: the mass  $M$ , and the angular momentum  $J$ .

This result was extended to Einstein-Maxwell theory by Mazur [54] and Bunting [55], where now  $(\mathcal{M}, g)$  must belong to the four-parameter Kerr-Newman family. In nature though, it is not expected for black holes to be charged, since if they were they would attract oppositely charged matter and swiftly become neutral. Hence, the expectation from the uniqueness theorems is that matter which collapses to form a black hole will settle down to a member of the Kerr family.

The essence of these theorems is the idea that a stationary black hole should be uniquely determined in terms of a small number of asymptotic charges. This led to the “no-hair” conjecture, which postulated that this was the case for stationary black holes in theories including other matter fields. Indeed this was verified in various set-ups [56–65], but has been shown to generally not be true by considering dilaton [66–68], non-Abelian [69–71], complex scalar [72], or Proca [73] fields.

### 1.2.2 Black hole thermodynamics

We have been calling the quantities  $M$ ,  $J$ ,  $Q$  and  $P$  asymptotic charges, despite the fact that so far we have treated them as parameters of the Kerr-Newman spacetimes, rather than quantities obtained by an integral at infinity. Let us now explain how these charges can be defined at infinity, and further go on to discuss how they satisfy the laws of thermodynamics.

Let us consider an asymptotically flat spacetime  $(\mathcal{M}, g)$  which is stationary w.r.t. a KVF,  $k^a$ , and axisymmetric w.r.t. a KVF,  $m^a$ , and with a Maxwell field with field strength tensor  $F_{ab}$ . Let  $\Sigma$  be a Cauchy surface of the spacetime, and  $\partial\Sigma$  its intersection with the asymptotic boundary. Then the electric charge and magnetic charge of the space are, respectively, defined by

$$Q = \frac{1}{4\pi} \int_{\partial\Sigma} \star F, \quad P = \frac{1}{4\pi} \int_{\partial\Sigma} F, \quad (1.11)$$

and the mass (or equivalently, the energy), and the angular momentum are, respectively, defined by the Komar integrals

$$M = -\frac{1}{8\pi} \int_{\partial\Sigma} \star dk, \quad J = \frac{1}{16\pi} \int_{\partial\Sigma} \star dm. \quad (1.12)$$

We have from the rigidity theorem that the horizon,  $\mathcal{H}^+$ , is generated by the Killing vector  $\xi^a = k^a + \Omega_H m^a$ , which is null on the horizon. Hence  $\xi^a \xi_a = 0$  is constant on the horizon, and thus its derivative must be normal to  $\mathcal{H}^+$  meaning that it will be proportional to  $\xi$ . That is,

$$\nabla_a (\xi^b \xi_b) = -2\kappa \xi_a, \quad (1.13)$$

where  $\kappa$  is named the *surface gravity* of the horizon.

The charges and the surface gravity satisfy a number of laws, often called the laws of black hole mechanics [74–77].

**Theorem 1.5 (Zeroth law of black hole mechanics)** *The surface gravity,  $\kappa$ , of the horizon of a stationary black hole spacetime satisfying the dominant energy condition is constant.*

**Theorem 1.6 (First law of black hole mechanics)** *Consider a variation within the space of Kerr-Newman solutions. The change in area of the black hole horizon is given by*

$$\frac{\kappa}{8\pi} \delta A = \delta M - \Omega_H \delta J - \Phi_H \delta Q - \Psi_H \delta P, \quad (1.14)$$

where  $\Phi_H$  and  $\Psi_H$  are the co-rotating electric and magnetic potentials, respectively. These are defined by  $\Phi_H = -\xi^a A_a|_{\mathcal{H}^+}$  and  $\Psi_H = -\xi^a B_a|_{\mathcal{H}^+}$  where  $F = dA$  and  $\star F = dB$  and  $A^a$  and  $B^a$  are taken in a gauge such that they vanish at infinity.

The first law is presented here in its weakest form, as a result regarding variations within the space of stationary black hole solutions. There is also a physical version describing how the charges of a black hole are perturbed when a small flux of matter enters the horizon [78]. Sudarsky and Wald strengthened the first law using the Hamiltonian formulation of GR to show that by considering small variations in the initial data leading towards a certain black hole solution one can also derive a first law relationship [42]. Indeed this proof extends to generic matter fields, so long as there is a well-defined Hamiltonian formulation [79].

**Theorem 1.7 (Second law of black hole mechanics)** *Assuming the weak energy condition, the area of the black hole horizon is non-decreasing.*

The evident similarity of the laws of black hole mechanics to those of thermodynamics led to the expectation that entropy of a black hole is proportional to its area, whilst the temperature of a black hole is proportional to its surface gravity. This led to some confusion, since classically, no particles can escape from black holes, and hence

one would expect that they would have zero temperature, whereas the surface gravity is generally non-zero. The mystery was solved by Hawking [80, 81], who revealed that when quantum effects of matter fields are taken into account, a black hole radiates at the so-called *Hawking temperature*:

$$T_H = \frac{\hbar\kappa}{2\pi} \quad (1.15)$$

Here we have included the factor of  $\hbar$  to stress that this is a quantum effect, though we will take  $\hbar = 1$  from now on.

This formula for the temperature fixes the constant of proportionality between the area and the entropy required such that the first law of black hole mechanics matches perfectly with the first law of thermodynamics. The entropy must be given by the *Bekenstein-Hawking formula*:

$$S_{BH} = \frac{A}{4G}. \quad (1.16)$$

One major mystery is precisely what the microscopic degrees of freedom are that are being counted by the entropy.

The black hole can now decrease area due to Hawking radiation, which violates the second law of black hole mechanics, as presented above. However, Bekenstein's *generalised second law* [82] dictates that the total entropy, combining that of the black hole and any matter fields, is always non-decreasing, which again matches with the second law of thermodynamics.

A black hole radiating at the Hawking temperature will eventually evaporate. Even if the state which collapsed to form the black hole was a pure state, Hawking's calculation implies that the end state of evaporation would be a mixed state, suggesting that information has been lost during this process, or more precisely, that the evolution is not unitary. One may at first think that the loss of information is not that problematic and arises in all sorts of physical processes — say we burn a book, it seems as though the information held within the pages is as irretrievably lost as if we had thrown it into a black hole. However, the difference is that if one were to capture the ashes as well as all of the photons emitted in the process of burning the book, one would, in theory, be able to be able to rebuild the book from scratch. The information is retained in the ashes and the radiation but one would need an unimaginably sophisticated quantum computer to access it. On the other hand, if one were to throw a book into a black hole, one could wait for half an eternity, capturing each and every quantum of Hawking radiation emitted during the black hole's lifetime, but according to Hawking's calculation, even with a perfect quantum computer, one wouldn't be able to deduce

whether the book thrown in was *The Brothers Karamazov*, *Fifty Shades of Grey*, or just a particularly large roll of toilet paper.<sup>4</sup>

This famous problem is called the information paradox [83]. A more modern version of the paradox is to say that the evaporation of a black hole implies that a theory of quantum gravity cannot satisfy all of the following: unitarity, locality, and regularity in the vicinity of a horizon [84]. The AdS/CFT correspondence, which maps a theory of quantum gravity to a field theory residing on the boundary (which we will review in Section 1.3.2) suggests that a full theory of quantum gravity may not be local.

In any case, the information paradox serves as an excellent example of how studying stationary solutions in general relativity can lead to pressing questions regarding the fundamental nature of the theory.

### 1.2.3 Higher dimensions

Though our Universe clearly appears to have four dimensions, there are a number of reasons for interest in higher dimensional black holes [85, 86]. Firstly, superstring theory is only mathematically consistent in ten dimensions, and therefore in order for it to be realised in the real world, there would need to be six extra dimensions which are in some sense small, and so unnoticeable for large observers. It is possible that microscopic black holes could be generated in colliders [87–89], and whilst they have failed to materialise in experiments in the LHC, future particle colliders [90–92] keep the hopes that they could be generated alive. Such microscopic black holes would provide excellent testing grounds for extra dimensions. Moreover, the AdS/CFT duality relates a  $d$ -dimensional black hole to a state of a  $(d - 1)$ -dimensional quantum field theory, hence in this case it is clear that studying other values of dimensionality will still be of great interest. Finally, black holes are some of the most fundamental objects in the theory of general relativity, and hence it is desirable to better understand their properties, in any number of dimensions, in order to better understand the theory. For example, one may wonder whether each of the uniqueness theorems reviewed in Section 1.2.1 is particular to four dimensions and asymptotic flatness, or holds in more generality.

By generalising the proof of Bunting and Masood-Ul-Alam it was shown that a static, higher-dimensional, asymptotically flat black hole spacetime with a non-degenerate horizon is isometric to the Schwarzschild-Tangherlini metric (the generalisation of Schwarzschild to higher dimensions) [93–95].

---

<sup>4</sup>We leave it to the reader to judge which two of these three are most similar.

The natural extensions of the rotating Kerr solutions to higher dimensions are the Myers-Perry black holes [96]. In  $d$ -dimensions, the spatial cross-section of the horizon of these black holes is topologically a sphere,  $S^{d-2}$ , and with  $d = 2n + 1$  or  $d = 2n + 2$  the solutions have  $n$  linearly independent axes of rotation. However, not all rotating black hole solutions belong to the Myers-Perry family; the first and most famous counterexamples, due to Emparan and Reall, are the five-dimensional black ring solutions [97], whose horizons have  $S^2 \times S^1$  topology.

Hence, unlike in four dimensions, it is not the case that all asymptotically flat, stationary black holes have horizons with spherical topology. Indeed, the space of higher dimensional black holes is far richer, not satisfying the natural analogue of the axisymmetric uniqueness theorem in four dimensions. That being said, there do exist theorems restricting the horizon topology to a wider family [98, 99], and the rigidity theorem does hold in higher dimensions under the assumption that the spatial cross-sections of the horizon are *compact* [100–102].

We shall shortly see that taking a non-zero cosmological constant allows for an even richer space of stationary black hole solutions. There are very few results regarding uniqueness in the presence of a positive cosmological constant. Indeed, recently, both static and axially rotating binary black hole solutions were obtained numerically in pure gravity in four dimensions with a positive cosmological constant [103, 104]. We will chiefly be interested though in the case of a negative cosmological constant.

## 1.3 Anti-de Sitter space

Let us now consider the vacuum Einstein equation with a negative cosmological constant:

$$R_{ab} + \frac{d-1}{\ell_d^2} g_{ab} = 0, \quad (1.17)$$

where  $\ell_d$  is called the *AdS radius* and is defined in terms of the cosmological constant by  $\Lambda = -(d-1)(d-2)/(2\ell_d^2)$ . The maximally symmetric solution to this equation is called *anti-de Sitter* (AdS) space.

### 1.3.1 The geometry of anti-de Sitter space

Anti-de Sitter space in  $d$  dimensions can be defined as the induced geometry of a hyperboloid

$$-Y_0^2 - Y_1^2 + \sum_{i=1}^{d-1} X_i^2 = -\ell_d^2 \quad (1.18)$$

embedded in  $\mathbb{R}^{2,d-1}$ , *i.e.* flat space with two timelike directions, which has metric

$$ds_{\mathbb{R}^{2,d-1}}^2 = -dY_0^2 - dY_1^2 + \sum_{i=1}^{d-1} dX_i^2. \quad (1.19)$$

The flat  $\mathbb{R}^{2,d-1}$  space possesses the isometry  $SO(2, d-1)$ , under which the constraint (1.18) is invariant, and hence anti-de Sitter space inherits this isometry.

We will find a number of different coordinate systems useful. Firstly, we can take *global coordinates* defined by

$$Y_0 = \ell_d \sec \theta \sin \tau, \quad Y_1 = \ell_d \sec \theta \cos \tau, \quad X_i = \ell_d y_i \tan \theta, \quad (1.20)$$

with  $y_i$  the standard Cartesian coordinates of a unit  $(d-1)$ -sphere, for  $i = 1, \dots, d-1$ , with  $\sum_{i=1}^{d-1} y_i^2 = 1$ . The metric of the hyperboloid in these coordinates is given by

$$ds_{\text{AdS}}^2 = \frac{\ell_d^2}{\cos^2 \theta} \left( -d\tau^2 + d\theta^2 + \sin^2 \theta d\Omega_{(d-2)}^2 \right), \quad (1.21)$$

and one can explicitly check it satisfies the vacuum Einstein equation with a negative cosmological constant, (1.17). From (1.20) the time coordinate appears to be periodic, which would lead to undesirable closed timelike curves. However, we can simply unravel the circle, taking  $\tau \in (-\infty, \infty)$  without any identifications, *i.e.* we take the universal covering of the hyperboloid. The  $\theta$  coordinate lies in the range  $\theta \in (0, \pi/2)$ . These coordinates parameterise the whole of the hyperboloid and hence the metric described by (1.21) is named *global anti-de Sitter space*. The asymptotic boundary is situated at  $\theta = \pi/2$ .

Another useful set of coordinates are the *Poincaré* coordinates, which are defined by

$$\begin{aligned} Y_0 &= \frac{\ell_d}{z} t, & X_{I+1} &= \frac{\ell_d}{z} x_I, \\ Y_1 - X_1 &= \frac{\ell_d}{z}, & Y_1 + X_1 &= \frac{\ell_d}{z} \left( z^2 - t^2 + \sum_{I=1}^{d-2} x_I^2 \right) \end{aligned} \quad (1.22)$$

where  $I = 1, \dots, d-2$ . The  $z$  coordinate runs over  $z \in (0, \infty)$  and hence these coordinates only cover half of the hyperboloid,  $\{Y_1 > X_1\}$ . This region of AdS space

parameterised by these coordinates is called the *Poincaré patch* and has metric

$$ds_{\text{Poincaré}}^2 = \frac{\ell_d^2}{z^2} \left( -dt^2 + dz^2 + \sum_{I=1}^{d-2} dx_I^2 \right). \quad (1.23)$$

We note that constant  $z$  slices of the Poincaré patch have flat geometry, with induced metric isometric to the Minkowski metric. The conformal boundary is situated at  $z = 0$ . The  $z \rightarrow \infty$  surface is called the Poincaré horizon. This surface appears to be singular in the Poincaré coordinates, but by considering the global coordinates or the original hyperboloid one can deduce that it is just a coordinate singularity.

Let us now consider the causal structure of AdS space, which is invariant under conformal transformations. Clearly the global AdS metric, (1.21), is conformal to (one half of)<sup>5</sup> the metric of the  $d$ -dimensional *Einstein static Universe* (ESU $_d$ ) which has the metric

$$ds_{\text{ESU}}^2 = -d\tau^2 + d\theta^2 + \sin^2 \theta d\Omega_{(d-2)}^2, \quad (1.24)$$

and is topologically a cylinder. The conformal boundary is situated where the conformal factor diverges, *i.e.* at  $\theta = \pi/2$ . The geometry of the boundary is conformal to ESU $_{d-1}$ .

Let us now specifically consider three dimensional anti-de Sitter space (AdS $_3$ ), though everything we'll see generalises to higher dimensions.<sup>6</sup> One can transform from global coordinates to Poincaré coordinates with the transformation

$$t = \frac{\sin \tau}{\cos \tau - \sin \theta \cos \phi}, \quad (1.25a)$$

$$r = \frac{\sin \theta \sin \phi}{\cos \tau - \sin \theta \cos \phi}, \quad (1.25b)$$

$$z = \frac{\cos \theta}{\cos \tau - \sin \theta \cos \phi}. \quad (1.25c)$$

As expected this transformation becomes singular at the Poincaré horizon, at  $z \rightarrow \infty$ , which in terms of the global coordinates is the surface defined by  $\cos \tau - \sin \theta \cos \phi = 0$ .

In Figure 1.1 we have shown the Penrose diagram of AdS $_3$ . In blue is the Penrose diagram for global AdS $_3$  which is topologically a cylinder with the time coordinate,  $\tau$ , running over the whole real line. The boundary of the cylinder is the conformal boundary of global AdS $_3$ . In orange is the embedding of the Poincaré patch in global AdS $_3$  according to the above coordinate transformations, which appears as a wedge. The region of the boundary of the wedge which also lies on the boundary of the cylinder

<sup>5</sup>The full ESU runs over  $\theta \in (0, \pi)$ .

<sup>6</sup>The Penrose diagram of AdS $_2$  though is slightly different.

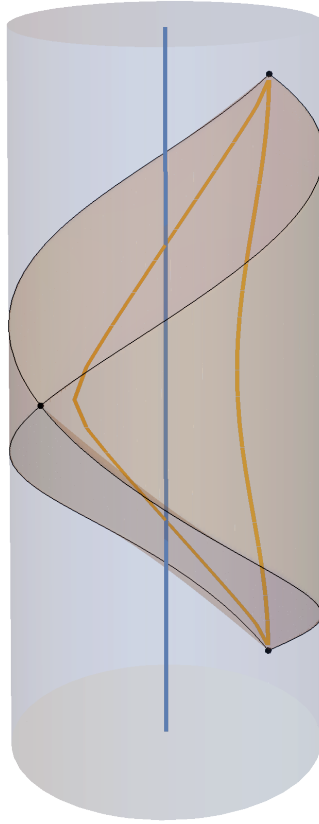


**Fig. 1.1:** In blue is the Penrose diagram of global  $\text{AdS}_3$ , which is topologically a cylinder. The orange region which lies wholly within the blue region is the Penrose diagram of the Poincaré patch of  $\text{AdS}_3$ . The Poincaré patch is bounded by the conformal boundary at  $z = 0$  (the boundary of the cylinder), and the Poincaré horizons at  $z \rightarrow \infty$ , which lie in the interior of the cylinder. The black lines show where the Poincaré horizon meets the boundary, at which the Poincaré coordinates become singular. The blue line shows an orbit of  $\partial_\tau$  where  $\tau$  is the time-coordinate of global  $\text{AdS}_3$ , whilst the orange curves show orbits of  $\partial_t$  where  $t$  is the time-coordinate use in the Poincaré patch.

is where  $z = 0$  and is the conformal boundary of the Poincaré patch. On the other hand the regions of the boundary of the wedge which lie within the interior of the cylinder are the past and future Poincaré horizons, at  $z \rightarrow \infty$ . The black lines show where the Poincaré horizons meet the conformal boundary. The  $z$  coordinate is singular at these edges, as can be seen from the definition of  $z$  in (1.25c) since at on these curves both the numerator and denominator of the expression for  $z$  go to zero.

The natural stationary Killing vector fields of the global AdS metric and the Poincaré metric are not the same. Orbits of the KVF associated to the time coordinate of the global AdS metric,  $\partial_\tau$ , are simply vertical lines in Figure 1.1, one of which is

indicated as a blue line. Clearly these pass straight through the Poincaré horizons. On the other hand, the orange curves in Figure 1.1 indicate the orbits of the KVF associated to the time coordinate of the Poincaré metric,  $\partial_t$ . These reach the conformal boundary at the points  $(\tau, \theta, \phi) = (\pm\pi/2, \pi/2, \pi/2)$ , at which  $t \rightarrow \pm\infty$  but  $r$  and  $z$  remain finite.

One notable feature of the Penrose diagram is that it shows that null curves can reach the conformal boundary of AdS in finite coordinate time. This has the consequence that AdS is *not* globally hyperbolic, *i.e.* there is no Cauchy surface on which a specification of initial data uniquely determines the future evolution of this data. Rather, one must additionally enforce boundary conditions on the conformal boundary in order to have well-defined dynamical evolution through anti-de Sitter space.

### 1.3.2 The AdS/CFT correspondence

The cosmological constant in our Universe does not appear to be negative. For a very long time it was thought to be exactly zero (so much so that Einstein himself called his inclusion of a cosmological constant his greatest blunder), however, experiments in the late 90s provided compelling evidence for an extremely small, but non-zero, positive cosmological constant [105–108].

Despite this, interest in anti-de Sitter space since the turn of the century has rocketed, motivated largely by the discovery of the AdS/CFT duality [109, 110], which describes a correspondence between a class of non-gravitational conformal field theories (CFT) which are quantum field theories that are invariant under conformal transformations, and string theories which, in particular, contain dynamical quantum gravity. The canonical early review of this correspondence is Ref. [111], though there now exists a myriad of reviews, lecture notes and textbooks into the subject, including, but not limited to, Refs. [112–119].

The duality equates the partition functions of the two theories:

$$\mathcal{Z}_{CFT} = \mathcal{Z}_{QG}. \quad (1.26)$$

The partition function on the left is only well-understood in the Euclidean section, whilst the full partition function of quantum gravity is barely understood at all. But let us focus on the Euclidean section for now and take some helpful limits to simplify things on the right hand side. There are two vital parameters of these CFTs that we will need to take into consideration: a coupling constant,  $\lambda$ , measuring the strength of

the interactions of the fields of the theory, and the number of degrees of freedom,  $N$ , which is usually associated to the central charge of the CFT.

Suppressing loop corrections in the string theory corresponds to taking the planar limit of the CFT,  $N \rightarrow \infty$ . In this limit, the CFT is dual to a theory of semi-classical strings about a geometry with AdS asymptotics. Moreover, at low energies, string theory is well approximated by theories of supergravity. Taking this limit corresponds to taking a limit of very strong coupling on the field theory side,  $\lambda \rightarrow \infty$ . Thus, the AdS/CFT correspondence is a strong-weak duality — taking the CFT to be strongly coupled is dual to taking the gravitational theory to be weakly coupled. All together, taking both  $\lambda$  and  $N$  are large yields a duality between a  $(d - 1)$ -dimensional CFT and a supergravity theory about an  $\text{AdS}_d \times X$  manifold, where  $X$  is a compact manifold. One can perform a Kaluza-Klein (KK) reduction on this compact manifold to obtain a theory on  $\text{AdS}_d$ , which has a consistent truncation to general relativity on  $\text{AdS}_d$ . Hence, studying classical gravity with a negative cosmological constant in  $d$  dimensions is dual to studying a very strongly coupled CFT with a large number of degrees of freedom living on a fixed  $(d - 1)$ -dimensional manifold.

The prototypical example of this duality is between type IIB string theory defined on  $\text{AdS}_5 \times S^5$  and a four-dimensional,  $\mathcal{N} = 4$ ,  $SU(N)$  super Yang-Mills CFT. In this case,  $\lambda = g_{\text{YM}}^2 N$ , is the 't Hooft coupling (with  $g_{\text{YM}}$  denoting the Yang-Mills coupling) and  $N$  is the rank of the  $SU(N)$  gauge group. The  $N \rightarrow \infty, \lambda \rightarrow \infty$  limit yields supergravity on  $\text{AdS}_5 \times S^5$  which can be truncated to general relativity on  $\text{AdS}_5$ . Let us however be agnostic regarding the precise details of the CFT and consider the duality in more generality.

The fundamental objects in a CFT are called *local operators*,  $\mathcal{O}$ . These respect the conformal symmetry of the CFT. Specifically, under a scaling transformation,  $x^\mu \rightarrow \alpha x^\mu$ , the operators transform as  $\mathcal{O}(x^\mu) \rightarrow \alpha^\Delta \mathcal{O}(\alpha x^\mu)$ , where  $\Delta$  is a number called the *scaling dimension* of  $\mathcal{O}$ . We can add additional source terms for such operators to the path integral directly:

$$\mathcal{Z}_{\text{CFT}}[\phi_0(x^\mu)] \supset \left\langle \exp \int d^D x^\mu \phi_0(x^\mu) \mathcal{O}(x^\mu) \right\rangle_E, \quad (1.27)$$

where  $D = d - 1$  is the number of boundary dimensions. The addition of the source terms corresponds to the addition of extra *fields*,  $\Phi$ , in the bulk theory with their boundary behaviour dictated by  $\phi_0(x^\mu)$ . In the  $N \rightarrow \infty, \lambda \rightarrow \infty$  limit, the gravitational theory becomes classical, and so we can evaluate the partition function by a saddle

point approximation:

$$\mathcal{Z}_{CFT}[\phi_0(x^\mu)] = \exp(-S_{gravity}[\Phi_c]) \Big|_{\lim_{z \rightarrow 0} (z^{-\gamma} \Phi_c(z, x^\mu)) = \phi_0}, \quad (1.28)$$

where  $S_{gravity}$  is the Einstein-Hilbert action including the negative cosmological constant and the Lagrangian arising from any matter fields, and  $\Phi_c$  is a solution to the equations arising from this theory satisfying certain boundary conditions at the conformal boundary, which is situated at  $z = 0$ , where  $z$  is the radial coordinate in Fefferman-Graham gauge, which we will define fully in Section 1.3.3.

The value of  $\gamma$  in (1.28) indicates the order in  $z$  at which a given boundary condition must be enforced at the conformal boundary, and is determined by the mass and spin of each the fields denoted by  $\Phi$ . For example, a scalar operator with scaling dimension,  $\Delta$ , is dual to a scalar field in the bulk with the boundary condition being enforced at order  $\gamma = \Delta - D$ , where  $\Delta$  can in turn be written in terms of the mass,  $m$ , of the scalar field via the mass-dimension formula:

$$\Delta = \frac{D}{2} + \sqrt{\frac{D^2}{4} + m^2 \ell_d^2}. \quad (1.29)$$

Meanwhile, the inclusion of a vector operator,  $J^\mu$ , excites a vector field,  $A^a$ . In particular a conserved current,  $J^\mu$ , is dual to a massless gauge field in the bulk and the boundary condition is enforced at  $\gamma = 0$ . This is an example of a typical principle: a global symmetry of the boundary leads to a gauge symmetry in the bulk. Such a conserved current in the CFT can be sourced by a chemical potential,  $A_\mu^{(0)}$

Finally, the stress tensor of the CFT,  $T_{\mu\nu}$ , is dual to metric perturbations in the bulk, with  $\gamma = -2$ . This last operator is of course present in any CFT, though we can still deform the CFT by adding a gravitational source term for the stress tensor, *i.e.* by taking the CFT to be on a curved background.

In each case though, both sides of (1.28) are divergent — on the left hand side the QFT partition function suffers from UV divergences, whereas the right hand side has IR divergences due to the infinite volume of AdS (for this reason the AdS/CFT is often called an UV/IR duality). These divergences can be dealt with via the process of holographic renormalization by setting a cutoff at  $z = \epsilon$  and adding counterterms to cancel the divergences that arise as  $\epsilon \rightarrow 0$ . Let us denote by  $S_{gravity}^{(R)}$  the action of the gravity theory with such counterterms included. We will briefly describe the results of this holographic renormalization in some cases, but for now let us neglect this subtlety.

As usual in QFT, the source terms play two roles. Firstly, one can perform functional derivatives with respect to the source in order to obtain the vacuum expectation value and correlation functions of operators:

$$\langle O(x) \rangle = \left. \frac{\delta S_{gravity}^{(R)}}{\delta \phi_0(x)} \right|_{\phi_0=0} \quad (1.30a)$$

$$\langle O(x_1) \dots O(x_n) \rangle = (-1)^{n+1} \left. \frac{\delta^n S_{gravity}^{(R)}}{\delta \phi_0(x_1) \dots \delta \phi_0(x_n)} \right|_{\phi_0=0}. \quad (1.30b)$$

Secondly, one can consider the sources to be external physical deformations of the theory, and the one-point function of an operator under the influence of the sources is given by

$$\langle O(x) \rangle_\phi = \frac{\delta S_{gravity}^{(R)}}{\delta \phi_0(x)}. \quad (1.31)$$

In this thesis, we will consider an Einstein-Maxwell theory in the bulk. Hence we shall be considering CFTs under the influence of electromagnetic and gravitational source terms. The gravitational source terms determine the background manifold that the CFT lives upon,  $\mathcal{B}_{d-1}$ . The addition of a non-trivial electromagnetic source can be thought of as further deforming the CFT theory by adding external electric or magnetic fields. States of the CFT residing on such a background will be dual to *asymptotically locally AdS* (AlAdS) geometries, which are solutions to the Einstein-Maxwell equations with a negative cosmological constant which possess conformal boundaries with induced geometry equal to the metric of  $\mathcal{B}_{d-1}$ . Once a bulk solution is obtained, one can then read off the one-point functions of the conserved current,  $J^\mu$ , and the stress tensor,  $T_{\mu\nu}$ , under the influence of these sources via (1.31). Let us now give a practical review of how this can be done via the process of holographic renormalization.

### 1.3.3 Holographic renormalization

The action we will consider in the bulk is that of Einstein-Maxwell theory with a negative cosmological constant, given in (1.2). The holographic quantities are extracted from a bulk solution via an asymptotic analysis of the solution near the conformal boundary [120]. It is helpful to transform the metric and the vector potential into

Fefferman-Graham gauge [121] in the asymptotic region:

$$ds^2 = \frac{\ell_d^2}{z^2} \left( dz^2 + \left( g_{\mu\nu}^{(0)} + g_{\mu\nu}^{(2)} z^2 + \dots + g_{\mu\nu}^{(D)} z^D + h_{\mu\nu}^{(D)} z^D \log z \right) dx^\mu dx^\nu + \mathcal{O}(z^{D+1}) \right), \quad (1.32a)$$

$$A = \left( A_\mu^{(0)} + \dots + A_\mu^{(D-2)} z^{D-2} + B_\mu^{(D-2)} z^{D-2} \log z \right) dx^\mu + \mathcal{O}(z^{D-1}), \quad (1.32b)$$

where, once again,  $D = d - 1$  is the number of dimensions of the boundary theory. The terms denoted by the ellipses contain only even powers of  $z$  up to  $\mathcal{O}(z^D)$  for the metric and up to  $\mathcal{O}(z^{D-2})$  for the vector potential. The logarithm terms are only present for  $D$  even, *i.e.* when the number of bulk dimensions is odd. These correspond to conformal anomalies arising for CFTs in even dimensions [122].

The leading order terms,  $g_{\mu\nu}^{(0)}$  and  $A_\mu^{(0)}$ , must be set as boundary conditions for the bulk problem. These correspond to the sources influencing the CFT. Many terms in the expansion are fixed explicitly in terms of the boundary data by the local analysis of the equations of motion near the boundary. However, in general,  $g_{\mu\nu}^{(D)}$ ,  $h_{\mu\nu}^{(D)}$ ,  $A_\mu^{(D-2)}$  and  $B_\mu^{(D-2)}$  are undetermined by this local analysis, and hence a full bulk solution must be found while setting additional boundary conditions deep within the bulk in order to attain them. All further subleading terms are fixed in terms of the boundary data and  $\{g_{\mu\nu}^{(D)}, h_{\mu\nu}^{(D)}, A_\mu^{(D-2)}, B_\mu^{(D-2)}\}$ .

The solutions of this thesis all possess either four or five dimensions, so let us focus on these dimensionalities. The case of five dimensions is far more complicated due to the presence of the logarithm terms. In each case, the one-point functions of the conserved current and the stress tensor are given by

$$\langle J^\mu \rangle = \frac{1}{\sqrt{g^{(0)}}} \frac{\delta S_{gravity}^{(R)}}{\delta A_\mu^{(0)}}, \quad (1.33a)$$

$$\langle T_{\mu\nu} \rangle = \frac{2}{\sqrt{g^{(0)}}} \frac{\delta S_{gravity}^{(R)}}{\delta g_{\mu\nu}^{(0)}}, \quad (1.33b)$$

where one must renormalize the Einstein-Hilbert action by adding counterterms which cancel the divergences arising in the above expressions for the VEVs. Here let us just state the results after this process of holographic renormalization, setting  $\ell_d = 1$ .

**$d = 4$ .** In any even bulk dimension, the counterterms provide no finite contributions, cancelling only the infinite divergences. The conserved current and stress tensor are

given by

$$\langle J_\mu \rangle = \frac{1}{4\pi G_4} A_\mu^{(1)}, \quad (1.34a)$$

$$\langle T_{\mu\nu} \rangle = \frac{3}{16\pi G_4} g_{\mu\nu}^{(3)}. \quad (1.34b)$$

There are no conformal anomalies of the CFT in this case, and hence the holographic stress tensor is traceless. Moreover, the one-point functions satisfy a Ward identity, given by

$$\nabla_\mu^{(0)} \langle T^\mu{}_\nu \rangle = F_{\mu\nu}^{(0)} \langle J^\mu \rangle, \quad (1.35)$$

where  $\nabla^{(0)}$  is the covariant derivative arising from the boundary metric,  $g_{\mu\nu}^{(0)}$ , and  $F_{\mu\nu}^{(0)}$  is the field strength tensor arising from the boundary vector potential,  $A_\mu^{(0)}$ .

**$d = 5$ .** Finite counterterms do arise in this case, making the holographic renormalization process more subtle (see, for example, [123] for details on this process for a more general theory). Ultimately, one finds

$$\langle J_\mu \rangle = \frac{1}{4\pi G_5} (2A_\mu^{(2)} + B_\mu^{(2)}), \quad (1.36a)$$

$$\langle T_{\mu\nu} \rangle = \frac{1}{4\pi G_5} \left\{ g_{\mu\nu}^{(4)} - \frac{1}{2} (g^{(2)})_{\mu\nu}^2 + \frac{1}{4} g_{\mu\nu}^{(2)} \text{Tr}[g^{(2)}] + \frac{3}{16} T_{\mu\nu}^{(0)\text{grav}} + \frac{1}{16} T_{\mu\nu}^{(0)\text{gauge}} \right. \\ \left. - \frac{1}{8} g_{\mu\nu}^{(0)} \left( (\text{Tr}[g^{(2)}])^2 - \text{Tr}[(g^{(2)})^2] \right) - \frac{1}{12} g_{\mu\nu}^{(0)} (F^{(0)})^{\rho\sigma} F_{\rho\sigma}^{(0)} \right\}, \quad (1.36b)$$

where  $(g^{(2)})_{\mu\nu}^2 = (g^{(0)})^{\rho\sigma} g_{\mu\rho}^{(2)} g_{\nu\sigma}^{(2)}$ , and  $T_{\mu\nu}^{(0)\text{grav}}$  and  $T_{\mu\nu}^{(0)\text{gauge}}$  are the gravity and gauge anomaly stress tensors, respectively, which can be written in terms of the curvature tensors of the boundary metric and the field strength tensor of the boundary vector potential as

$$T_{\mu\nu}^{(0)\text{grav}} = R_{\mu\rho\nu\sigma}^{(0)} (R^{(0)})^{\rho\sigma} - \frac{1}{4} g_{\mu\nu}^{(0)} R_{\rho\sigma}^{(0)} (R^{(0)})^{\rho\sigma} - \frac{1}{3} R^{(0)} R_{\mu\nu}^{(0)} + \frac{1}{6} \nabla_\mu^{(0)} \nabla_\nu^{(0)} R^{(0)} \\ + \frac{1}{2} (\nabla^{(0)})^2 R_{\mu\nu}^{(0)} + \frac{1}{12} g_{\mu\nu}^{(0)} \left( (R^{(0)})^2 - (\nabla^{(0)})^2 R^{(0)} \right) \quad (1.37a)$$

$$T_{\mu\nu}^{(0)\text{gauge}} = -F_{\mu\rho}^{(0)} (F^{(0)})_{\nu}{}^\rho + g_{\mu\nu}^{(0)} (F^{(0)})^{\rho\sigma} F_{\rho\sigma}^{(0)}. \quad (1.37b)$$

Due to the presence of the anomaly stress tensors, the trace of  $\langle T_{\mu\nu} \rangle$  is no longer automatically vanishing:

$$\langle T^\mu{}_\mu \rangle = \frac{1}{64\pi G_5} \left( R_{\rho\sigma}^{(0)} (R^{(0)})^{\rho\sigma} - \frac{1}{3} (R^{(0)})^2 - 4(F^{(0)})^{\rho\sigma} F_{\rho\sigma}^{(0)} \right). \quad (1.38)$$

This is the expected conformal anomaly of the CFT. The Ward identity given in (1.35) still holds in this case.

### 1.3.4 Asymptotically AdS black holes

Under the AdS/CFT duality, asymptotically AdS black hole solutions correspond to thermal states of the CFT. The most simple black hole solution in anti-de Sitter space is that of the  $d$ -dimensional<sup>7</sup> AdS-Schwarzschild metric, given by

$$ds_{AdS-Schw}^2 = -f(r) dt^2 + f(r)^{-1} dr^2 + r^2 d\Omega_{(d-2)}^2. \quad (1.39a)$$

with

$$f(r) = 1 + \frac{r^2}{\ell_d^2} - \left( 1 + \frac{r_h^2}{\ell_d^2} \right) \left( \frac{r_h}{r} \right)^{d-3}, \quad (1.39b)$$

where the parameter  $r_h$  is the radius of the horizon. This vacuum solution is asymptotic to global AdS. The temperature of the horizon is given by

$$T_H = \frac{(d-1)r_h^2 + (d-3)\ell_d^2}{4\pi r_h \ell_d^2}. \quad (1.40)$$

The dependence of this temperature on the radius is shown graphically in Figure 1.2. One striking difference between this formula and that describing the temperature of the asymptotically flat Schwarzschild solution, in which the temperature is inversely proportional to the radius of the horizon, is that there is a minimum temperature of the AdS-Schwarzschild black hole, given by

$$T_0 = \frac{\sqrt{(d-3)(d-1)}}{2\pi\ell_d}. \quad (1.41)$$

For any temperature  $T_H > T_0$ , there are two distinct black hole solutions, called a small and a large AdS black hole, and thus two saddles of the Euclidean gravitational path integral. Moreover, for any temperature there is another thermal state called

<sup>7</sup>Let us here focus on  $d \geq 4$  since the case of the three-dimensional BTZ black hole [124] is qualitatively different, *e.g.* there is at most one BTZ black hole for a given temperature.

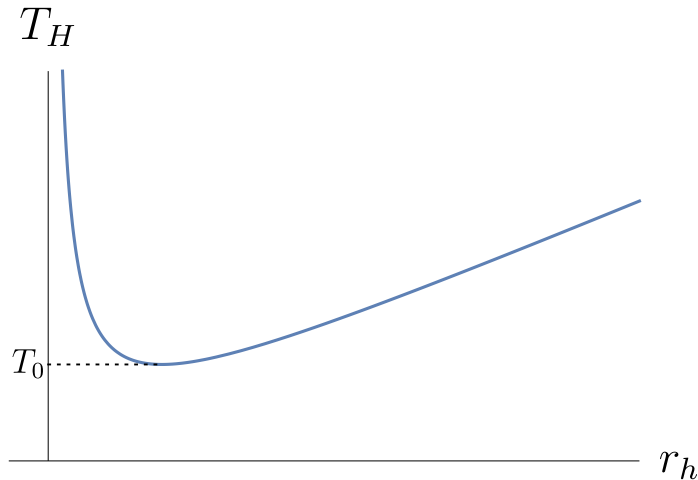


**Fig. 1.2:** The temperature,  $T_H$ , for four-dimensional AdS-Schwarzschild black holes of different radius. There is a non-zero minimum temperature of vacuum black holes in AdS.

thermal AdS simply formed by taking the global AdS solution, given in (1.21), and periodically identifying the imaginary time coordinate,  $\tau_E = i\tau$ , with a period given by the inverse temperature,  $\beta = T_H^{-1}$ .

In the canonical ensemble we must compare the free energy of these three saddles at fixed temperature to see which solution dominates. Hawking and Page [125] first carried out this analysis long before the AdS/CFT duality was discovered. In order to calculate the energy, we can use the method of holographic renormalization described in the previous section. For, example, in four dimensions, writing the AdS-Schwarzschild metric in Fefferman-Graham gauge gives:

$$ds^2 = \frac{\ell_4}{z^2} \left[ dz^2 - \left( 1 + \frac{z^2}{2\ell_4^2} + \frac{2}{3} (r_h^2 + \ell_4^2) \frac{r_h z^3}{\ell_4^6} + \dots \right) d\tau^2 \right. \\ \left. + \ell_4^2 \left( 1 - \frac{z^2}{2\ell_4^2} + \frac{1}{3} (r_h^2 + \ell_4^2) \frac{r_h z^3}{\ell_4^6} + \dots \right) d\Omega_{(2)}^2 \right], \quad (1.42)$$

where here the boundary metric,  $g_{\mu\nu}^{(0)}$ , is that of the  $ESU_3$  with radius  $\ell_4$ :

$$g_{\mu\nu}^{(0)} dx^\mu dx^\nu = -d\tau^2 + \ell_4^2 d\Omega_{(2)}^2. \quad (1.43)$$

From this expansion, one can read off the holographic stress tensor,  $\langle T_{\mu\nu} \rangle$ , using (1.34):

$$\langle T^\tau{}_\tau \rangle = -\frac{r_h}{8\pi G_4} \left( 1 + \frac{r_h^2}{\ell_4^2} \right), \quad \langle T^{\Omega_i}{}_{\Omega_i} \rangle = \frac{r_h}{16\pi G_4} \left( 1 + \frac{r_h^2}{\ell_4^2} \right), \quad (1.44)$$

where  $\Omega_i$  denotes any of the angular directions on the two-sphere. The results are qualitatively similar in other dimensionalities, once one has subtracted off the Casimir energy of empty global AdS (*i.e.* the value of  $\langle T_{\mu\nu} \rangle$  found with  $r_h = 0$ ). In general,

$$\langle T^\tau{}_\tau \rangle = -\frac{(d-2)r_h^{d-3}}{16\pi G_d \ell_d} \left( 1 + \frac{r_h^2}{\ell_d^2} \right), \quad \langle T^{\Omega_i}{}_{\Omega_i} \rangle = \frac{r_h^{d-3}}{16\pi G_d \ell_d} \left( 1 + \frac{r_h^2}{\ell_d^2} \right). \quad (1.45)$$

The total energy can be found by integrating the energy density,  $\langle T^\tau{}_\tau \rangle$ , over the boundary  $(d-2)$ -sphere:

$$E = \frac{(d-2)\omega_{d-2}r_h^{d-3}}{16\pi G_d} \left( 1 + \frac{r_h^2}{\ell_d^2} \right), \quad (1.46)$$

where  $\omega_{d-2}$  is the area of a unit  $S^{d-2}$  sphere. The horizon is spherical with radius,  $r_h$ , hence the entropy is given by

$$S = \frac{\omega_{d-2}}{4G_d} r_h^{d-2}. \quad (1.47)$$

These two equations, along with temperature of the black hole, given in (1.40), allow one to compute the free energy:

$$F = E - T_H S = \frac{\omega_{d-2}r_h^{d-3}}{16\pi G_d} \left( 1 - \frac{r_h^2}{\ell_d^2} \right). \quad (1.48)$$

Since we subtracted the Casimir energy of the global AdS solution, this really is the relative free energy when compared with thermal AdS. In the canonical ensemble, the dominant solution will be the solution which minimises the free energy for a given temperature.

For  $T_H < T_0$ , thermal global AdS is the only saddle, so is dominant by default. For  $T_H > T_0$ , the small black holes always have positive free energy and hence are always subdominant. However, if  $r_h > \ell_d$ , then we see from (1.48) that the large black hole solution has lower free energy than thermal AdS, and hence dominates the canonical ensemble. Thus, there is a first-order phase transition between the two phases called the *Hawking-Page transition*. It occurs at the temperature,

$$T_{HP} = \frac{d-2}{2\pi\ell_d}. \quad (1.49)$$

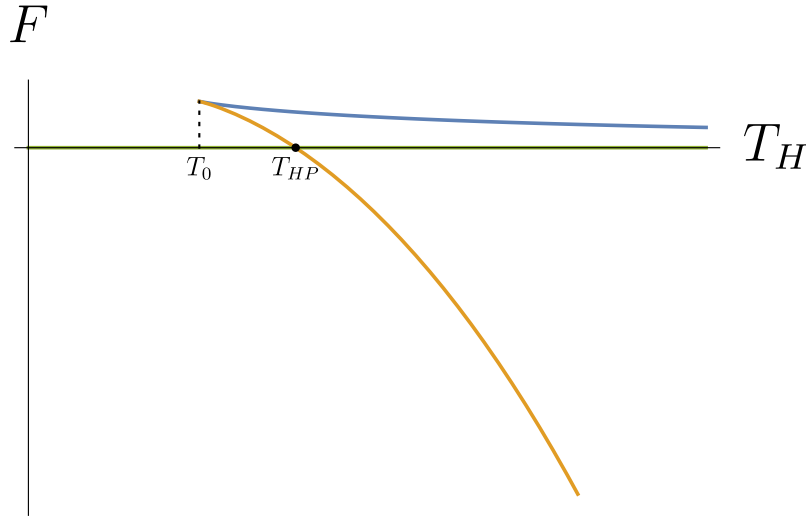


**Fig. 1.3:** The phase diagram of the thermal solutions in four-dimensional AdS space. The blue and orange correspond to the values of the free energy,  $F$ , of the small and large AdS-Schwarzschild solutions, respectively, whilst the green line (at  $F = 0$ ) is that of the thermal AdS solution. There are no black hole solutions for  $T_H < T_0$ . The solution which dominates the ensemble for a given temperature,  $T_H$ , is the one with the least value of the free energy. For  $T_H < T_{HP}$ , this is the thermal AdS solution, but for  $T_H > T_{HP}$  the large black hole dominates.

Figure 1.3 shows the phase diagram which makes this phase transition evident.

This phase transition also occurs on the field theory side. Witten argued that the Hawking-Page transition was dual to a transition between a confined phase and a deconfined phase of the CFT when living on a spatial sphere [126]. At low temperatures relative to the radius of the sphere,  $\ell_d$ , the different species (or colours) of the fields combine together to form composites often called glue balls, with the energy density resultantly being  $\mathcal{O}(1)$ . At high temperatures relative to  $\ell_d$ , the fields escape from these composites and thus the energy density instead behaves as  $\mathcal{O}(N^2)$ . Witten argued that the confined phase corresponds the thermal global AdS solution, whereas the deconfined phase corresponds to the AdS-Schwarzschild solution.

Hence, this extremely complicated property of confinement of a strongly coupled QFT is mapped to a far simpler property in the bulk, that of the presence of a black hole horizon.

By Birkhoff's theorem in AdS, these are the only finite temperature, vacuum, static, spherically symmetric solutions which are asymptotic to global AdS. However the structure of the space of solutions will be far richer if we include gravitational and electromagnetic source terms at the boundary. One key aim of this thesis will be to explore this avenue of investigation.

Moreover, not all black holes in AdS have horizons with spherical topology, even in four dimensions. Another simple metric is that of the planar AdS black hole given by

$$ds_{\text{planar}}^2 = \frac{\ell_d^2}{z^2} \left( -g(z) dt^2 + \frac{dz^2}{g(z)} + \delta_{IJ} dx^I dx^J \right), \quad (1.50a)$$

with

$$g(z) = 1 - \left( \frac{z}{z_h} \right)^{d-1}. \quad (1.50b)$$

In these coordinates, the horizon lies at  $z = z_h$ , and the conformal boundary is at  $z = 0$  where the metric approaches that of the Poincaré patch of AdS. The temperature of the planar black hole is

$$T_H = \frac{d-1}{4\pi z_h}, \quad (1.51)$$

which can take any positive value. Just as above, one could find another saddle in the canonical ensemble by identifying the imaginary time coordinate in the metric of the Poincaré patch, (1.23), with a period given by the inverse temperature. However, the planar black *always* dominates over the thermal planar AdS solution, hence there is no Hawking-Page transition in this case. This means that the deconfined state of the CFT dominates when the background manifold is the Minkowski manifold.

## 1.4 Black droplets and funnels

The case of the Hawking-Page transition exemplifies how holography can often take complicated aspects of a quantum field theory and give them a geometrical interpretation in terms of the gravity theory. We'll see a further example of the geometrization of a complicated phase transition of the strongly coupled CFT in this section — this time for a CFT living on a fixed black hole background. Studying a QFT on black hole background was what led Hawking to the discovery that black holes emit Hawking radiation and hence behave as thermodynamic objects [80], as we reviewed in Section 1.2.2. However the direct study of quantum fields on curved backgrounds has been largely restricted by difficulty to free or weakly interacting fields. One would expect qualitative differences if the fields were instead strongly coupled.

Fortunately, the AdS/CFT duality provides an approach to indirectly study a strongly coupled CFT on a curved background,  $\mathcal{B}_{d-1}$ , by studying AlAdS spacetimes with conformal boundaries on which the induced metric is equal to that of  $\mathcal{B}_{d-1}$  (see, for example, [127] for an excellent review on this method). Taking  $\mathcal{B}_{d-1}$  to be a black

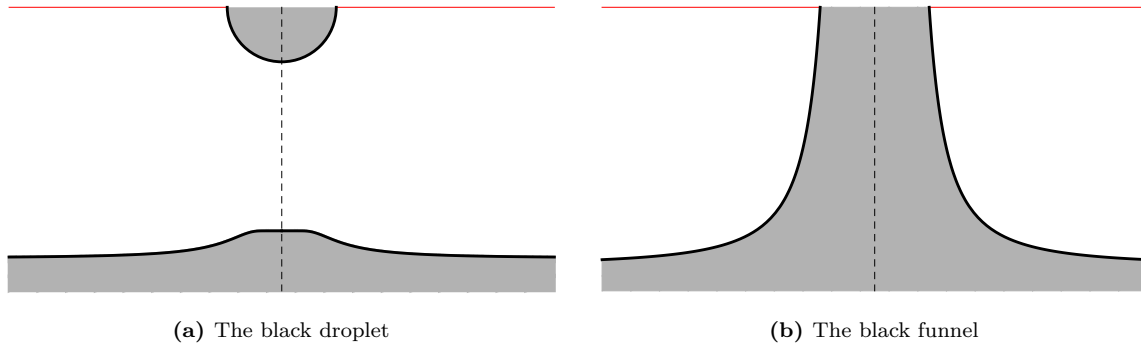


**Fig. 1.4:** Schematic drawings of spatial cross-sections of the black droplet and black funnel spacetimes. In each case the red boundary is the conformal boundary on which the metric is that of the Schwarzschild black hole. The dashed line is an axis of rotation. The droplet contains two disconnected horizons: one extending from the boundary horizon and the other the deformed planar horizon deep within the bulk. The funnel has a single connected horizon, extending from the boundary horizon and asymptoting to the planar horizon deep within the bulk.

hole spacetime will provide insight into the properties of Hawking radiation at strong coupling via wholly classical calculations. Since the black hole background is fixed, this study will not elucidate how the CFT backreacts with gravity, and thus will give us little information on the nature of black hole evaporation. Instead the boundary black hole behaves as an infinite thermal source for the CFT.

### 1.4.1 The gravitational duals to a CFT on Schwarzschild

Let us first consider  $\mathcal{B}_{d-1}$  to be a Schwarzschild black hole, with temperature  $T_H$ . The boundary horizon will extend into the bulk, necessarily generating a bulk horizon which is anchored on the conformal boundary. Moreover, the CFT state must asymptotically approach a thermal state with temperature  $T_\infty$  on flat space, since Schwarzschild is asymptotically flat. Hence, in the bulk one expects a (deformed) planar horizon deep within the bulk with temperature  $T_\infty$ . If the CFT is in the Unruh state with  $T_\infty = 0$ , then this horizon becomes the Poincaré horizon.

There are two classes of dual bulk gravitational solutions which are distinguished by the nature of the horizons in the bulk. One, called the *black droplet* contains two disconnected horizons in the bulk, the black hole horizon anchored on the boundary horizon and the perturbed planar horizon. The other, the *black funnel*, instead contains a single, connected horizon, running from the boundary horizon to an asymptotic region at which it approaches the expected planar horizon. Figure 1.4 depicts sketches of spatial cross-sections of these two spacetimes.

The connected horizon of the black funnel allows classical flow along it. This means that (unless the CFT is in the Hartle-Hawking state with  $T_H = T_\infty$ ) the horizon of the black funnel is not a Killing horizon, evading the rigidity theorems due to the fact it is non-compact. On the field theory side, this classical flow corresponds to  $\mathcal{O}(N^2)$  Hawking radiation of the CFT fields from the black hole to the asymptotic region, which is precisely what one would expect if instead one were studying  $N^2$  free or weakly interacting fields on the black hole background.

On the other hand, there is no energy flux between the two disconnected horizons of the black droplet at leading order in  $N$  (*i.e.* at a classical level in the bulk) even if they have different temperatures. Including stringy corrections in the bulk, which arise at subleading order in  $N$ , will lead to Hawking radiation between the two horizons. This means that on the field theory side the Hawking radiation from the black hole to the asymptotic region of the CFT fields is greatly suppressed to  $\mathcal{O}(N^0)$ . The field theory mechanism behind this behaviour is not well understood.

Overall then, the black funnel corresponds to a *deconfined* phase of the CFT living on the black hole background, whilst the black droplet corresponds to a *confined* phase [128, 129]. The first solutions were found by considering the CFT on the lower dimensional Bañados-Teitelboim-Zanelli (BTZ) black hole [130–132]. The black droplet dual to the CFT in the Unruh state,  $T_\infty = 0$ , on a four-dimensional Schwarzschild background was obtained in [133], and the black funnel dual to the CFT in the Hartle-Hawking state,  $T_\infty = T_H$ , was found in [134]. Black droplets and funnels were found for various values of the ratio  $T_\infty/T_H$  in [135], which correspond to Frolov-Page states of the CFT [136]. Droplets were found only to exist for  $T_\infty/T_H \lesssim 0.93$  and funnels were found only for  $T_\infty/T_H \gtrsim 0.55$ , suggesting there must be a phase transition at some intermediate value. One can also detune the temperature of the bulk horizon as it approaches the boundary horizon [137], though this corresponds to a CFT state that is singular at the horizon.

One interesting aspect of these solutions is precisely the sense in which they are in equilibrium. The droplet solutions are always static and the funnel solutions are stationary, hence they are *dynamically* in equilibrium. However, for  $T_\infty \neq T_H$ , the bulk solutions are not in *thermodynamic* equilibrium; the temperatures of the two horizons in the black droplet are unequal and the horizon of the black funnel is generally not even a Killing horizon at all. This lack of thermodynamic equilibrium means that, except in special cases, there is no well-defined definition of the free energy of the solutions, meaning that it is very difficult to argue which of them will dominate the ensemble at a value of  $T_\infty/T_H$  for which they both exist. This difference between

dynamical equilibrium and thermodynamic equilibrium will be one of the key themes of this thesis.

### 1.4.2 Global black droplets and funnels

One can adapt the above considerations to other black hole spacetimes, for example, those compactified onto the ESU. Such solutions are called global droplets and funnels [138–140]. Though such spacetimes are less relevant to astrophysical Hawking radiation, they provide fascinating case studies for the different phases of the CFT, with the multiple boundary horizons acting like infinite heat sources and sinks inducing heat flow in the boundary theory.

Specifically, in [140], the boundary geometry was formed by compactifying two BTZ black holes and patching them together at their asymptotic boundaries. This yields two black hole horizons antipodally situated on the ESU. In that work the boundary black holes were taken to have the same temperature and the authors were able to find a number of different droplet and funnel bulk solutions each of which are in thermodynamic equilibrium, allowing for a comparison of the free energy. We will be interested in deforming such solutions by taking them out of equilibrium. This leads to an even richer space of solutions and allows one to study flowing states of the CFT with the flow being induced by sources, though unfortunately the thermodynamic analysis of the out-of-equilibrium solutions becomes far more difficult.

## 1.5 The Randall-Sundrum model

As described above, the AdS/CFT duality allows us to study, via gravitational calculations, a strongly coupled conformal field theory on a fixed background. But what if we would like the field theory also to couple to *dynamical* gravity? The Randall-Sundrum (RS) braneworld paradigm provides a possible avenue towards studying such a system.

Matter in the RS models is restricted to a  $(3 + 1)$ -dimensional submanifold (a “3-brane”) embedded in a higher dimensional space which has a negative cosmological constant. There are two Randall-Sundrum models, often called RSI and RSII.

These models also have an interest outside of the world of AdS/CFT, since they provide mechanisms for including extra dimensions without losing the apparent four-dimensional behaviour of gravity at low energies for observers restricted to the brane. Since superstring theory is mathematically consistent in only ten dimensions, such

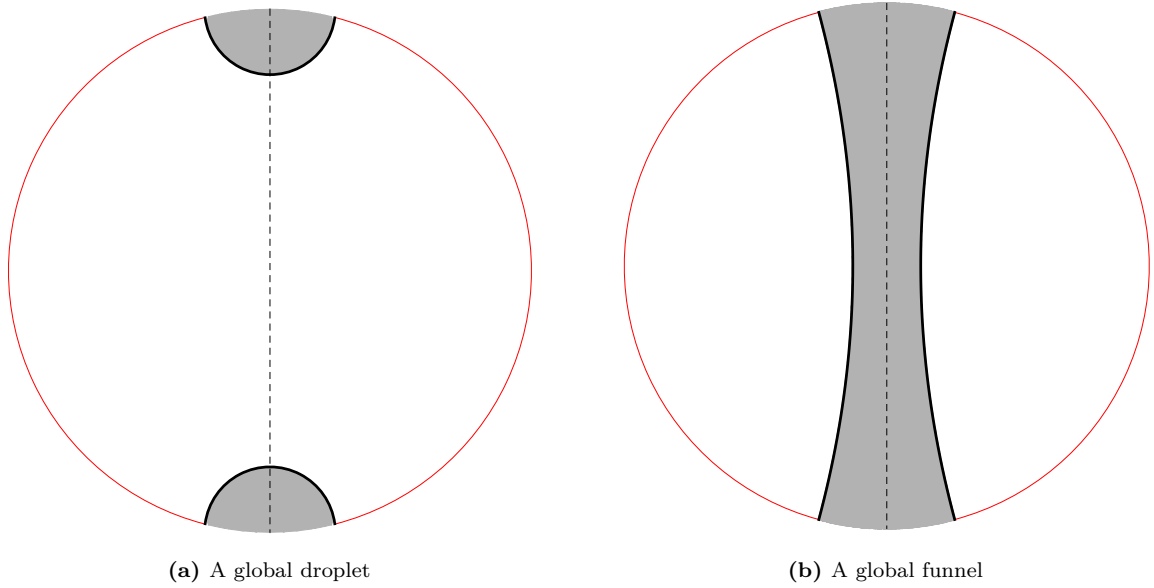


**Fig. 1.5:** Schematic drawings of spatial cross-sections of global droplets and funnels. The conformal boundary is shown by the red curve. The boundary metric contains two black hole horizons antipodally situated on the ESU. The dashed line is an axis of rotation.

mechanisms for extra dimensions are vital in order for string theory to be a feasible fundamental theory for describing the physics of our Universe.

We'll be particularly interested in the RSII model but let us quickly describe the RSI model first.

### 1.5.1 The RSI model

The first Randall-Sundrum (RSI) solution [141] was introduced as a possible solution of the hierarchy problem, which pertains to the question of why the force of gravity is so many orders of magnitude weaker than the other fundamental forces of nature. The metric of the ambient space is given by

$$ds^2 = dY^2 + \exp(-2|Y|\ell_5) \eta_{\mu\nu} dx^\mu dx^\nu, \quad (1.52)$$

where  $x^\mu$  run over the coordinates on the brane and the extra  $Y$  coordinate in the RSI model lies in the range  $Y \in (0, b)$  with the spacetime being bounded by two branes at  $Y = 0$  and  $Y = b$ . The bulk spacetime has a negative cosmological constant, the brane at  $Y = 0$  has positive tension and the brane at  $Y = b$  has negative tension. Matter is restricted to the  $Y = b$  brane. Via a careful balancing act between the values of the

tensions of the branes and the cosmological constant, one can enforce that the effective gravitational theory on the  $Y = b$  brane is four-dimensional GR at low energies.

The warping factor in the metric (1.52) means that the effective mass,  $m_4$ , of a particle on the brane is exponentially suppressed compared with its true five-dimensional mass,  $m_5$ :

$$m_4 = e^{-b/\ell_5} m_5. \quad (1.53)$$

Therefore, the strength of gravity is exponentially suppressed on the brane, which is how the extra dimension of the RSII model provides a possible solution to the hierarchy problem.

### 1.5.2 The RSII model

The RSII model [142] also contains a 3-brane on which matter is restricted. This time though, there is an extra dimension which is infinite in extent. Taking the 3-brane to have an induced geometry of flat space, the metric of the ambient space must also be as described in (1.52), however now the extra coordinate,  $Y$  extends infinitely, with the brane on which matter is confined being situated at  $Y = 0$ , across which there is a  $\mathbb{Z}_2$  symmetry.

In [142], the authors carried out a Kaluza-Klein (KK) reduction of the 5d gravitational perturbations about this metric down to the 4d brane. From the KK spectrum, the non-relativistic gravitational potential between two particles on the brane of mass  $m_1$  and  $m_2$  at a distance of  $r$  apart was computed to be

$$V(r) = G_4 \frac{m_1 m_2}{r} \left( 1 + \frac{\ell_5^2}{r^2} \right). \quad (1.54)$$

The first term is a contribution from a massless KK mode which plays the role of the four-dimensional graviton on the brane and agrees with the standard Newtonian potential of four-dimensional gravity. The second term arises from a tower of massive KK modes and provides a correction to the effective theory of gravity on the brane. However, the correction is very small when  $r \gg \ell_5$ , hence there is very little sign of the extra dimension for observers living on the brane except at small scales or, equivalently, at high energies. Therefore, despite the extra dimension being infinite in extent, the effective theory of gravity at low energies still reduces to four-dimensional GR. Heuristically speaking, despite the extra dimension being infinite, the exponential warping factor of the RSII metric, (1.52), leads to a steep potential well trapping the five-dimensional graviton to the vicinity of the brane at low energies, giving the

effective four-dimensional behaviour in the leading order term in (1.54). Only at high energies can the graviton overcome this potential well and escape from the brane deep into the bulk, which is what leads to the departure from four-dimensional GR at high energies represented by the second term in (1.54).

Focusing on the  $Y \geq 0$  side of the spacetime, one can take the coordinate transformation

$$z = \ell_5 e^{Y/\ell_5}, \quad (1.55)$$

to bring the metric (1.52) into a familiar form:

$$ds^2 = \frac{\ell_5^2}{z^2} (dz^2 + \eta_{\mu\nu} dx^\mu dx^\nu). \quad (1.56)$$

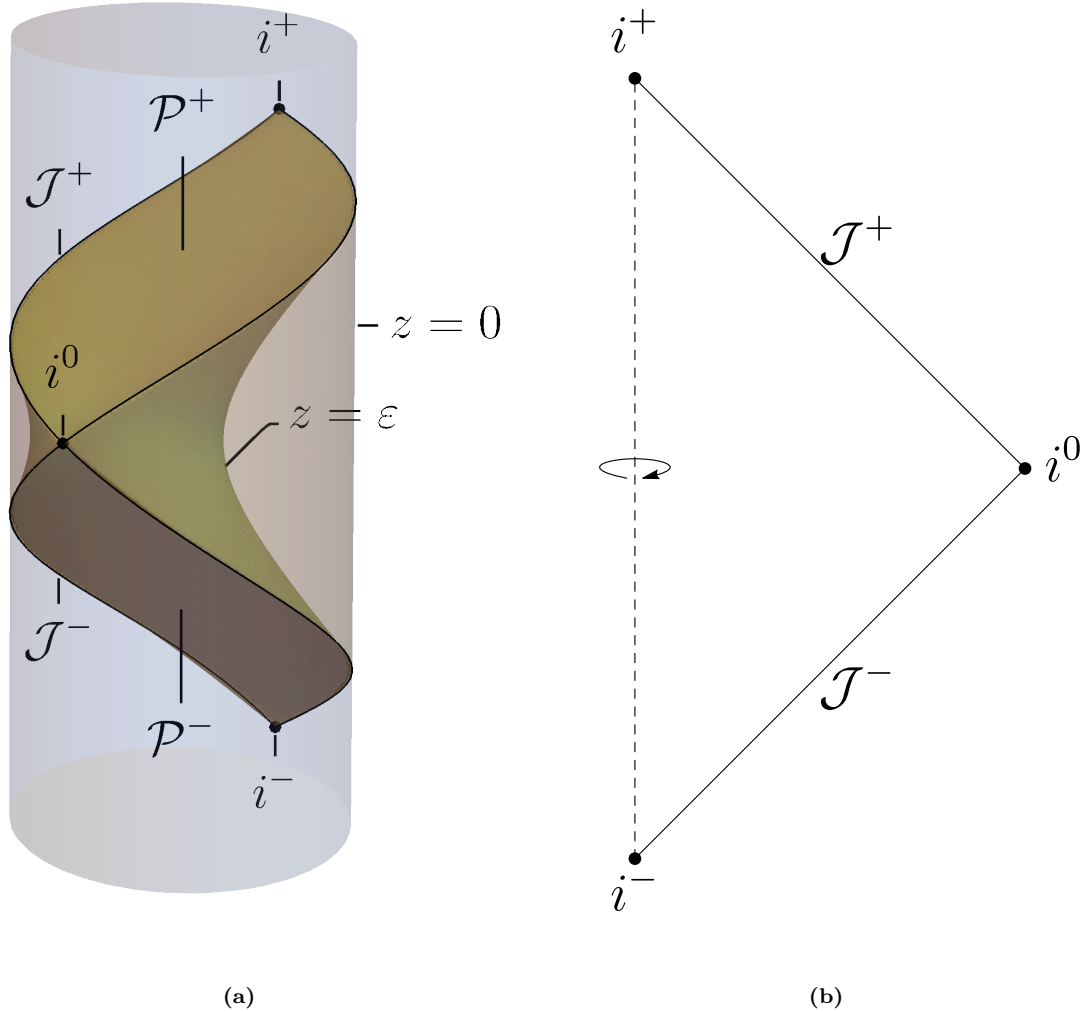
In these coordinates, the brane lies at  $z = \ell_5$  and (one side of) the bulk is the region  $z \in [\ell_5, \infty)$ . In fact, by rescaling the coordinates, the brane can be taken to be at any constant  $z$  slice,  $z = \varepsilon$ . The metric given in (1.56) is that of the Poincaré patch of AdS space, in which the coordinate  $z$  runs from the conformal boundary at  $z = 0$  to the Poincaré horizons at  $z = \infty$ . Therefore, the RSII bulk can be thought of as a subregion of the Poincaré patch of AdS<sub>5</sub>, specifically the region between a constant  $z$  slice (the brane) and the Poincaré horizons at  $z = \infty$ , still with a  $\mathbb{Z}_2$  symmetry imposed across the brane.

Figure 1.1 showed the Penrose diagram of global AdS in blue and shaded in orange the Poincaré patch of the AdS space. In Figure 1.6a we also include the RSII bulk shaded in green. This region is defined by  $z \in [\varepsilon, \infty)$ , and the transformation given by (1.25c) is utilised in order to embed it in the Penrose diagram of global AdS. The brane is the  $z = \varepsilon$  surface, and the RSII bulk lies between this brane and the past and future Poincaré horizons of the Poincaré patch, labelled as  $\mathcal{P}^-$  and  $\mathcal{P}^+$ , respectively. The black lines,  $\mathcal{J}^\pm$  and the points  $i^\pm$  and  $i^0$  are where the brane meets the conformal boundary.

Unwrapping the brane around the cylinder yields the Penrose diagram according to an observer on the brane, as shown in Figure 1.6b, where we have now shown the axis of rotation of the two suppressed angular directions as the dashed vertical line. The induced geometry on the brane is flat space, and hence the Penrose diagram is the same as that of the four-dimensional Minkowski metric. The observer on the brane

would perceive the asymptotic boundaries,  $i^0$ ,  $i^\pm$  and  $\mathcal{J}^\pm$  as, respectively, spacelike, past/future timelike and past/future null infinity.<sup>8</sup>

<sup>8</sup>Note, we have labelled null infinity on the brane using the symbols  $\mathcal{J}^\pm$  in order to distinguish between these boundaries of the brane and the conformal boundary of the whole AdS space, which is often written as  $\mathcal{I}^\pm$ .



**Fig. 1.6:** In (a), we have Penrose diagram of  $\text{AdS}_5$  and the RSII bulk, after suppressing two angular directions. The blue region is global AdS, the pale orange region is the Poincaré patch and the green region is one side of the RSII bulk. Each region described above fully contains those following it, *i.e.* blue  $\supset$  orange  $\supset$  green. The RSII bulk is the region between the past and future Poincaré horizons, annotated, respectively, by  $\mathcal{P}^-$  and  $\mathcal{P}^+$ , and the brane which is a surface of constant  $z = \varepsilon$ . The induced geometry on the brane is Minkowski. Unwrapping the  $z = \varepsilon$  gives the Penrose diagram according to an observer on the brane, shown in (b), with the vertical line being the axis of rotation of the two suppressed angular directions. The observer would perceive  $i^0$ ,  $i^\pm$ ,  $\mathcal{J}^\pm$  as spacelike, past/future timelike and past/future null infinity, respectively. From the perspective of the bulk,  $\{i^0, i^\pm, \mathcal{J}^\pm\}$  make up the intersection of the brane with the conformal boundary.

### 1.5.3 The connection between the RSII model and AdS/CFT

The fact that the RSII spacetime is a region of AdS space gives us a useful perspective on the effective theory on the brane. Specifically, the AdS/CFT duality implies that five-dimensional GR in the RSII bulk is dual to a “quantum-corrected” theory on the brane, given by four-dimensional GR coupled to a strongly coupled CFT with a UV cut-off. To see how this interpretation arises, let us follow the argument given in [143], which is in turn based upon the calculation of the holographic Weyl anomaly [122].

As we reviewed in Section 1.3.2, general relativity in AdS<sub>5</sub> is dual to a large  $N$  super Yang-Mills (SYM) theory in the ’t Hooft limit ( $\lambda \rightarrow \infty$ ) residing on a fixed four-dimensional background,  $\mathcal{B}_{d-1}$ . Considering gravitational excitations in the bulk and taking the logarithm of (1.28) yields

$$\mathcal{W}_{\text{CFT}}[\gamma_{\mu\nu}] = \text{ext}_{g_{\mu\nu}^{(0)} = \gamma_{\mu\nu}} \left( S_{\text{bulk}}[g_{ab}] + S_{\text{bdy}}[g_{\mu\nu}^{(0)}] \right), \quad (1.57)$$

where  $\gamma_{\mu\nu}$  is the metric of the manifold,  $\mathcal{B}_{d-1}$ , on which we wish to study the CFT, whilst  $g_{\mu\nu}^{(0)}$  is the leading order term in the Fefferman-Graham expansion of the five-dimensional metric asymptotically locally AdS metric, as defined in (1.32a). Here  $S = S_{\text{bulk}} + S_{\text{bdy}}$  is the classical action of the gravitational theory, and we have now included the Gibbons-Hawking-York boundary term required to give a well-defined variational principle [144, 145]. Moreover, now we are taking the dominant saddle by taking an extremum over all asymptotically locally AdS metrics which have induced metric on the conformal boundary equal to  $\gamma_{\mu\nu}$ . The logarithm of the partition function,  $\mathcal{W}_{\text{CFT}} = \log \mathcal{Z}_{\text{CFT}}$ , is the generating functional of connected Green’s functions of the CFT. In the usual AdS/CFT correspondence, the gravitational modes in the AdS side that extend to the conformal boundary are non-normalizable, *i.e.* they diverge and do not fluctuate as one approaches the boundary. Therefore, in order to have a well-defined theory one must add counterterms that cancel out these divergences. The effect of this is that the boundary metric,  $\gamma_{\mu\nu}$ , is fixed and is not corrected by the CFT.

In the AdS/CFT correspondence, the radial direction (the  $z$ -direction) is understood to be dual to the energy of the boundary CFT, with  $z = 0$  being dual to the UV limit of the CFT. Since the RSII spacetime is a chunk of the Poincaré patch of AdS<sub>5</sub> that has been cut off at the brane at some  $z = \varepsilon$ , this curtailing of the spacetime on the gravitational side will equate to introducing a UV cut-off to the CFT at some energy scale,  $\Lambda_\varepsilon$ . As described in [143, 146], this suggests the following extension of

the AdS/CFT correspondence to the RSII braneworld:

$$\mathcal{W}_{\text{CFT}}[\gamma_{\mu\nu}] + S_{4d \text{ gravity}}[\gamma_{\mu\nu}] = \text{ext}_{g_{\mu\nu}^{(0)} \sim \gamma_{\mu\nu}} \left( S_{\text{bulk}}[g_{ab}] + S_{\text{brane}}[g_{\mu\nu}^{(0)}] \right), \quad (1.58)$$

where now  $\mathcal{W}_{\text{CFT}}$  is the generating functional of connected Green's functions of the CFT, which now lives on the brane, with some UV cutoff  $\Lambda_\varepsilon$ , and the extremum is now over metrics that have induced metric on the brane isometric to  $\gamma_{\mu\nu}$ . One can also add terms to both sides of (1.58) which describe the other matter fields that are restricted to the brane, however, here we'll simply consider the vacuum case. Note that we now have an additional term on the left hand side,  $S_{4d \text{ gravity}}[\gamma_{\mu\nu}]$ , which is the action of gravity on the brane. This means that gravity is dynamical on the brane, with the CFT coupling to it. The presence of this extra term is due to the fact that now that we have a cutoff at  $z = \varepsilon$ , the gravitational modes mentioned above, which in standard AdS/CFT must be cancelled out with counterterms, simply don't diverge as we approach the brane at  $z = \varepsilon$ . Thus, we need not add any counterterms, meaning that we retain terms that describe how the CFT living on the brane interacts with gravity.

To see how this works explicitly, let's consider the right-hand side of (1.58) a little more closely. Let's take  $\ell_5 = 1$  here, so that  $\Lambda = -6$ . We know that any asymptotically locally AdS metric can be written in Fefferman-Graham gauge:

$$ds^2 = \frac{1}{z^2} \left( dz^2 + \bar{g}_{\mu\nu} dx^\mu dx^\nu \right), \quad (1.59a)$$

where  $\bar{g}$  has an expansion in  $z$  given by

$$\bar{g}_{\mu\nu} = g_{\mu\nu}^{(0)} + z^2 g_{\mu\nu}^{(2)} + z^4 g_{\mu\nu}^{(4)} + z^4 \log z h_{\mu\nu}^{(4)} + \dots \quad (1.59b)$$

with  $g_{\mu\nu}^{(i)}$  and  $h_{\mu\nu}^{(4)}$  being independent of  $z$ . Note that the above metric has determinant given by

$$\sqrt{-g} = \frac{1}{z^5} \sqrt{-\bar{g}} = \sqrt{-g^{(0)}} \left( \frac{1}{z^5} + \frac{1}{2z^3} (g^{(0)})^{\mu\nu} g_{\mu\nu}^{(2)} + \mathcal{O}(z^{-1}) \right), \quad (1.60)$$

where we have used the expansion (1.59b) and a standard identity regarding determinants<sup>9</sup> in order to derive the second equality. We will not be concerned with the

<sup>9</sup>The identity is given by  $\det(A+B) = \det A + \det B + \det A \cdot \text{Tr}(A^{-1}B)$ , where  $A$  and  $B$  are two matrices with  $A$  invertible.

precise coefficient of the order  $z^{-1}$  term here, though this can also be written in terms of  $g_{\mu\nu}^{(i)}$ .

For  $g_{ab}$ , when written in this gauge, to satisfy the boundary condition on the brane (situated at  $z = \varepsilon$ ) on the right hand side of (1.58), we require that  $g_{\mu\nu}^{(0)} = \varepsilon^2 \gamma_{\mu\nu}$ . We seek to take an extremum over classical solutions which satisfy the bulk equations of motion and this boundary condition. These bulk equations are the vacuum Einstein equations with  $\Lambda = -6$ , thus in the bulk  $R = -20$ . Therefore the evaluation of the bulk action on-shell is

$$\begin{aligned}
16\pi G_5 S_{\text{bulk}}[g_{ab}] &= \int_{z=\varepsilon} dz \int d^4x \sqrt{-g} (R - 2\Lambda) \\
&= -8 \int_{z=\varepsilon} dz \int d^4x \left( \frac{1}{z^5} \sqrt{-\bar{g}} \right) \\
&= -8 \int_{z=\varepsilon} dz \int d^4x \sqrt{-g^{(0)}} \left( \frac{1}{z^5} + \frac{1}{2z^3} (g^{(0)})^{\mu\nu} g_{\mu\nu}^{(2)} + \mathcal{O}(z^{-1}) \right) \\
&= 2 \int d^4x \sqrt{-g^{(0)}} \left( \frac{1}{\varepsilon^4} + \frac{1}{\varepsilon^2} (g^{(0)})^{\mu\nu} g_{\mu\nu}^{(2)} + a_{(4)} \log \varepsilon + \mathcal{O}(\varepsilon^0) \right), \quad (1.61)
\end{aligned}$$

where we have carried out the  $z$  integral in the final line, with the  $\mathcal{O}(z^{-1})$  term in the integrand giving a logarithm term and a term which is finite in the limit  $\varepsilon \rightarrow 0$ .

Meanwhile, the boundary action, in the case where there is no matter on the brane, is given by the Gibbons-Hawking-York term as well as a term coming from the tension of the brane:

$$16\pi G_5 S_{\text{brane}}[\gamma_{\mu\nu}] = \int d^4x \sqrt{-\gamma} (2K + 16\pi G_5 \lambda), \quad (1.62)$$

where  $\lambda$  is the tension of the brane and  $K$  is the trace of the extrinsic curvature of the brane, which is given in terms of the normal,  $n_\mu$ , to the brane by

$$K_{\mu\nu} = \gamma_\mu^\rho \gamma_\nu^\sigma \nabla_\rho n_\sigma = -\frac{1}{\varepsilon^2} \bar{g}_{\mu\nu} + \frac{1}{2\varepsilon} \partial_z \bar{g}_{\mu\nu}. \quad (1.63)$$

Taking the trace

$$K = -4 + \frac{\varepsilon}{2} \bar{g}^{\mu\nu} \partial_z \bar{g}_{\mu\nu} = -4 + \varepsilon^2 (g^{(0)})^{\mu\nu} g_{\mu\nu}^{(2)} + \mathcal{O}(\varepsilon^4). \quad (1.64)$$

Combining the above results, we find that

$$16\pi G_5 (S_{\text{bulk}} + S_{\text{brane}}) = \int d^4x \mathcal{L}, \quad (1.65a)$$

with

$$\mathcal{L} = \sqrt{g^{(0)}} \left( \frac{16\pi G_5 \lambda - 6}{\varepsilon^4} + \frac{8\pi G_5 \lambda}{\varepsilon^2} (g^{(0)})^{\mu\nu} g_{\mu\nu}^{(2)} + a_{(4)} \log \varepsilon + \dots \right). \quad (1.65b)$$

where the omitted terms are all finite as  $\varepsilon \rightarrow 0$ . The quantity,  $a_{(4)}$ , which can be defined in terms of covariant quantities derived from  $g_{\mu\nu}^{(0)}$ , is the Weyl anomaly of the CFT, and is of great interest generally, though in our case we do not need to find it explicitly.

The order  $\varepsilon^{-2}$  term can be calculated by considering the 5d Einstein equation, which, as shown in [122], enforces that

$$R_{\mu\nu}^{(0)} = 2g_{\mu\nu}^{(2)} + \left( (g^{(0)})^{\rho\sigma} g_{\rho\sigma}^{(2)} \right) g_{\mu\nu}^{(0)} + \mathcal{O}(\varepsilon^2) \quad \implies \quad R^{(0)} = 6(g^{(0)})^{\rho\sigma} g_{\rho\sigma}^{(2)} + \mathcal{O}(\varepsilon^2), \quad (1.66)$$

where here  $R_{\mu\nu}^{(0)}$  and  $R^{(0)}$  are, respectively, the Ricci tensor and Ricci scalar associated to  $g_{\mu\nu}^{(0)}$ . Thus

$$\mathcal{L} = \sqrt{-g^{(0)}} \left( \frac{16\pi G_5 \lambda - 6}{\varepsilon^4} + \frac{4\pi G_5 \lambda R^{(0)}}{3\varepsilon^2} + a_{(4)} \log \varepsilon + \dots \right). \quad (1.67)$$

Now, in standard AdS/CFT, we take  $\varepsilon \rightarrow 0$ , and hence all the terms explicitly written above diverge, meaning that they must be removed by the addition of local counterterms. This is the procedure of holographic renormalization yielding the results given in Section 1.3.3. In particular, we remove the term proportional to  $R^{(0)}$ , meaning that gravity is non-dynamical in the boundary theory.

However, in the case of the RSII model,  $\varepsilon$  is non-zero, and hence all terms in (1.67) are finite, and there's no need to add counterterms. This is the crux: we retain the term proportional to  $R^{(0)}$ , and hence we will find that gravity on the brane is dynamical in the dual picture.

So far, to keep in touch with the AdS/CFT calculation, we've been treating the RSII bulk as one-sided, but recall that really it is two-sided, with a  $\mathbb{Z}_2$  symmetry across the brane. This means that in the above calculation we really should have taken two lots of the bulk integral and the Gibbons-Hawking term (one from each of the sides of the brane), but still only a single contribution of the term coming from the brane tension. This has the effect of adding a factor of two to each term in (1.67) except those involving a factor of  $\lambda$ . Taking this into account, and rewriting in terms of the

metric  $\gamma_{\mu\nu} = \varepsilon^{-2}g_{\mu\nu}^{(0)}$ , we find

$$\mathcal{L} = \sqrt{-\gamma} \left( 16\pi G_5 \lambda - 12 + \frac{4\pi G_5 \lambda \mathcal{R}}{3} + a'_{(4)} \log \varepsilon + \dots \right), \quad (1.68)$$

where now  $\mathcal{R}$  is the Ricci scalar associated to  $\gamma_{\mu\nu}$ . In order for effective cosmological constant on the brane to be zero, we must tune the tension of the brane by taking  $\lambda = 3/(4\pi G_5)$  so that the first two terms cancel one another. Reinstating the factors of  $\ell_5$ , we find overall that

$$\text{ext}_{g_{\mu\nu}^{(0)}=\gamma_{\mu\nu}} \left( S_{\text{bulk}}[g_{ab}] + S_{\text{brane}}[g_{\mu\nu}^{(0)}] \right) = \mathcal{W}_{\text{CFT}}[\gamma_{\mu\nu}] + \frac{\ell_5}{16\pi G_5} \int d^4x \sqrt{-\gamma} \mathcal{R}, \quad (1.69)$$

where  $\mathcal{W}_{\text{CFT}}$  contains the  $\log \varepsilon$  term, as well as the terms annotated by the ellipsis in (1.68). This implies that the effective Newton's constant for gravity on the brane is given by  $G_4 = G_5/\ell_5$ . Having reinstated the factor of  $\ell_5$ , the brane tension is given by  $\lambda = 3/(4\pi G_5 \ell_5)$ .

Therefore, the five-dimensional theory of gravity in the RSII bulk is dual to a four-dimensional strongly coupled CFT defined on the brane, coupled to four-dimensional GR. This gives an interesting alternative interpretation to differences of the effective theory on the brane from general relativity. In the bulk picture, one sees that these differences arise from the graviton being able to access the extra dimension at high energies. On the other hand, in the brane picture of the duality, the differences come from corrections to the propagator of the graviton due to loops of CFT fields in a solely four-dimensional theory. Of course, the CFT in the latter picture is strongly coupled, and hence it is generally easier to make calculations in the former, bulk picture.

#### 1.5.4 Static RSII black holes

The analysis yielding the effective non-relativistic potential, (1.54), for gravity on the brane is a perturbative analysis about flat space on the brane. However, black holes are non-perturbative solutions, so this analysis *a priori* does not guarantee that braneworld black holes resemble standard four-dimensional black holes at large scales. Therefore it is desirable to directly derive black hole solutions in the RSII model to substantiate the viability of the RSII model as a mechanism for extra dimensions in our Universe.

Recall that the original RSII model is given by the metric (1.56) in the region  $z \in [\ell_5, \infty)$ . However, one can, in fact, replace the Minkowski metric,  $\eta_{\mu\nu}$ , by any 4d

Einstein metric,  $h_{\mu\nu}$ , and still have a solution to the 5d Einstein equation:

$$ds^2 = \frac{\ell_5^2}{z^2} \left( dz^2 + h_{\mu\nu} dx^\mu dx^\nu \right). \quad (1.70)$$

In search of a braneworld black hole, one may initially take  $h_{\mu\nu}$  in the above equation to be the 4d Schwarzschild metric. In this case, the induced metric on the brane is the Schwarzschild black hole, and its horizon extends throughout the bulk all the way to the Poincaré horizon, hence it is named the *AdS black string*. However, such a spacetime has a curvature singularity where the event horizon meets the Poincaré horizon and, indeed, it is unstable near this region. Therefore the AdS black string cannot be the final state of gravitational collapse of matter on the brane. It was conjectured in [147] that the string would decay to a “black cigar” geometry with a regular horizon, in which the induced geometry on the brane is very close to the Schwarzschild geometry but the black hole horizon “pinches off” some way into the bulk before reaching the Poincaré horizon.

However, there was some debate over whether such a “pinched off” black hole in the RSII model could exist with sizes large relative to the AdS length scale,  $\ell_5$ . Due to the connection to the AdS/CFT correspondence described in Section 1.5.3, the dual to a black hole in the RSII bulk would be a *quantum corrected* black hole [148], *i.e.* a black hole whose geometry is corrected by the contributions coming from the large  $N$ , strongly-coupled CFT. If the CFT were free, then the  $\mathcal{O}(N^2)$  extra degrees of freedom arising from the CFT fields would lead to  $\mathcal{O}(N^2)$  extra radiation away from the quantum-corrected black hole on the brane side of the duality. In the dual, bulk picture, this  $\mathcal{O}(N^2)$  extra radiation would correspond to a *classical* instability, and hence the bulk black hole would be classically time-dependent, disallowing the existence of stationary bulk black holes in RSII braneworlds.

It was contended, however, that the key step in this argument depends upon intuition from free field theory, whereas in the dual to the RSII braneworld, the CFT is strongly coupled [128]. It was postulated that this strong coupling may lead to some confinement mechanism of the CFT in the vicinity of the quantum corrected black hole, which would reduce the amount of radiation away from the black hole down to  $\mathcal{O}(N^0)$ . On the bulk side this reduced radiation would correspond to the emission of usual Hawking quanta from the bulk black hole, and hence does not imply an instability of the classical black hole solution.

This debate occurred before the discovery of the black droplet and funnel solutions that we reviewed in Section 1.4. The obtainment of the static black droplet solution

[133] showed that indeed there is a confined phase, with only  $\mathcal{O}(N^0)$  radiation, of the CFT when it resides on a fixed black hole background. This suggested heavily that braneworld black holes would exist, and that the black droplet would be the limit of them as the brane is taken all the way to the conformal boundary, or dually, as gravity is taken to be non-dynamical in the CFT theory.

Indeed, fairly quickly, the method to obtain the black droplet was altered in order to numerically attain static black holes in the RSII model for a large range of sizes compared with the AdS length scale [149], settling the debate once and for all. These solutions were also found via another method in [150] by perturbing away from the black droplet solutions, and in [151] they were shown to be the final state of gravitational collapse of spherically symmetric matter on the brane.

The induced metric of the static RSII black holes on the brane very closely resemble the Schwarzschild solution when they are large relative to the AdS radius. However, the black holes in our universe are generally rotating and uncharged, therefore in order for the RSII model to be phenomenologically viable, it must exhibit rotating black hole solutions as well as static ones.

## 1.6 The black hole solutions of this thesis

This thesis is concerned with numerically obtaining stationary solutions to the Einstein equation with a negative cosmological constant. As we've seen throughout this introduction, there are number of reasons that such solutions are of interest. Under the AdS/CFT duality, these classical black holes corresponds to studying thermal states of very strongly coupled conformal field theories (CFTs) with a large number of degrees of freedom — an extremely challenging feat without the aid of holography. Whilst also being related to the AdS/CFT correspondence, the Randall-Sundrum II model, which is a braneworld scenario in which matter is restricted to a submanifold of a larger space with a negative cosmological constant, is a genuine candidate for the inclusion of extra dimensions in our Universe. Last, but not least, the discovery of such a large and diverse set of black hole solutions shows the old idea of black hole uniqueness does not easily extend into anti-de Sitter space. These are the avenues of research that this thesis considers. A common theme shall be that in AdS black hole solutions can be stationary and even static and yet not be in thermodynamic equilibrium.

Chapters 3-6 are each based on a different paper [1–4] constituted by original work undertaken in collaboration with Jorge E. Santos.

We'll begin in Chapter 2 by describing the various numerical methods used throughout the thesis to obtain stationary black hole solutions in general relativity. Many of these techniques are standard. The key is that in order for the Einstein equation to have elliptic character, so that they can be solved as a boundary value problem, a suitable gauge must be chosen. We'll review two possible choices, the DeTurck gauge and Bondi-Sachs gauge. Once an elliptic problem is obtained, one still is faced with a very complicated set of coupled, non-linear PDEs. We'll discuss how these can be approximated by a very large set of non-linear algebraic equations which can be solved with the Newton-Raphson method.

In Chapter 3, based on the work of [1], we will turn to the black holes in the Randall-Sundrum II model. These braneworld set-ups must be shown to exhibit rotating black holes in order to be phenomenologically viable. In this chapter we obtain such rotating RSII black holes, and show clearly that when they are large compared with the AdS radius, they very closely resemble four-dimensional Kerr black holes according to observers on the brane. On the other hand when they become small they exhibit signs of the extra dimension, tending instead towards the geometry of a singly rotating Myers-Perry black hole.

Next, in Chapter 4, we'll study a strongly-coupled CFT on a four-dimensional de Sitter-Schwarzschild background (dS-S), *i.e.* a spherically symmetric black hole solution to the Einstein equation with a positive cosmological constant. The dS-S spacetime contains two horizons, the event horizon of the black hole and a cosmological horizon, which generically have two different temperatures. We construct the asymptotically locally AdS gravitational dual solutions, which have a conformal boundary on which the metric is dS-S. Similarly to the case of the black droplets and funnels, reviewed in Section 1.4, there are two possible bulk solutions, distinguished by the horizon structure in the bulk. We first presented these solutions, named *black tunnels* and *black hammocks*, in [2]. Since dS-S naturally has two non-equal temperature scales associated to it, these dual solutions are not in thermal equilibrium, despite being stationary. We argue that this set-up could provide a very natural case-study for investigating the mysterious phase transition between confinement and deconfinement to which the two different bulk solutions correspond.

So far we have considered solutions in AdS without the presence of any matter fields. In terms of the dual field theory, this means that the CFT is only deformed by a gravitational source, *i.e.* the boundary metric on which it resides. However, it is also of great interest to understand how the CFT behaves under other sources, for example, a background electric field. Global droplets and funnels, reviewed in Section 1.4.2,

provide a useful set-up in which such a system can be studied. We add a chemical potential to the field theory which induces a conserved current,  $J^\mu$ . This corresponds to the addition of a Maxwell field in the bulk. In Chapter 5, we define the chemical potential to vary on the boundary geometry, and in particular fix that it approaches two different values at the two black hole horizons in the boundary geometry, which induces an electric current between the two horizons. We dub these solutions as *holographic batteries* [3]. The ratio of the induced current and the applied external electric field gives the *conductivity* of the CFT on the boundary background, and this quantity can be extracted from the bulk solution. In this case, even though the boundary horizons are fixed to have the same temperature, the fact that the electric potential is chosen to vary between them once again causes the bulk solutions not to be in thermodynamic equilibrium.

Finally in Chapter 6 we approach the question of whether multi-horizon solutions can exist in AdS. With zero cosmological constant it appears that the only binary solutions are members of the Majumdar-Papapetrou family with the black holes needing to have extremal charge to balance their gravitational attraction. The negative cosmological constant contributes an additional attractive term to the gravitational potential well, and so one may expect that any analogous configuration of two charged black holes in AdS will be doomed to collapse, even if they are extremally charged. Hence, one may expect that the existence of static, charged binary solutions are prohibited in AdS. However, a key difference to flat space is that one can easily add source terms at the conformal boundary in AdS. This allows one to add a background electric field which may aid to keep the black holes apart. We'll discuss precisely how this can be done in Chapter 6, which is based on the work of [4]. Interestingly, for given boundary charges, there is a continuous family of binary solutions, parameterised by quantities defined on the horizons of black holes. Therefore these binary solutions represent continuous non-uniqueness. Despite being static, not all of the solutions are in thermoelectric equilibrium. The solutions are dual to states of the CFT under the influence of an electric source, though a great deal of mystery still remains as to the precise nature of these states.

Finally, in Chapter 7 we will conclude with an overall discussion of the stationary solutions described in this thesis, in particular touching upon the ways in which each of them fail or succeed to be in equilibrium.

## Chapter 2

# Numerical methods for finding stationary black holes solutions

Finding stationary solutions to the Einstein equation is a completely different, though equally ferocious, beast to studying a time-dependent problem in general relativity. More complete reviews of the methods described in this chapter are given in [152, 153], though these do not include detail on the Bondi-Sachs gauge (which we will discuss in Section 2.2) which was only used subsequently for stationary problems.

When faced with a dynamical problem, one seeks to formulate the Einstein equation as a set of hyperbolic PDEs, and then solves them as an initial value problem, evolving the initial data through time. This can be thought of as similar in character to solving the wave equation.

On the other hand, when seeking stationary solutions, one should instead formulate the equations to have elliptic character. One must set boundary conditions on the boundaries of the spacetime (which may include horizon of black holes or axes of symmetry) and then solve the PDEs as a boundary value problem. This time, the problem is much more akin to solving a Poisson equation.

Unfortunately, the PDEs arising from the Einstein equation (even when one explicitly assumes stationarity, or staticity) turn out to have mixed hyperbolic-elliptic character. To see this, let us consider linearising the vacuum equations, given in (1.17), about a background metric,  $g_{ab}$ , by considering small perturbations about this background,  $g_{ab} \rightarrow g_{ab} + h_{ab}$ :

$$\Delta h_{ab} := \delta \left( R_{ab} + \frac{d-1}{\ell_d^2} g_{ab} \right) = \delta R_{ab} + \frac{d-1}{\ell_d^2} h_{ab}, \quad (2.1a)$$

where the variation of the Ricci tensor is given by

$$\delta R_{ab} = \Delta_L h_{ab} + \nabla_{(a} m_{b)}, \quad (2.1b)$$

with  $\Delta_L$  is the standard Lichnerowicz operator

$$\Delta_L h_{ab} = -\frac{1}{2} \nabla^2 h_{ab} - h^{cd} R_{acbd} + h^c_{(a} R_{b)c} \quad (2.1c)$$

and

$$m_a = \nabla_b h^b_a - \frac{1}{2} \nabla_a h, \quad (2.1d)$$

where  $h$  is the trace of  $h_{ab}$ .

To consider the character of the equations, one must investigate the principal part,  $\sigma$  of the second-order differential operator  $\Delta$ , which is simply the terms within it containing two derivatives, and is given in this case by

$$\sigma[h_{ab}] = \frac{1}{2} g^{cd} (-\partial_c \partial_d h_{ab} + \partial_c \partial_a h_{bd} + \partial_c \partial_b h_{ad} - \partial_a \partial_b h_{cd}). \quad (2.2)$$

If we replace all the derivatives above by a general one-form,  $\omega_a$ , giving

$$\sigma[h_{ab}; \omega_a] = \frac{1}{2} g^{cd} (-\omega_c \omega_d h_{ab} + \omega_c \omega_a h_{bd} + \omega_c \omega_b h_{ad} - \omega_a \omega_b h_{cd}), \quad (2.3)$$

then we say the equations are *elliptic* if  $\sigma[h_{ab}; \omega] \neq 0$  for any non-zero one-form  $\omega_a$  and any perturbation  $h_{ab}$ . However, in this case, we can take  $h_{ab} = \omega_{(a} v_{b)}$  for any vector  $v^a$ , and we find that  $\sigma[h_{ab}; \omega_a] = 0$ . Of course, in a coordinate basis, this is a perturbation of the form  $h_{ab} = \partial_{(a} v_{b)}$ , which we recognise as a local diffeomorphism. Hence, we see that the failure for Einstein's equations to be elliptic arises due to the diffeomorphism invariance of general relativity. This suggests that the remedy to this issue may be to fix the gauge of the problem.

In Sections 2.1 and 2.2, we will introduce a couple of choices of the gauge which can be used to alleviate this issue, specifically the DeTurck gauge and the Bondi-Sachs gauge, respectively. However, even once a well-defined boundary value problem has been attained by fixing the gauge there is still great difficulty in solving it except in the most basic cases due to the non-linear nature of general relativity. Our approach will be to discretize the coordinate domain on which the equations are defined, and use this discretization to approximate the coupled non-linear PDEs by a very large set of non-linear algebraic equations. In Section 2.3, we describe the way in which the procedure is carried out and how the resultant algebraic equations are solved iteratively

via the Newton-Raphson method. Lots of problems tend to arise in the numerical method described above. In Section 2.4, we discuss a number of standard tricks that can be used to deal with a great deal of these issues.

## 2.1 The DeTurck method

One approach is to slightly alter the Einstein equation by adding on a term which makes it manifestly elliptic for a static *Ansatz*. Let us begin by considering a case with no matter. Here, one instead solves the *Einstein-DeTurck equation*, also known as the harmonic Einstein equation, given by

$$0 = R_{ab} + \frac{d-1}{\ell_d^2} g_{ab} - \nabla_{(a} \xi_{b)} \quad (2.4a)$$

where the *DeTurck vector*,  $\xi^a$ , is defined by

$$\xi^a = g^{bc} (\Gamma_{bc}^a(g) - \Gamma_{bc}^a(\bar{g})), \quad (2.4b)$$

with  $\bar{g}_{ab}$  a reference metric that we are free to choose, and  $\Gamma_{cd}^a(\mathbf{g})$  denoting the Christoffel connection associated to a metric  $\mathbf{g}$ . Note that though each Christoffel symbol is not a tensor, the difference between them is, and thus the DeTurck vector,  $\xi^a$ , is a tensor.

For the Einstein-DeTurck equation, the principal part of the linearisation about a background is

$$\sigma[h_{ab}] = -\frac{1}{2} g^{cd} \partial_c \partial_d h_{ab}. \quad (2.5)$$

If  $g_{ab}$  possesses a timelike Killing vector field, under which the variation  $h_{ab}$  is invariant, then  $\sigma[h_{ab}]$  must be non-zero. Hence for stationary problems, the Einstein-DeTurck equation is elliptic.<sup>1</sup>

Note however, that in order for solutions of (2.4a) to also be a solution to the Einstein equation, (1.17), we require that  $\xi^a = 0$ . Solutions to (2.4a) with non-zero  $\xi^a$  are called *Ricci solitons*. In certain cases there exist theorems which prohibit the existence of Ricci solitons [133, 154]. However, even in scenarios in which these theorems do not hold, the DeTurck method can still be extremely useful, though one must be careful to explicitly check that the solution being obtained is not a Ricci soliton by carrying out convergence tests.

<sup>1</sup>Strictly speaking, this is only true outside of any ergoregions of the spacetime; it is the timelike nature of the KVF which ensures ellipticity. Inside of an ergoregion where the stationary KVF becomes spacelike, the Einstein-DeTurck equation in fact ceases to be elliptic. However, we shall still find that it is still a useful numerical formulation for stationary problems including ergoregions.

### 2.1.1 Including a Maxwell field

The above analysis refers to the use of the DeTurck method in the case of pure gravity, but it can be easily generalised to the case of Einstein-Maxwell theory, which has the equations of motion given by

$$0 = R_{ab} + \frac{d-1}{\ell^2} g_{ab} - 2\tilde{T}_{ab}, \quad (2.6a)$$

$$0 = \nabla^a F_{ab} \quad (2.6b)$$

where in the case of a Maxwell field, the trace-reversed stress tensor,  $\tilde{T}_{ab}$  is given by

$$\tilde{T}_{ab} = F_a{}^c F_{bc} - \frac{1}{2(d-2)} g_{ab} F_{cd} F^{cd}. \quad (2.6c)$$

The Maxwell equation will similarly yield mixed hyperbolic-elliptic PDEs in general, once again with the failure of ellipticity originating from the gauge invariance of the equation. In the DeTurck method, one adds terms to each of these equations, in particular, taking

$$0 = R_{ab} + \frac{d-1}{\ell^2} g_{ab} - 2\tilde{T}_{ab} - \nabla_{(a} \xi_{b)}, \quad (2.7a)$$

$$0 = \nabla^a F_{ab} - \nabla_b \zeta \quad (2.7b)$$

where  $\xi^a$  is again the DeTurck vector defined in terms of a reference metric by (2.4b), and

$$\zeta = g^{cd} \nabla_c (A_d - \bar{A}_d), \quad (2.8)$$

with  $\bar{A}$  a reference vector potential which again one is free to choose.

The situation simplifies if the vector potential is assumed to be proportional to the stationary KVF,  $A_a \propto k_a$ , in which case the Maxwell equation is in fact already automatically elliptic, and so one can take  $\zeta = 0$ .

There are as yet no theorems prohibiting Ricci solitons *a priori* in Einstein-Maxwell theory. Thus, one must check that the solutions to (2.7) are not Ricci solitons by running convergence tests to check that both  $\xi^a$  and  $\zeta$  tend towards zero in the continuum limit.

## 2.2 Bondi-Sachs gauge

The Bondi-Sachs gauge is another choice one can take in order to obtain stationary solutions. We will find it is particularly useful to obtain solutions similar to the black funnels described in Section 1.4, which are asymptotically locally anti-de Sitter solutions with a horizon anchored at two different points of the conformal boundary. This gauge was discussed in references [155–157] in four dimensions in the context of time-dependent problems. It was first used as a gauge choice to numerically solve a stationary problem in [2] in the context of pure gravity and in [158, 3] for Einstein-Maxwell theory. One particularly favourable feature of Bondi-Sachs gauge is that, unlike in DeTurck gauge, no non-analytic terms arise in an expansion of an Einstein metric near the conformal boundary [159].

For a general AlAdS metric in  $d$  dimensions, with conformal boundary at  $y = 0$ , the metric can be locally written in Bondi-Sachs gauge as

$$ds^2 = \frac{L^2}{y^2} \left[ e^{2\beta} (-V dv^2 - 2 dv dy) + e^{2\chi} h_{IJ} (dx^I - U^I dv) (dx^J - U^J dv) \right], \quad (2.9)$$

where the stationary Killing vector field in these coordinates is given by  $k^a = (\partial/\partial v)^a$ , and the  $I, J, \dots$  indices run over all coordinates except  $v$  and  $y$ . We take  $\det h_{IJ} = 1$ , so that the determinant of the induced geometry on constant  $y$  slices is contained within the function  $\chi$ . For the current analysis, let us assume one can take coordinates such that  $U^I \neq 0$  for only one of the  $x^I$  coordinates and that the other  $x^J$  coordinates span a conserved  $(d-3)$ -sphere,<sup>2</sup> in which case the metric can be written as

$$ds^2 = \frac{L^2}{y^2} \left[ e^{2\beta} (-V dv^2 - 2 dv dy) + e^{2\chi} \left( \frac{1}{A^{d-3}} (dx - U^x dv)^2 + A d\Omega_{(d-3)}^2 \right) \right], \quad (2.10)$$

with five functions,  $V, U^x, \beta, A, \chi$ , depending upon  $\{x, y\}$  for a stationary problem. Note that by redefining the radial coordinate,  $y$ , we also have the freedom to fix one of  $\beta$  or  $\chi$  (or a combination thereof).

In the vacuum case, we wish to solve the Einstein equation with negative cosmological constant:

$$E_{ab} := R_{ab} + \frac{d-1}{\ell_d^2} g_{ab} = 0. \quad (2.11)$$

---

<sup>2</sup>All uses of the Bondi-Sachs gauge in this thesis satisfy these assumptions, but one can also use this gauge for more general stationary problems, with the analysis of this section generalising in a fairly trivial fashion.

The Einstein equation has more non-trivial components than the number of free functions,  $\{V, U^x, \beta, A, \chi\}$ , but it so happens that not all of these components are independent. Following [155–157], it turns out that one need only solve the four independent equations of motion coming from  $E_{ij} = 0$ , with  $i, j \neq v$  in the bulk — we call these *the bulk equations*. This leaves three other non-trivial equations,  $E_{va} = 0$ , which must also be satisfied in order to have a full solution to the Einstein equation. However, it can be shown using the contracted Bianchi identity that if these additional equations are satisfied at some constant  $y$  slice, then actually they are necessarily satisfied throughout the whole of the bulk, so long as the bulk equations are also satisfied there. The contracted Bianchi identity is given by

$$\nabla_a R^a{}_b = -\frac{1}{2}\nabla_b R. \quad (2.12)$$

In a coordinate basis, the Bianchi identity can be expanded to the equality

$$0 = g^{bc} \left( \partial_b R_{ac} - \frac{1}{2} \partial_a R_{bc} - \Gamma_{bc}^d R_{ad} \right). \quad (2.13)$$

We'll assume that the bulk equations hold, *i.e.* we have

$$R_{yy} = 0, \quad R_{yx} = 0, \quad R_{Ax} = 0, \quad R_{xx} = -\frac{d-1}{\ell_d^2} g_{xx}, \quad R_{AB} = -\frac{d-1}{\ell_d^2} g_{AB}, \quad (2.14)$$

where we'll use  $A, B, \dots$  to denote the indices of the coordinates spanning the  $(d-3)$ -sphere. Let us first consider the  $y$ -component of the contracted Bianchi identity, given in (2.13). Noting that the inverse metric has  $g^{\nu\mu} = 0$ , where  $\mu \neq y$ , and after applying the bulk equations, one finds that the  $y$ -component of the contracted Bianchi identity simplifies to

$$0 = \frac{2}{\ell_d^2} g^{IJ} \partial_y g_{IJ} - g^{ab} \Gamma_{ab}^v R_{yv}. \quad (2.15)$$

One can directly calculate the inverse metric and the Christoffel symbols, and find that (2.15) is solved by

$$R_{yv} = -\frac{d-1}{\ell_d^2} g_{yv}. \quad (2.16)$$

Thus the bulk equations automatically solve  $E_{yv} = 0$  algebraically.

It still remains to satisfy the  $(v, v)$  and the  $(v, x)$  components of the Einstein equation. For the latter, consider the  $x$ -component of the contracted Bianchi identity.

We have

$$0 = g^{bc} \left( \partial_b R_{xc} - \frac{1}{2} \partial_x R_{bc} - \Gamma_{bc}^d R_{xd} \right). \quad (2.17)$$

Expanding all of these terms, applying the bulk equations, as well as (2.16) yields

$$g^{vy} \partial_y R_{vx} - g^{ab} \Gamma_{ab}^v R_{vx} = \frac{d-1}{\ell_d^2} \left[ -g^{vy} \partial_x g_{vy} + g^{xy} \partial_y g^{vy} + g^{xy} \partial_y g_{xx} + \frac{1}{2} g^{xx} \partial_x g_{xx} - \frac{1}{2} g^{AB} \partial_x g_{AB} - g^{ab} \Gamma_{ab}^x g_{xx} \right]. \quad (2.18)$$

Now by direct calculation, one can check that  $R_{vx} = -(d-1)\ell_d^{-2}g_{vx}$ , or equivalently  $E_{vx} = 0$ , solves the above equation. Since the equation is a first-order PDE, possessing only a  $y$ -derivative, this means that so long as we set  $E_{vx} = 0$  on some constant  $y$  slice, then the contracted Bianchi identity ensures that the unique solution must satisfy  $E_{vx} = 0$  throughout the whole bulk, via Picard's theorem.

We can deal with the  $(v, v)$  component of the Einstein equation in a similar fashion by considering the  $v$ -component of the contracted Bianchi identity:

$$0 = g^{bc} \left( \partial_b R_{vc} - \frac{1}{2} \partial_v R_{bc} - \Gamma_{bc}^d R_{vd} \right). \quad (2.19)$$

Once again, we expand each term, apply the bulk equations, (2.16), and now additionally  $E_{vx} = 0$ . This gives

$$g^{vy} \partial_y R_{vv} - g^{ab} \Gamma_{ab}^v R_{vv} = \frac{d-1}{\ell_d^2} \left[ g^{yy} \partial_y g_{vy} + g^{yx} (\partial_y g_{vx} + \partial_x g_{vy}) + g^{xx} \left( \partial_x g_{vx} - \frac{1}{2} \partial_v g_{xx} \right) - \frac{1}{2} g^{AB} \partial_v g_{AB} - g^{ab} (\Gamma_{ab}^y g_{vy} + \Gamma_{ab}^x g_{vx}) \right]. \quad (2.20)$$

Again by direct calculation, one can verify that  $R_{vv} = -(d-1)\ell_d^{-2}g_{vv}$  solves this equation, hence by a similar argument to the  $(v, x)$  component, so long as we enforce  $E_{vv} = 0$  on a constant  $y$  slice, it will be satisfied throughout the whole bulk.

Hence, in summary, when working with a metric in Bondi-Sachs gauge, one need only solve the bulk equations coming from  $E_{ij} = 0$  for  $i, j \neq v$ , and additionally set  $E_{va} = 0$  as boundary conditions at some constant  $y$  hypersurface, and then the contracted Bianchi identity enforces that  $E_{va} = 0$  holds throughout the whole spacetime.

Since we are not directly enforcing  $E_{va} = 0$  everywhere across the bulk, one way to monitor the convergence of our numerical method is to measure the magnitude of  $E_{va}$

throughout spacetime on the numerical solution. In the continuum limit, this should vanish even away from where  $E_{va} = 0$  was imposed as a boundary condition. In this way, the method we outline here is not very different from the DeTurck method, where we also have to check that the DeTurck vector vanishes in the continuum limit. Though practically this method has proved to be extremely useful for finding solutions, it still remains to be fully understood whether this integration scheme leads to a well-defined elliptic boundary value problem for a stationary spacetime in a precise mathematical sense.

### 2.2.1 Including a Maxwell field

The Bondi-Sachs gauge can also be used to solve stationary problems in Einstein-Maxwell theory, with equations of motion (2.6). With the metric in Bondi-Sachs gauge, as described in (2.9), the vector potential must be taken in a gauge with  $A_y = 0$  where  $y$ , once again, is the AdS radial direction. Likewise to the Einstein equation, one solves only a subset of the PDEs arising from the Maxwell equations throughout the bulk directly, setting the remainder as boundary conditions at a constant  $y$  slice. Specifically, one must solve  $\nabla^a F_{ai} = 0$  where  $i \neq v$  but only set the  $\nabla^a F_{av} = 0$  equation as a boundary condition. By a similar argument as for the Einstein equation presented above, this ensures that the full Maxwell equation is satisfied throughout the bulk.

## 2.3 The Newton-Raphson method

By considering an *Ansatz* with  $N$  unknown metric functions and using either the DeTurck method, or by directly fixing the gauge to be Bondi-Sachs and considering the bulk equations, one obtains a set of  $N$  coupled, non-linear PDEs:

$$\mathcal{G}_i[\vec{x}, F_1, \dots, F_N] = 0, \quad (2.21)$$

where  $\mathcal{G}_i$ , for  $i = 1, \dots, N$ , are differential operators that may also depend on the derivatives of  $F_j$ . We will solve these numerically by using collocation methods to estimate derivatives and the Newton-Raphson algorithm to iteratively approach the solution. Such methods are reviewed fully in [153].

The *Newton-Raphson algorithm*, sometimes just called Newton's method, was first introduced for the root finding of complicated functions, but can also be useful for numerically solving PDEs. One expands about an estimate,  $F_j^{[n]}$ , for the functions to

linear order:

$$0 = \mathcal{G}_i[\vec{x}, F_1, \dots, F_N] = \mathcal{G}_i[\vec{x}, F_1^{[n]}, \dots, F_N^{[n]}] + \frac{\delta \mathcal{G}_i}{\delta F_j}[\vec{x}, F_1^{[n]}, \dots, F_N^{[n]}] \delta F_j + \mathcal{O}(\delta F_j^2), \quad (2.22)$$

where  $\delta F_j = F_j - F_j^{[n]}$ , and  $\delta \mathcal{G}_i / \delta F_j$  is a linear second order differential operator acting on  $\delta F_j$ , which can be found by linearising the equations by taking  $F_j = F_j + \varepsilon \delta F_j$  in  $\mathcal{G}_i$ , differentiating with respect to  $\varepsilon$  and then setting  $\varepsilon$  to zero. If the estimate,  $F_j^{[n]}$ , is close to a true solution of  $\mathcal{G}_i$ , then the  $\mathcal{O}(\delta F_j^2)$  term is very small, and hence

$$\frac{\delta \mathcal{G}_i}{\delta F_j}[\vec{x}, F_1^{[n]}, \dots, F_N^{[n]}] \delta F_j \simeq -\mathcal{G}_i[\vec{x}, F_1^{[n]}, \dots, F_N^{[n]}]. \quad (2.23)$$

Therefore, if we can evaluate  $\mathcal{G}_i$  and  $\delta \mathcal{G}_i / \delta F_j$  for our given estimate,  $F_j^{[n]}$ , we can solve (2.23) for  $\delta F_i$  and then take as our next estimate

$$F_i^{[n+1]} = F_i^{[n]} + \delta F_i. \quad (2.24)$$

Repeating this iteratively will yield a quadratic convergence to the solution, as long as we start with a seed sufficiently close to the solution.

The linear PDEs given by (2.23) still depend on derivatives of the functions, so they are remain tricky to solve. In order to do so we discretize and use *collocation methods*, which are reviewed in [160], to approximate them with algebraic equations.

To elucidate how these collocation methods work, let's first consider the simpler case of a single function,  $f(x)$ , depending upon a single coordinate,  $x \in [x_-, x_+]$ . We take a set of points  $x_i$  called collocation points, spanning this coordinate patch. Let  $f_i := f(x_i)$  be the value of the function at these points. The purpose of collocation methods is to approximate the derivatives  $f_i^{(n)} := (d/dx)^n f|_{x=x_i}$  in terms of the evaluations,  $f_j$ , of the function at *each* of the lattice points. That is, we seek *differentiation matrices*,  $D_{ij}^{(n)}$ , such that

$$f_i^{(n)} \simeq D_{ij}^{(n)} f_j, \quad (2.25)$$

where we've summed over the repeated  $j$  index. The simplest choice is the standard finite differences approximation. One takes  $x_i$  to be evenly space, with spacing  $\delta x$  and then (for internal points) one takes the estimate

$$f_i^{(1)} = \frac{f_{i+1} - f_{i-1}}{2\delta x}, \quad f_i^{(2)} = \frac{f_{i+1} - 2f_i + f_{i-1}}{(\delta x)^2}, \dots \quad (2.26)$$

The derivatives at the endpoints of the domain can also be estimated. In the case of finite differences, the differentiation matrices are very sparse, but the approximation of the derivatives is not particularly accurate. One may envisage improving the accuracy of the approximation by taking the differentiation matrices to be extremely dense, so that, for example,  $f_i^{(1)}$ , depends on  $f_j$  for all  $j$ . However, if one does this with evenly spaced points, one finds that the interpolant has large oscillations near the endpoints.

The solution to this issue is to instead take unequally spaced collocation points, which are particularly clustered towards the endpoints. One example of this is using a *Chebyshev-Gauss-Lobatto grid*, defined by taking

$$x_j = \frac{x_+ - x_-}{2} + \frac{x_+ + x_-}{2} \cos\left(\frac{j\pi}{n}\right), \quad \text{for } j = 0, \dots, n \quad (2.27)$$

where  $x_+ = x_0, \dots, x_n = x_-$  are the collocation points in descending order. The first-order differentiation matrix is given by

$$D_{ii}^{(1)} = \sum_{k \neq i} \frac{1}{x_i - x_k}, \quad D_{ij}^{(1)} = \frac{a_i}{a_j (x_i - x_j)} \quad (i \neq j),$$

where  $a_i = \prod_{k \neq i} (x_i - x_k)$ .

(2.28)

Higher order derivatives can be found simply by repeatedly applying the first order differentiation matrix, or alternatively from specifically defining higher order differentiation matrices which are not too much more complex. Such differentiation matrices can easily be generalized to more dimensions by taking a lattice of collocation points spanning the higher dimensional coordinate space and estimating derivatives in each direction using the one-dimensional differentiation matrices given above.

Now, let us discuss how we can use such collocation methods to solve the linear PDEs, (2.23), that are given to us by each iteration of Newton's method. Given an estimate  $F_j^{[n]}$ , we seek to solve this equation for  $\delta F_j$ . The difficulty of solving this equation comes down to the fact that  $\mathcal{G}_i$  are differential equations, and so depend not only upon the evaluation of each function  $F_j$ , but also their derivatives.

Suppose we know the value of each of the functions at each of the collocation points,  $F_j(\vec{x}_\ell)$ . We can then estimate the derivatives of each function using differentiation matrices as described above, and then plug these into  $\mathcal{G}_i$ . Therefore, we can approximate the differential operator,  $\mathcal{G}_i$ , at these points by a function  $G_i$ :

$$\mathcal{G}_i[\vec{x}_k, F_1, \dots, F_N] \simeq G_i(\vec{x}_k, F_1(\vec{x}_\ell), \dots, F_N(\vec{x}_\ell)). \quad (2.29)$$

The key difference is that, whilst  $\mathcal{G}_i$  is a differential operator, depending on the evaluations and the derivatives of the functions,  $F_j$ , at a single point,  $G_i$  is simply a function that now depends only on the *evaluation* of the functions,  $F_j$ , at *all* of the lattice points, but not on derivatives. Plugging an estimate  $F_j^{[n]}$  for the evaluation of the functions at each lattice point yields a numerical vector of length  $NM$  (where  $N$  is the number of PDEs and  $M$  is the number of lattice points) representing the evaluation of the differential operator on the estimate  $F_j^{[n]}$ . Similarly, by plugging in the estimates  $F_j^{[n]}$ , one can replace the second order differential operator  $\delta\mathcal{G}_i/\delta F_j$  by an  $NM \times NM$  numerical matrix. Finally, the unknown functions,  $\delta F_j$  in (2.23) is replaced by the value of that function at each lattice point, yielding an unknown vector of length  $NM$  denoted by  $\delta F_j(\vec{x}_\ell)$ .

Therefore, the use of collocation methods allows for the approximation of the linear PDEs described in (2.23) by a very large set of linear algebraic equations in which the only unknown quantity is the vector  $\delta F_j(\vec{x}_\ell)$ , which can then be calculated via a linear solve algorithm. Here we have presented the overall approach as a process of first linearising the PDEs and then using collocation methods to approximate these by linear algebraic equation. However, really these two methods must be utilised in tandem, and so one could equally consider the approach as approximating the non-linear PDEs by non-linear algebraic equations using collocation methods which are then solved iteratively using the Newton-Raphson method.

As discussed above, once one has obtained  $\delta F_j(\vec{x}_\ell)$ , one can update the estimate for the solution using (2.24). If the infinity norm of  $\delta F_j(\vec{x}_\ell)$  is less than some pre-chosen small value,  $\epsilon_{min}$ , then this suggests we are very close to a true solution of the original non-linear PDEs, (2.21), and so we can take  $F_j^{[n+1]}$  to be the numerical solution. If the norm of  $\delta F_j(\vec{x}_\ell)$  is extremely large, say greater than  $\epsilon_{max}$  then this implies the seed is outside the radius of convergence of the Newton-Raphson algorithm, meaning that the algorithm will diverge, and suggesting one needs to use a different seed closer to the solution. Let us now consider a number of tricks which can aid in order to ensure convergence to the desired solution.

## 2.4 A toolbox of tricks

### 2.4.1 Damping

The first thing one can do if the Newton-Raphson method is quickly diverging is use damping. Effectively, in doing so, one is being sceptical about the accuracy of

the update  $\delta F_i$  obtained, and so only adding a fraction of this value to the previous estimate:

$$F_i^{[n+1]} = F_i^{[n]} + \alpha \delta F_i, \quad (2.30)$$

for  $0 < \alpha \leq 1$ . This will reduce the risk of the Newton method diverging, though will slow down convergence once one is close to a solution. However, one could also take the value of  $\alpha$  to depend upon the infinity norm of  $\delta F_i$ , so that it is taken to be small when one is far away from a solution but equal to one when very nearby the solution. For example, one can take

$$\alpha = \begin{cases} \frac{\beta}{\|\delta F_i\|_\infty} & \text{if } \|\delta F_i\|_\infty > \beta \\ 1 & \text{otherwise,} \end{cases} \quad (2.31)$$

where  $\|\delta F_i\|_\infty$  denotes the maximum value across each of the functions and each of the lattice points, and  $\beta$  can be chosen as the number at which one wishes to introduce damping.

### 2.4.2 Obtaining a good seed

For complicated problems though, if one starts with a seed too far away from a solution, no amount of damping will stop the Newton-Raphson algorithm from diverging. Hence, the choice of a good seed is imperative.

Often there are natural choices for a seed. As a toy example, let us imagine we possessed these numerical methods in the fifty years between the discovery of the analytical expressions for the Schwarzschild and Kerr solutions. In that case one could have found the Kerr solution numerically by using the Schwarzschild solution as a seed for a very slowly rotating black hole. Then one could increase the angular velocity each time taking the previously found Kerr solution as a seed, so that the seed is always a fairly good estimate for the next solution. This is an example of “marching”, where one starts at some point within a continuous parameter space, and slowly alters the parameters, each time using the nearby solution as a seed. This is a very effective method for exploring a parameter space, though it requires a solution within that space to already be known.

However, if one wants to find an entirely new class of solutions, say with a different asymptotic structure, or with multiple horizons, it is often much more difficult to find a first solution within the parameter space. One sometimes can take a seed which satisfies all of the boundary conditions, but not necessarily any field equations (indeed,

in the DeTurck method, the reference metric must satisfy all the boundary conditions so it can often provide a useful seed). In general, though, this still will not be a good enough first guess in order to ensure convergence.

One method to overcome this issue is named the  $\delta$ -trick, used in [161, 103, 4]. The philosophy is effectively to begin by artificially altering the equations of motion to ones that are automatically solved by some metric, and then to slowly deform the equations back to the true equations of motion of the problem, using the previous solution as a seed each time. Specifically, say the equations of motion in question are denoted all together by  $E[g] = 0$ , where  $g$  denotes the solution metric (and vector potential in the case of Einstein-Maxwell) that one is seeking to obtain numerically. Suppose one knows that another configuration,  $g_0$ , satisfies some alternative equations of motion,  $E_0[g_0] = 0$ . Then one could define

$$\hat{E}[g; \delta] = (1 - \delta)E[g] + \delta E_0[g]. \quad (2.32)$$

It is clear that  $g_0$  is a solution to  $\hat{E}[g; 1] = 0$ , and that a solution to  $\hat{E}[g; 0] = 0$  would be the desired solution to our original problem. Hence, one can start with  $\delta = 1$  and  $g_0$  as a seed, and solve  $\hat{E}[g; \delta] = 0$  iteratively, each time slightly decreasing  $\delta$  and using the previous intermediate solution as a seed. If, via this process,  $\delta$  can be reduced all the way to zero, then a solution to the original problem has been obtained.

One particular example of the  $\delta$ -method which is useful when solving the Einstein-DeTurck equation is to define  $E_0$  to be an equation which is automatically solved by the reference metric,  $g_0 = \bar{g}$ , say by taking  $E_0[g] = E[g] - E[\bar{g}]$ . This yields

$$\hat{E}[g; \delta] = E[g] - \delta E[\bar{g}]. \quad (2.33)$$

### 2.4.3 Patching

Sometimes if the solutions exhibit very large derivatives, it can be useful to split the coordinate domain into multiple patches, which increases the accuracy of the estimation of the derivatives via the pseudospectral collocation methods described above.

More fundamentally though, the pseudospectral collocation methods described above work well on only rectangular (or cuboid in higher dimensions) coordinate domains, and therefore, patching methods are necessary in the case that the coordinate domain is not rectangular. One splits the non-rectangular domain into multiple rectangular patches on which the collocation methods can be used to estimate derivatives as usual. This also allows one to use an entirely different coordinate systems in different

regions of the space, which can be very extremely useful when designing a reference metric.

There are a number of ways to interpolate between the patches. Firstly, one can take the patches to overlap and then ensure that the functions agree in either patch in the region where they overlap [162–164]. Alternatively, one can take the patches to meet only at their boundaries, and enforce that the functions and their derivatives (when written in the same coordinate system) agree at the interface between the two patches [161, 165–167, 103, 104, 4]. This latter method called *transfinite interpolation* is the method used in Chapter 6, where we will explain it in far more detail.

#### 2.4.4 Turning points

Sometimes when varying parameters in a space of solutions, one approaches what is known as a *turning point*. Say, for simplicity, there is only a single parameter,  $\lambda$ . Then it may be that solutions cease to exist as  $\lambda$  increases to a certain value,  $\lambda^*$ . Often this is a sign of the solutions becoming singular at this point in the parameter space, however, this is not always the case.

Instead it can be that the solutions remain regular, but certain physical quantities (say, some charge  $Q$ ) begin to have very large derivatives with respect to  $\lambda$ . Thus at  $\lambda^*$ , one has  $d\lambda/dQ \rightarrow 0$ . This suggests that new solutions can be found by instead *decreasing*  $\lambda$  once again. Hence, a new branch of solutions can be found, meaning that near  $\lambda^*$  there are two distinct solutions with the same input value of  $\lambda$ .

It can be tricky to jump between the two branches when starting on one of them, since the Newton-Raphson algorithm will naturally converge to the most nearby solution, which will generally be on the same branch as the seed. One way to prevent this from occurring is to slightly alter the seed in order to induce the Newton-Raphson algorithm to land on the other branch. Say one has two solutions, denoted by  $g_1$  and  $g_2$ , which solve the equations of motion with parameters  $\lambda_1$  and  $\lambda_2$ , respectively, where  $\lambda_1 < \lambda_2 < \lambda^*$ . Then consider taking

$$g_{seed} = g_2 + \gamma(g_2 - g_1) \tag{2.34}$$

as the new seed. If  $\gamma = 0$ , then  $g_{seed} = g_2$ , the solution on the first branch. However, if we take  $\gamma$  to be large, then it may kick the seed far enough that we converge to a new solution with  $\lambda = \lambda_2$  on the second branch. The intuition between why this may work is based on an assumption that the change in solution between  $\lambda = \lambda_1$  and  $\lambda = \lambda_2$  may be similar to the change between the first  $\lambda = \lambda_2$  solution and the second  $\lambda = \lambda_2$  on

the next branch. However, in order for this assumption to be accurate, one needs both  $\lambda_2 - \lambda_1$  and  $\lambda^* - \lambda_2$  to be very small. This method was used in [165, 166, 4] to find solutions either side of turning points — the last of these citations refers to the paper reviewed in Chapter 6.

# Chapter 3

## Rotating Randall-Sundrum II black holes

### Abstract

We find rotating black hole solutions in the Randall-Sundrum II (RSII) model by numerically solving a three-dimensional PDE problem using pseudospectral collocation methods. We compute the area and equatorial inner-most stable orbits of these solutions. For large black holes compared with the AdS length scale,  $\ell$ , the black hole exhibits four-dimensional behaviour, approaching the Kerr metric on the brane, whilst for small black holes, the solution tends instead towards a five-dimensional Myers-Perry black hole with a single non-zero rotation parameter aligned with the brane. This departure from exact four-dimensional gravity may lead to different phenomenological predictions for rotating black holes in the RSII model to those in standard four-dimensional general relativity. This work, first presented in [1], provides a stepping stone for studying such modifications.

### 3.1 Introduction

In the century since the discovery of general relativity, there has been much excitement over the possibility that our universe may contain extra dimensions. For a large part, this has originated from the fact that superstring theory is known to be mathematically consistent only in ten dimensions (nine spatial and one temporal). However, such considerations lead to an inevitable question: *If the universe does contain extra dimensions, why does it appear so stubbornly four-dimensional?*

For matter fields, this can be answered fairly simply — it is perfectly consistent for the fields of the standard model to be restricted to a 3-brane (which is slice of spacetime made up of the temporal dimension as well as three spatial dimensions) in a higher dimensional space. However, gravity is not so easily dealt with. Through his theory of general relativity, Einstein taught us that gravity is simply the curvature of spacetime, and therefore it necessarily must be able to propagate in all directions and all dimensions. Gravity in our universe, however, seems to exhibit four-dimensional behaviour; in particular, it satisfies Newton’s inverse square law of gravitation at low energies. In general, adding extra spatial dimensions will break this inverse square behaviour. And so, to really tackle the problem at hand, we must slightly update the question posed in the previous paragraph: *If the universe does contain extra dimensions, why does **gravity** appear so stubbornly four-dimensional?*

Generally, in order to answer this, the extra dimensions in such theories are taken to be compactified and curled up very small, so that they have no effect on observers at large distances. However, to some surprise, Lisa Randall and Raman Sundrum showed in 1999 that this is not the only possibility. They introduced a five-dimensional model, now called the Randall-Sundrum II (RSII) model [142], which contains a single extra dimension that is non-compact and infinite in extent. However, vitally, the extra dimension is heavily warped so that the low-energy behaviour of gravity on a 3-brane on which the matter fields are confined still resembles four-dimensional general relativity. The Randall-Sundrum paradigm was first introduced in [141] in order to provide a possible solution to the hierarchy problem: the question regarding why gravity is so many orders of magnitude weaker than the other forces.

Section 1.5.2 of the introduction presented a brief review of the key features of the RSII model. Roughly speaking, the warping causes the graviton to be trapped in the vicinity of the 3-brane at low energies by a very steep potential well, leading to apparent four-dimensional behaviour according to the observers living on the brane. However, at high energies, the graviton is able to overcome this potential well and access the extra dimension. Therefore, at these scales there may be deviations from four-dimensional general relativity in the effective theory of gravity on the RSII brane. This motivates finding black hole solutions in the RSII model, since these will explore the high energy behaviour of gravity, and hence may exhibit different properties to standard four-dimensional black holes.

As we discussed in Section 1.5.3, due to the AdS/CFT correspondence [109–111], the RSII model has an alternative interpretation, as a four-dimensional theory in which gravity is corrected by the addition of a strongly coupled CFT with a UV

cut-off [168, 143, 146]. Therefore there are two reasons to be interested in the RSII model: as a genuine candidate for an extra dimension in our Universe, and also as a way to study the behaviour of a strongly coupled CFT when coupled to gravity.

This duality also initially led to some debate regarding whether large, static black holes could exist in the RSII braneworld at all. Therefore a black hole in the five-dimensional RSII bulk would correspond holographically to a *quantum-corrected* black hole on the brane [148]. It was thought that the black hole would quickly evaporate due to extra radiation arising from the CFT degrees of freedom, meaning any bulk black hole solution would be time-dependent. However, it was contended that this argument neglects the strong coupling of the CFT [128].

The debate was settled in [149], where static, stable black hole solutions on the brane were found for both small and large radii. This solution is closely related to black droplets and funnels [129–135, 137–140, 165], which are the gravitational duals to the limit where the CFT decouples from gravity, and were summarised in Section 1.4.

However, observed black holes in our universe tend to be rotating, and hence in order for the RSII model to be phenomenologically viable, it must exhibit not only static black hole solutions, but also rotating ones. In this chapter, we describe such rotating black hole solutions in the RSII braneworld. We were able to find these black hole solutions over a two parameter space. One parameter runs over the possible angular velocity of the black holes and the other measures the size of the black hole, relative to the AdS length scale.

Large RSII black holes exhibit four-dimensional behaviour, with the induced metric on the brane closely resembling that of the usual Kerr metric of a four-dimensional rotating black hole. However, smaller RSII black holes instead show five-dimensional behaviour, seeming to approach the five-dimensional Myers-Perry black hole [96] with single rotation.

We'll see this transition particularly clearly by considering the area of the event horizon of the black holes in the five-dimensional spacetime. In the limit where the black holes are very small, the area scales roughly as the radius cubed, which is indicative of five-dimensional behaviour, meaning that the black hole is roughly spherical in the five-dimensional spacetime. On the other hand, in the limit where the black holes become large, the area instead scales with the radius squared, revealing four-dimensional behaviour. This means that in this large limit, the black holes become more and more pancake-like, flattened in line with the brane and extend little into the extra dimension (relative to the other dimensions along the brane).

This transition from four-dimensional to five-dimensional behaviour means that braneworld black holes of a finite size will have a slightly different geometry on the brane to the Kerr black hole, and hence, may lead to different phenomenological predictions to those arising from standard four-dimensional general relativity.

One quantity that changes as a result of this transition is the position of the inner-most stable circular orbits (ISCO) around the equator of the rotating RSII black holes. In general, stable orbits around a black hole cannot come arbitrarily close to the event horizon, and so for a given black hole, there is a location of where the closest possible stable circular orbit to the event horizon would be situated. This is called the ISCO. The motivation for finding this quantity for the rotating RSII black holes is the fact that, unlike their four-dimensional counterparts, standard five-dimensional black holes do not exhibit stable orbits at all. Since the RSII black holes exhibit a transition from four-dimensional to five-dimensional behaviour as they decrease in size, one may therefore expect that, under this transition, the position of the ISCO diverges away from the corresponding value for the four-dimensional black hole. We find that the rotating RSII black holes do exhibit stable orbits, and that their ISCO has greater radius than the standard four-dimensional Kerr black hole. Moreover, the value of the ISCO tends towards that of the Kerr black hole as the braneworld black holes become large, yielding more evidence that in this limit the braneworld black hole very closely resembles a standard four-dimensional black hole on the brane.

The fact that we do obtain different predictions for finitely sized rotating RSII black holes to standard black holes provides a glimpse of the possibility of using astrophysical measurements of rotating black holes to test the viability of the RSII model in our Universe. However, since large rotating RSII black holes very closely resemble standard four-dimensional black holes, for this to really be an experimental possibility, much more finely-grained features of the rotating RSII black holes, such as their quasi-normal mode spectra, would need to be calculated in order to provide sharper contrast with Kerr black holes. It is also hoped that microscopic black holes may be produced in future in high-energy particle colliders, such as the International Linear Collider [90, 91] and the Compact Linear Collider [92]. If the Universe did contain a Randall-Sundrum extra dimension, then these microscopic black holes would be much more likely to exhibit five-dimensional behaviour than astrophysical black holes, being so many orders of magnitude smaller. Therefore, they would provide an excellent testing ground for seeking and constraining a Randall-Sundrum extra dimension.

In Section 3.2 we will present the *Ansatz* for the rotating RSII black hole, written in some particularly useful coordinates. We'll go on to describe some of the key features

of the solutions in Section 3.3, in particular, showing the aforementioned transition from five-dimensional to four-dimensional behaviour of the RSII black holes as they increase in size by considering the entropy, the inner-most stable circular orbits, and the geometry of the bifurcating sphere of the rotating RSII black hole solutions. Finally, we will end with a discussion in Section 3.4 and highlight some possible avenues for further study.

## 3.2 Obtaining braneworld black holes

### 3.2.1 The Ansatz

The bulk of the RSII model is a solution to Einstein's equation with negative cosmological constant in five dimensions,

$$R_{ab} + \frac{4}{\ell_5^2} g_{ab} = 0. \quad (3.1)$$

As discussed in Section 1.5.2, the original RSII spacetime, in which the induced metric on the brane is flat, can be expressed as a region of the Poincaré patch of AdS, given by

$$ds^2 = \frac{\ell_5^2}{z^2} \left( dz^2 - dt^2 + dr^2 + r^2 d\Omega_{(2)}^2 \right), \quad (3.2)$$

between a constant  $z$  slice and the Poincaré horizon at  $z = \infty$ . If we assume that a black hole in the RSII would indeed “pinch off” at some point in the bulk, then this implies that if we were to use similar  $\{z, r\}$  coordinates as used above to describe the empty RSII spacetime then the black hole would be described by some non-trivial surface in the  $\{z, r\}$  plane. Therefore, the coordinate domain would have five boundaries in these coordinates, which would need to be split up in order to carry out numerics. However, these issues can be alleviated by considering the following coordinate transformation

$$z = \frac{\Delta(x, y)}{1 - y^2}, \quad r = \frac{x\sqrt{2 - x^2}}{1 - y^2}, \quad \text{where} \quad \Delta(x, y) = 1 - x^2 + \beta^{-1}(1 - y^2). \quad (3.3)$$

Now the metric of the empty RSII spacetime becomes

$$ds^2 = \frac{\ell_5^2}{\Delta(x, y)^2} \left[ -h(y)^2 dt^2 + \frac{4y^2}{h(y)^2} dy^2 + \frac{4}{g(x)} dx^2 + x^2 g(x) d\Omega_{(2)}^2 \right], \quad (3.4)$$

where, here and for the remainder of the chapter,  $g(x) = 2 - x^2$  and  $h(y) = 1 - y^2$ . The coordinates  $x \in (0, 1), y \in (0, 1)$  parameterize the RSII bulk with the brane situated at

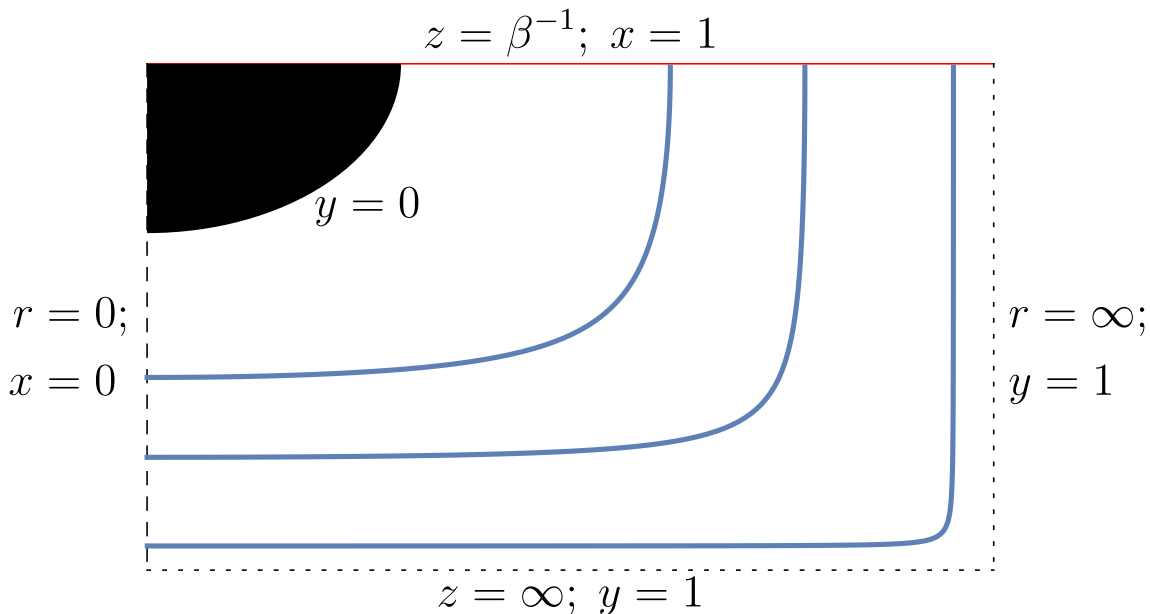


**Fig. 3.1:** The coordinate domain of a static RSII black hole. The red boundary is the brane. The dashed line is where the  $S^2$  shrinks to zero size and the dotted boundaries are asymptotic boundaries. In  $\{z, r\}$  coordinates there are five boundaries, but the  $y = 1$  surface encompasses both  $z \rightarrow \infty$  and  $r \rightarrow \infty$ , so that there are only four boundaries in the  $\{x, y\}$  coordinates. Constant  $y$  surfaces in the bulk are depicted as blue lines. The horizon is given by  $y = 0$  in these coordinates.

$x = 1$ , which is a surface of constant  $z = \beta^{-1}$ , and the Poincaré horizon at  $y = 1$ , and so they are particularly useful coordinates to search for solutions in the RSII bulk. Indeed, these were the coordinates used in [149] to find a static RSII black hole. Figure 3.1 shows a sketch of the coordinate domain of the static RSII black hole. Horizontal and vertical lines are constant  $z$  and  $r$  surfaces, respectively, whereas the blue curves are curves of constant  $y$ .

To obtain an *Ansatz* for the static RSII black hole, the metric (3.4) was adapted to include a bifurcating Killing horizon at  $y = 0$  (this is done by moving the factor of  $y^2$  multiplying the  $dy^2$  term in (3.4) to instead be multiplying the  $dt^2$  term), and adding unknown functions multiplying each term in the metric, whilst ensuring that the metric remains spherically symmetric and static.

In our case, we are seeking a rotating black hole solution, which will be neither spherically symmetric nor static. However, we do assume it will be stationary, axisymmetric (with associated Killing vector fields  $\partial_t$  and  $\partial_\phi$ , respectively) and symmetric under the transformation of simultaneously flipping the signs of both  $t$  and  $\phi$ . The most general *Ansatz* that is consistent with these symmetries and that possesses a

bifurcating Killing horizon at  $y = 0$  is given by

$$\begin{aligned}
ds^2 = \frac{\ell_5^2}{\Delta(x, y)^2} & \left\{ -\frac{h(y)^2 y^2 P(y)}{A(y, \xi)} F_1 dt^2 + \frac{4F_2}{P(y)h(y)^2} dy^2 + \frac{4x^2 g(x) F_3}{2 - \xi^2} \left( d\xi + \frac{F_7}{xh(y)} dy \right)^2 \right. \\
& + (1 - \xi^2)^2 S(x, y, \xi) x^2 g(x) F_4 \left( d\phi + y^2 W(y, \xi) F_6 dt \right)^2 \\
& \left. + \frac{4F_5}{g(x)} \left( dx + \frac{F_8}{h(y)} dy + F_9 d\xi \right)^2 \right\}. \tag{3.5}
\end{aligned}$$

where the coordinate  $\xi$  measures the inclination from the equatorial plane and, in pure AdS<sub>5</sub>, is related to the usual polar angle,  $\theta$ , on the  $S^2$  via  $\xi(2 - \xi^2)^{1/2} = \cos\theta$ . The coordinates not associated to any isometries run over the cube  $\{x, y, \xi\} \in (0, 1)^3$ . A constant  $\xi$  slice of this coordinate domain will resemble Figure 3.1. We will describe each of these boundaries of this cube momentarily. The functions  $A$ ,  $P$ ,  $S$  and  $W$  depend upon a parameter  $\alpha$  which measures the rotation of the black hole and are given by

$$A(y, \xi) = 1 + h(y)^2 \alpha^2 (2 + \alpha^2 - y^2 (1 + \alpha^2 - \xi^2 (2 - \xi^2) (1 - h(y) \alpha^2))) \tag{3.6a}$$

$$P(y) = 1 - h(y) \alpha^2 \tag{3.6b}$$

$$S(x, y, \xi) = \frac{1 + h(y)^2 \alpha^2 x^2 (2 + \alpha^2 x^2 - y^2 (1 + \alpha^2 x^2 - \xi^2 (2 - \xi^2) (1 - h(y) \alpha^2 x^2)))}{(1 + h(y)^2 \xi^2 (2 - \xi^2) \alpha^2 x^2)^2} \tag{3.6c}$$

$$W(y, \xi) = \frac{3 - 3y^2 + y^4 + h(y)^2 (1 + \xi^2 (2 - \xi^2)) \alpha^2 - h(y)^3 \xi^2 (2 - \xi^2) \alpha^4}{1 + h(y)^2 \alpha^2 (2 + \alpha^2 - y^2 (1 + \alpha^2 - \xi^2 (2 - \xi^2) (1 - h(y) \alpha^2)))}, \tag{3.6d}$$

where, recall,  $h(y) = 1 - y^2$ . The functions  $F_i(x, y, \xi)$  for  $i = 1, \dots, 9$  are unknown; it is these functions that we must determine numerically in order to obtain the metric of the rotating RSII black hole. Note that this *Ansatz* reduces to that used to obtain the static RSII black hole of [149] by taking  $F_3 = F_4$  and  $F_6 = F_7 = F_9 = \alpha = 0$ .

In order to find the  $F_i$  functions, we use the numerical methods described in Chapter 2. Specifically, we solve the Einstein-DeTurck equation which now yields nine elliptic PDEs for the nine unknown  $F_i$  functions. We choose the reference metric to be

given by the *Ansatz*, with

$$F_i(x, y, u) = \begin{cases} 1 & \text{for } 1 \leq i \leq 5 \\ \frac{\alpha}{1+\alpha^2} & \text{for } i = 6 \\ 0 & \text{for } 7 \leq i \leq 9. \end{cases} \quad (3.7)$$

This reference metric has a horizon at  $y = 0$ . Let us quickly consider properties of this horizon, such as its temperature and angular velocity, since the horizon of the full solution will necessarily inherit the same values of those quantities. We wish to evaluate the quantities in terms of an asymptotic observer living on the brane, *i.e.* at  $x = 1$  and  $y = 1$ . This requires rescaling the time coordinate by taking  $t = T/(\ell_5\beta)$ . From the metric we can immediately read off the angular velocity of the horizon, measured in units of  $T$ :

$$\Omega_H = \frac{\alpha}{\ell_5\beta(1+\alpha^2)}. \quad (3.8)$$

To obtain the temperature we must investigate the near horizon geometry a little closer. Taking the transformation

$$y = \frac{\sqrt{1-\alpha^2}(\beta(1-x^2)+1)}{2\beta\ell_5}\rho, \quad (3.9)$$

and then expanding near the horizon, one finds that the reference metric becomes

$$d\bar{s}^2 = -(\kappa^2\rho^2 + \mathcal{O}(\rho^3))dt^2 + (1 + \mathcal{O}(\rho))d\rho^2 + \dots, \quad (3.10a)$$

where the  $\dots$  denotes the other components of the metric and  $\kappa$  is the surface gravity,

$$\kappa = \frac{1-\alpha^2}{2\ell_5\beta(1+\alpha^2)}. \quad (3.10b)$$

As usual we can calculate the temperature by Wick rotating to Euclidean time, noting the Euclidean time must have a certain periodicity in order for the metric to be smooth, and then associating this periodicity with the inverse temperature. Specifically, the Hawking temperature is given by

$$T_H = \frac{1}{2\pi}\kappa = \frac{1-\alpha^2}{4\pi\ell_5\beta(1+\alpha^2)}. \quad (3.11)$$

The full solutions to the Einstein equations will inherit these values of the temperature and angular velocity from the reference metric. They also provide clarification regarding the meaning of the two parameters of the metric,  $\alpha \in (0, 1)$  and  $\beta \in (0, \infty)$ . The *rotation parameter*,  $\alpha$ , controls the rotation of the black hole, with  $\alpha = 1$  being an extremal black hole and  $\alpha = 0$  the static braneworld black hole of [149]. The size of the black hole relative to the AdS length scale  $\ell_5$  is in turn controlled by the *length parameter*,  $\beta$ . Note that the ratio  $\Omega_H/T_H$  is independent of  $\beta$  and  $\ell_5$ , and it is this quantity we fix when comparing different black holes of the same rotation but of different sizes relative to  $\ell_5$ .

### 3.2.2 Boundary conditions

Via the DeTurck method, we have obtained an elliptic set of nine coupled PDEs defined on the cube  $\{x, y, \xi\} \in (0, 1)^3$ , in terms of the nine unknown functions,  $F_i$ . In order to have a well-defined boundary value problem we need to set nine boundary conditions on each of the six faces.

Firstly, let us consider the fictitious boundaries of our domain at each of which the conditions are given by requiring regularity of the metric at the boundary. At the axis of symmetry where the  $S^2$  shrinks to zero size,  $x = 0$ , we require that

$$\begin{aligned}\partial_x F_i(0, y, \xi) &= 0 \quad \text{for } 1 \leq i \leq 6 \\ F_i(0, y, \xi) &= 0 \quad \text{for } 7 \leq i \leq 9.\end{aligned}\tag{3.12}$$

At the bifurcating Killing horizon,  $y = 0$ , we have that

$$\begin{aligned}\partial_y F_i(x, 0, \xi) &= 0 \quad \text{for } 1 \leq i \leq 6 \text{ or } i = 9 \\ F_i(x, 0, \xi) &= 0 \quad \text{for } 7 \leq i \leq 8.\end{aligned}\tag{3.13}$$

The boundary conditions on the equatorial plane,  $\xi = 0$ , are given by

$$\begin{aligned}\partial_\xi F_i(x, y, 0) &= 0 \quad \text{for } 1 \leq i \leq 6 \text{ or } i = 8 \\ F_i(x, y, 0) &= 0 \quad \text{for } i \in \{7, 9\}.\end{aligned}\tag{3.14}$$

Finally, at the north pole,  $\xi = 1$ , we require that

$$\begin{aligned}\partial_\xi F_i(x, y, 1) &= 0 \quad \text{for } i \in \{1, 2, 4, 5, 6, 8\} \\ F_i(x, y, 1) &= 0 \quad \text{for } i \in \{7, 9\} \\ F_3(x, y, 1) &= F_4(x, y, 1).\end{aligned}\tag{3.15}$$

At the  $y = 1$  boundary, we require that the metric approaches the Poincaré horizon of AdS<sub>5</sub>, that is, far away from the black hole, the metric tends asymptotically towards the same geometry as the vacuum RSII solution. In order to do this, we set the metric to be equal to the reference metric, given by (3.7), at this boundary. Since  $A$ ,  $P$ ,  $S$  and  $W$  are all equal to one at  $y = 1$ , note that this boundary condition means the metric matches (3.4) as  $y \rightarrow 1^-$  after the identification,  $d\varphi = d\phi + \alpha/(1 + \alpha^2) dt$ .

Finally, we have to consider boundary conditions on the brane,  $x = 1$ . Recall that in the RSII model there is a  $\mathbb{Z}_2$  symmetry across the brane. However, the fact that the stress tensor, including the tension of the brane itself, is concentrated to the brane leads to discontinuities in the solution. These discontinuities are described by the *Israel junction conditions* [169], which, in this case where there is no matter on the brane, yield the following condition:

$$0 = K_{ab} - K\gamma_{ab} + \frac{3}{\ell_5}\gamma_{ab},\tag{3.16}$$

where,  $\gamma_{ab}$  is the induced metric on the brane and  $K_{ab} = \gamma_{ac}\nabla^c n_b$  is the extrinsic curvature, with  $n_b$  being the inward unit normal to the brane. These provide six conditions at the brane. We additionally impose that the component of the DeTurck vector normal to the brane is zero, *i.e.*  $\xi_x = 0$ , and that  $F_8 = F_9 = 0$ , comprising a total of nine boundary conditions.

Note that the reference metric satisfies all of these boundary conditions. However, it should be noted that due to the rotation of the black holes, the solutions contain an ergoregion, meaning that the Killing vector field is not timelike in the entirety of the exterior of the black hole. Hence, this case does *not* satisfy the assumptions of any proof forbidding Ricci solitons, and so, *a priori*, there is no guarantee that the solutions to the Einstein-DeTurck equations will also be solutions to the Einstein equation. However, we were able to find solutions to the Einstein-DeTurck equation by discretizing onto a Chebyshev-Gauss-Lobatto grid and using the Newton-Raphson method, as described in Section 2.3. To inspect the validity of the solutions, we then check that the DeTurck vector is small and tending towards zero in the continuum

limit, suggesting we have a true solution to the Einstein equation. These convergence tests are shown in Appendix A.1.

### 3.3 Properties of the braneworld black holes

We were able to find solutions with the rotation parameter,  $\alpha$ , running from zero rotation to near extremality, and the length parameter,  $\beta$ , in a range of values, chiefly within an order or two of magnitude of unity. Our results clearly show that for large  $\beta$  our solutions exhibit four-dimensional behaviour, with their induced metric on the brane appearing to approach that of the Kerr metric with the same  $\Omega_H/T_H$ . Meanwhile, for small  $\beta$  the black holes show five-dimensional behaviour, and approach five-dimensional Myers-Perry black holes [96] with a single non-zero rotation parameter, again with the same  $\Omega_H/T_H$ . This behaviour can be glimpsed by investigating the properties of the braneworld black holes, a few of which we describe here.

#### 3.3.1 Entropy of the horizon

Firstly, in Figure 3.2 we plot the area (which is proportional to the entropy) of the bifurcating Killing horizon of the rotating RSII in the five-dimensional bulk against their proper radius on the brane,  $\rho_H$ , in a log-log plot. This proper radius is computed by dividing the proper distance around the equator of the intersection of the black hole horizon and the brane by  $2\pi$ . In each subfigure in Figure 3.2, the rotation parameter,  $\alpha$ , (or, equivalently  $\Omega_H/T_H$ ) is fixed, and the length parameter,  $\beta$ , varies between the different braneworld black holes (the black dots). For reference, we have also added the corresponding plots for the four-dimensional Kerr black hole (the dotted, red line), and the five-dimensional single-rotation Myers-Perry black hole (the dashed, green line), each with the same  $\Omega_H/T_H$ . Moreover, we have scaled each axis by the appropriate powers of the AdS length,  $\ell_5$ , to ensure we are comparing dimensionless quantities.

The small braneworld black holes exhibit five-dimensional behaviour, tending towards the Myers-Perry area, which is cubic in terms of  $\rho_H$ . This means that as the black holes become small, they extend roughly the same proper distance into direction perpendicular to the brane as those transverse to it. On the other hand, the large braneworld black holes exhibit four-dimensional behaviour, tending to the Kerr area, which is quadratic in terms of  $\rho_H$ . Therefore, in this limit, the braneworld black holes become flattened in line with the brane, extending very little into the extra dimension normal to the brane relative to the directions along the brane.

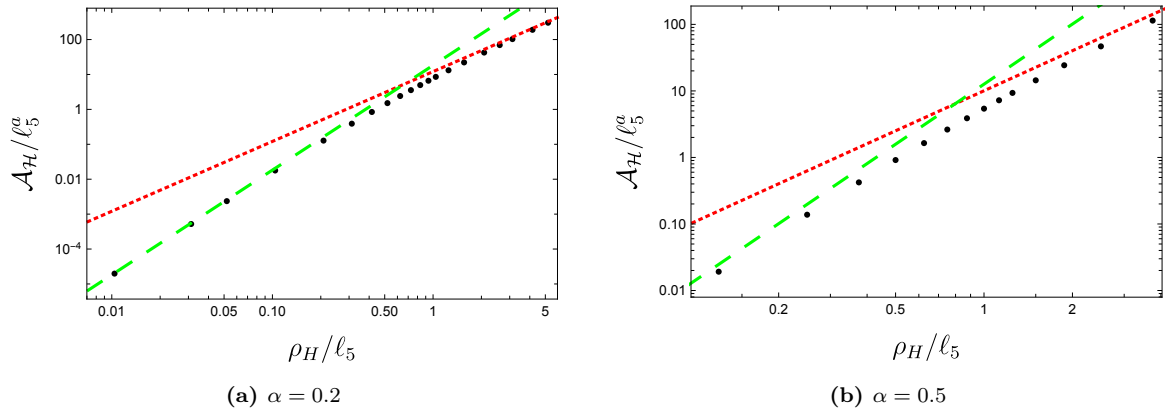


**Fig. 3.2:** The area of the bifurcating Killing surface of rotating RSII black holes, with fixed  $\alpha$  (or, equivalently  $\Omega_H/T_H$ ) as a function of the proper radius  $\rho_H$  (black dots) in a log-log plot. The dotted, red line is the area of a four-dimensional Kerr black hole, whilst the dashed, green line is the area of a five-dimensional single rotating Myers Perry black hole, both of which have the same  $\Omega_H/T_H$ . We have divided the quantities on both axes by powers of  $\ell_5$  to make them dimensionless, for example on the  $y$ -axis, we have  $\mathcal{A}_H/\ell_5^a$  where  $a = 3$  for both the RSII black holes and the Myers-Perry black holes, whereas  $a = 2$  for the Kerr black holes.

We see this behaviour particularly well for small values of  $\alpha$ , for example  $\alpha = 0.2$  in Subfigure 3.2a. The numerics became more and more difficult as  $\alpha$  was increased, particularly for relatively small or large  $\beta$ , and hence the trend is less clear for larger  $\alpha$ , as seen in Subfigure 3.2b where  $\alpha = 0.5$ . However, even for large  $\alpha$ , the data is still consistent with this transition between four-dimensional and five-dimensional behaviour of areas.

### 3.3.2 Geometry of the bifurcating Killing horizon

To explore a little more closely the behaviour of the braneworld black holes in the limit where they become large we also consider the induced geometry of the braneworld bifurcating Killing surface. That is, we consider the 2d geometry obtained by taking the intersection of the brane ( $x = 1$ ) and the event horizon ( $y = 0$ ) at a constant time slice. We retain the axisymmetry of the solution in the  $\phi$  direction, and hence we are considering an axisymmetric 2d geometry, parameterised by  $\xi$  and  $\phi$ .

Two-dimensional geometries are completely determined by the Ricci scalar, and hence such an axisymmetric 2d is determined by the Ricci scalar as a function of the inclination from the axis of symmetry. This geometry has spherical topology, and so each constant  $\xi$  slice is a circle. Of course, the coordinate  $\xi$  is not a gauge invariant quantity. In order to express the inclination in a gauge independent way, we introduce the function  $\rho(\xi)$  which measures the proper radius of the circle at fixed  $\xi$ , which once

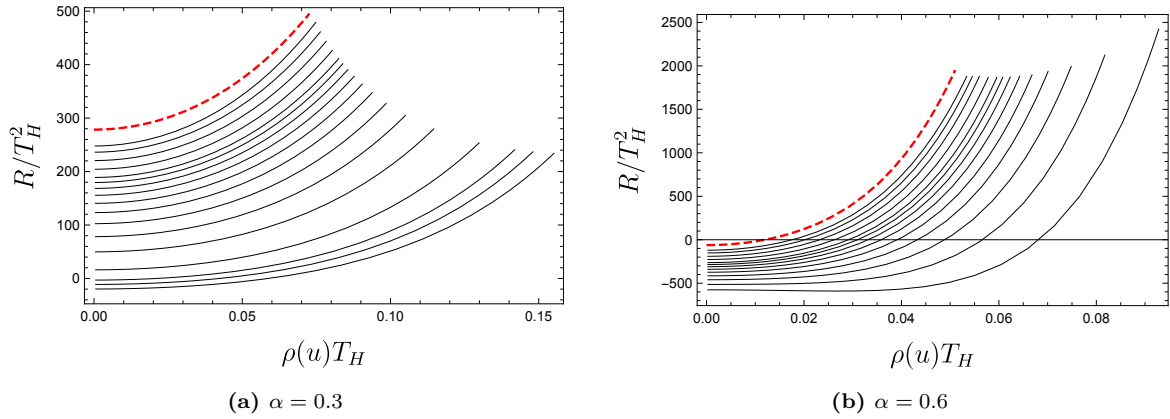


**Fig. 3.3:** The Ricci scalar,  $R$ , of the two-dimensional induced geometry of the intersection of the event horizon with the brane at a constant time slice is plotted against  $\rho(\xi)$ , which is the proper radius of the circle in the geometry at a given value of  $\xi$ , the inclination from the axis of symmetry. Quantities on both axes have been multiplied by the suitable powers of the temperature,  $T_H$ , to make them dimensionless. Such a plot uniquely determines a two-dimensional axisymmetric geometry. The plots for the braneworld black holes for a fixed value of  $\alpha$  (or, equivalently  $\Omega_H/T_H$ ) are given by solid, black curves and the corresponding plot for a four-dimensional Kerr black hole, with the same  $\Omega_H/T_H$ , is given by the dashed, red curve. The braneworld curves closest to the Kerr line are those with largest length parameter,  $\beta$ , with this parameter decreasing monotonically as one moves between the curves from left to right.

again is found by dividing the proper distance around these circles by  $2\pi$ . Therefore, at the north pole,  $\rho(\xi = 1) = 0$ , and  $\rho(\xi)$  increases as  $\xi$  decreases.

In Figure 3.3 we plot the Ricci scalar as a function of  $\rho(\xi)$  over  $\xi \in (0, 1)$  for each of the braneworld black holes (solid, black lines) for a fixed value of  $\Omega_H/T_H$ , along with the corresponding plot for the Kerr black hole (dashed, red line). Here, and for the remainder of the chapter, we multiply the quantities of both axes by the required factors of the temperature,  $T_H$ , to make them dimensionless. Such a plot uniquely determines the geometry of a two-dimensional axisymmetric manifold with spherical topology. In each of the two subfigures in Figure 3.3, the length parameter,  $\beta$ , is decreasing as one moves from left to right between the different black curves. The curves approach that of the Kerr black hole as  $\beta$  becomes large, adding further evidence that the induced geometry on the brane of braneworld black holes approaches the Kerr geometry as they become large.

### 3.3.3 Orbits

Another interesting quantity that allows for comparison to Kerr is the position of the (equatorial) inner-most stable circular orbit (ISCO) around the black hole. We consider the motion of a particle that is restricted to the brane, at  $x = 1$ , and the equatorial

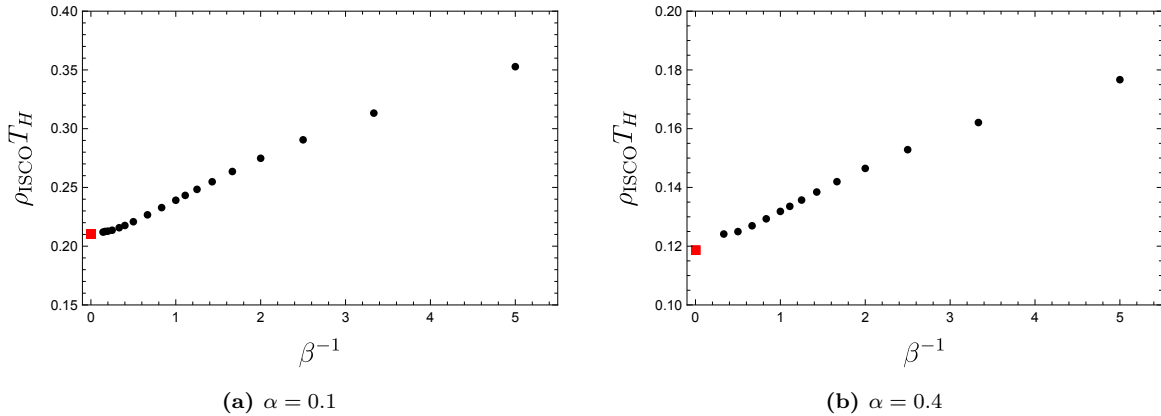


**Fig. 3.4:** Plots of the proper radius,  $\rho_{ISCO}$ , of the ISCO for braneworld black holes for a given value of  $\alpha$  (or, equivalently  $\Omega_H/T_H$ ) against  $\beta^{-1}$  (black dots). We have added the corresponding value for the Kerr black hole with the same value of  $\Omega_H/T_H$  at  $\beta^{-1} = 0$  (red square). We have multiplied  $\rho_{ISCO}$  by the temperature,  $T_H$ , of the black holes to obtain a dimensionless quantity.

plane of the rotation of the black hole, at  $\xi = 0$ . Both of these planes lie at the centre of a  $\mathbb{Z}_2$  symmetry, and so any geodesic that starts with motion within this region will remain within it. Just as in the calculation of the ISCO in the Kerr or Schwarzschild black holes, we can use the fact that there are conserved quantities along the path of such a geodesic. In particular, we have two conserved quantities associated to the two Killing vector fields: the energy,  $E$  and the angular momentum,  $h$ . As usual, the use of these allows one to find an ordinary differential equation that governs the radial profile of a normalised timelike geodesic. In our coordinates, this is an equation for the position  $y(t)$  of the particle, which can be written as  $\dot{y}(t)^2 = V(y; E, h)$ .

In order to find the ISCO, we require that  $V = V' = 0$ , where the derivative is with respect to  $y$ . These two equations can be solved to give a family of circular geodesics depending on  $(E, h)$ . From this family, the ISCO will be the solution with the minimal angular momentum (minimising with respect to the energy gives similar results). We computed the proper radius  $\rho_{ISCO}$  of the ISCO, which once again is the proper distance around the circumference of the orbit divided by  $2\pi$ , and multiplied by the temperature,  $T_H$ , to get a dimensionless quantity.

In Figure 3.4, we plot the value of  $\rho_{ISCO} T_H$  against  $\beta^{-1}$  for two fixed values of the rotation parameter,  $\alpha$ . The reason for using the inverse of the length parameter,  $\beta$ , on the  $x$ -axis is that we expect that in the large  $\beta$  limit, the braneworld black hole tends towards a Kerr geometry. Kerr black holes do exhibit stable circular orbits, thus we have added, for reference, the value for  $\rho_{ISCO} T_H$  of a Kerr black hole of the same  $\Omega_H/T_H$  at  $\beta^{-1} = 0$  as a red square in the figure.

We see that the value of the ISCO of the braneworld black hole tends to the value for the Kerr black hole as they become large. On the other hand, as  $\beta$  decreases the proper radius of the ISCO increases. Note that, five-dimensional black holes do not contain bound orbits for timelike particles, and we find that the value of  $\rho_{ISCO}T_H$  begins to increase as  $\beta$  becomes smaller, where the black holes begin to exhibit five-dimensional behaviour. It would be of great interest to obtain braneworld black holes with much smaller values of  $\beta$ , which more and more exhibit five-dimensional behaviour to see if the value of  $\rho_{ISCO}T_H$  diverges as  $\beta$  tends towards zero.

### 3.4 Discussion

The results presented in the previous section provide compelling evidence that the induced geometry of the rotating RSII black holes on the brane tends to that of the Kerr metric in the large  $\beta$  limit. This is a necessary requirement for the Randall-Sundrum II model to phenomenologically viable, since the astrophysical black holes observed in our Universe appear to be very well described by the Kerr metric.

However, we also see evidence that, as one takes  $\beta$  to be smaller, the black holes transition to having five-dimensional behaviour. As a result of this transition, one would expect finitely-sized rotating black holes in the RSII model to have slightly different induced geometry on the brane to the standard four-dimensional Kerr black holes of general relativity. Hence, this could provide a stepping-stone to putting constraints upon a Randall-Sundrum extra dimension via astrophysical measurements.

It should be noted, however, that there are still many more steps that would need to be taken before this is a realistic possibility. Table-top experiments have probed corrections to Newtonian gravity of the form (1.54) induced by a Randall-Sundrum extra dimension and constrained the AdS length scale,  $\ell_5$ , in the RSII model to be at most about the order of a millimetre [170]. Astrophysical black holes are of course many orders of magnitude large than this, and so, in order to test the RSII model using astrophysical black holes, one would firstly have to extend our results to find rotating black holes in the RSII model for much larger values of the length parameter,  $\beta$ . Unfortunately, the numerical method used to obtain these solutions became extremely slow for large  $\beta$ , however, it is possible that using a different reference metric in the DeTurck method may ease the computation. Alternatively, the method used in [150] perhaps provided a more natural way of finding large static RSII black holes by directly perturbing away from a black droplet solution (which in a sense is the  $\beta \rightarrow \infty$  limit of a static RSII black hole), and so if one generalised this method to the rotating case,

one may be able to find rotating RSII black holes for larger values of  $\beta$  than in this work.<sup>1</sup>

Furthermore, this work has provided evidence that, even if one did obtain these very large RSII black holes, their induced metric on the brane would be extremely similar to the Kerr metric. Therefore, one would need to find much more finely-grained features of the RSII black holes, in order to provide sharper comparison to the Kerr black hole. For example, it would be very interesting to calculate the quasi-normal modes of the braneworld black holes, which may allow for comparison to data from gravitational wave detectors.

Another possibility of using these black holes to experimentally test the RSII model would arise if, as is hoped, microscopic black holes were produced in future particle colliders, such as the International Linear Collider [90, 91] and the Compact Linear Collider [92]. As shown in this work, such small black holes would be very likely to exhibit five-dimensional behaviour if there were a Randall-Sundrum extra dimension, and hence they would provide an excellent testing ground for constraining the Randall-Sundrum II model.

Another further point of study could be to examine the superradiance instability of the RSII black holes. We did obtain the ergoregion of the rotating RSII black holes in the five-dimensional bulk and found in each case that the region has spherical topology. It would be interesting to investigate whether the slightly different geometries of the braneworld black hole ergoregions compared to that of Kerr could result in different superradiance instabilities [171, 172].

It would also be of great interest to study further the rotating RSII close to extremality,  $\alpha \rightarrow 1$ . One reason for that it has recently been shown that effective field theory corrections to general relativity generically lead the horizons of rotating black holes becoming singular in the extremal limit [158, 173, 174]. In these cases, all scalar curvature invariants are non-singular, but the tidal forces felt by infalling observers were found to diverge at the horizon in the extremal limit. The effective equations on the brane are given by the Einstein equation with some complicated correction term and hence one may expect that the RSII black holes should have diverging tidal forces as one approaches extremality. We found that the tidal forces, as measured by a four-dimensional observer falling through the horizon, increase more quickly with the rotation parameter,  $\alpha$ , than is the case for standard Kerr black holes, but the evidence is inconclusive on whether these forces are truly diverging as  $\alpha \rightarrow 1$ . This

---

<sup>1</sup>Indeed, we were able to find rotating black droplets, which have a Kerr metric on the boundary, by a very similar method as described in this chapter, though this work remains unpublished. These would be the starting point of finding large  $\beta$  rotating RSII black holes by generalising [150].

leaves it highly desirable to study more quickly rotating solutions, or even analysing the extremal limit directly, as was done for extremal charged RSII black holes [175].

Finally, in this work we have considered the exterior geometry of these rotating RSII black holes, but it would be extremely interesting if one could explore the interiors of the solutions. The Kerr black hole contains an inner, Cauchy horizon, however, it has been shown in various cases that when gravity is coupled to other fields, the inner horizon of a charged black hole can “collapse” [176–178], in accordance with the strong cosmic censorship conjecture [22], leaving a hairy black hole solution that does not possess a Cauchy horizon before the singularity. It is postulated that similar behaviour may occur for the Cauchy horizon within a rotating black hole when gravity is coupled to other fields. Following from the connection to the AdS/CFT correspondence reviewed in Section 1.5.3, we know that the five-dimensional RSII rotating black hole is dual to a four-dimensional rotating black hole whose geometry is quantum-corrected by a large  $N$ , strongly coupled CFT. Therefore, one may conjecture that such a quantum-corrected black hole does not possess an inner horizon, and that the dual bulk RSII black hole would also be free of a Cauchy horizon in its interior. It would be very interesting, though extremely numerically challenging, to check directly whether this is indeed the case.

# Chapter 4

## Black tunnels and hammocks

### Abstract

We construct the holographic duals to a large  $N$ , strongly coupled,  $\mathcal{N} = 4$  super Yang-Mills conformal field theory defined on a four-dimensional de Sitter-Schwarzschild background. There are two distinct five-dimensional bulk solutions. One, named the black tunnel, is static and possesses two disconnected horizons. The other, the black hammock, contains only one horizon in the bulk. The hammock horizon is not a Killing horizon, and hence possesses interesting properties, such as non-vanishing expansion and shear, as well as allowing classical flow along it. The DeTurck method was used in order to attain the black tunnel solutions, whilst the black hammocks were found in Bondi-Sachs gauge. This work was first presented in [2].

### 4.1 Introduction

One of the most fascinating results in theoretical physics was the discovery of Hawking radiation — that quantum fields radiate on fixed black hole backgrounds [80]. Famously, this phenomenon leads to the information paradox [83], posing deep and fundamental questions about the way a theory of quantum gravity must behave. However, for the most part, the study of Hawking radiation and, more generally, quantum field theory in curved spacetime has been focused on free or weakly interacting fields. A natural question is to ask whether taking the quantum fields to be strongly coupled affects the way they behave on a curved background, though the two difficulties of strong coupling and curved space make it extremely challenging to make any headway tackling this problem via first-principles field theory calculations.

Fortunately, gauge/gravity duality has provided an approach to study precisely such a system. The AdS/CFT correspondence [109–111] describes a duality between an  $\mathcal{N} = 4$  super Yang-Mills (SYM) conformal field theory (CFT) on a fixed, but possibly curved, manifold  $\mathcal{B}$  and type IIB string theory on an asymptotically locally anti-de Sitter (AlAdS) spacetime which has conformal boundary given by  $\mathcal{B}$ . Taking the limit where the CFT possesses a large number of colours,  $N$ , and is strongly coupled (specifically taking the 't Hooft coupling to infinity) corresponds to taking a classical limit on the gravitational side. Hence, in order to study how such a large  $N$ , strongly coupled CFT behaves on a manifold  $\mathcal{B}$ , one can find AlAdS solutions to the Einstein equation with conformal boundary  $\mathcal{B}$ . See, for example, [127] for an excellent review on this method.

Much work has been done in the case where the boundary metric  $\mathcal{B}$  is taken to be the Schwarzschild metric [129–135, 137, 165]. As reviewed in Section 1.4, two classes of gravitational duals have been found. One family of solutions are called black droplets, which contain two, disconnected horizons in the bulk: a horizon which extends from the boundary black hole and a perturbed planar black hole deep within the bulk. The other class are called black funnels, and these contain a single, connected horizon in the bulk which extends from the horizon of the boundary black hole into the bulk and into an asymptotic region.

The two solutions correspond to different phases of the CFT on the Schwarzschild background. The connected, funnel solution corresponds to a *deconfined* phase. In the bulk, the single horizon allows flow along it at a classical level (it is a non-Killing horizon, evading rigidity theorems due to its non-compact nature), meaning that on the field theory side there is Hawking radiation from the horizon to the asymptotic region of order  $\mathcal{O}(N^2)$ . On the other hand, the disconnected, droplet solution corresponds to a *confined* phase; there is no classical flow between the two bulk horizons, meaning that on the field theory side the Hawking radiation of the CFT is greatly suppressed to  $\mathcal{O}(N^0)$ . If one were to instead excite  $N^2$  free fields on a black hole background, one would always expect  $\mathcal{O}(N^2)$  radiation from the horizon, and hence, this confined phase is a novel property of strongly coupled fields. The field theory mechanism behind this behaviour is still not well understood.

In such a set up, one can dial the temperature,  $T_H$ , of the boundary black hole and the temperature,  $T_\infty$ , of the limiting thermal CFT at infinity. It is interesting to investigate which of these phases dominates across values of the dimensionless parameter  $T_\infty/T_H$ . In [135], evidence was provided that for small values of  $T_\infty/T_H$ ,

the droplet phase dominates, whilst for large values of  $T_\infty/T_H$ , the funnels phase dominates.

In this chapter, we investigate a similar set-up, this time considering the holographic duals to a large  $N$ , strongly coupled CFT on a de Sitter-Schwarzschild background. There are two horizons in the de Sitter-Schwarzschild spacetime, the event horizon and the cosmological horizon, which have different temperatures (except at extremality). This background provides a very natural set-up in which to investigate the phases of the CFT, since rather than having to impose that the CFT is in some unphysical thermal state asymptotically, here the geometry naturally imposes that the two horizons radiate with given temperatures.

The space of such de Sitter-Schwarzschild geometries (up to an overall scale) is parameterized by the ratio between the temperatures of the two horizons, or equivalently, by the ratio of the radii of the horizons,  $\rho_h = r_h/r_c \in (0, 1)$ , where  $r_h$  and  $r_c$  are the proper radii of the event and cosmological horizons, respectively. Throughout this chapter, we will refer to the parameter,  $\rho_h$ , as the *radius ratio*. Note that  $\rho_h$  is gauge invariant in this context, due to the background spherical symmetry of the de Sitter-Schwarzschild black hole.

Once again, two dual bulk solutions arise, depending on whether the boundary horizons are connected via a bulk horizon or not. The *black tunnel* is a solution in which there are two disconnected bulk horizons, one of which extends from the boundary event horizon and the other from the boundary cosmological horizon. Each of these horizons closes in on itself some way into the bulk. In the other solution, which we call the *black hammock*, the boundary event horizon and boundary cosmological horizons are connected by a single horizon in the bulk. See Figure 4.1 for schematic drawings of these two geometries. Similarly to the black funnels (and other flowing, non-equilibrium steady state solutions [179–187]), the black hammocks allow classical flow along their horizons, which again is dual to a deconfined phase of the CFT, with  $\mathcal{O}(N^2)$  Hawking radiation on the field theory side of the duality. There is no classical flow between the two horizons of the black tunnel, so this is dual to a confined phase of the CFT fields with  $\mathcal{O}(N^0)$  Hawking radiation.

It would be of great interest to investigate which of these solutions dominates for different values of the radius ratio,  $\rho_h$ , since this would be dual to which phase of the CFT matter is dominant on the field theory side. One would expect a similar phase transition to that of the droplets and funnels, as evidenced by [135]. For a number of reasons, which we will discuss, this problem is difficult and may require

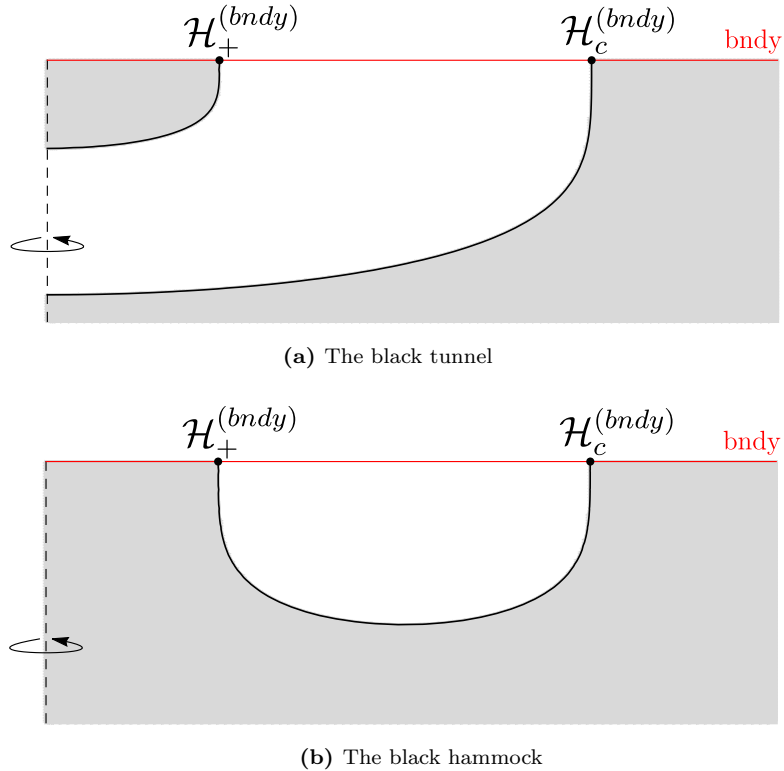


**Fig. 4.1:** Some schematic drawings of spatial cross-sections of the black tunnel and hammock after suppressing two angular directions. In each case the dotted line is the axis of symmetry where the  $S^2$  shrinks to zero size. The hammocks only have one horizon which doesn't cross the axis of symmetry, whereas the tunnels have two horizons both of which cross the axis of symmetry. In each diagram, the red line is the conformal boundary, on which there is a de Sitter-Schwarzschild geometry.

direct calculation of the stability of the solutions under time-evolution after a small perturbation.

Another point of interest is that the black tunnel and black hammock solutions are closely related to black hole solutions in the Randall-Sundrum II (RSII) model [142]. Following the methods used in [149, 1] to find other RSII black hole solutions, discussed in Chapter 3, one could envisage adapting the black tunnels in order to find black hole solutions in the RSII model where one takes a positive effective cosmological constant on the brane. Such solutions would be dual to spherically symmetric four-dimensional black holes with a positive cosmological constant that receive “quantum corrections” from a large  $N$ , strongly coupled CFT.

We used different gauge choices in order to solve the Einstein equation numerically for the two different solutions. For the black tunnels, we used *the DeTurck method* [162, 152, 153], reviewed in Section 2.1. It turns out in this case that the added term

must actually vanish on any solution, hence we necessarily obtain a solution to the Einstein equation rather than a Ricci soliton.

One could also use the DeTurck method to find the black hammock solutions, and indeed we were able to do so, but we found that we had to use an extremely high number of lattice points and precision in the numerical method in order to extract the quantities of interest from the solutions, making the process extremely computationally expensive. Instead, we found that a different gauge choice, specifically *Bondi-Sachs gauge*, was a lot more effective. The use of this gauge to solve stationary problems was reviewed in Section 2.2. Indeed, it seems as though Bondi-Sachs gauge is particularly well-adapted to stationary problems with a null hypersurface in the bulk “opposite” the conformal boundary, and so is useful for finding black hammock solutions. The use of the two complementary methods allowed us to find both solutions for a large range of the parameter space  $\rho_h \in (0, 1)$ . This work, first presented in [2], was the first instance where flowing solutions were found by solving a boundary value problem in Bondi-Sachs gauge.

One additional benefit of finding the black hammocks in Bondi-Sachs gauge is that it is a very natural gauge in which to time-evolve the solutions after a slight perturbation. Hence, it could provide a way to directly test the dynamical stability of the hammocks across the parameter space.

In Sections 4.2 and 4.3 we present the methods used to find the black tunnels and black hammocks, respectively, and we extract the holographic stress tensor from the bulk solution in each case. In Section 4.4, we discuss some of the properties of the solutions. The hammocks have particularly interesting properties due to the fact their horizon are non-Killing. This means there is classical flow along the horizon and the expansion and shear of the horizon are non-zero. In Section 4.5, we end with a discussion focusing particularly on the difficulties of deducing which of the black tunnel or black hammock solution, and hence which phase of the dual CFT, dominates for a given value of the radius ratio,  $\rho_h$ . This difficulty arises from the fact that, despite the two solutions being stationary, neither of them is in thermodynamic equilibrium. We argue that in order to obtain the phase diagram of the dual CFT, one would have to directly investigate the stability of the two dual solutions.

## 4.2 Black tunnels

In order to find the black tunnel solutions we used the DeTurck method, which was described in Section 2.1. The solutions are five-dimensional, and the Einstein-DeTurck

equation in this dimensionality is given by

$$R_{ab} + \frac{4}{\ell^2} g_{ab} - \nabla_{(a} \xi_{b)} = 0, \quad (4.1)$$

with  $\xi^a$  denoting the DeTurck vector defined by (2.4b) in terms of a reference metric which we will soon choose explicitly.

### 4.2.1 Ansatz for the black tunnels

We assume the solutions will be static and spherically symmetric. On the conformal boundary, which we set at  $y = 0$ , we will enforce the metric to be conformal to that of de Sitter-Schwarzschild. In the bulk there will be two disconnected horizons, one emanating from the event horizon on the boundary and the other from the cosmological horizon. We'll call these the bulk event horizon (at  $x = 0$ ) and bulk cosmological horizon (at  $x = 1$ ), respectively. Finally, between the two horizons in the bulk, there will be an axis where the  $S^2$  shrinks to zero size, given by  $y = 1$ . Hence, the black tunnels naturally live in a rectangular coordinate domain,  $\{x, y\} \in (0, 1)^2$ . In Figure 4.2, we've drawn the tunnel again schematically, along with the integration domain that naturally arises.

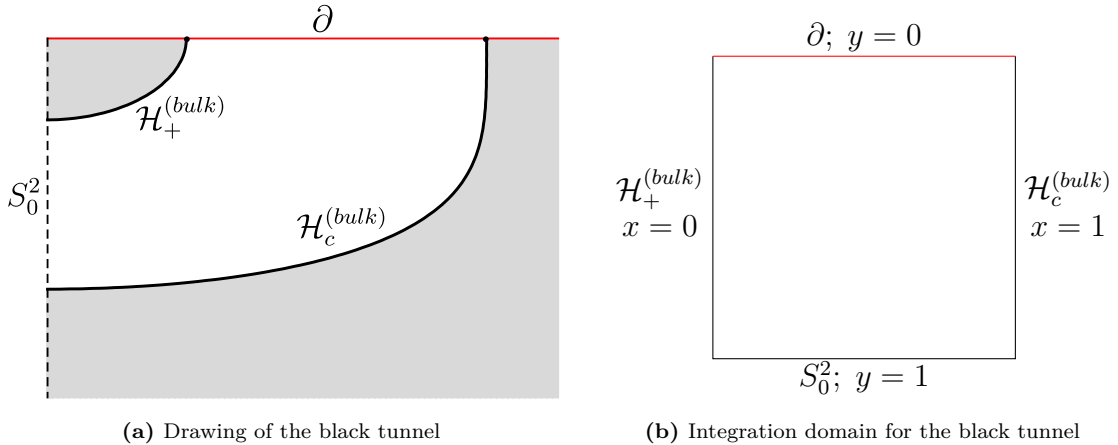


**Fig. 4.2:** The black tunnel naturally has four boundaries; the conformal boundary,  $\partial$ ; the bulk event horizon,  $\mathcal{H}_+^{(bulk)}$ ; the axis of symmetry where the two-sphere shrinks to zero size,  $S_0^2$ ; and the bulk cosmological horizon,  $\mathcal{H}_c^{(bulk)}$ . Hence, we automatically have a square integration domain.

The line element we use to describe such solutions is given by the following *Ansatz*:

$$ds_{\text{tunnel}}^2 = \frac{\ell_5^2}{y} \left[ -x^2 (1-x^2)^2 \frac{(1-\rho_h)^2}{\rho_h^2} G(x) q_1(x, y) dT^2 + \frac{16}{G(x)} q_2(x, y) dx^2 \right. \\ \left. + (1-y) q_3(x, y) d\Omega_{(2)}^2 + \frac{q_4(x, y) (dy + (1-y) q_5(x, y) dx)^2}{4(1-y)y} \right], \quad (4.2a)$$

where

$$G(x) = \frac{(2-x^2) (1+2\rho_h - x^2(2-x^2)(1-\rho_h^2))}{1+\rho_h+\rho_h^2}, \quad (4.2b)$$

and  $d\Omega_{(2)}^2$  is the metric on a round, unit radius two-sphere. We recall that the parameter,  $\rho_h$ , is the ratio of the radii of the event and cosmological horizons in the boundary de Sitter-Schwarzschild geometry. Hence  $\rho_h \rightarrow 1$  is the extremal limit at which the event and cosmological horizons are coincident, whilst  $\rho_h \rightarrow 0$  is the limit where the horizons become infinitely far apart. We found black tunnel solutions across the whole of the parameter space  $\rho_h \in (0, 1)$ .

The reference metric we used to define the DeTurck vector is given by the *Ansatz* above with  $q_1 = q_2 = q_3 = q_4 = 1$  and  $q_5 = 0$ . We will see that this reference metric satisfies all the boundary conditions that we will describe in the next subsection.

The DeTurck method in this case cannot yield Ricci solitons, since all the conditions of the theorem of [133] forbidding their existence are satisfied. In any case, we present convergence tests in Appendix A.2 showing that the DeTurck vector vanishes in the continuum limit.

## 4.2.2 Boundary conditions

The Einstein-DeTurck equation evaluated for the *Ansatz* given by (4.2a) yields a system of five second-order PDEs on the integration domain  $\{x, y\} \in (0, 1)^2$ . In order to solve such a system, we need to set five boundary conditions on each of the sides of the square.

### The conformal boundary $y = 0$

Here, we enforce Dirichlet boundary conditions in order to set the induced metric on the conformal boundary to be conformal to the de Sitter-Schwarzschild metric in four

dimensions, which is given by

$$ds_{dS-S}^2 = -f(r) dt^2 + \frac{dr^2}{f(r)} + r^2 d\Omega_{(2)}^2, \quad (4.3)$$

where

$$\begin{aligned} f(r) &= 1 - \frac{2M}{r} - \frac{\Lambda_4 r^2}{3} \\ &= -\frac{(r-r_c)(r-r_h)(r+r_c+r_h)}{r(r_c^2+r_c r_h+r_h^2)}, \end{aligned} \quad (4.4)$$

with  $\Lambda_4$  the positive cosmological constant of the four-dimensional geometry,  $M$  the mass of the black hole and  $r_h$  and  $r_c$  the radii of the event and cosmological horizons, respectively. Taking the transformations

$$r = \frac{r_h}{1 - \xi^2(2 - \xi^2)(1 - \rho_h)}, \quad \text{with} \quad \rho_h = \frac{r_h}{r_c}, \quad (4.5)$$

the metric becomes

$$ds_{dS-S}^2 = r(\xi)^2 \left[ -\xi^2(1 - \xi^2)^2 \frac{(1 - \rho_h)^2}{\rho_h^2 r_c^2} G(\xi) dt^2 + \frac{16 d\xi^2}{G(\xi)} + d\Omega_{(2)}^2 \right], \quad (4.6)$$

where  $r = r(\xi)$ , given by (4.5) is now thought of as a function of  $\xi$ , rather than a coordinate, and  $G$  is defined by (4.2b). In these coordinates, the event horizon lies at  $\xi = 0$  and the cosmological horizon is situated at  $\xi = 1$ . With respect to the usual  $t$ -coordinate, the temperature of the event and cosmological horizons are, respectively, given by

$$T_H = \frac{(1 - \rho_h)(1 + 2\rho_h)}{4\pi r_h (1 + \rho_h + \rho_h^2)}, \quad T_c = \frac{(1 - \rho_h)(2 + \rho_h)}{4\pi r_c (1 + \rho_h + \rho_h^2)}. \quad (4.7)$$

Now we are ready to define our boundary conditions at  $y = 0$ , the conformal boundary. Here, we set  $q_1 = q_2 = q_3 = q_4 = 1$ , and  $q_5 = 0$ . With such a choice, and taking

$$y = \frac{(1 - \xi^2(2 - \xi^2)(1 - \rho_h))^2}{r_h^2} z^2, \quad x = \xi, \quad T = \frac{t}{r_c}, \quad (4.8)$$

one finds that at leading order in  $z$  near the conformal boundary

$$ds_{\text{tunnel}}^2 \Big|_{z=0} = \frac{\ell_5^2}{z^2} (dz^2 + ds_{dS-S}^2), \quad (4.9)$$

with the de Sitter-Schwarzschild metric being given by (4.6). Hence, this boundary condition enforces that the black tunnel is an AlAdS spacetime with the metric on the conformal boundary being conformal to de Sitter-Schwarzschild.

### The fictitious boundaries

The remaining three boundaries of the integration domain are fictitious boundaries. At  $x = 0$  and  $x = 1$ , respectively, we have the bulk event and cosmological horizons and at  $y = 1$  we have the axis between the two bulk horizons where the two-sphere collapses to zero size.

At each of these boundaries we require that the metric is regular. This can be imposed with Neumann boundary conditions. In particular, at each fictitious boundary we set the normal derivative of each function to the boundary to zero. That is for  $i = 1, \dots, 5$ , we set

$$\partial_x q_i(0, y) = 0, \quad \partial_x q_i(1, y) = 0, \quad \partial_y q_i(x, 1) = 0. \quad (4.10)$$

### 4.2.3 Extracting the holographic stress tensor

Now let us briefly discuss how we can extract the holographic stress tensor once we have obtained the solution numerically, as discussed more generally in Section 1.3.3. Firstly, one can solve the equations of motion defined by (4.1) order by order in  $y$  off the boundary  $y = 0$ . This fixes that

$$\begin{aligned} q_1(x, y) &= 1 + \alpha_1(x)y + \beta_1(x)y^2 + \hat{\gamma}_1(x)y^{1+\sqrt{3}} + \dots \\ q_2(x, y) &= 1 + \alpha_1(x)y + \beta_2(x)y^2 + \hat{\gamma}_1(x)y^{1+\sqrt{3}} + \dots \\ q_3(x, y) &= 1 - \frac{1}{2}\alpha_1(x)y + \beta_3(x)y^2 + \hat{\gamma}_1(x)y^{1+\sqrt{3}} + \dots \\ q_4(x, y) &= 1 + \beta_4(x)y^2 + \hat{\gamma}_4(x)y^{1+\sqrt{3}} + \dots \\ q_5(x, y) &= \beta_5(x)y^2 + \gamma_5(x)y^3 + \tilde{\gamma}_5(x)y^3 \log y + \dots \end{aligned} \quad (4.11)$$

Some of these functions are fixed by the equations of motion as

$$\alpha_1(x) = -\frac{1 + \rho_h}{1 + \rho_h + \rho_h^2} g(x) \quad (4.12a)$$

$$\beta_3(x) + \frac{\beta_1(x)}{2} + \frac{\beta_2(x)}{2} = \frac{5(1 + \rho_h)^2 g(x)^2 - 2(1 + \rho_h)(1 + \rho_h + \rho_h^2) g(x)}{8(1 + \rho_h + \rho_h^2)^2} \quad (4.12b)$$

$$\beta_4(x) = \frac{2(1 + \rho_h + \rho_h^2)(1 + \rho_h)g(x) - (1 + \rho_h)^2g(x)^2}{4(1 + \rho_h + \rho_h^2)^2} \quad (4.12c)$$

$$\beta_5(x) = -\frac{(1 + \rho_h)}{2(1 + \rho_h + \rho_h^2)}g'(x) \quad (4.12d)$$

$$\tilde{\gamma}_5(x) = \frac{3(1 + \rho_h)^2}{8(1 + \rho_h + \rho_h^2)^2}g(x)g'(x), \quad (4.12e)$$

where

$$g(x) = 1 - x^2(2 - x^2)(1 - \rho_h). \quad (4.12f)$$

The only functions not fixed by a local analysis of the Einstein-DeTurck equation off the conformal boundary are  $\{\beta_1, \beta_2, \gamma_5, \hat{\gamma}_1, \hat{\gamma}_4\}$ . In order to find these functions, we need to solve the equations in the full spacetime, after having imposed regularity deep in the bulk. It turns out only the  $\beta_i$  functions are needed to calculate the stress tensor. Note that, once we have numerical approximations of the full functions  $q_i$ , we can easily evaluate an estimate for  $\beta_i$  from the second derivative of  $q_i$  with respect to  $y$  at  $y = 0$ .

Armed with this expansion near  $y = 0$ , we can go to Fefferman-Graham gauge [121] near the conformal boundary and fix the conformal frame. That is, we seek a coordinate transformation such that near the conformal boundary the metric takes the form given in (1.32a), which in five dimensions becomes

$$ds^2 = \frac{\ell_d^2}{z^2} \left( dz^2 + \left( g_{\mu\nu}^{(0)} + g_{\mu\nu}^{(2)}z^2 + g_{\mu\nu}^{(4)}z^4 + h_{\mu\nu}^{(4)}z^4 \log z \right) dx^\mu dx^\nu + \mathcal{O}(z^5) \right), \quad (4.13)$$

where we pick the conformal frame so that  $g_{\mu\nu}^{(0)}$  is the de Sitter-Schwarzschild metric given by (4.6). This can be achieved with a transformation

$$\begin{aligned} x &= \xi + \sum_{j=1}^6 \delta_j(\xi)z^j \\ y &= \sum_{j=2}^6 \epsilon_j(\xi)z^j. \end{aligned} \quad (4.14)$$

The explicit expressions of  $\delta_j(\xi)$  and  $\epsilon_j(\xi)$  can be determined by substituting the above transformation into the metric given by the *Ansatz* after expanding each of the functions off the boundary with (4.11). One can then work order by order in  $z$  to match the resultant metric with (4.13). Such a procedure fixes  $g_{\mu\nu}^{(2)}$ ,  $g_{\mu\nu}^{(4)}$  and  $h_{\mu\nu}^{(4)}$  uniquely. In this case  $h_{\mu\nu}^{(4)} = 0$ , due to the fact that the boundary metric is Einstein.

With the metric in Fefferman-Graham coordinates, one can readily read off the holographic stress tensor using (1.36b). Finally, we can make the identification from the standard AdS/CFT dictionary that

$$G_5 = \frac{\pi}{2} \frac{\ell_5^3}{N^2}. \quad (4.15)$$

One can check that the stress tensor is conserved and has a fixed trace:

$$\nabla_\mu^{(0)} T^{\mu\nu} = 0, \quad T^\mu{}_\mu = -\frac{3\ell_5^3}{16\pi G_5 r_c^4 (1 + \rho_h + \rho_h^2)^2} = -\frac{3\ell_5^3}{16\pi G_5 \ell_4^4}, \quad (4.16)$$

where, respectively,  $\nabla^{(0)}$  and  $\ell_4 = \sqrt{3/\Lambda_4}$  are the covariant derivative and the de Sitter length scale of the four-dimensional boundary geometry. The fact that the stress tensor has a constant but non-zero trace originates from the fact the boundary metric is a solution to the Einstein equation with a positive cosmological constant, agreeing with (1.38).

After the dust settles, we find

$$\langle T^t_t \rangle = \frac{N^2 g(\xi)^4}{2\pi^2 r_c^4 \rho_h^4} \left\{ \beta_1(x) - \frac{1}{16(1 + \rho_h + \rho_h^2)^2} \left[ \frac{3\rho_h^4}{g(\xi)^4} + \frac{4\rho_h^2(1 + \rho_h)}{g(\xi)} \right. \right. \\ \left. \left. - 12(1 + \rho_h)(1 + \rho_h + \rho_h^2)g(\xi) + 12(1 + \rho_h)^2 g(\xi)^2 \right] \right\}, \quad (4.17a)$$

$$\langle T^\xi_\xi \rangle = \frac{N^2 g(\xi)^4}{2\pi^2 r_c^4 \rho_h^4} \left\{ \beta_2(x) - \frac{1}{16(1 + \rho_h + \rho_h^2)^2} \left[ \frac{3\rho_h^4}{g(\xi)^4} \right. \right. \\ \left. \left. - 8(1 + \rho_h)(1 + \rho_h + \rho_h^2)g(\xi) + 8(1 + \rho_h)^2 g(\xi)^2 \right] \right\}, \quad (4.17b)$$

$$\langle T^{\Omega_i}_{\Omega_i} \rangle = \frac{N^2 g(\xi)^4}{2\pi^2 r_c^4 \rho_h^4} \left\{ \beta_3(x) - \frac{1}{16(1 + \rho_h + \rho_h^2)^2} \left[ \frac{3\rho_h^4}{g(\xi)^4} - \frac{2\rho_h^2(1 + \rho_h)}{g(\xi)} \right. \right. \\ \left. \left. + 6(1 + \rho_h)(1 + \rho_h + \rho_h^2)g(\xi) \right] \right\}, \quad (4.17c)$$

where  $\Omega_i$  stands for any of the angles on the round  $S^2$ .

## 4.3 Black hammocks

### 4.3.1 The integration domain for the black hammocks

The black hammocks share many similarities with the black funnel solutions of [134, 135, 137], which were gravitational duals to a CFT living on a flat Schwarzschild background. The key difference is the horizons of such black funnel solutions approach a planar black hole in the bulk far from the boundary event horizon, due to the fact the flat Schwarzschild boundary metric possesses only one horizon. On the other hand, the black hammocks will have no such asymptotic region; the bulk horizon will return to the conformal boundary to intersect the boundary cosmological horizon.

At first sight, it seems as though the black hammocks will only have two boundaries: the conformal boundary and the horizon of the bulk black hole, which now hangs down in the bulk between the positions of the boundary event horizon and the boundary cosmological horizon, motivating the name “hammock”. We’ve schematically drawn the shape of this geometry again in Figure 4.3a.

Attempting naively to carry out numerics on a domain with only two boundaries would be very difficult. Fortunately though, we can use a trick to “blow up” the points at which the horizon meets the boundary into lines, as was done in [134, 135, 137, 139]. This trick is based on the fact that at leading order, the geometry near the conformal boundary must be hyperbolic, and hyperbolic black holes are the only family of static geometries which are manifestly hyperbolic for each time slice as one approaches

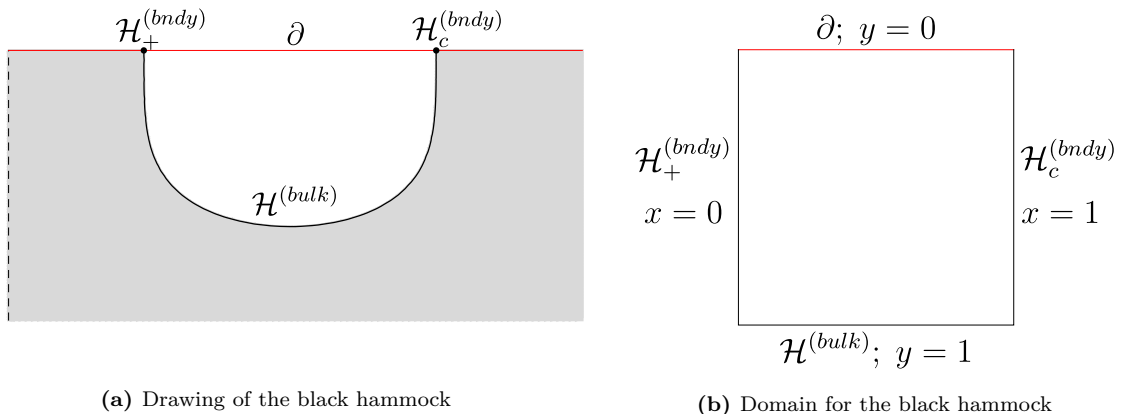


**Fig. 4.3:** Here we sketch the black hammock in (a). It initially appears to have only two boundaries: the conformal boundary and the bulk horizon. However, the bulk horizon must approach hyperbolic black holes as it approaches the conformal boundary, where it meets the boundary event horizon and the boundary cosmological horizon. This allows us one to add two extra boundaries to the integration domain at  $x = 0$  and  $x = 1$ , where this limiting behaviour will be imposed. Hence, we obtain a rectangular integration domain as shown in (b).

the boundary. Hence, one can add two extra boundaries at the points at which the hammock horizon is anchored on the boundary and enforce this limiting behaviour as boundary conditions. The family of hyperbolic black holes runs over one parameter: the temperature. It is likely that one could find *detuned* black hammock solutions, that is, solutions where the temperature of the hyperbolic black hole is different to the temperature of boundary horizon that the bulk horizon is approaching. Such detuned solutions were found in the context of field theories living on an asymptotically flat Schwarzschild black hole [137]. In this work however, we choose to study the solutions in which the temperatures of the hyperbolic black holes match the temperatures of the horizons of the boundary de Sitter-Schwarzschild geometry.

The metric of a hyperbolic black hole is given by

$$ds_{\mathbb{H}}^2 = \frac{\ell_5^2}{z^2} \left[ -(1 - z^2) d\hat{t} + \frac{dz^2}{1 - z^2} + d\eta^2 + \sinh^2 \eta d\Omega_{(2)}^2 \right], \quad (4.18)$$

which has temperature  $(4\pi)^{-1}$  with respect to the time coordinate  $\hat{t}$ .

By blowing up the point where the bulk horizon meets the conformal boundary into lines, we obtain a rectangular integration domain, as shown in Figure 4.3b. We'll pick coordinates such that the boundaries are the conformal boundary at  $y = 0$ , the two hyperbolic black hole limits at  $x = 0$  and  $x = 1$ .

### 4.3.2 Ansatz for the black hammocks

We were able to obtain the black hammocks both by using the DeTurck method and by directly gauge-fixing to Bondi-Sachs gauge. These two methods were reviewed in Sections 2.1 and 2.2, respectively. Both the numerical calculation of solutions and the extraction of quantities of interest were far easier and quicker in Bondi-Sachs gauge, and so we present the solutions in this gauge here.

A five-dimensional stationary,  $SO(3)$ -symmetric solution in Bondi-Sachs can be written as

$$ds^2 = \frac{\ell_5^2}{y^2} \left[ e^{2\beta} (-V dv^2 - 2 dv dy) + e^{2\chi} \left( \frac{1}{A^2} (dx - U^x dv)^2 + A d\Omega_{(2)}^2 \right) \right], \quad (4.19)$$

with five functions,  $V$ ,  $U^x$ ,  $\beta$ ,  $A$ ,  $\chi$ , which can depend upon  $\{x, y\}$ . We can use the freedom of redefining the radial coordinate to fix the radial dependence of the  $\chi$  function. We desire there to be a null hypersurface opposite the conformal boundary, at  $y = 1$ , which we will later check is an event horizon. We will also explicitly take some

functions of  $x$  and  $y$  out of the unknown functions  $V$ ,  $U^x$ ,  $\beta$ ,  $A$ ,  $\chi$ , with the purpose of making the boundary conditions and reference metric more easy to apply in the numerics. Altogether, we take the *Ansatz* for the black hammocks to be

$$ds^2 = \frac{\ell_5^2}{y^2} \left[ \left( -(1-y^2) \frac{(1-\rho_h)^2}{\rho_h^2} H(x)^2 p_1(x,y) dv^2 - 2 \frac{(1-\rho_h)}{\rho_h} H(x) dv dy \right) p_3(x,y)^2 + \frac{1}{4x(1-x)(1+y^4 p_5(x))^2} \left( \frac{(dx - x(1-x)p_2(x,y) dv)^2}{(1-x)x p_4(x,y)^2} + H(x)p_4(x,y) d\Omega_{(2)}^2 \right) \right], \quad (4.20)$$

where

$$H(x) = \frac{1 + 2\rho_h - x(1 - \rho_h^2)}{1 + \rho_h + \rho_h^2}. \quad (4.21)$$

The bulk equations,  $E_{ij} = 0$ , provide four PDEs for the functions  $p_k(x,y)$  for  $k = 1, \dots, 4$  and  $p_5(x)$ . It's worth noting that  $p_5$  is independent of  $y$ , and moreover, the  $E_{xy} = 0$  equation evaluated at  $y = 1$  actually provides a simple algebraic condition for  $p_5(x)$  in terms of the four other functions and their derivatives at  $y = 1$ . However, we found that the convergence of the numerical method was faster if we promoted  $p_5$  to a function of both  $x$  and  $y$  and imposed as a fifth bulk equation that  $\partial_y p_5(x,y) = 0$ .

The highest  $y$ -derivative of the functions arising in the bulk equations are

$$\{\partial_y p_1, \partial_y^2 p_2, \partial_y p_3, \partial_y^2 p_4\}, \quad (4.22)$$

that is, two second order derivatives and two first order derivatives with respect to  $y$ . This suggests that when we expand the functions about the conformal boundary, we should find there are three free functions in order for us to have a well-defined PDE problem. Moreover, we should find we need to set three boundary conditions deep in the bulk at  $y = 1$ .

We will enforce that  $E_{va} = 0$  at the  $y = 1$  hypersurface. As discussed in Section 2.2, the contracted Bianchi identity implies that, so long as the bulk equations are satisfied, such boundary conditions actually enforce that  $E_{va} = 0$  throughout the whole bulk, yielding a full solution to the Einstein equation. Indeed, once a solution is found we can explicitly track the  $E_{va}$  components, providing a test of the convergence properties of the numerical method to find the black hammocks, which we present in Appendix A.3.

In order to numerically solve the bulk equations, we must firstly set boundary conditions, which we discuss in the next subsection, and then, once again, we use collocation methods and the Newton-Raphson algorithm, described in Section 2.3,

to numerically solve the system of PDEs obtained. Originally to obtain the black hammocks, we used a grid of size  $120 \times 120$  when discretizing, however, it seems likely that a use of the patching methods described in Section 2.4.3 would speed up the numerics.

It's also worth reiterating that we have no proof that the system of PDEs that result from the Einstein equation applied to our *Ansatz* in Bondi-Sachs gauge is elliptic, though the speed and accuracy of the numerical method would seem to suggest ellipticity. It would be very interesting to explore further whether this gauge naturally gives elliptic PDEs for such stationary problems in general relativity.

### 4.3.3 Boundary conditions

#### The conformal boundary $y = 0$

Just as with the black tunnels, at the conformal boundary we wish to set Dirichlet boundary conditions enforcing that the metric on the conformal boundary is conformal to the de Sitter-Schwarzschild metric, given by (4.3). This time, consider a coordinate transformation given by

$$r = \frac{r_h}{1 - (1 - \rho_h)w}, \quad \text{with} \quad \rho_h = \frac{r_h}{r_c}, \quad (4.23)$$

so that the event horizon is the  $w = 0$  surface and the cosmological is the  $w = 1$  surface, and the metric is given by

$$ds_{dS-S}^2 = \frac{r_h^2}{(1 - w(1 - \rho_h))^2} \left[ -w(1 - w) \frac{(1 - \rho_h)^2}{\rho_h^2 r_c^2} H(w) dt^2 + \frac{dw^2}{H(w)w(1 - w)} + d\Omega_{(2)}^2 \right], \quad (4.24)$$

where  $H$  is defined by (4.21). We set at  $y = 0$  the boundary conditions that  $p_1 = p_3 = p_4 = 1$  and  $p_2 = 0$ , and then take the transformations

$$v = \frac{t}{2r_c} - \frac{\rho_h}{H(w)(1 - \rho_h)} y, \quad y = z \frac{(1 - w(1 - \rho_h))\sqrt{H(w)}}{2r_h\sqrt{w(1 - w)}}, \quad x = w, \quad (4.25)$$

then at leading order in  $z$ , the metric near the  $z = 0$  boundary is

$$ds^2 = \frac{\ell_5^2}{z^2} \left( dz^2 + ds_{dS-S}^2 \right), \quad (4.26)$$

with the de Sitter-Schwarzschild metric in the coordinates of (4.24). Therefore, the black hammocks will also be an AlAdS spacetime with de Sitter-Schwarzschild on the boundary.

### The hyperbolic black hole $x = 0$

As discussed above, we use the fact that the bulk horizon must approach the geometry of the horizon of a hyperbolic black hole as it approaches the conformal boundary to add another boundary to the integration domain. In order to enforce that the metric takes the form (4.18) at this boundary,  $x = 0$ , we take the Dirichlet boundary conditions:  $p_1 = p_3 = p_4 = 1$  and  $p_2 = 0$ . Moreover, we also set  $p_5 = 0$  at  $x = 0$ , though it can be easily shown that this follows from the equations of motion. Now, if we take new coordinates

$$dv = \frac{1}{r_c} d\hat{t} - \frac{\rho_h}{H(0)(1 - \rho_h)(1 - y^2)} dy, \quad x = H(0)\xi, \quad (4.27)$$

then at leading order in  $\xi$  for each component, the metric becomes

$$ds^2 \Big|_{\xi=0} = \frac{\ell_5^2}{y^2} \left[ -\frac{(1 - y^2)(1 - \rho_h)^2 H(0)^2}{\rho_h^2 r_c^2} d\hat{t}^2 + \frac{dy^2}{1 - y^2} + \frac{1}{4\xi^2} d\xi^2 + \frac{1}{4\xi} d\Omega_{(2)}^2 \right]. \quad (4.28)$$

After taking

$$\xi = e^{-2\eta}, \quad y = z, \quad (4.29)$$

then the above metric matches the large  $\eta$  limit of (4.18), so indeed we are imposing we are approaching a hyperbolic black hole as we go towards the boundary. Moreover, the temperature of this hyperbolic black hole is

$$T_{\mathbb{H}_h} = \frac{(1 - \rho_h)H(0)}{4\pi\rho_h r_c} = T_H, \quad (4.30)$$

where  $T_H$  is the temperature of the boundary event horizon, given in (4.7).

### The hyperbolic black hole $x = 1$

Of course, the bulk horizon meets the conformal boundary not only at the boundary event horizon, but also at the boundary cosmological horizon. Hence we can similarly expand this point into another line in the integration domain by enforcing that the geometry approaches that of another hyperbolic black hole horizon.

The work is very similar to the  $x = 0$  boundary. At  $x = 1$ , we set the Dirichlet boundary conditions:  $p_1 = p_3 = p_4 = 1$  and  $p_2 = p_5 = 0$ . This time take

$$dv = \frac{1}{r_c} d\hat{t} - \frac{\rho_h}{H(1)(1 - \rho_h)(1 - y^2)} dy, \quad x = 1 - H(1)\xi, \quad (4.31)$$

then at the boundary  $x = 1$ , which has become the surface  $\xi = 0$ , the metric, to leading order in  $\xi$  for each term, becomes

$$ds^2 \Big|_{\xi=0} = \frac{\ell_5^2}{y^2} \left[ -\frac{(1 - y^2)(1 - \rho_h)^2 H(1)^2}{\rho_h^2 r_c^2} d\hat{t}^2 + \frac{dy^2}{1 - y^2} + \frac{1}{4\xi^2} d\xi^2 + \frac{1}{4\xi} d\Omega_{(2)}^2 \right], \quad (4.32)$$

hence, just as above, the geometry is that of the limit of a hyperbolic black hole, this time with temperature

$$T_{\mathbb{H}_c} = \frac{(1 - \rho_h)H(1)}{4\pi\rho_h r_c} = T_c. \quad (4.33)$$

### The null hypersurface $y = 1$

We have one final boundary of our integration domain at  $y = 1$ . Note that, the *Ansatz* gives an inverse metric with a factor of  $(1 - y^2)$  in the  $g^{yy}$  component, and hence the  $y = 1$  is a null hypersurface.

Recall that in Bondi-Sachs gauge, only a subset of the components Einstein equation need to be explicitly solved in the bulk, with the remainder being set as boundary conditions at some constant  $y$  slice. The null hypersurface at  $y = 1$  provides a perfect place to set these conditions. Hence, we set three Robin boundary conditions at  $y = 1$  by requiring that,

$$E_{vv} = E_{vy} = E_{vx} = 0. \quad (4.34)$$

Note that, *a priori*, we cannot be sure whether this null hypersurface is the horizon of the bulk black hole. In Section 4.4.1 we'll provide numerical evidence that it is indeed the horizon by checking that there are future-directed, radial, null curves from any point with  $y < 1$  to the conformal boundary at  $y = 0$ .

### 4.3.4 Extracting the holographic stress tensor

Once again, we can expand the functions off the boundary by ensuring order-by-order they solve the equations of motion. It can be shown that in Bondi gauge, no non-analytic terms will arise in such an expansion [159]. This lack of non-analytic terms ensures that the numerical method has exponential convergence even when reading

asymptotic charges. This is in stark contrast with the DeTurck method which is typically plagued by non-analytic terms close to the AdS boundary, such as those in (4.11). We obtain

$$p_i(x, y) = \sum_{j=0}^5 \psi_i^{(j)}(x) y^j + \dots, \quad \text{for } i = 1, \dots, 4, \quad (4.35)$$

where  $\psi_1^{(0)} = \psi_3^{(0)} = \psi_4^{(0)} = 1$  and  $\psi_2^{(0)} = 0$ . The only functions not fixed by the local analysis of the equations of motion are  $\{\psi_1^{(4)}, \psi_2^{(4)}, \psi_4^{(4)}\}$ , so as expected we have three free functions at the conformal boundary. Moreover  $\psi_2^{(4)}$  is fixed by the local analysis up to a constant:

$$\psi_2^{(4)} = C_1 \frac{(1-x)x}{\left(1 + 2\rho_h - x(1 - \rho_h^2)\right)^2}. \quad (4.36)$$

We'll see that the value of this constant,  $C_1$ , plays a key role when we consider the flow along the horizon of the hammock. Next we go into Fefferman-Graham coordinates, so that the metric is in the form given by (4.13). To do so, we take a transformation

$$x = w + \sum_{k=1}^5 \zeta_j(w) z^j \quad (4.37a)$$

$$y = \sum_{k=1}^5 \eta_j(w) z^j \quad (4.37b)$$

$$v = \frac{t}{2r_c} + \sum_{k=1}^5 \theta_j(w) z^j, \quad (4.37c)$$

with the functions  $\zeta_i$ ,  $\eta_i$  and  $\theta_i$  being defined order-by-order so that the metric is of the form given in (4.13), where still  $g_{\mu\nu}^{(0)}$  is taken to be the de Sitter-Schwarzschild metric. However, if we take the holographic stress tensor in the coordinates of (4.24), we'll find that it's not regular at the horizons, due to the flow along the bulk horizon. To alleviate this, we can take coordinates which are regular at *both* the future event and future cosmological horizons in the boundary spacetime. That is, with the de Sitter-Schwarzschild we define a new time coordinate,  $V$ , by

$$dt = dV - \frac{\rho_h(1-2w)}{(1-\rho_h)H(w)(1-w)w} dw. \quad (4.38)$$

This brings the de Sitter-Schwarzschild metric to the form

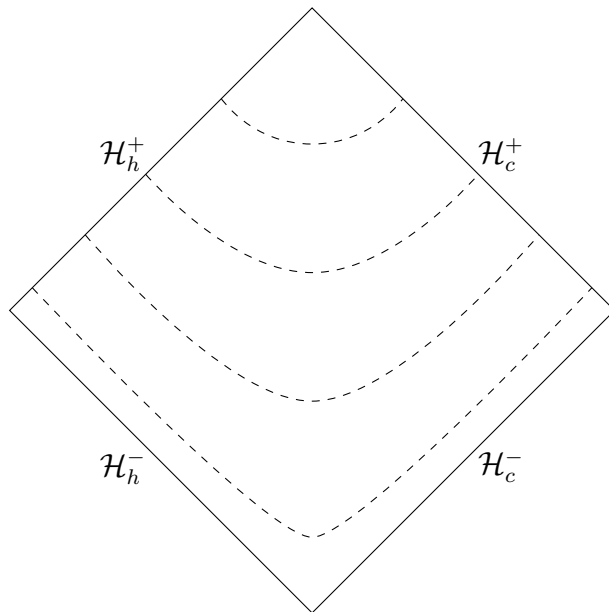


**Fig. 4.4:** The Penrose diagram of the four-dimensional de Sitter-Schwarzschild spacetime. The dashed curves are spacelike hypersurfaces of constant  $V$ , where  $V$  is the coordinate defined in (4.38). Hence the coordinate  $V$  is regular at both the future event horizon,  $\mathcal{H}_h^+$ , and the future cosmological horizon,  $\mathcal{H}_c^+$ .

$$ds^2 = \frac{r_h^2}{(1 - w(1 - \rho_h))^2} \left[ -w(1 - w) \frac{(1 - \rho_h)^2}{\rho_h^2 r_c^2} H(w) dV^2 - \frac{2(1 - 2w)(1 - \rho_h)}{r_c \rho_h} dV dw + \frac{4(1 + \rho_h + \rho_h^2)}{1 + 2\rho_h - w(1 - \rho_h^2)} dw^2 + d\Omega_{(2)}^2 \right]. \quad (4.39)$$

In Figure 4.4, we draw the Penrose diagram for the de Sitter-Schwarzschild geometry. The dashed curves are hypersurfaces of constant  $V$ .

Now we can finally evaluate the holographic stress tensor via (1.36b). We find that the stress tensor is regular everywhere, is conserved and has fixed trace, once again given by (4.16).

### 4.3.5 Properties of the hammock horizon

Due to the fact that the bulk horizon of the black hammock is not Killing it can have further interesting properties, for example, it can have non-trivial expansion and shear. This has been observed in other flowing geometries such as those in [179, 139, 135]. In order to investigate these properties, one must consider the geometry of the bulk horizon,  $\mathcal{H}^{(bulk)}$ . From the *Ansatz*, we know that the  $y = 1$  slice is a null hypersurface, but we cannot be immediately sure that it really is the horizon of the hammock. In

the next section, we'll provide evidence that indeed the horizon is the  $y = 1$  slice of the bulk spacetime, so let us for now assume that as a given.

In general calculating the expansion and shear can be difficult, however, we follow [139, 135], which introduced a number of tricks that allows one to calculate the affine parameter along a generator of the horizon and from this quickly calculate the expansion and shear.

We assume the horizon is the  $y = 1$  hypersurface of the bulk spacetime, thus it is parameterised by  $\{v, x, \theta, \phi\}$ , where  $\theta$  and  $\phi$  are the usual angular coordinates in the two-sphere. Hence,  $\mathcal{H}^{(bulk)}$  is a four-dimensional null hypersurface with a three-dimensional space of generators. Due to stationarity and spherical symmetry, the spacetime also possesses three Killing vector fields, which we will denote as  $\partial_I$ , for  $I = v, \theta, \phi$ , none of which are generators of the horizon, which is non-Killing. Thus, any two generators of the horizon will be related by the action of a combination of the  $\partial_I$  vector fields. This means for a given value of  $x$ , we can arbitrarily pick a horizon generator, say with affine parameter,  $\lambda$ . We can extend  $\lambda$  to a function of  $x$  along the horizon by requiring that it is independent of  $v, \theta$  and  $\phi$ , so that  $\lambda = \lambda(x)$ .

Let  $U^a$  be the tangent vector to the horizon generator with affine parameter  $\lambda$ . We know that each of the  $\partial_I$  vectors is tangent to  $\mathcal{H}^{(bulk)}$ , hence  $U \perp \partial_I$ . Now, one can choose another vector field  $S^a$  such that  $S^a U_a = -1$ ,  $S \perp \partial_I$ .

In order to find the expansion and shear, first one defines the tensor  $B_{ab} = \nabla_b U_a$ , which is symmetric since  $U^a$  is hypersurface orthogonal. Now let us consider a deviation vector,  $\eta$ , orthogonal to both  $U$  and  $S$ . Then

$$\eta^b B^a_b = U^b \nabla_b \eta^a, \quad (4.40)$$

that is,  $B^a_b$  measures the failure of a deviation vector to be parallelly transported along  $U$ . Since  $U$  and  $\partial_I$  commute,  $\partial_I$  are deviation vectors for the geodesic congruence, so from the above equation,

$$(\partial_I)^b B^a_b = U^b \nabla_b (\partial_I)^a. \quad (4.41)$$

Now let us consider  $h_{IJ} = \partial_I \cdot \partial_J$ . In the  $\{v, x, y, \theta, \phi\}$  coordinates,  $h_{IJ} = g_{IJ}$ , so it is simply the induced metric on a constant  $x$  and constant  $y$  slice. If one differentiates

the component of  $h_{IJ}$  with respect to the affine parameter  $\lambda$ , one finds that

$$\begin{aligned}
\frac{d}{d\lambda}h_{IJ} &= U^b \nabla_b (\partial_I \cdot \partial_J) \\
&= (\partial_I)^b B^a_b (\partial_J)_a + (\partial_J)^b B^a_b (\partial_I)_a \\
&= 2B_{ab} (\partial_I)^a (\partial_J)^b \\
&= 2B_{IJ}.
\end{aligned} \tag{4.42}$$

Now, when calculating the expansion, shear and twist of a null geodesic congruence, it turns out the space one has to work with is an equivalence class of deviation vectors, where first we restrict to vectors which are orthogonal to  $U^a$ , and then consider two such deviation vectors as equivalent if they differ by a multiple of  $U^a$  (see, for example, Section 9.2 of [11] or Appendix F of [12] for further details). Let us denote the vector space of such an equivalence class as  $\hat{V}$ . This is a  $3 = 5 - 2$  dimensional vector space in our case, where we have five bulk dimensions. A vector/covector in the spacetime naturally gives rise to a vector/covector in  $\hat{V}$  if and only if its contraction with  $U$  is zero. Furthermore, a general tensor  $T^{a_1 \dots a_k}_{b_1 \dots b_\ell}$  in the spacetime naturally gives rise to a tensor  $\hat{T}^{a_1 \dots a_k}_{b_1 \dots b_\ell}$  if and only if contracting any one of its upper or lower indices with  $U_a$  or  $U^a$  and then the remainder of indices with vectors or covectors with natural realisations in  $\hat{V}$  gives zero.

Each of  $g_{ab}$ ,  $B_{ab}$  and  $(\partial_I)^a$  satisfy the above definitions, so they naturally give rise to tensors in  $\hat{V}$ . Therefore, the three linearly independent vectors  $(\partial_I)^a$  provide a basis for  $\hat{V}$ , so for any spacetime tensor  $T$  satisfying the above condition, we can find  $\hat{T}$  simply by reading off the  $\{v, \theta, \phi\}$  components of  $T$ . That is,

$$\hat{h}_{IJ} = h_{IJ} = g_{IJ}, \tag{4.43}$$

$$\hat{B}_{IJ} = B_{IJ} = \frac{1}{2} \frac{d}{d\lambda} h_{IJ}. \tag{4.44}$$

Now that we're working in the vector space  $\hat{V}$ , we can define the *expansion* and *shear*, respectively, as

$$\Theta = \hat{B}^I_I = \hat{h}_{IJ} \hat{B}^{IJ} = h_{IJ} B^{IJ}, \tag{4.45}$$

$$\sigma_{IJ} = \hat{B}_{IJ} - \frac{1}{d-2} \Theta \hat{h}_{IJ} = B_{IJ} - \frac{1}{d-2} \Theta h_{IJ}, \tag{4.46}$$

where  $d$  is the dimension of the bulk spacetime, so that, in our case  $d = 5$ . The *twist* is the anti-symmetric part of  $\hat{B}_{IJ}$ , which vanishes here, due to the symmetry of  $B_{IJ}$ .

We already have  $h$ , so we need only calculate  $B$  to find the expansion and shear. This can be done by finding the affine parameter  $\lambda(x)$ , and then solving (4.44) for  $B$ . In order to find the affine parameter, we can utilise Raychaudhuri's equation, which is given by

$$\frac{d\Theta}{d\lambda} = -\hat{B}^b{}_a \hat{B}^a{}_b - R_{ab} U^a U^b. \quad (4.47)$$

By the Einstein equation,  $R_{ab} \propto g_{ab}$ , and moreover  $U^a$  is null, so that the final term above vanishes. Also,  $\hat{B}^{ab}$  is symmetric and orthogonal to both  $U$  and  $S$ , so the above equation simplifies to

$$\frac{d\Theta}{d\lambda} = -\hat{B}^{IJ} \hat{B}_{IJ}. \quad (4.48)$$

One can then substitute  $\Theta$  and  $\hat{B}_{IJ}$  in the above equation for expressions in terms of  $h_{IJ}$  by using (4.44) and (4.45), which yields the following second order ODE for  $\lambda$ :

$$\lambda'' = \lambda' \left( h^{IJ} h'_{IJ} \right)^{-1} \left[ \frac{1}{2} h^{IJ} h^{KL} h'_{IK} h'_{JL} + \left( h^{IJ} h'_{IJ} \right)' \right], \quad (4.49)$$

where  $'$  denotes a derivative with respect to  $x$ , the coordinate along the horizon. A more general ODE is given in [135] in the case where the horizon is not necessarily a constant  $y$  slice, but rather some non-trivial surface in the  $(x, y)$  plane.

Once one has a numerical solution for the line element of the black hammock, one can numerically solve the above ODE for the affine parameter  $\lambda(x)$ . Finally with such an affine parameter, one can evaluate  $\hat{B}_{IJ}$  since (4.44) implies that

$$\hat{B}_{IJ} = \frac{1}{2} \left( \lambda'(x) \right)^{-1} \frac{d}{dx} h_{IJ}. \quad (4.50)$$

From this the expansion and shear along the horizon can easily be computed using (4.45) and (4.46).

## 4.4 Results

### 4.4.1 The position of the hammock horizon

The *Ansatz* for the black hammock fixed that the  $y = 1$  slice was a null hypersurface in the bulk spacetime, however, at no point in the *Ansatz* or in the boundary conditions did we explicitly set that it really was the bulk horizon. In particular, we cannot be sure it is not instead some inner horizon, and that the real event horizon lies outside of it.

We can check this isn't the case by ensuring we can reach the conformal boundary via a future-directed, causal curve starting at any given point outside the  $y = 1$  hypersurface.

Let us consider, in  $(v, x, y, \theta, \phi)$  coordinates, a radial curve with tangent vector given by

$$U^a = \left( \frac{1}{x(1-x)p_2(x,y)} U^x, U^x, U^y, 0, 0 \right). \quad (4.51)$$

The condition for such a curve to be null leads to the equation

$$\frac{dy}{dx} = - \frac{(1 - \rho_h)(1 - y^2)p_1(x, y)H(x)}{2\rho_h(1 - x)x p_2(x, y)}. \quad (4.52)$$

We numerically solve the above ODE for  $y(x)$ . This provides a family of null curves, parameterised by the choice of initial condition of the ODE. The  $y$  coordinate depends monotonically on the  $x$  coordinate, so we can indeed use  $x$  as a parameter along the curve. One finds that if one takes as an initial condition that  $y = 1$  for some value of  $x$ , then one finds that the curve remains on the  $y = 1$  hypersurface for all time. On the other hand, if one takes  $y = 1 - \epsilon$  as an initial condition for any  $\epsilon > 0$ , then the curve will always intersect the conformal boundary at  $y = 0$ . Moreover, we can easily see that the vector  $U^a$  is future-directed, since its inner product with  $\partial/\partial v$  is negative in the asymptotic region where  $\partial/\partial v$  defines the time-orientation. Thus we can find a future-directed causal curve from any point in the exterior of  $y = 1$  to the conformal boundary at  $y = 0$ . This proves that  $y = 1$  is not an inner horizon, and provides strong evidence that the  $y = 1$  hypersurface is indeed the event horizon of the black hammock.

#### 4.4.2 Embeddings of the horizons

In order to aid with visualisation of the geometries, we can embed a spatial cross-section of the horizons into hyperbolic space. The cross-section of the horizon of the black hammock and each of the horizons of the black tunnel are three-dimensional, so we can embed them into four-dimensional hyperbolic space  $\mathbb{H}^4$ , which has metric

$$ds_{\mathbb{H}^4}^2 = \frac{L_4^2}{Z^2} \left( dZ^2 + dR^2 + R^2 d\Omega_{(2)}^2 \right). \quad (4.53)$$

Let us consider finding an embedding of the horizons of the black tunnel. The bulk event and bulk cosmological horizons are, respectively, the  $x = 0$  and  $x = 1$  surfaces, and are parameterised by the  $y$  coordinate. Hence, for each of the horizons we seek an

embedding of the form  $(R(y), Z(y))$ . Such a surface in  $\mathbb{H}_4$  has induced metric

$$ds_{emb}^2 = \frac{L_4^2}{Z(y)^2} \left( (Z'(y)^2 + R'(y)^2) dy^2 + R(y)^2 d\Omega_{(2)}^2 \right). \quad (4.54)$$

We compare the above line element with the induced metric of a constant time slice of each of the bulk event and bulk cosmological horizons. In each case, this yields a simple first-order ODE and an algebraic equation which can be solved numerically for  $R(y)$  and  $Z(y)$ . Note that the embeddings of the two horizons (the bulk event horizon at  $x = 0$  and the bulk cosmological horizon at  $x = 1$ ) must be found separately, but can be embedded into the same space. There is a fair amount of freedom in the embeddings corresponding to the initial conditions of the ODEs, so really it is only the shape of the horizons that matters. We choose  $L_4 = \ell_5$ , and take for the cosmological horizon the initial condition that  $R(0) = 1$ , and for the event horizon we pick the initial condition that  $R(0) = \rho_h$ .

To obtain the embedding diagram, one then plots the resultant values of  $\{R(y), Z(y)\}$  across the range  $y \in (0, 1)$  for each of the horizons. In Figure 4.5a, we've plotted together the embedding diagrams for the two horizons of the black tunnel, with a value of the parameter  $\rho_h = 0.5$ .

We can apply a similar procedure for the black hammocks, which only has one horizon, which in the coordinates of our *Ansatz* is the  $y = 1$  hypersurface, hence this time is parameterised by the  $x$  coordinate. Once again we compare the line element of the embedding  $(R(x), Z(x))$  in  $\mathbb{H}_4$  to the induced metric on a constant time slice of the bulk horizon of the hammock. This yields an ODE, which we solve with the

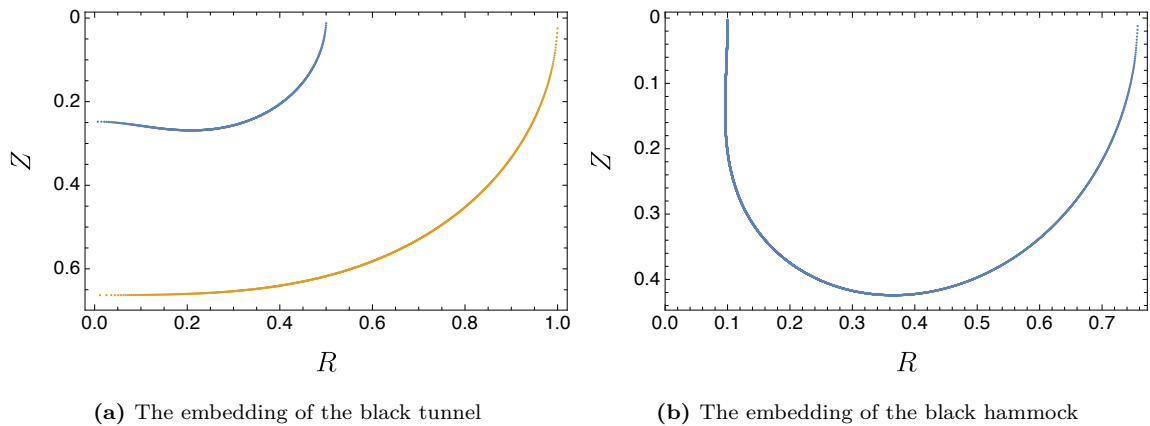


**Fig. 4.5:** The embedding diagrams of the black tunnel and hammock with  $\rho_h = 0.5$  in four-dimensional hyperbolic space. The tunnel has two disconnected horizons; the blue curve is the bulk event horizon whilst the orange curve is the bulk cosmological horizon. The hammock possesses a single connected horizon.

initial condition  $R(0) = 0.1$ , though again we stress that it is only the shape of the embedding that matters rather than any numerical values. The embedding diagram obtained for the black hammock is plotted in Figure 4.5b.

### 4.4.3 The ergoregion of the hammocks

The results described in Section 4.4.1 provide strong evidence that the horizon of the black hammock is the  $y = 1$  null hypersurface. However, the fact that the stationary Killing vector field  $k^a = (\partial/\partial v)^a$  does not generate the horizon means that there must be an ergoregion in which  $k^a$  is spacelike. The ergosurface is the boundary of this ergoregion, where necessarily  $k^2 = 0$ .

We find that for large values of the radius ratio,  $\rho_h$ , the ergosurface is very close to the horizon, meaning the ergoregion is extremely small. For smaller values of  $\rho_h$ , however, the ergoregion is noticeably larger. In Figure 4.6 we have plotted the ergoregion as a surface in the  $(x, y)$  plane for a black hammock with  $\rho_h = 0.1$ . As one would expect from the *Ansatz*, the ergosurface approaches the horizon as one goes towards  $x = 0$  or  $x = 1$ , which we recall are the points on the conformal boundary at which the bulk horizon approaches the geometry of a hyperbolic black hole.

In general, the presence of an ergoregion can lead to superradiant instabilities of black holes [188]. Noting the fact that as the radius ratio,  $\rho_h$ , is taken to be small (*i.e.* as the horizons of the de Sitter-Schwarzschild boundary geometry are taken to be far apart) the ergoregion becomes larger and larger, it would be particularly

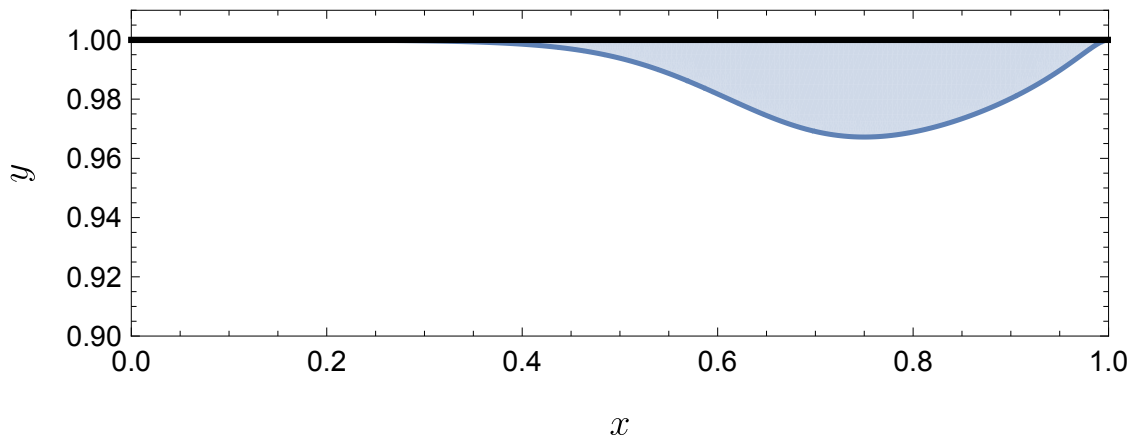


**Fig. 4.6:** The ergoregion of the black hammock, with  $\rho_h = 0.1$ , plotted as in the  $(x, y)$  coordinate space. The black line at  $y = 1$  is the horizon of the black hammock. The blue curve is the ergosurface where the Killing vector  $k = \partial/\partial v$  is null and the shaded region is the ergoregion where  $k$  is spacelike.

interesting to investigate whether the black hammocks for these values of  $\rho_h$  do suffer such superradiant instabilities.

#### 4.4.4 Energy

Now we'll turn to some of the conserved charges that the solutions possess. Firstly we'll look at the energy of both the tunnels and the hammocks, and then the flow which is non-zero only for the hammocks. Before we do so let us stress one particularly interesting point regarding the normalisation of these quantities. The energy and flow are dimensionful quantities, so in order to compare the quantities between solutions, one has to multiply by a suitable power of a dimensionful parameter of the solutions. Often the temperature of the black hole is used as this normalising factor. However, in our case, we have two temperatures which are not equal: the temperature of the event horizon,  $T_H$ , and the temperature of the cosmological horizon,  $T_c$ . This is connected to the fact that in de Sitter-Schwarzschild, one has two scales, the mass of the black hole and the de Sitter length scale. It is not immediately clear which of the temperatures,  $T_H$  or  $T_c$ , is the meaningful quantity to normalise with, or if instead we should use some combination of them. Indeed, the fact that the two temperatures of the horizons are different means that it is difficult to define a canonical ensemble, and hence it is hard to discuss the solutions using thermodynamic analysis. We'll return to this point in the discussion in Section 4.5. For now, let us present the charges which we choose to make dimensionless using  $T_H$ , which seems to yield results without divergent behaviour at the endpoints of the parameter space.

The energy of the black tunnels and hammocks can be defined from the holographic stress tensor,  $T_{\mu\nu}$ , in the standard way [122, 189]. One takes a Cauchy slice  $\Sigma$  of the boundary de Sitter-Schwarzschild geometry and then the energy is defined by an integral over this slice as

$$E := - \int_{\Sigma} d^3x \sqrt{h} n^{\mu} k^{\nu} T_{\mu\nu}, \quad (4.55)$$

where  $k^{\mu}$  is the stationary Killing vector field of the de Sitter-Schwarzschild metric and  $h$  the determinant of the induced metric on  $\Sigma$  and  $n^{\mu}$  the unit normal to  $\Sigma$ .

For the hammocks, we have to be careful to use coordinates on which the stress tensor is regular at both horizons, which can be done by taking the de Sitter-Schwarzschild metric in the form given in (4.39). We pick the surface  $\Sigma$  to be a constant  $V$  slice, and so  $n_{\mu} \propto (dV)_{\mu}$ . Such surfaces are shown as dashed curves in the Penrose diagram for de Sitter-Schwarzschild, which is shown in Figure 4.4. In these coordinates, the stationary Killing vector field is given by  $k^{\mu} = (\partial/\partial V)^{\mu}$ . With these choices, the integral for the

energy becomes

$$E = -2\pi r_c^3 \rho_h^3 (1 - \rho_h) \int_0^1 dw \frac{T^V_V}{(1 - w(1 - \rho_h))^4}. \quad (4.56)$$

The integral can be computed numerically for both the tunnels and the hammocks using the holographic stress tensors found in Section 4.2.3 and Section 4.3.4, respectively. It is immediately clear that the stress tensor for the tunnels is regular and finite at the horizons, so there are no difficulties in calculating the energy for each of the values of the radius ratio,  $\rho_h$ . We've plotted the energy of each tunnel solution in Figure 4.7a. Turning points of the energy can often signify transitions between stability and instability and so one particularly interesting and surprising feature of this plot is that the energy of the tunnels (when normalised by the event horizon temperature) is a non-monotonic function of the parameter  $\rho_h$ . However, the fact that one finds a non-monotonic function, and moreover the position of the maximum, is dependent on the fact we've used  $T_H$  to make the energy dimensionless, and thus it is difficult to argue that this maximum is meaningful given that  $T_H$  is not the only scale in the system.

The regularity of the stress tensor of the black hammocks depends on non-trivial relations between (fourth) derivatives of the metric functions. It is expected that the true, full solutions will satisfy these relations, however there is some noise in the numerical solutions due to the fact the solutions have been found on a discrete grid. Thus, in order to ensure these relations are satisfied when finding the metric functions numerically, we needed to use high precision and a large number of lattice points in the discretization (we used a precision of 50 decimal places on the  $120 \times 120$  grid).<sup>1</sup> We found that the smaller the value of  $\rho_h$ , the more difficult it is to ensure that one attains a regular stress tensor numerically. We were able to get sensible results for  $\rho_h \geq 0.1$ , and have plotted the energy for these solutions in Figure 4.7b. We did find hammock solutions for smaller values of  $\rho_h$ , but not at a high enough resolution to ensure we obtained a regular stress tensor numerically and hence we've omitted these points from the plot.

---

<sup>1</sup>The numerical work carried out to comprise the paper [2], on which this chapter is based, used only a single patch. It is possible that using the patching methods described in Section 2.4.3, one could be able to derive this energy accurately without having to go to such high precision and resolution. To do so, one could take one patch to be localised very close to the asymptotic region, to improve the accuracy of the derivatives at infinity.

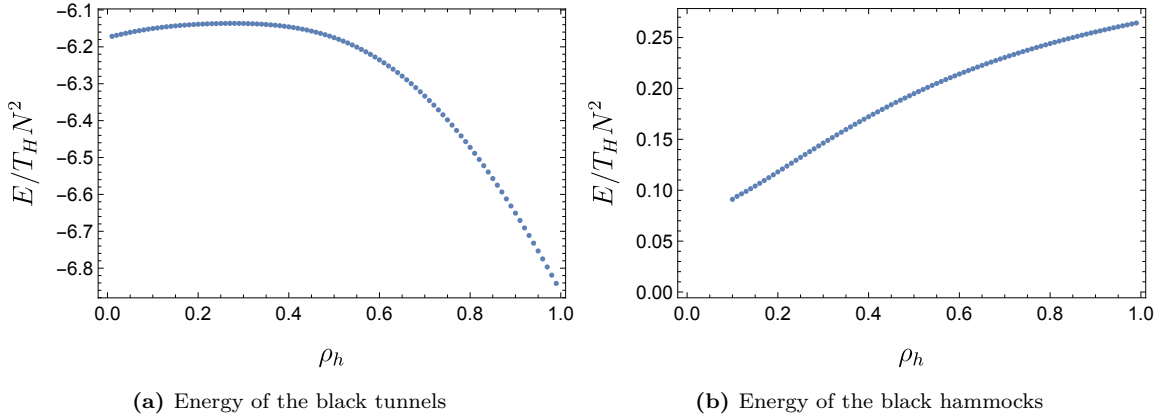


**Fig. 4.7:** The plots of the energy of the black tunnel and black hammock solutions across different values of the parameter  $\rho_h$ . Here we have divided the energy,  $E$ , by the temperature of the event horizon,  $T_H$ , in order to obtain a dimensionless quantity.

#### 4.4.5 Flow

Now let us turn our attention to some additional properties of the hammocks. Unlike the tunnel, the hammock is not a static solution in the bulk. This is due to the fact that the horizon is not a Killing horizon; there is flow along it. This flow represents the deconfined phase of the CFT corresponding to the hammock solution, and can be defined in terms of the holographic stress tensor by an integral over a two-sphere of fixed radius  $r$  as follows:

$$\Phi := - \int_{S^2} d^2x \sqrt{-\gamma} m^\mu k^\nu T_{\mu\nu}, \quad (4.57)$$

where  $\gamma_{\mu\nu}$  is the induced metric on a constant radius slice of the boundary de Sitter-Schwarzschild geometry with determinant  $\gamma$  and unit normal  $m^\mu$ , whilst  $k^\mu$  is again the stationary Killing vector field. Due to the conservation of the stress tensor, this integral is invariant of the choice of the radius of the two-sphere one integrates over.

Once again, we work in the coordinates  $(V, w, \theta, \phi)$  of (4.39) in which the stress tensor is regular at the horizons. Thus, we consider a constant  $w$  slice, with  $m_\mu \propto (dw)_\mu$  and  $k^\mu = (\partial/\partial V)^\mu$ . By expanding the equations of motion about the conformal boundary, as done in Section 4.3.4, one can show that the flow is given by

$$\Phi = \frac{N^2(1 - \rho_h)}{32\pi r_c^2 \rho_h (1 + \rho_h + \rho_h^2)^2} C_1, \quad (4.58)$$

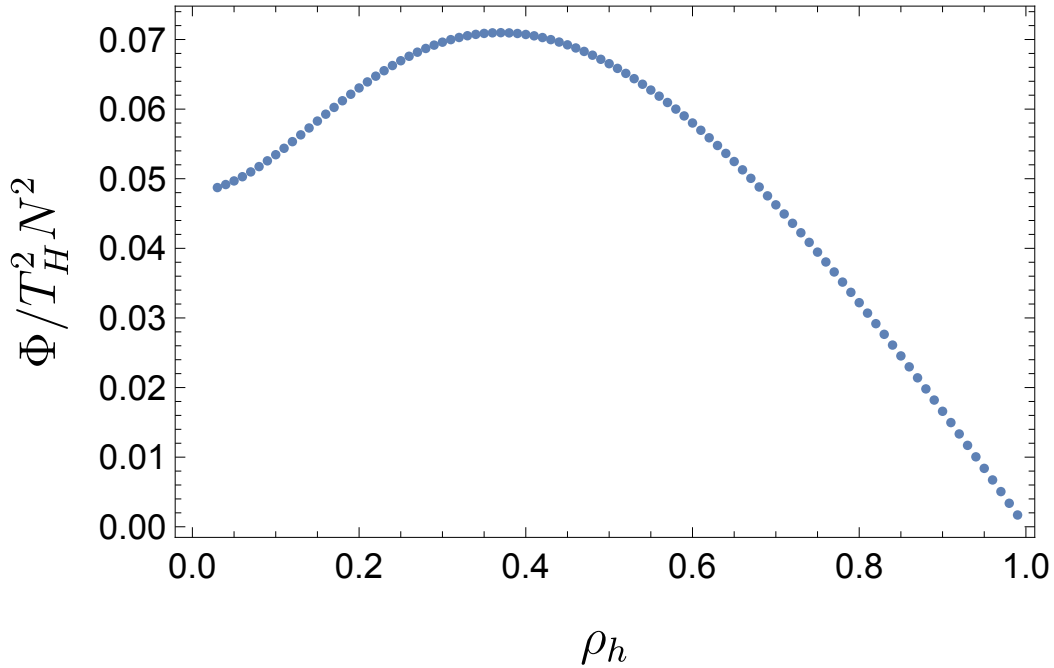


**Fig. 4.8:** The flow along the black hammock, divided by the temperature of the event horizon squared, for different values of the radius ratio,  $\rho_h$ . The flow,  $\Phi$ , is a non-monotonic function of  $\rho_h$ .

where  $C_1$  can be obtained numerically from a fourth derivative of the metric function  $p_2(x, y)$  using the equation (4.36). As expected this result is independent of the radial coordinate  $w$ .

This calculation confirms that in the deconfined hammock phase, the CFT on the field theory side of the duality flows at order  $\mathcal{O}(N^2)$ .

Since one only needs to extract a constant using the metric functions found numerically, the flow can be found to a high degree of accuracy for each of the black hammock solutions obtained. In Figure 4.8, we have plotted the flow as a function of the radius ratio,  $\rho_h$ . As expected,  $\Phi$  is positive for each of the solutions, which corresponds to flow from the hotter event horizon to the cooler cosmological horizon. Moreover, the flow tends towards zero in the extremal limit ( $\rho_h \rightarrow 1$ ) in which the event and cosmological horizons are aligned and have the same temperature.

Interestingly, the flow is a non-monotonic function of  $\rho_h$ , with a maximum at  $\rho_h \simeq 0.396$ . This property was also found in the flowing black funnel solutions of [135], which are dual to a CFT on a flat Schwarzschild background with the CFT asymptotically in a thermal state with non-zero temperature. As of yet, there is no field theory explanation of this non-monotonic behaviour of the flow for either the flowing funnels or the hammocks. The position of the maximum of the flow for the black hammocks is at a different value of the ratio of the two temperatures than the

flowing funnels, which is perhaps to be expected since in the case of the hammocks, the distance between the two horizons is finite and naturally varies as one changes the ratio of their temperatures, whereas the event horizon in the flowing funnels is always an infinite distance from the asymptotic region.

In [135] it was conjectured, with evidence provided by considering local Penrose inequalities [190], that the turning point of the flow may indicate the phase transition between the confined and deconfined phase of the CFT. It would be of great interest to investigate whether this also holds in the current case, with the turning point of the flow similarly signifying a transition from dominance of the tunnel solution to that of the hammock solution.

However, let us once again stress that the fact that one finds a non-monotonic function, and moreover the position of the maximum, depends on the quantity one uses to make the flow dimensionless. If one uses  $T_c$  instead of  $T_H$ , one finds that the flow diverges as  $\rho_h \rightarrow 0$ . It is not obvious which scale one should use to normalise.

#### 4.4.6 Expansion and shear of the hammock horizon

The fact that the bulk horizon of the hammock is non-Killing allows it to have interesting properties, for example, non-trivial expansion and shear.

Firstly, let us consider the behaviour of  $h_{IJ}$ , which was defined in Section 4.3.5, along the horizon, the  $y = 1$  hypersurface. In particular, we plot its determinant,  $h = \det h_{IJ}$ , in Figure 4.9a. Clearly,  $h$  monotonically increases with  $x$ , as one moves along the horizon from the boundary event horizon (at  $x = 0$ ) to the boundary cosmological horizon (at  $x = 1$ ).

Moreover, from the line element, (4.20), the coordinate velocity along the horizon is given by  $\Omega(x) = x(1-x)p_2(x, 1)$ . We plot this in Figure 4.9b against the  $x$  coordinate. For each value of the radius ratio,  $\rho_h$ , the coordinate velocity is positive across the horizon, which supports the fact that the flow along the horizon is from the hotter boundary event horizon at  $x = 0$  to the cooler boundary cosmological horizon at  $x = 1$ . This fact, together, with the fact that the determinant of  $h_{IJ}$  is an increasing function of  $x$ , suggests strongly that the past horizon lies at  $x = 0$ .

Now let us turn our attention to the affine parameter, the expansion and the shear. Following the discussion in Section 4.3.5, in order to obtain the affine parameter,  $\lambda(x)$ , we can numerically solve the ODE given by (4.49). In Figure 4.9c, we plot  $\lambda(x)$  against  $x$ . As one would expect,  $\lambda$  increases monotonically with  $x$ . It diverges as  $x \rightarrow 1$  at the boundary cosmological horizon. At the event horizon,  $x = 0$ ,  $\lambda$  goes instead to a finite value, which we are free to choose by rescaling the affine parameter. We have

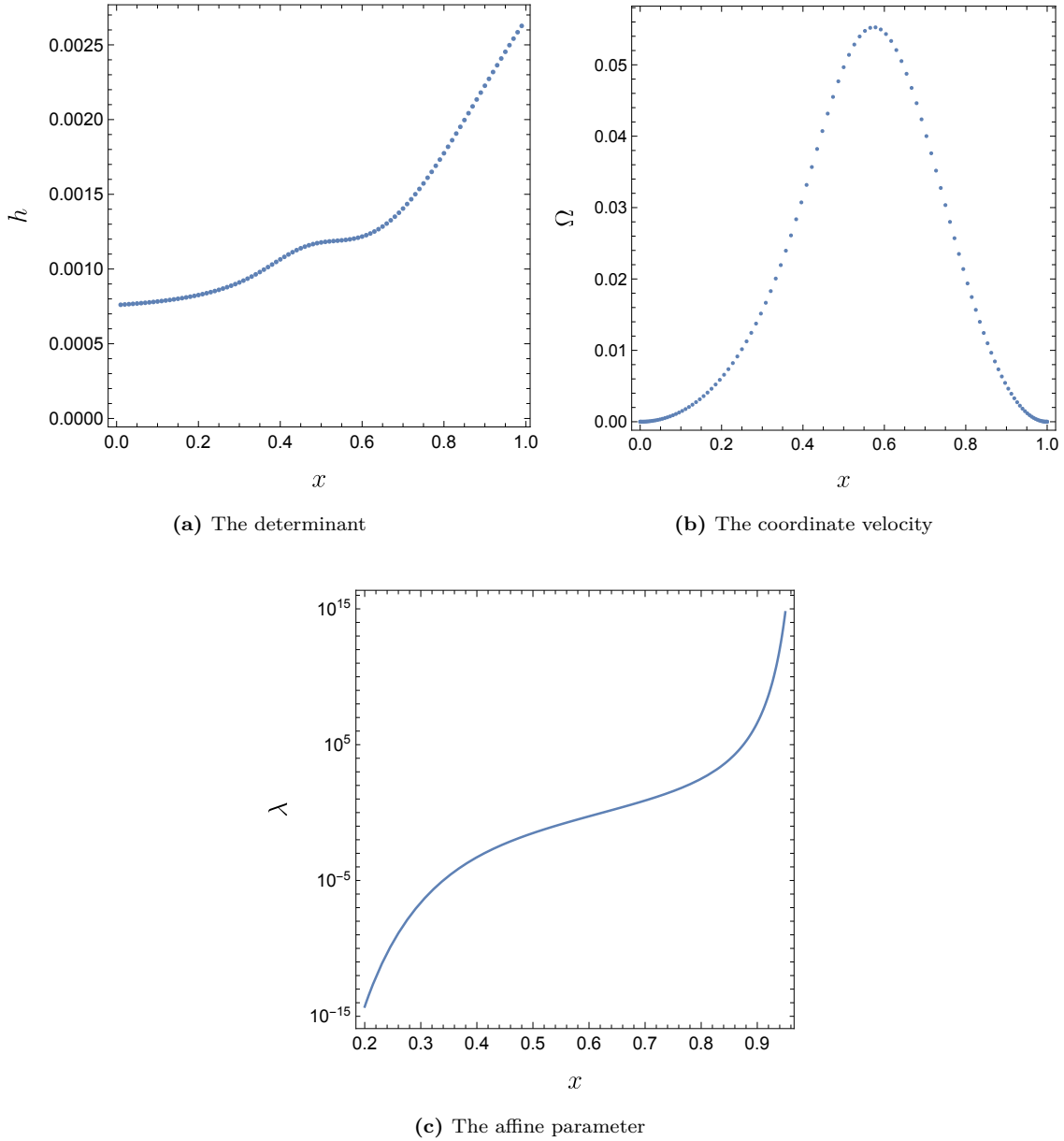


**Fig. 4.9:** Here we plot the the determinant,  $h = \det h_{IJ}$ , the coordinate velocity  $\Omega(x)$ , and the affine parameter,  $\lambda(x)$ , in **(a)**, **(b)** and **(c)**, respectively, against the coordinate  $x$  along the horizon for the black hammock with  $\rho_h = 0.4$ . Clearly, the determinant is a monotonically increasing function of  $x$ . Meanwhile the coordinate velocity  $\Omega(x)$  is positive, showing that the flow will be from the boundary event horizon to the boundary cosmological horizon. The affine parameter is also monotonically increasing, from zero at  $x = 0$ , at the boundary event horizon, up to positive infinity at  $x = 1$ , at the boundary cosmological horizon.

used such freedom to fix  $\lambda(0) = 0$  and  $\lambda'(0.5) = 1$ . Hence the boundary event horizon is the past boundary of the bulk horizon.

Once we have the affine parameter, the expansion and shear are easy to calculate using (4.50) followed by (4.45) and (4.46). In Figure 4.10, we plot the expansion along the horizon (now parameterised by the affine parameter  $\lambda$ ) in a log-log plot. As expected by Raychaudhuri's equation, we find that  $d\Theta/d\lambda < 0$  everywhere. For small and large values of  $\lambda$ , the expansion follows a line in the log-log plot. However, there is some interesting non-trivial behaviour of the expansion, in this case at around  $\lambda \simeq 0.2$ . This behaviour is partially explained by the behaviour of the shear.

The shear in  $\{v, \theta, \phi\}$  coordinates is given by a diagonal, traceless  $3 \times 3$  matrix, with its  $\theta$  and  $\phi$  components related due to spherical symmetry. Hence, the shear at each point is completely determined by its  $vv$  component:

$$\sigma^I{}_J = \text{Diag} \left( \sigma^v{}_v, -\frac{1}{2}\sigma^v{}_v, -\frac{1}{2}\sigma^v{}_v \right). \quad (4.59)$$

In Figure 4.11, we plot  $\sigma^v{}_v$  against the affine parameter, after taking the absolute value so that we can plot in a log-log plot. For small values of  $\lambda$  (nearer to the boundary event horizon) the  $\sigma^v{}_v$  component of the shear is positive, whereas, for large values of  $\lambda$  (nearer the boundary cosmological horizon),  $\sigma^v{}_v$  is negative. By continuity, the shear must vanish at some point along the horizon. This leads to the ‘‘kink’’ in the

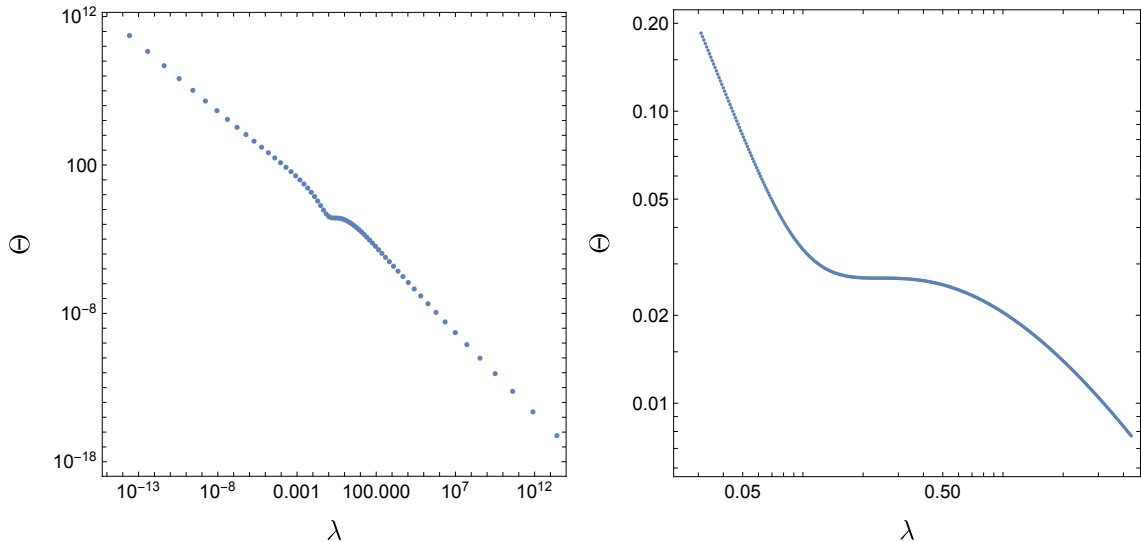


**Fig. 4.10:** The expansion,  $\Theta$ , of the horizon plotted against the affine parameter,  $\lambda$ . The left-hand panel is a log-log plot of this curve across a large portion of the horizon. The right hand panel is a zoom (still with a logarithm scale of both axes) of the plot on the left, focusing on the portion of the curve with non-linear behaviour of the expansion.

curve of the logarithm of the absolute value of  $\sigma^v_v$ , seen in Figure 4.11, located at around  $\lambda \simeq 0.2437$ . In the top-right panel of Figure 4.11, we've zoomed in on this point further, after interpolating between the lattice points. However, this apparent “kink” is only an artifact of the fact we've taken the absolute value so that we can plot in a log-log plot. To explain the behaviour more clearly, we've plotted  $\sigma^v_v$  in the region of interest without taking the absolute value or the logarithm on either axis in the bottom panel of Figure 4.11. Indeed, the shear vanishes at  $\lambda \simeq 0.2437$ , and  $\sigma^v_v$  has a minimum value at  $\lambda \simeq 0.2738$  before returning to zero as  $\lambda$  becomes large. This behaviour of the shear vanishing at a single point along the horizon, and flipping signs across it seems to occur for each of the hammocks we found across the parameter space. This behaviour was not found for the flowing funnels of [135]. Hence, it may be indicative of the horizon returning to the conformal boundary rather than tending towards the geometry of a planar horizon.

As discussed above, the expansion also seems to have interesting behaviour near this value of the affine parameter, which we've focused in on on the right hand panel of Figure 4.10. This behaviour follows from the behaviour of the shear, since by Raychaudhuri's equation,

$$\frac{d\Theta}{d\lambda} = -\frac{1}{3}\Theta^2 - \sigma^{IJ}\sigma_{IJ}, \quad (4.60)$$

so that when the shear vanishes, the magnitude of  $d\Theta/d\lambda$  decreases, so that the plot of  $\Theta$  temporarily flattens out near this point (though the gradient never vanishes completely). Indeed, we checked explicitly that the values found for the expansion and shear accurately satisfy Raychaudhuri's equation.

## 4.5 Discussion

We constructed the holographic duals to a large  $N$ , strongly coupled CFT living on a de Sitter-Schwarzschild background. These are five-dimensional, AlAdS spacetimes with a de Sitter-Schwarzschild geometry on the conformal boundary. There are two solutions: the black tunnel solution with two disconnected bulk horizons, which is dual to a confined phase of the CFT, and the black hammock solution with a single connected bulk horizon, which is dual to a deconfined phase of the CFT. We were able to find black tunnel solutions across the whole of the parameter space,  $\rho_h \in (0, 1)$ , where the radius ratio,  $\rho_h$ , is the ratio of the proper radii of the boundary event and cosmological horizons, and we were able to find black hammock solutions for a large range of the parameter space ( $\rho_h \geq 0.03$ ).

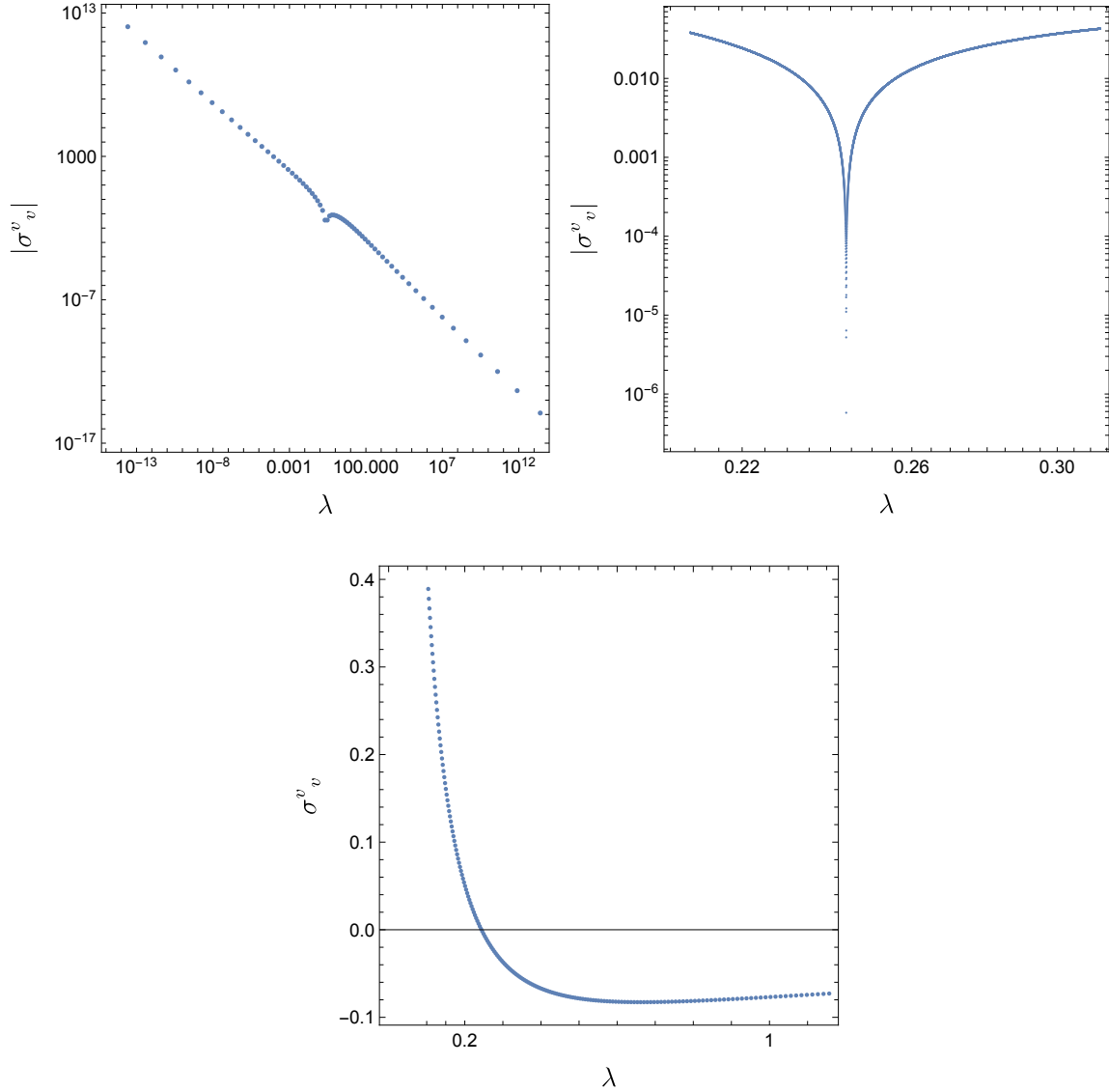


**Fig. 4.11:** In the top-left panel, the absolute value of the  $vv$  component of the shear,  $|\sigma^v_v|$ , is plotted against the affine parameter,  $\lambda$ , along the horizon of the black hammock with  $\rho_h = 0.4$  in a log-log plot. We have simply taken the absolute value in order to be able to take the logarithm. The plot in the top-left panel indicates some interesting behaviour of  $|\sigma^v_v|$  near  $\lambda \simeq 0.24$ , which we have zoomed in on in the top-right panel, after interpolating between lattice points. The behaviour near this point is more easily understood by looking at the behaviour of  $\sigma^v_v$  nearby, which is plotted (in a standard plot, without taking logs on either axis) in the bottom panel. The shear vanishes at  $\lambda \simeq 0.2437$ , with each of its non-trivial components,  $\sigma^I_J$ , flipping signs across this point on the horizon. We find  $\sigma^v_v$  is positive below this value of  $\lambda$  and negative for large values of  $\lambda$ , taking its minimum value at  $\lambda \simeq 0.2738$ , before tending towards zero as  $\lambda$  diverges.

We used complementary methods to obtain the two families of solutions. In order to find the black tunnels, we used the DeTurck method, which is very effective for static problems, yielding elliptic PDEs. Moreover with the boundary conditions in our case, it can be proven that Ricci solitons cannot exist, so that any solution found via the DeTurck method is necessarily a solution to the Einstein equation. On the other hand, we calculated the black hammocks in Bondi-Sachs gauge. This was the first use of such a gauge to find flowing ALAdS spacetimes in five dimensions. It seems as though Bondi-Sachs gauge works particularly well for spacetimes with a null hypersurface “deep” in the bulk, *i.e.* opposite the conformal boundary in the integration domain. Such solutions, for example, the hammocks of this work, as well as flowing funnel solutions can also be found using the DeTurck method, though generally in these cases one cannot say with absolute certainty that the solutions are not Ricci solitons, and moreover, the solutions need to be found to a high degree of precision and on a large number of lattice points in order for quantities like the holographic stress tensor to be extracted. For example, we found that extracting the stress tensor of the black hammock solutions in DeTurck gauge required around twice the number of lattice points in the radial direction compared with when using the solutions found in Bondi-Sachs gauge. Not only this, but to find the hammocks in DeTurck gauge, one has to solve for seven metric functions, rather than just the five in Bondi-Sachs gauge. Moreover, in Bondi-Sachs gauge we were able to explore far more of the parameter space. It would be very interesting to explore the efficacy of the Bondi-Sachs gauge in this context in more detail, and its use may open a door to solving other difficult problems, particularly those with the presence of a flowing horizon.

The horizon of the black hammock is not a Killing horizon, allowing it to have interesting properties, such as classical flow along it, as well as non-vanishing expansion and shear. This does not contradict the rigidity theorems, since these apply only to geometries with horizons with compactly generated spatial cross-sections. The boundary event horizon is always hotter than the boundary cosmological horizon, and hence, as one would expect, we found that the classical flow along the black hammock is always from the event horizon to the cosmological horizon. The results of the shear and expansion are interesting, particularly the result that the shear vanishes at a point along the horizon, with all of its components swapping signs across this point.

It would be of great interest to be able to investigate the phase diagram of the CFT living on the de Sitter-Schwarzschild background. This would be achieved by deducing which of the gravitational duals dominates for a given value of the parameter,  $\rho_h$ . It would be expected that for very small  $\rho_h$ , when the boundary horizons are very far

apart, the confined, tunnel phase would dominate, whilst for large  $\rho_h \simeq 1$ , where the horizons are almost aligned, the deconfined, hammock phase would dominate. Hence, the expectation is that there is a phase transition at some intermediate value of  $\rho_h$ . However, there is much difficulty in confirming this behaviour and finding the location of this phase transition.

In [135], it was suggested that a similar transition between black droplet and funnel solutions, which are dual to a CFT on a flat Schwarzschild background, occurs at the point in the parameter space at which the flow,  $\Phi$ , is maximised. We find a maximum of the flow, as seen in Figure 4.8, so one may conjecture that this is signifying the phase transition. However, the position of this maximum depends on the choice of quantity used to make the flow dimensionless. We used the temperature of the boundary event horizon,  $T_H$ . It is not clear to us that this is the meaningful quantity to use, as opposed to the temperature of the boundary cosmological horizon,  $T_c$ , or indeed some combination of these two temperatures.

This issue is linked to the difficulty to undergo a thermodynamic study of the two solutions in order to deduce which dominates. For example, in [140], the phases of similar solutions was investigated by comparing the free energy,  $F = E - TS$ , of each of the solutions, with the solution with least free energy dominating. However, in our case, the solutions are not in thermal equilibrium which means that the free energy is very difficult to define.

Moreover, we found there was some difficulty in extracting the difference in the entropy of the two solutions. In particular, we found that the difference between the sum of the areas of the two tunnel horizons and the area of the hammock horizon is infinite, even after matching the conformal frame. Divergences in extremal surface area can depend only upon the boundary metric, so this suggests that the hammock horizon is not the minimal extremal surface.<sup>2</sup> Therefore, in order to find the entropy difference, one would have to extend the geometry of the hammock through the bulk horizon, find the extremal surface and compare the area of it to the area of the two bulk horizons of the black tunnel. It would be very interesting to further understand this divergence of the difference between the horizon areas of the two solutions, and to explicitly find the extremal surface for the hammock.

In lieu of a thermodynamic argument to determine the dominance of either the tunnel or hammock, it appears that the best course to take in order to investigate the phase diagram may be to explicitly test the stability of the two bulk solutions across the parameter space. Fortunately, Bondi-Sachs gauge is extremely well-adapted to allow

---

<sup>2</sup>I would like to thank Don Marolf for his insight into this issue.

for one to slightly perturb the black hammock solutions and track over a time-evolution whether this perturbation leads to an instability. One would perhaps expect that for small values of  $\rho_h$ , the black hammock would be unstable to such a perturbation, and hence would decay into a black tunnel. However, in order for such a transition to occur, the single bulk horizon of the hammock would have to “pinch off” and split into two disconnected horizons. Such evolution would violate the weak cosmic censorship conjecture [15], perhaps in a similar manner to the Gregory-Laflamme instability of the black string [191, 192]. It has previously been shown that weak cosmic censorship can be violated in AdS [193–196], though the current set-up may prove to be an easier problem in which to explicitly find the evolution towards a naked singularity.

# Chapter 5

## Holographic batteries

### Abstract

We study a three-dimensional holographic CFT under the influence of a background electric field on a spacetime containing two black hole horizons. The electric background is fixed such that there is potential difference between the two boundary black holes, inducing a conserved current. By constructing the holographic duals to this set-up, which are solutions to the Einstein-Maxwell equations with a negative cosmological constant in four dimensions, we calculate, to a fully non-linear level, the conductivity of the CFT in this background. Interestingly, we find that the conductivity depends non-trivially on the potential difference. The bulk solutions are flowing geometries containing black hole horizons which are non-Killing and have non-zero expansion. We find a novel property that the past boundary of the future horizon lies deep in the bulk and show this property remains present after small perturbations of the temperature difference of the boundary black holes. This work was first published in [3].

### 5.1 Introduction

Given a quantum field theory (QFT), a natural avenue of investigation is to test how it behaves under an external electric field. Studying such behaviour for a strongly coupled QFT using direct field theory techniques is computationally very challenging (though progress has been made when the system is in the proximity of quantum critical points [197]; see also [198] for a holographic description of a similar setup). However, since its advent, the AdS/CFT correspondence [109–111] has allowed for the indirect study of strongly coupled condensed matter systems via gravitational calculations (see for instance [199] for an excellent review on the topic).

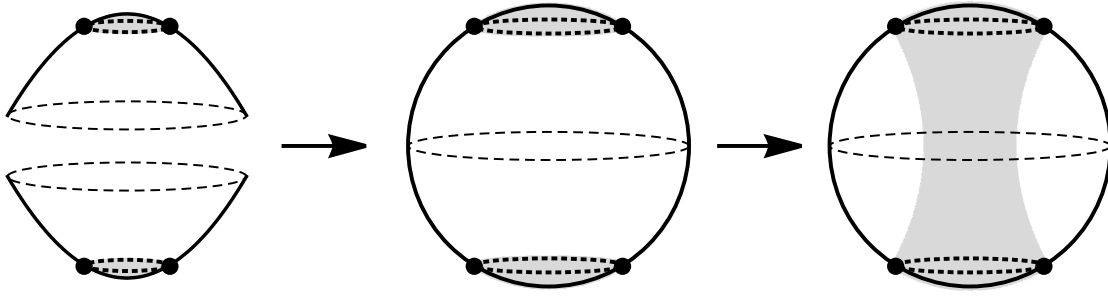


**Fig. 5.1:** Some sketches of spatial cross-sections of spacetimes of interest. **Left:** Two BTZ black holes with the dashed curves being their asymptotic boundaries and the dotted line their horizons. The interior is shaded. **Middle:** The boundary geometry found by patching the BTZ spacetimes together at infinity and then compactifying onto the ESU. **Right:** The global funnel, a solution in the bulk with a horizon connecting the two boundary horizons.

Specifically, we work in the limit of the AdS/CFT duality in which the gravitational theory is well described by classical gravity. In this limit, the duality maps a problem of studying a strongly coupled CFT with a large number of degrees of freedom living on a fixed (but possibly curved) background,  $\mathcal{B}$ , to a gravitational problem in which one must find a corresponding *asymptotically locally AdS*, (AlAdS), spacetime, called the *bulk*, which possesses a conformal boundary on which the induced metric is conformal to  $\mathcal{B}$ .

Taking  $\mathcal{B}$  to be an asymptotically flat black hole background led to the black droplet and funnels reviewed in Section 1.4, whilst considering  $\mathcal{B}$  to be a black hole in de Sitter space led to the solutions of the previous chapter.

In this chapter, we will focus on four-dimensional global funnels. The boundary geometry will be given by the conformal compactification of the geometry obtained by “patching together” two identical Bañados-Teitelboim-Zanelli (BTZ) black holes [124] (shown on the left in Figure 5.1) at their asymptotic boundaries. This yields two black holes antipodally situated in the Einstein Static Universe (ESU) as sketched in the middle in Figure 5.1. There is a well-known solution called the BTZ black string or uniform funnel which connects these two boundary black holes, however, even in the case of vacuum gravity in the bulk, there is a rich structure of bulk solutions beyond this uniform funnel [138–140, 200]. The right hand sketch in Figure 5.1 is a schematic drawing of a global funnel.

We add a chemical potential,  $A_\mu^{(0)}$ , to the field theory which induces a conserved current,  $J^\mu$ , and, on the gravitational side of the duality, causes a deformation of the bulk geometry away from the uniform funnel to a new solution to the Einstein-Maxwell equations with a negative cosmological constant. We will define the chemical potential

to vary on the boundary background, and in particular fix that it approaches two different values at the two BTZ black hole horizons in the boundary geometry. Since these charged global funnels correspond to the QFT sourced by the two horizons at the same temperature but with a potential difference between them, we dub the solutions as *holographic batteries*.

The background electric field caused by the chemical potential is  $E^\mu = (F^{(0)})^{t\mu}$  where  $F^{(0)}$  is the field strength tensor arising from  $A^{(0)}$  and  $t$  is the coordinate associated to the stationary Killing vector field of the boundary geometry. Ohm's law tells us that the conductivity,  $\sigma$ , of the field theory is the ratio between the induced current and the background electric field:

$$J^\mu = \sigma^\mu{}_\nu E^\nu. \quad (5.1)$$

Calculating the bulk solution allows one to extract the conserved current,  $J^\mu$ , induced by the source on the field theory side, and hence the conductivity of the boundary field theory (see [201] for a nice introduction to computing conductivity holographically).

In much previous work, only the linear response of the field theory to a small background electric field was computed [202–210]. However, the computation of a full bulk solution to the non-linear equations allows one to compute the conductivity of the field theory non-linearly, and so the behaviour of the field theory under strong electric fields can be calculated. Interestingly, we find that the conductivity is not a constant value, *i.e.* the current,  $J^\mu$ , depends non-trivially on the magnitude of the chemical potential, despite there being no net energy flow, in contrast to what was observed in [211, 212].

Moreover, the chemical potential varying across the boundary geometry induces classical flow along the bulk horizon. Unlike previously found solutions containing flowing horizons [179, 139, 135, 2], this flow is not caused by a temperature difference between two asymptotic regions of the bulk horizon, and this means the properties of the holographic batteries are subtly different to these other flowing solutions. In particular, we show that the past boundary of the bulk horizon lies deep in the bulk, as opposed to on one of the points at which the bulk horizon is anchored on the boundary, as seen in all previous flowing black hole geometries. We show that this property is generic by considering holographic batteries in which the boundary black holes can also have a small temperature difference.

## 5.2 Finding the holographic batteries

First let us consider the metric of the BTZ black hole:

$$ds_{BTZ}^2 = -f(r) dT^2 + \frac{dr^2}{f(r)} + r^2 d\varphi^2, \quad (5.2)$$

with  $f(r) = (r^2 - r_0^2)/\ell_3^2$ , where  $r_0$  is the radius of the BTZ black hole and  $\ell_3$  is the three-dimensional AdS length scale. Taking

$$r = \frac{r_0}{x\sqrt{2-x^2}}, \quad T = \frac{\ell_3^2}{r_0} t, \quad \varphi = \frac{\ell_3}{r_0} \phi, \quad (5.3)$$

so that  $x = 1$  is the horizon and  $x = 0$  is infinity, yields

$$\begin{aligned} d\tilde{s}_{BTZ}^2 &= \Omega(x)^2 ds_{BTZ}^2 \\ &= \ell_3^2 \left[ -dt^2 + \frac{1}{(1-x^2)^2} \left( \frac{4dx^2}{2-x^2} + d\phi^2 \right) \right], \end{aligned} \quad (5.4)$$

where we've multiplied the metric by a conformal factor

$$\Omega(x) = \frac{x\sqrt{2-x^2}}{1-x^2}. \quad (5.5)$$

Note that  $\phi$  has a period of  $2\pi r_0/\ell_3$ , which we must take into account when calculating any global properties of the solutions. The geometry upon which we wish to study the CFT is obtained by patching two copies of the metric given by  $d\tilde{s}_{BTZ}^2$  at their boundaries, *i.e.* at  $x = 0$ . Thus the boundary metric is given by the metric in (5.4), with  $x \in [-1, 1]$  and  $x = \pm 1$  being the two boundary black hole horizons. The temperature of each horizon, measured in units of the original  $T$  coordinate, is given by  $T_H = r_0/(2\pi\ell_3^2)$ .

The idea is to add an electric field on this background which acts as a source and to fix the chemical potential at the two boundary horizons,  $x = \pm 1$ . Specifically, let us add an electrical source given by the following vector potential:

$$A^{(0)} = \mu g(x) dt, \quad (5.6)$$

where  $g(x)$  is a profile we are free to choose and which we will design so that  $g(1) = +1$  and  $g(-1) = -1$ . The potential difference between the two horizons is

$$V := \left[ A^{(0)} \cdot k \right]_{x=-1}^{x=1} = 4\pi\mu T_H, \quad (5.7)$$

where  $k = \partial/\partial T$ . For the majority of this chapter we take

$$g(x) := \sin\left(\frac{\pi}{2}x\sqrt{2-x^2}\right), \quad (5.8)$$

which we call the *sine profile*.

The addition of an electric source in the boundary theory means that the bulk theory is Einstein-Maxwell with a negative cosmological constant in four dimensions, with the following equations of motion:

$$0 = E_{ab} := R_{ab} + \frac{3}{\ell_4^2}g_{ab} - 2T_{ab} \quad (5.9a)$$

$$0 = \nabla^a F_{ab} \quad (5.9b)$$

where  $\ell_4$  is the four-dimensional AdS length scale,  $F = dA$  is the field strength tensor of the Maxwell field and the bulk stress tensor<sup>1</sup> is given by

$$T_{ab} = F_a{}^c F_{bc} - \frac{1}{4}g_{ab}F^{cd}F_{cd}. \quad (5.10)$$

We obtained the solutions in both Bondi-Sachs gauge and using the DeTurck method. Each gauge has different uses. The numerical computation is far quicker in Bondi-Sachs gauge and quantities of interest, such as properties of the horizon and the asymptotic quantities, are far easier to read off. On the other hand, we found that solutions with larger values of the amplitude,  $\mu$ , of the boundary potential could be found using the DeTurck method.<sup>2</sup> Non-analytic terms do arise in the expansion of the metric near the horizon in DeTurck gauge, unlike in Bondi-Sachs gauge, which leads to some difficulties in reading off asymptotic quantities.

Thus, the solutions in Bondi-Sachs gauge are far more user-friendly, and we present an *Ansatz* for the holographic batteries in this gauge in Section 5.2.1. We also describe explicitly the process of holographic renormalization in this case as it turns out to be quite simple. We will also briefly discuss how these solutions can be found using the

<sup>1</sup>In four dimensions, the trace of the stress tensor of a Maxwell field necessarily vanishes, so that the stress tensor agrees with the trace-reversed stress tensor.

<sup>2</sup>By using the patching methods of Section 2.4.3, one may be able to also access this part of the parameter space using Bondi-Sachs gauge.

DeTurck method in Section 5.2.2. Obtaining the solutions in two different gauges also greatly supports their validity, and indeed we found that in the region of the parameter space in which solutions were found in both gauges, all gauge invariant quantities extracted were in agreement between the two gauges.

### 5.2.1 Bondi-Sachs gauge

We begin with an *Ansatz* in Bondi-Sachs gauge which possesses a null hypersurface at  $y = 1$  and a conformal boundary at  $y = 0$ . We also assume the solutions will be stationary and axisymmetric, with corresponding Killing vector fields  $\partial_v$  and  $\partial_\phi$ , respectively. For the gauge field we pick a gauge in which  $A_y = 0$ . In such a gauge, the *Ansatz* is given by

$$ds^2 = \frac{\ell_4^2}{y^2} \left[ q_2^2 \left( -(1-y^2)q_1 dv^2 - 2 dv dy \right) + \frac{q_5^2}{(1-x^2)^2} \left( \frac{4(dx - (1-x^2)q_4 dv)^2}{(2-x^2)q_3} + q_3 d\phi^2 \right) \right] \quad (5.11a)$$

and

$$A = \ell_4 \left( q_6 dv + \frac{q_7}{1-x^2} dx \right), \quad (5.11b)$$

where  $q_i(x, y)$  are unknown functions which depend upon  $x$  and  $y$ . Schematically, this spacetime also looks like the right-hand sketch in Figure 5.1.

There is still some gauge freedom in the *Ansatz* which can be used to fix the radial dependence of either  $q_2$  or  $q_5$  completely. In our case we fix that of  $q_5$ , by enforcing

$$q_5(x, y) = 1 + y^2 S_2(x). \quad (5.12)$$

The Einstein-Maxwell equations yield ten equations for the seven unknown functions in the metric and vector potential given by the *Ansatz*, (5.11), in Bondi-Sachs gauge. On the face of it, one may worry that the equations are over-determined, but in reality not all of the equations of motion are independent. In fact, one can solve the *bulk equations*, which are given by  $E_{ij} = 0$  and  $\nabla^a F_{ai} = 0$  for  $i, j \neq v$  where  $v$  is the temporal direction, throughout the whole of the space and the remaining equations, named the *supplementary equations*,  $E_{va} = 0$  and  $\nabla^a F_{av} = 0$ , on a constant  $y$  slice, which in our case we choose to be the  $y = 1$  null hypersurface, and which we check *a posteriori* is the event horizon.

Having set the supplementary equations as Robin boundary conditions at  $y = 1$ , the contracted Bianchi identity, together with the bulk equations, enforce that the supplementary equations must be satisfied throughout the whole spacetime, as shown in Section 2.2. It still remains to be fully understood whether this integration scheme leads to a well-defined elliptic PDE problem for a stationary spacetime.

Now let us address the boundary conditions at the remaining boundaries of the integration domain. Recall that the radial dependence of the  $q_5$  function is fixed as (5.12) as a gauge choice, so we need not prescribe boundary conditions for this function. At  $y = 0$ , the conformal boundary, we set Dirichlet boundary conditions enforcing that the induced metric on the boundary is conformal to (5.4). To do so, we set  $q_1 = q_2 = q_3 = 1$  and  $q_4 = 0$ . Then after taking the transformations:

$$dv = dt - \frac{1}{1-y^2} dy, \quad y = \frac{z}{\ell_3} \quad (5.13)$$

we find that to leading order in  $z$ ,

$$ds^2 = \frac{L^2}{z^2} \left( dz^2 + d\tilde{s}_{BTZ} \right) + \mathcal{O}(z^{-1}), \quad (5.14)$$

where  $d\tilde{s}_{BTZ}$  is the desired boundary metric, given by (5.4). As for the gauge field, we want it to approach the desired electric source (5.6) at leading order at the conformal boundary. As such, we enforce at  $y = 0$  that

$$q_6 = \mu g(x), \quad q_7 = 0. \quad (5.15)$$

The funnels naturally lie on a coordinate domain with only two boundaries, the conformal boundary and the bulk horizon. However, running numerics on such a domain is very difficult, and so, similarly to what was done in [139, 135, 2], the two points at which the horizon meets the boundary are “blown up” to two extra sides of the coordinate domain, given by  $x = \pm 1$ . This is possible because the horizon must approach the geometry of a hyperbolic black hole asymptotically as it approaches the conformal boundary. Hence at  $x = \pm 1$ , we fix that the horizon has this limiting behaviour. This is also done by setting  $q_1 = q_2 = q_3 = 1$  and  $q_4 = 0$  at these boundaries. Moreover, to match the vector potential at these boundaries to the conformal boundary, we take  $q_6(1, y) = \mu$ ,  $q_6(-1, y) = -\mu$  and  $q_7(\pm 1, y) = 0$ .

Finally, in order to numerically solve the bulk equations, we use pseudo-spectral collocation methods on a Chebyshev-Gauss-Lobatto grid to approximate the PDEs

with non-linear algebraic equations which are solved iteratively by Newton's method, as described in Section 2.3.

Due to the fact the supplementary equations are not enforced explicitly throughout the bulk, they give us a way to test the veracity of the solutions, since they should still tend to zero across the bulk in the continuum limit. This convergence test is shown in Appendix A.4.

**Holographic renormalization.** Having set the Dirichlet boundary conditions at the conformal boundary,  $y = 0$ , a local, order-by-order analysis of the equations of motion near  $y = 0$  determine the asymptotic behaviour of the  $q_i$  functions to a large extent. Expanding about this boundary, one discovers that

$$q_1(x, y) = 1 + 3S_2(x)y^2 + \alpha_1(x)y^3 + \mathcal{O}(y^4) \quad (5.16a)$$

$$q_2(x, y) = 1 - \frac{1}{2}S_2(x)y^2 + \mathcal{O}(y^4) \quad (5.16b)$$

$$q_3(x, y) = 1 + \alpha_3(x)y^3 + \mathcal{O}(y^4) \quad (5.16c)$$

$$q_4(x, y) = \alpha_4(x)y^3 + \mathcal{O}(y^4) \quad (5.16d)$$

$$q_5(x, y) = 1 + y^2S_2(x) \quad (5.16e)$$

$$q_6(x, y) = \mu g(x) + \beta_6(x)y + \mathcal{O}(y^2) \quad (5.16f)$$

$$q_7(x, y) = \beta_7(x)y + \mathcal{O}(y^2) \quad (5.16g)$$

where, we recall that the radial profile of the  $q_5$  was actually a gauge choice we were free to make. All higher order terms are fixed in terms of  $\{\alpha_1, \alpha_3, \alpha_4, \beta_6, \beta_7\}$ , which are the free functions that are not fixed by any local analysis of the equations of motion near the boundary. Instead, in order to find these five functions, we need to solve the equations of motion fully, whilst enforcing regularity deep in the bulk. The local analysis of the equations of motion does, however, provide some information on the functional form of  $\beta_7$  and  $\alpha_4$ :

$$\beta_7(x) = (1 - x^2) \left( \frac{C_1}{\sqrt{2 - x^2}} - \mu g'(x) \right) \quad (5.17)$$

$$\alpha_4(x) = (1 - x^2) \left[ \sqrt{2 - x^2} \left( C_2 + \frac{1}{3}\mu C_1 g(x) \right) - \frac{1}{4}(2 - x^2)S_2'(x) \right], \quad (5.18)$$

where  $C_1$  and  $C_2$  are unknown constants not fixed by the asymptotic expansion, which we will see are intimately connected to the conductivity and the flow of the field theory. Once the  $\{\alpha_1, \alpha_3, \alpha_4, \beta_6, \beta_7\}$  functions are obtained via the bulk calculation, one can

proceed with the standard approach of holographic renormalization [120], explained in Section 1.3.3, by transforming to Fefferman-Graham gauge, in which the metric and vector potential in four dimensions take the form:

$$ds^2 = \frac{\ell_4^2}{z^2} \left[ dz^2 + \left( g_{\mu\nu}^{(0)} + g_{\mu\nu}^{(2)} z^2 + g_{\mu\nu}^{(3)} z^3 + \dots \right) dx^\mu dx^\nu \right], \quad (5.19a)$$

$$A = \ell_4 \left( A_\mu^{(0)} + z A_\mu^{(1)} \right) dx^\mu + \mathcal{O}(z^2), \quad (5.19b)$$

where  $g_{\mu\nu}^{(0)}$  is the boundary metric,  $A_\mu^{(0)}$  is the boundary electric source and the Greek indices run over all coordinates other than the AdS radial direction,  $z$ . This can be achieved with a coordinate transformation

$$x = w + \sum_{j=1}^4 \gamma_j(w) z^j, \quad y = \sum_{j=1}^4 \delta_j(w) z^j, \quad (5.20a)$$

as well as a gauge transformation of the vector potential,  $A \rightarrow A + d\chi$ , with

$$\chi = \sum_{j=1}^2 \varepsilon_j(w) z^j. \quad (5.20b)$$

The explicit expressions for  $\gamma_j(w)$ ,  $\delta_j(w)$  and  $\varepsilon_j(w)$  can be found by taking the expansion of the metric and gauge field given by (5.16), transforming with (5.20) and then matching with the Fefferman-Graham form of the metric and vector potential order-by-order in  $z$ .

Finally, the vacuum expectation value of the holographic stress tensor and the conserved current can be simply read off as

$$\langle T_{\mu\nu} \rangle = \frac{3\ell_4^2}{16\pi G_4} g_{\mu\nu}^{(3)}, \quad \langle J_\mu \rangle = \frac{\ell_4^2}{4\pi G_4} A_\mu^{(1)}. \quad (5.21)$$

Note that the holographic stress tensor,  $\langle T_{\mu\nu} \rangle$ , is distinct from the bulk stress tensor,  $T_{ab}$ , arising from the bulk Maxwell field. Explicitly, we find

$$\begin{aligned} \langle T_{tt} \rangle &= -\frac{\nu \alpha_1(x)}{2\ell_3}, & \langle T_{xx} \rangle &= -\frac{\nu (\alpha_1(x) + 3\alpha_3(x))}{\ell_3(2-x^2)(1-x^2)^2}, & \langle T_{\phi\phi} \rangle &= \frac{\nu (3\alpha_3(x) - \alpha_1(x))}{4\ell_3(1-x^2)^2}, \\ \langle T_{tx} \rangle &= -\frac{3\nu}{4\ell_3} \left( S_2'(x) + \frac{4\alpha_4(x)}{(2-x^2)(1-x^2)} \right) & &= -\frac{\nu (\mu g(x) C_1 + 3C_2)}{\ell_3 \sqrt{2-x^2}} \end{aligned} \quad (5.22a)$$

and

$$\langle J_t \rangle = \frac{\nu \beta_6(x)}{\ell_3}, \quad \langle J_x \rangle = \frac{\nu}{\ell_3} \left( \frac{\beta_7(x)}{(1-x^2)} + \mu g'(x) \right) = \frac{\nu C_1}{\ell_3 \sqrt{2-x^2}}, \quad (5.22b)$$

with  $\nu = \ell_4^2/(4\pi G_4)$  which on the field theory side is a parameter measuring the number of degrees of freedom of the CFT, and where we have made use of (5.17) and (5.18) which fix the functional forms of  $\langle T_{tx} \rangle$  and  $\langle J_x \rangle$ , though one must still compute the bulk solution in order to extract the value of the integration constants,  $C_1$  and  $C_2$ .

One can explicitly check that the current is conserved:

$$D_\mu \langle J^\mu \rangle = 0, \quad (5.23)$$

where  $D_\mu$  is the covariant derivative associated to the boundary geometry, and moreover the stress tensor is traceless and satisfies a Ward relation:

$$\langle T_\mu{}^\mu \rangle = 0, \quad D^\mu \langle T_{\mu\nu} \rangle - F_{\mu\nu}^{(0)} \langle J^\mu \rangle = 0, \quad (5.24)$$

where  $F^0$  is the field strength tensor arising from the source, (5.6).

## 5.2.2 DeTurck gauge

We also obtained the solutions via the DeTurck method, in which one adds additional terms to the equations of motion in order to make them elliptic. One solves the *Einstein-DeTurck equations* given by

$$0 = R_{ab} + \frac{3}{\ell^2} g_{ab} - 2T_{ab} - \nabla_{(a} \xi_{b)}, \quad (5.25a)$$

$$0 = \nabla^a F_{ab} - \nabla_b \zeta \quad (5.25b)$$

with

$$\xi^a = g^{cd} [\Gamma_{cd}^a(g) - \Gamma_{cd}^a(\bar{g})] \quad (5.25c)$$

$$\zeta = g^{cd} \nabla_c (A_d - \bar{A}_d) \quad (5.25d)$$

where  $\bar{g}_{ab}$  and  $\bar{A}_a$  are, respectively, a reference metric and a reference vector potential which we are free to choose. In this case there are no guarantees the solutions will not be Ricci solitons, hence we must check after the fact that  $\xi$  and  $\zeta$  are small and

tending to zero in the continuum limit. These convergence tests are also presented in Appendix A.4.

The *Ansatz* for the holographic batteries in DeTurck gauge is given by

$$ds^2 = \frac{\ell_4^2}{y^2} \left[ -p_1 dv^2 - 2p_2 dv dy + p_5 dy^2 + \frac{p_4 d\phi^2}{(1-x^2)^2} + \frac{4p_3}{2-x^2} \left( \frac{dx}{1-x^2} + p_6 dy + p_7 dv \right)^2 \right] \quad (5.26a)$$

and

$$A = \ell_4 \left( p_8 dv + p_9 dy + \frac{p_{10}}{1-x^2} dx \right), \quad (5.26b)$$

where the unknown  $p_i$  functions depend on  $x$  and  $y$ . The reference metric and vector potential are obtained by setting

$$p_i(x, y) = \begin{cases} 1 - y^2 & \text{for } i = 1 \\ 1 & \text{for } 2 \leq i \leq 4 \\ \mu g(x) & \text{for } i = 8 \\ 0 & \text{otherwise} \end{cases} \quad (5.27)$$

The equations are again solved as a boundary value problem. Dirichlet boundary conditions are set at the conformal boundary,  $y = 0$ , and the two asymptotic regions where the horizon meets the boundary at  $x = \pm 1$  simply by setting that the metric and vector potential are equal to the reference metric and reference vector potential, *i.e.*  $p_i$  is given by (5.27) at these boundaries. Similarly to in Bondi-Sachs gauge, these conditions enforce that the boundary metric is conformal to (5.4), the vector potential at the conformal boundary is equal to (5.6) up to a factor of  $\ell_4$ , and that the bulk horizon approaches the geometry of a hyperbolic horizon near the boundary.

We do not set boundary conditions at the  $y = 1$  boundary. Instead, following the pioneering work of [179], we solve the equations of motion to a larger value of  $y = y_{max} > 1$ , ensuring that the horizon of the obtained solution lies within the integration domain. This method implicitly enforces the condition that the metric is regular at the horizon, due to the fact that using pseudo-spectral method yields regular solutions throughout the interior of the integration domain.

Once the solutions are obtained, one can again extract the holographic stress tensor and conserved current via a process of holographic renormalization, though in DeTurck gauge one must contend with non-analyticities in the expansion.

In this gauge the horizon is not necessarily the  $y = 1$  slice. One can find the position of the bulk horizon by assuming it takes the form  $y = P(x)$  such that  $P(1) = P(-1) = 1$ , and then the fact that the horizon must be a null hypersurface provides a first order ODE for  $P$  which can be solved numerically. We find that the horizon “bends inwards” in the coordinate domain so that  $P(x) \leq 1$  for all  $x \in [-1, 1]$ , and so we are free to take  $y_{max}$  as close to 1 as we like.

Having found the solutions in two different gauges strongly supports that they are valid solutions to the Einstein-Maxwell equations, and we find that in the region of the parameter space in which we found solutions in both gauges all physical quantities matched. Though the use of Bondi-Sachs gauge is numerically less expensive and allows for the easier extraction of physical quantities, we found that the DeTurck gauge allowed us to obtain solutions with larger values of  $\mu$  than was possible in Bondi-Sachs gauge.

## 5.3 Results

### 5.3.1 Stress tensor and conserved current

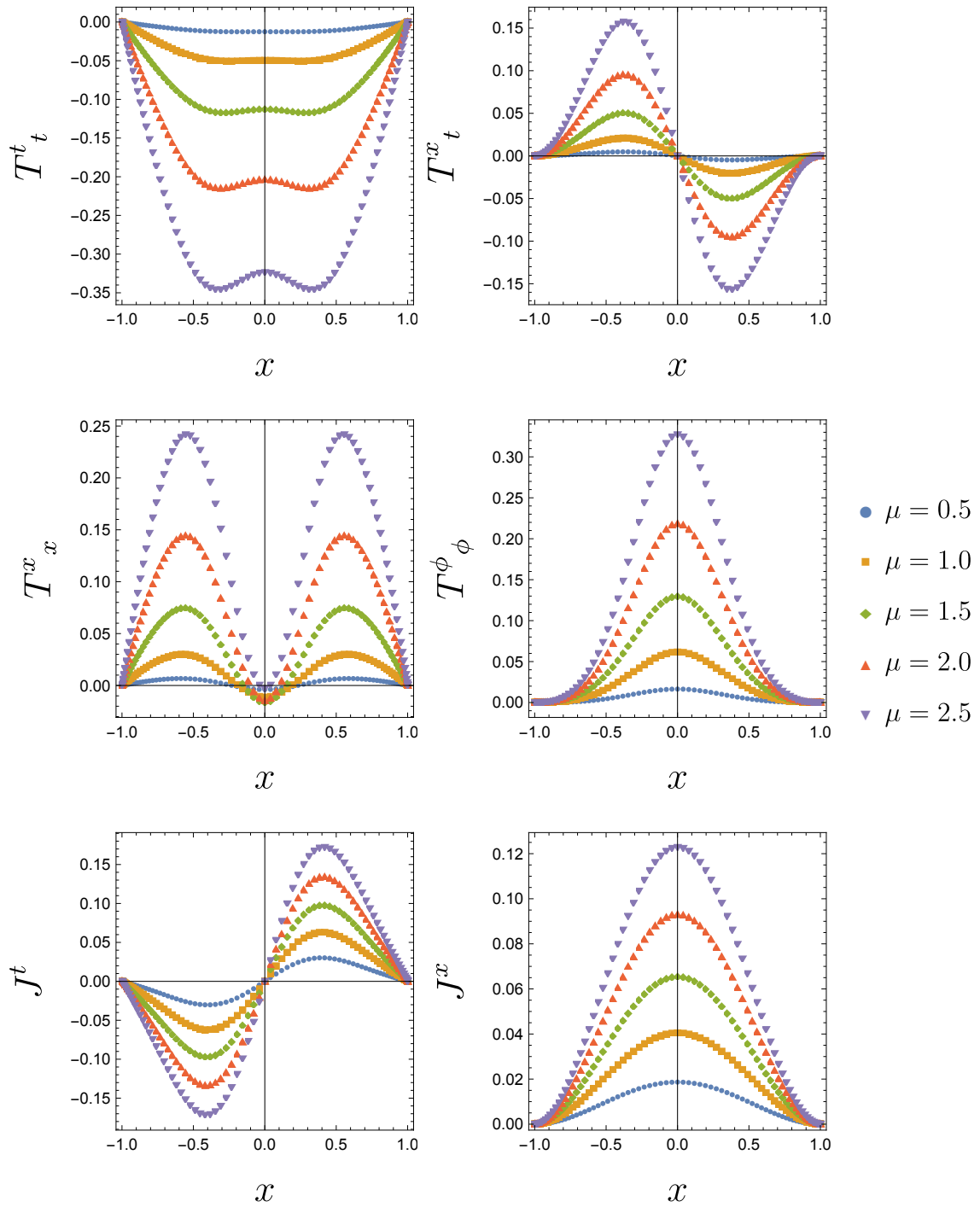
As described above, the holographic stress tensor,  $\langle T_{\mu\nu} \rangle$ , and conserved current,  $\langle J^\mu \rangle$ , can be extracted from the numerical solutions using the standard procedure of holographic renormalization in either gauge. Explicit formulae for these quantities in this case are given for the Bondi-Sachs gauge in (5.22). Analogous expressions in DeTurck gauge can be similarly obtained after transforming to Fefferman-Graham gauge and making use of (1.34).

Figure 5.2 gives plots for the non-zero components of the holographic stress tensor and the conserved current for various values of the magnitude,  $\mu$ , for the sine profile chemical potential with the magnitude of each component increasing as  $\mu$  increases.

### 5.3.2 Conductivity

Of particular interest will be the conserved current,  $\langle J^\mu \rangle$ . We can define the *total current*,  $I$ , by integrating  $\langle J^\mu \rangle$  over a circle,  $S_x^1$ , of fixed  $x$  at a fixed time-slice in the boundary geometry:

$$I := \int_{S_x^1} d\phi \sqrt{g_{\phi\phi}} m_\mu \langle J^\mu \rangle = 2\nu\pi^2 T_H C_1 \quad (5.28)$$



**Fig. 5.2:** Plots of the components of the holographic stress tensor,  $T^\nu_\rho$ , against the  $x$  coordinate. The different curves correspond to different values of the magnitude,  $\mu$ , of the sine profile chemical potential. The magnitude of each component increases as  $\mu$  increases.

where  $m^\mu$  unit normal is the unit normal to the circle  $S_x^1$ . Let us note again that  $\phi$  has periodicity  $2\pi r_0/\ell_3$ , which must be taken into account when computing this integral. Note that the value of  $I$  is independent of the choice of  $x$  at which one fixes the circle,  $S_x^1$ , which follows as a direct consequence of the conservation of the current, (5.23).

We can describe the *conductance*,  $G$ , of the holographic battery by dividing the total current by the potential difference between the two horizons, *i.e.*

$$G := \frac{I}{V} = \frac{\nu\pi C_1}{2\mu}. \quad (5.29)$$

The conductance depends upon both the choice of profile,  $g(x)$ , and the magnitude of the chemical potential,  $\mu$ , or equivalently the potential difference between the two horizons,  $V$ . In Figure 5.3, we plot the conductance of the holographic batteries, with the sine profile defined by (5.8), against the potential difference.

As  $V/T_H \rightarrow 0$ , the conductance tends to two and it increases with the voltage. Moreover, the gradient of the curve at  $V = 0$  is zero, meaning that one has to go beyond the linear regime in order to see the non-trivial dependence of the conductance on the potential difference. The derivative of the conductance with respect to  $V/T_H$  possesses a turning point, in this case at  $V/T_H \simeq 6.62$ , with the gradient of the curve

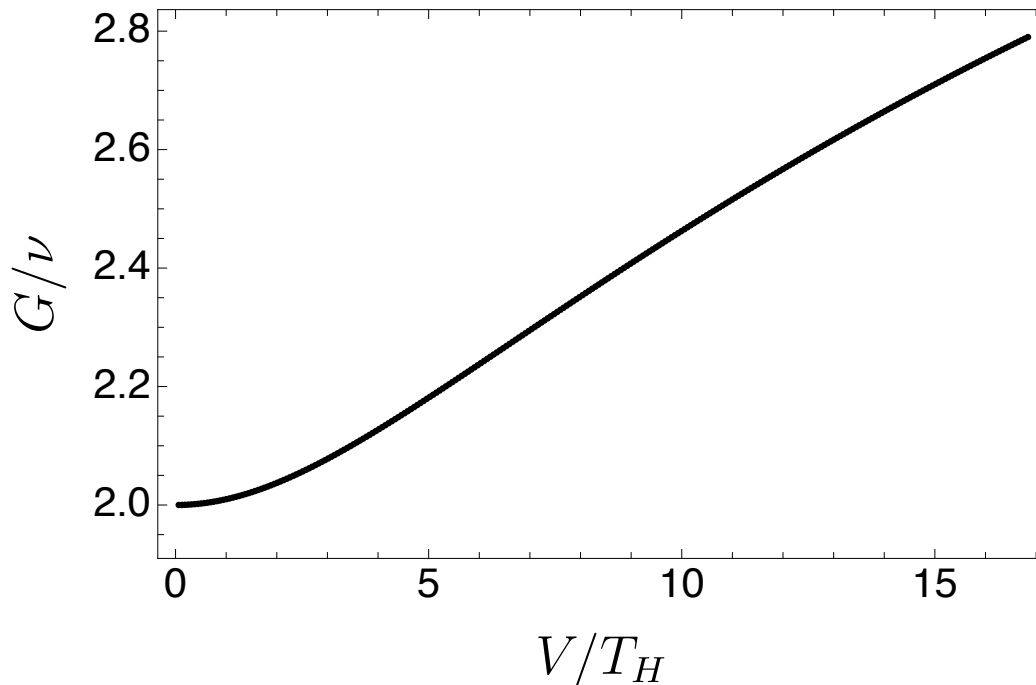


**Fig. 5.3:** The conductance of the holographic batteries with the sine profile, against the potential difference,  $V$ , normalised by the temperature of the black hole horizons,  $T_H$ .

decreasing for larger values of  $V/T_H$ . It would be of interest to investigate further what happens to  $G$  as  $V/T_H$  becomes very large, though there are numerical challenges in extending to this region of the parameter space.

The behaviour of the conductance appears qualitatively similar for other choices of the profile,  $g(x)$ , which each satisfy  $g(1) = 1 = -g(-1)$ . In Appendix B we provide plots of the conductance for other such profiles as well as a proof that  $G/\nu \rightarrow 2$  as  $V/T_H \rightarrow 0$  for *any* choice of odd profile  $g(x)$  by conducting an analysis of the linearised equations of motion.

One can also compute the local *conductivity* of the field by computing the ratio between the  $x$ -components of the induced current and the source electric field,

$$\begin{aligned} \sigma(x) &:= \frac{\langle J^x \rangle}{(F^{(0)})^{tx}} \\ &= \frac{2G}{\pi} \cdot \frac{1}{g'(x)\sqrt{2-x^2}}. \end{aligned} \quad (5.30)$$

Since the external electric field is not homogeneous, the conductivity is not constant. However, for a given profile its functional form is always the same, with its magnitude determined by the value of the overall conductance,  $G$ .

### 5.3.3 Energy Flow

The addition of a chemical potential causes some heating of the dual CFT by the Joule effect and hence there is flow in the boundary field theory. As was observed in other flowing solutions [179, 139, 135, 2], this means that the bulk horizon is not a Killing horizon. The flow can be expressed via an integral of the holographic stress tensor over a circle,  $S_x^1$ , of fixed  $x$  in the boundary geometry as follows:

$$\begin{aligned} \Phi(x) &= - \int_{S_x^1} d\phi \sqrt{-\gamma} m_\mu k^\nu \langle T^\mu{}_\nu \rangle \\ &= 2\pi T_H \left( 2G\mu^2 g(x) + 3\pi\nu C_2 \right), \end{aligned} \quad (5.31)$$

where  $\gamma_{\mu\nu}$  is the induced metric on a constant  $x$  slice of the boundary geometry with determinant  $\gamma$  and unit normal  $m_\mu \propto (dx)_\mu$ , whilst  $k^\mu \propto (dt)^\mu$  is the normalised stationary Killing vector field. Note therefore, that the flow is simply proportional to the  $T^x{}_t$  component of the holographic stress tensor, which is given in (5.22). The constant  $C_2$  is an integration constant arising in asymptotic expansion of the  $q_4$  function, given in (5.18), though its value is not fixed by a local analysis of the equations of motion.

In the current case, in which the two boundary horizons have the same temperature and the chemical potential,  $g(x)$ , is odd, we find empirically, as one would expect, that  $C_2 = 0$ , and hence there is no net flow between the two horizons. Thus, the flow,  $\Phi(x)$ , is proportional to the chemical potential, and is odd with  $\Phi(x) > 0$  for  $x > 0$ , meaning that there is flow in both directions originating from the point  $x = 0$  and moving outwards towards the boundary. As we will see this behaviour near  $x = 0$  has an interesting effect on the structure of the horizon of the bulk geometry.

### 5.3.4 Properties of the bulk horizon

By design, the  $y = 1$  surface is a null hypersurface. In a similar manner to what was done in Section 4.4.1, we checked explicitly that there exist future-directed radial null curves from anywhere outside of this hypersurface to the boundary, suggesting it is the event horizon.

Let us consider a generator of the horizon,  $U_a \propto (dy)_a$ , which can be parameterised by the  $x$  coordinate. The affine parameter,  $\lambda(x)$ , can be obtained from the geodesic equation or from Raychaudhuri's equation. At the axis of symmetry at  $x = 0$ , we find that  $\lambda'(x) \rightarrow 0$ , with  $\lambda(0)$  taking a finite value, which we are free to choose via an affine transformation as  $\lambda(0) = 0$ . Moreover, we find that  $U^a$  is future-directed in both directions moving away from  $x = 0$ . This suggests that the horizon is better thought of as being generated by two separate future-directed generators, both described by  $U^a$  and originating at  $x = 0$ , one moving in the positive  $x$ -direction and the other moving in the negative  $x$ -direction. Hence, the point  $x = 0$  is the *past boundary of the future horizon* of the solutions.

Let us restrict to the  $x \geq 0$  region of the horizon, since the behaviour in the  $x \leq 0$  region is similar by symmetry. In the left-hand panel of Figure 5.4, we plot the affine parameter along the generator against the  $x$  coordinate in a log plot.

Given our affinely-parameterised null geodesic,  $U^a$ , the  $B$ -tensor is given by  $B_{IJ} = \nabla_I U_J$ , where  $I$  and  $J$  run over  $\{v, \phi\}$ . The expansion,  $\Theta$ , and shear,  $\sigma_{IJ}$ , are the trace and symmetric-traceless parts of this tensor, respectively. These can be derived by the method described in Section 4.3.5. The fact that  $\lambda'(x) \rightarrow 0$  as  $x \rightarrow 0$  means that the expansion and shear diverge as  $x \rightarrow 0$  along the horizon. In the right-hand panel of Figure 5.4 we have plotted the expansion against the affine parameter along the generator of the  $x > 0$  region of the horizon.

In flowing horizons, the past boundary is generally situated at the point at which the flow along the horizon emanates from and, moreover, the expansion diverges at this point. In the previous cases [139, 135, 2], the flow was induced by a temperature

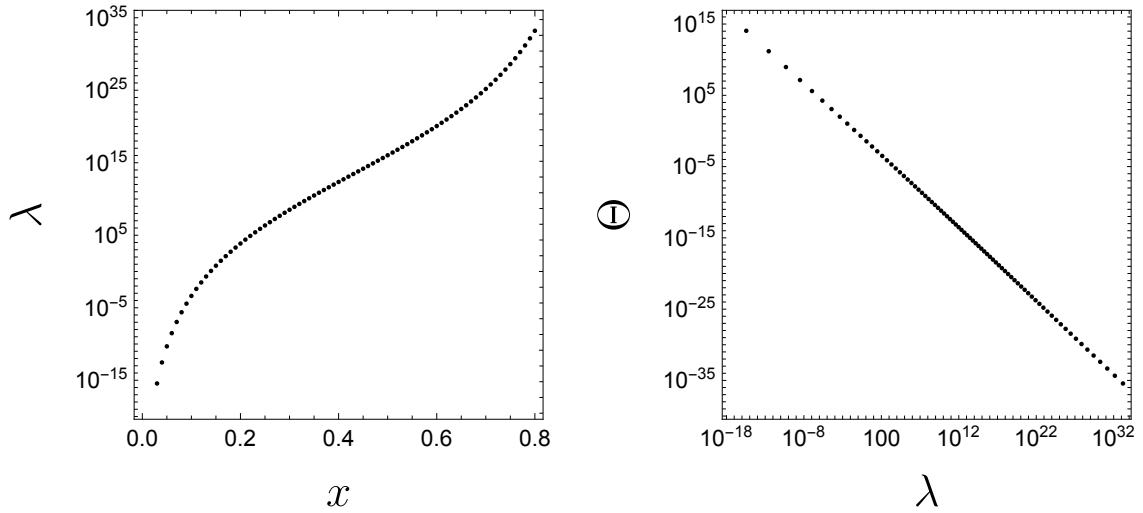


**Fig. 5.4: Left:** The affine parameter,  $\lambda$ , along the generator of the  $x > 0$  region of the horizon, plotted in a log plot against the coordinate  $x$ , for a holographic battery with  $\mu = 0.24$ . Here we have made the choice that  $\lambda(0) = 0$  and  $\lambda'(0.1) = 0.1$ . **Right:** The expansion,  $\Theta$ , along the generator for this holographic battery, plotted in a log-log plot against  $\lambda$ . The expansion diverges at  $\lambda = 0$ .

difference between the boundary black holes meaning that the past boundary tended to be the hotter boundary horizon. However, in the current case there is no temperature difference; the flow is instead induced by the Joule effect, emerging from  $x = 0$  and proceeding outwards, towards the boundary black holes, situated at  $x = \pm 1$ . Hence, our case is distinct in that the past boundary is situated spatially in the *centre* of the horizon with the future-directed horizon generators extending outwards in either direction. This has another interesting consequence: at  $x = 0$  (and only at  $x = 0$ ), the generator  $U^a$  coincides with the stationary Killing vector,  $U^a \propto (\partial_v)^a$ , meaning that the Killing vector is a generator of the horizon only on a proper submanifold of the horizon. To our knowledge, this feature has so far not been found to occur in any other instances of flowing horizons. It would be interesting to better understand how this bulk horizon fits within the classification of black hole horizons described in [213].

The divergent expansion at  $x = 0$  suggests that the tidal forces between neighbouring horizon generators diverges at this point. However, since the future-directed generators emerge from this point, this singularity is always in their far past. If we instead consider the geodesics of infalling observers, then we find no infinite tidal forces are felt for such neighbouring geodesics, even near  $x = 0$ , hence these solutions do not contain any physical singularities.

### 5.3.5 Detuning the temperatures

One may wonder whether this property of the past boundary of the future horizon of the holographic batteries lying deep in the bulk is generic or simply a product of the symmetry of the set-up. To investigate this, we detune the temperatures by adding a non-trivial profile to the  $g_{tt}$  component of the boundary geometry:

$$ds_{detuned}^2 = -\ell_3^2 h(x)^2 dt^2 + \frac{\ell_3^2}{(1-x^2)^2} \left( \frac{4 dx^2}{2-x^2} + d\phi^2 \right) \quad (5.32a)$$

where

$$h(x) := 1 + \beta \sin \left( \frac{\pi}{2} x \sqrt{2-x^2} \right), \quad (5.32b)$$

so that the ratio between the temperatures of the two boundary horizons is given by  $T_+/T_- = (1+\beta)/(1-\beta)$ . The *detuned holographic batteries* are the bulk duals to the CFT on this background, still under the influence of an additional chemical potential, given by (5.8). The method to find the detuned solutions is almost identical to the previous, tuned case, with the *Ansatz* only slightly modified to accommodate for the non-trivial  $h(x)$  profile. Note, one can recover the tuned holographic batteries by taking  $\beta = 0$ .

Interestingly, we find that there is an open set in the parameter space, depicted by the shaded region in Figure 5.5, in which the flow vanishes at some point along the horizon and hence the past boundary of the future horizon lies deep in the bulk. Roughly speaking, for these solutions, the contribution to the flow from the temperature difference is not large enough to everywhere overcome the flow due to the Joule effect and cause the flow to be in the same direction throughout the boundary geometry. This shows that the property of the tuned holographic batteries of having the past boundary of the future horizon lying spatially deep within the bulk is not simply an artifact of the  $\mathbb{Z}_2$  symmetry of the original set-up.

## 5.4 Discussion

We constructed charged global funnel solutions in four dimensions. These bulk solutions are dual to a CFT sourced by two black holes with the same temperature but with a potential difference between them, which generates a current. By considering the ratio between this induced current and the enforced potential difference, we obtained the conductivity of the CFT in this background at a non-linear level, showing that it has a non-trivial dependence on the voltage. The response of a strongly coupled field theory under an external electric field is a very difficult quantity to calculate directly,

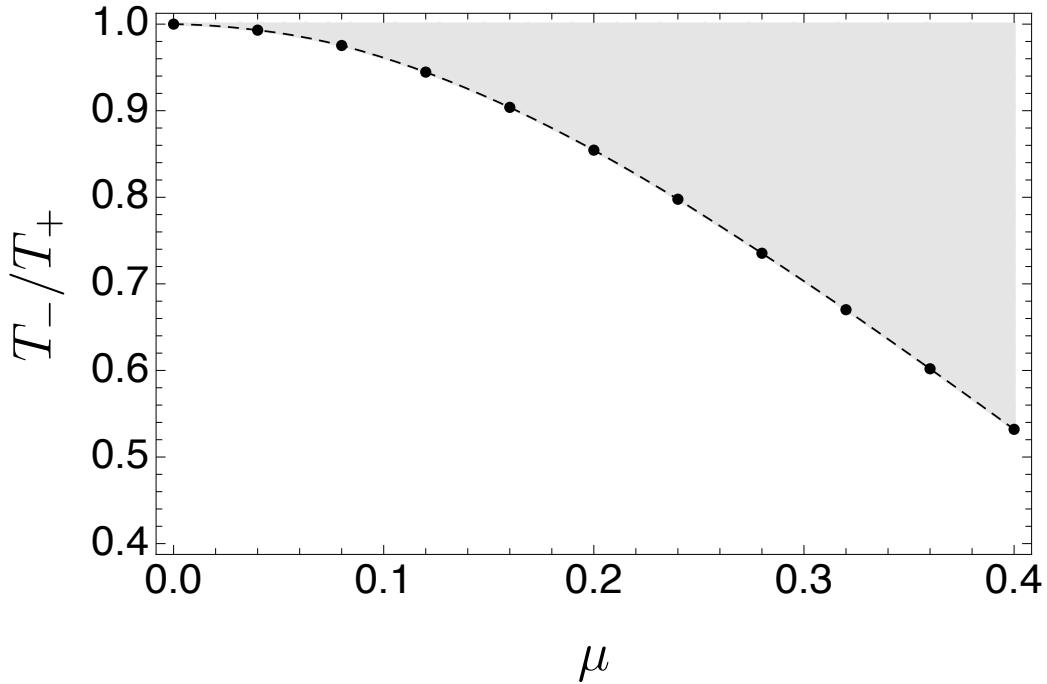


**Fig. 5.5:** The region in the parameter space of the detuned holographic batteries in which the past boundary of the horizon lies in the bulk rather than being anchored on the conformal boundary at the hotter boundary black hole. The chemical potential is fixed to be  $\pm\mu$  on the horizon with temperature  $T_{\pm}$ , respectively, where without loss of generality  $T_+ > T_-$ .

especially away from the linear response, and this work provides an interesting toy example to study such systems holographically.

Due to the Joule effect, the addition of the source chemical potential in the boundary theory causes some heating of the CFT, leading to the flow of energy. On the bulk side of the duality this manifests in the fact that the generators of the event horizon are not Killing vectors. Unlike in previous flowing geometries, however, the flow is not from one boundary horizon to the other, which has the result that the past boundary of the future bulk horizon lies deep within the bulk, rather than being anchored on the boundary as seen in previous examples. By perturbing the solutions away from the  $\mathbb{Z}_2$  symmetry of the original set-up, we showed that this feature is generic and not just an artifact of the symmetry.

The fact that the horizon is not Killing again leads to difficulties in carrying out a thermodynamic analysis of the solutions. This time, despite the two boundary horizons having the same temperature, the addition of the chemical potential still takes the bulk solution, and hence the boundary state, out of thermodynamic equilibrium meaning that there is no well-defined notion of free energy. This leads to difficulties on the question as to whether the charged funnels dominate over a solution with the same

boundary geometry in which two droplets emerge from the boundary horizons but do not connect in the bulk.<sup>3</sup> However, it is known that the uniform funnel dominates for a BTZ black hole with a large enough radius [131], and physically one would expect that by adding a small charge difference between the two boundary black holes one would remain in the phase in which the funnel dominates. It is less clear that as one increases the amplitude  $\mu$  that the deconfined phase corresponding the funnel will dominate.

Indeed, it would be very desirable to continue to obtain the funnel solution for larger values of  $\mu$ , perhaps using the patching methods described in Section 2.4.3 in order to extend the parameter space. In particular, it would be interesting to ascertain whether these solutions continue to exist for larger and larger  $\mu$ , or whether they cease to exist, perhaps becoming singular at a certain value of the amplitude. In the case of the former, the limiting behaviour of the conductance for large amplitude would also be of great interest.

One could also envisage obtaining analogous solutions which are not charged, but rotating. In this new set-up, the boundary geometry would be formed of two rotating BTZ black holes, with their horizons rotating in opposite directions. The bulk geometry would be a funnel which is rotating in one direction in the vicinity of one boundary horizon and in the opposite direction near the other. Hence the angular velocity would be non-constant along the horizon and it would vanish somewhere deep within the bulk. One would expect such a twisting horizon would once again be non-Killing, though again the stationary Killing vector would be a generator on the submanifold of the horizon on which the angular momentum vanishes. Hence, even in this case of pure gravity, it seems the horizon structure of these rotating funnels may well be similar to that of the holographic batteries. It would be interesting to see how flow of the CFT is induced by the rotating background on the field theory side, and whether this again takes the solutions out of thermodynamic equilibrium.

---

<sup>3</sup>It is yet to be explicitly shown that such a solution exists for  $\mu \neq 0$ , though it would be extremely surprising if they did not, at least for small  $\mu$

# Chapter 6

## Charged static AdS black hole binaries

### Abstract

We construct the first binary black hole solutions of Einstein-Maxwell theory in asymptotically anti-de Sitter space. The attractive force between the two black holes is balanced by the addition of a background electric field, sourced at the conformal boundary. There is a continuous family of bulk solutions for a given boundary profile and temperature, suggesting there is continuous non-uniqueness. We investigate the charges of the solutions and verify numerically that they satisfy a first law of black hole mechanics relation. This work was first presented in [4].

### 6.1 Introduction

Very few stationary multi-black hole solutions are known to exist. Indeed, stationary black holes are often hypothesised to be uniquely defined in terms of a small number of asymptotic properties, such as their energy, charge and angular momentum, which would forbid the existence of multi-horizon solutions. This hypothesis, generally referred to as the “no-hair theorem”, has been proven to hold under certain assumptions [32, 37, 56–61, 214, 33, 62–65].

However, the no-hair theorem is known to be violated in various other circumstances. For example, there exist black hole solutions with matter hair [215–218, 72, 73], and in higher dimensions, black hole horizons can have non-spherical topology [97, 164].

Solutions containing multiple black holes also exist, in each of which the gravitational attraction between the black holes is balanced by some other force. In Einstein-Maxwell theory, the famous Majumdar-Papapetrou solution [38, 39] is a configuration of extremally charged, four-dimensional black holes in which their electric repulsion balances their gravitational attraction. Similar exact systems of extremal black holes are also known in higher dimensions [219, 220]. Indeed, there are many more multi-black hole solutions known to exist in higher dimensions, some supported by the centrifugal force arising from rotation [221–224], and others [225–229] supported by gravitational solitons known as “bubbles of nothing” [230]. Finally, stationary black binaries with de Sitter asymptotics have also been obtained in pure gravity [103, 104], this time being held apart by the expansion due to a positive cosmological constant.

In this chapter we turn our attention to the question of whether binary solutions can exist in anti-de Sitter (AdS) space. The presence of a negative cosmological constant contributes an additional gravitational potential well (compared with asymptotically flat space), and so one may expect that binaries cannot exist in Einstein-Maxwell theory, since it seems even electrically extremal black holes wouldn’t have sufficient electric repulsion to balance the gravitational attraction. However, in AdS there is also the possibility to add a background electric field which is non-zero at the conformal boundary. We will show that the addition of such a electric potential allows for the existence of static, charged, binary black hole solutions with AdS asymptotics in both four and five dimensions.

Such solutions have an additional source of interest due to the AdS/CFT correspondence [109–111], which is a duality between a theory containing a strongly coupled conformal field theory (CFT) and a gravitational theory in AdS space in one higher dimension.

We will enforce that the bulk solutions are asymptotically globally AdS, tending towards the geometry of  $d$ -dimensional global AdS space, which is described by the metric:

$$ds_{\text{AdS}}^2 = -f(R) dt^2 + f(R)^{-1} dR^2 + R^2 d\Omega_{(d-2)}^2, \quad (6.1a)$$

with

$$f(R) = 1 + \frac{R^2}{\ell_d^2}. \quad (6.1b)$$

In these coordinates, the conformal boundary is situated at  $R \rightarrow \infty$ . From the perspective of the field theory, we are studying a CFT situated on the metric of the boundary of this bulk spacetime, a  $(d - 1)$ -dimensional Einstein static Universe (ESU) of radius  $\ell_d$ .

We deform this theory by adding a chemical potential, which acts as an electric source for the theory, given by

$$A^{(0)} = \mu(\theta) dt, \quad (6.2)$$

where  $\theta$  is the polar angle of the sphere, and  $\mu(\theta)$  is a profile which we are free to choose. This chemical potential excites a Maxwell field in the bulk theory, with its leading order behaviour at infinity dictated by the profile,  $\mu(\theta)$ . As we will discuss, this allows for the existence of binary solutions, which correspond holographically to states of the CFT living on the ESU under the influence of this electric source. In [231], other bulk solutions with the same boundary conditions were investigated, one, a soliton with no horizon, and another, a single black hole whose horizon is polarized due to the background electric field.

We first begin by considering a background electric field which is excited on an  $\ell = 1$  mode of the boundary sphere, *i.e.*  $\mu(\theta) = \mu_1 \cos \theta$ . Roughly speaking, for suitable values of  $\mu_1$ , this allows for the existence of binary solutions with black holes which are oppositely charged, since they will be attracted to opposite sides of the conformal boundary, which can balance their mutual gravitational and electric attraction. Figure 6.1 shows a very rough sketch of such a spacetime.

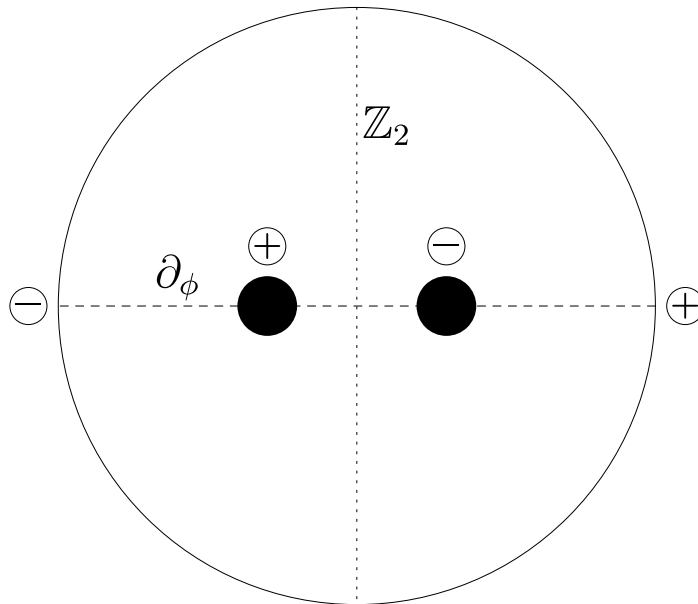


**Fig. 6.1:** A schematic drawing of a symmetric binary solution in AdS with an  $\ell = 1$  boundary profile. The vertical, dotted line is a plane of reflective symmetry, whilst the horizontal, dashed line is an axis of rotation. The plus and minus symbols represent the charges of the horizons and the poles of the conformal boundary. The system is in static equilibrium since the two black holes are attracted to opposite sides of the boundary, balancing their mutual attraction.

Interestingly, we find that for fixed choices of the temperature and the amplitude,  $\mu_1$ , of the electric field, there is a *two-dimensional* solution space of binaries, with the two continuous parameters corresponding to a local chemical potential of each of the black hole horizon. Only a one-dimensional sub-family of this space preserves the  $\mathbb{Z}_2$  symmetry of the boundary data.

We begin with a brief overview of the numerical construction of the binary solutions, before exploring their associated holographic quantities and charges, and showing that they satisfy a first law relationship.

## 6.2 The numerical construction of AdS binaries

The black hole binaries are solutions to the Einstein-Maxwell equations with a negative cosmological constant, which we repeat here:

$$0 = R_{ab} + \frac{d-1}{\ell_d^2} g_{ab} - 2\tilde{T}_{ab}, \quad (6.3a)$$

$$0 = \nabla^a F_{ab}, \quad (6.3b)$$

where  $\tilde{T}_{ab}$  is the trace-reversed stress tensor given by

$$\tilde{T}_{ab} = F_a{}^c F_{bc} - \frac{1}{2(d-2)} g_{ab} F_{cd} F^{cd}. \quad (6.3c)$$

We seek solutions containing two black hole horizons and possessing a static Killing vector field,  $\partial_t$ . Moreover, let us assume axisymmetry in four dimensions and  $SO(3)$  symmetry in five dimensions, so that the solutions are cohomogeneity-two.

As for the asymptotic behaviour, we require that the solutions are asymptotic to global AdS, (6.1a), and we will impose a non-zero profile for the gauge field at infinity, given by (6.2). This latter condition will excite a Maxwell field in the bulk. We enforce the black holes are electrically charged, by allowing only the  $t$ -component of the gauge potential to be non-zero.

We shall use the DeTurck method, described in Section 2.1, to obtain these solutions, solving the *Einstein-DeTurck equation*, defined by

$$0 = R_{ab} + \frac{d-1}{\ell_d^2} g_{ab} - 2\tilde{T}_{ab} - \nabla_{(a}\xi_{b)} \quad (6.4)$$

with  $\xi$  being the *DeTurck vector* defined in terms of a reference metric which we are free to choose. For the symmetry class of interest, the Einstein-DeTurck equation

yields a set of elliptic PDEs [133]. No reference gauge potential is required in this case since, by assumption, the gauge vector is proportional to the static Killing vector field, which has the consequence that the Maxwell equation, (6.3b), is already elliptic.

The reference metric must satisfy all the symmetry and boundary conditions we wish to enforce for the binary solution, hence must contain two black hole horizons and be asymptotically AdS. Fortunately though, it need not be a solution to the Einstein equation.

It is, in theory, possible to write down a global *Ansatz* for the solution, in terms of which one would define the reference metric, however, this is very difficult and not necessary. Instead the approach will be to define two different *Ansätze*, one of which will be used to calculate the metric in a region near the black holes and the other in the asymptotic region. These *Ansätze* will be based on other solutions which share properties of the desired solution in the relevant region. Near the black holes, the cosmological constant has a smaller effect, so we will make use of an exact binary black hole solution of the four-dimensional vacuum Einstein equation with zero cosmological constant called the *Israel-Khan* solution [232]. On the other hand, the presence of the cosmological constant has much larger effect on the asymptotic structure than the presence of black holes in the bulk, and so in the asymptotic region we will instead base our *Ansatz* on the metric of empty global AdS.

These two metrics will also be of great use when designing a reference metric which satisfies all the required boundary conditions. Let us now briefly review these two metrics before explaining how they are used to define the *Ansätze* and the reference metric. For the majority of this section, we will focus on the method used to find four-dimensional solutions, though we will discuss briefly how it generalises to five dimensions quite simply.

### 6.2.1 The Israel-Khan solution

The Israel-Khan solution is an exact solution to the vacuum Einstein equation in four dimensions with  $\Lambda = 0$ . It contains two black holes which are held apart by a conical strut. This solution can be written in ring-like coordinates,  $\{x, y\}$ , with the metric

being given by

$$ds_{IK}^2 = -\Delta_x m_{xy}^2 (1-x^2)^2 dt^2 + \frac{\lambda^2}{m_{xy}^2 \Delta_{xy}^2} \left[ w_y^2 \left( \frac{4 dx^2}{(2-x^2)\Delta_x} + \frac{4 dy^2}{(2-y^2)\Delta_y} \right) + y^2(2-y^2)(1-y^2)^2 d\phi^2 \right], \quad (6.5)$$

where

$$\Delta_x(x) = 1 - k^2 x^2 (2 - x^2), \quad (6.6a)$$

$$\Delta_y(y) = 1 - (1 - k^2) y^2 (2 - y^2), \quad (6.6b)$$

$$\Delta_{xy}(x, y) = (1 - y^2)^2 + k^2 x^2 (2 - x^2) y^2 (2 - y^2), \quad (6.6c)$$

$$w_y(y) = \frac{k}{(1+k)^2} \left( 1 + \sqrt{\Delta_y} \right)^2, \quad (6.6d)$$

$$m_{xy}(x, y) = \frac{k \left( 1 - (1-k) y^2 (2 - y^2) + \sqrt{\Delta_y} \right)}{(1-k)\Delta_x (1-y^2)^2 + \left( k + \sqrt{\Delta_y} \right) \left( \Delta_x + (1-k) \left( \sqrt{\Delta_{xy}} - 1 \right) \right)}. \quad (6.6e)$$

The space of solutions is parameterised by  $k \in (0, 1)$  and  $\lambda \in (0, \infty)$  with the temperature of each of the two horizons being given by

$$T_H = \frac{1}{2\pi} \frac{k(1+k)}{4\lambda(1-k)}. \quad (6.7)$$

The Israel-Khan solution is static and axisymmetric with respect to the Killing vector fields  $\partial_t$  and  $\partial_\phi$ , respectively. The other two coordinates lie in the range  $x \in (-1, 1)$  and  $y \in (0, 1)$ . The horizons of the two black holes are situated at  $x = \pm 1$ , and there is a  $\mathbb{Z}_2$  symmetry across the  $x = 0$  plane. Meanwhile, the  $y = 0$  and  $y = 1$  coordinate boundaries make up the  $\partial_\phi$  axis of rotation, with the  $y = 0$  segment being the *inner axis* which is the line between the two black hole horizons (at which the conical singularity is situated), and the  $y = 1$  segment constituting the *outer axis* which stretches from the horizons to the poles of the conformal boundary. The asymptotic boundary is situated the single coordinate point  $(x, y) = (0, 1)$  at which  $\Delta_{xy}$  vanishes. Hence, there is a coordinate singularity at infinity in these coordinates. We have drawn a schematic diagram of a constant time slice of the Israel-Khan spacetime in Figure 6.2.

If we were to use the Israel-Khan solution as a reference metric for the AdS binaries, they would inherit the conical singularity at  $y = 0$ . We, however, wish to obtain regular

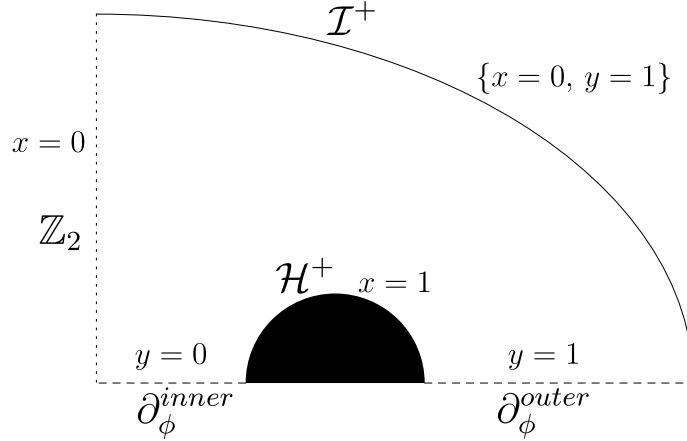


**Fig. 6.2:** A sketch of the Israel-Khan spacetime. There is a plane of reflective symmetry at  $x = 0$ , shown as a dotted line, and a black hole horizon at  $x = 1$ . The  $y = 0$  and  $y = 1$  boundaries, shown as dashed lines, constitute the  $\partial_\phi$  axis of rotation on the inside and outside of the binary system, respectively. The conical singularity is situated along the  $y = 0$  axis for the Israel-Khan metric. The ring-like  $\{x, y\}$  coordinates are singular at infinity, with the boundary being described by the single coordinate point,  $\{x = 0, y = 1\}$ .

binary solutions, so let us generalise the Israel-Khan metric by multiplying the  $d\phi^2$  term by a function  $\Sigma(y)$  given by

$$\Sigma(y) = 1 - \alpha(1 - y^2)^2. \quad (6.8)$$

This gives us a family of metrics parameterised by  $\alpha$ :

$$ds_{IK;\Sigma}^2 = -\Delta_x m_{xy}^2 (1 - x^2)^2 dt^2 + \frac{\lambda^2}{m_{xy}^2 \Delta_{xy}^2} \left[ w_y^2 \left( \frac{4 dx^2}{(2 - x^2) \Delta_x} + \frac{4 dy^2}{(2 - y^2) \Delta_y} \right) + y^2 (2 - y^2) (1 - y^2)^2 \Sigma(y) d\phi^2 \right]. \quad (6.9)$$

By adjusting the new parameter,  $\alpha$ , we can remove the conical singularity at  $y = 0$ . In particular, if we take

$$\alpha = \frac{(1 - k)^2 (1 + 6k + k^2)}{(1 + k)^4}, \quad (6.10)$$

then the metric,  $ds_{IK;\Sigma}^2$ , contains no conical singularities. Let us name the metric given by  $ds_{IK;\Sigma}^2$  for this value of  $\alpha$  the *warped Israel-Khan metric*. Of course,  $ds_{IK;\Sigma}^2$  is only a solution to the Einstein equation when  $\alpha = 0$ , but we will find that using the value of  $\alpha$  which removes the conical singularity to be far more useful.

## 6.2.2 Empty global AdS

Global anti-de Sitter space in four dimensions is often written as

$$ds_{AdS}^2 = - \left(1 + \frac{R^2}{\ell_4^2}\right) dt^2 + \left(1 + \frac{R^2}{\ell_4^2}\right)^{-1} dR^2 + R^2 (d\theta^2 + \sin^2 \theta d\phi^2), \quad (6.11)$$

where  $\ell_4$  is the AdS radius. For our uses, we will take new coordinates

$$R = \frac{r}{1-r^2}, \quad \sin \theta = 1 - \xi^2, \quad (6.12)$$

so that the metric is given by

$$ds_{AdS}^2 = \frac{1}{(1-r^2)^2} \left\{ -g(r) dt^2 + \frac{(1+r^2)^2}{g(r)} dr^2 + r^2 \left[ \frac{4 d\xi^2}{2-\xi^2} + (1-\xi^2)^2 d\phi^2 \right] \right\}, \quad (6.13)$$

with

$$g(r) := \frac{r^2}{\ell_4^2} + (1-r^2)^2. \quad (6.14)$$

The radial coordinate transformation is necessary in order to compactify the coordinate,  $r \in (0, 1)$  with  $r = 0$  being the origin, and  $r = 1$  the conformal boundary which is topologically  $\mathbb{R}_t \times S^2$ . The transformation of the angular coordinate removes trigonometric functions from the metric which speeds up the numerics considerably. The  $\partial_\phi$  axis is given by  $\xi = \pm 1$ , and there is a  $\mathbb{Z}_2$  symmetry across  $\xi = 0$ .

## 6.2.3 The *Ansätze*

As described above, we will have two *Ansätze*, one for the region near the horizons based on the warped Israel-Khan metric and one for the asymptotic region based on empty global AdS. In each case, we will take the *Ansatz* to be the most general deformation of the relevant metric which still satisfies all our symmetry assumptions. The binary solution in AdS will also be charged, and so we need also to define an *Ansatz* for the Maxwell field. We will assume they are electrically charged, so that the vector potential satisfies  $A_a \propto (dt)_a$ .

**The inner *Ansatz*.** We define the *Ansatz* in the region near the black holes in the  $\{x, y\}$  coordinates of the Israel-Khan solution. We simply add unknown functions multiplying each metric component of the warped Israel-Khan metric, as well as adding

an unknown  $dx dy$  cross-term, yielding

$$ds_{inner}^2 = -\Delta_x m_{xy}^2 (1-x^2)^2 \mathcal{T}_{in} dt^2 + \frac{\lambda^2}{m_{xy}^2 \Delta_{xy}^2} \left[ y^2 (2-y^2) (1-y^2)^2 \Sigma(y) \mathcal{S}_{in} d\phi^2 + w_y^2 \left( \frac{4\mathcal{C}_{in} dx^2}{(2-x^2)\Delta_x} + \frac{4\mathcal{B}_{in}}{(2-y^2)\Delta_y} (dy - \mathcal{F}_{in} dx)^2 \right) \right]. \quad (6.15a)$$

For the gauge field, we simply take

$$A = \mathcal{A}_{in} dt. \quad (6.15b)$$

Hence, we have six unknown functions in the in region that we have to solve for,  $\{\mathcal{T}_{in}, \mathcal{C}_{in}, \mathcal{B}_{in}, \mathcal{S}_{in}, \mathcal{F}_{in}, \mathcal{A}_{in}\}$ , each of which depend on  $\{x, y\}$ . Note that by taking  $\mathcal{T}_{in} = \mathcal{C}_{in} = \mathcal{B}_{in} = \mathcal{S}_{in} = 1$  and  $\mathcal{F}_{in} = 0$ , we obtain  $ds_{IK;\Sigma}^2$ , which we can then either take to be the Israel-Khan metric by setting  $\alpha = 0$ , or instead eradicate the conical singularity by taking  $\alpha$  to be as given in (6.10).

Though the whole spacetime is given by  $x \in (-1, 1)$ , we will initially assume a  $\mathbb{Z}_2$  symmetry at  $x = 0$  for the bulk solutions, and so we will focus on the  $x \in (0, 1)$  region, setting boundary conditions to enforce this symmetry.

**The outer *Ansatz*.** In the outer region we build the *Ansatz* by considering a general deformation of the global AdS metric, whilst still respecting the desired symmetries. We take

$$ds_{outer}^2 = \frac{1}{(1-r^2)^2} \left[ -g(r) \mathcal{T}_{out} dt^2 + \frac{(1+r^2)^2}{g(r)} \mathcal{C}_{out} dr^2 + r^2 \left( \frac{4\mathcal{B}_{out}}{2-\xi^2} (d\xi - \mathcal{F}_{out} dr)^2 + (1-\xi^2)^2 \mathcal{S}_{out} d\phi^2 \right) \right], \quad (6.16a)$$

and for the gauge field

$$A = \mathcal{A}_{out} dt. \quad (6.16b)$$

This time the unknown functions  $\{\mathcal{T}_{out}, \mathcal{C}_{out}, \mathcal{B}_{out}, \mathcal{S}_{out}, \mathcal{F}_{out}, \mathcal{A}_{out}\}$  depend upon the coordinates  $\{r, \xi\}$ . The global AdS metric is obtained by setting  $\mathcal{T}_{out} = \mathcal{C}_{out} = \mathcal{B}_{out} = \mathcal{S}_{out} = 1$  and  $\mathcal{F}_{out} = 0$ .

### 6.2.4 Coordinate transformations

We have a large amount of freedom in interpolating between the two coordinate domains. Firstly we can choose the position and shape of the interface between the two regions. In our case, we use a constant  $r$  surface,  $r = r_0$ , as the interface. Moreover, we have a further freedom in defining the coordinate transformation between the inner  $\{x, y\}$  coordinates and the outer  $\{r, \xi\}$  coordinates.

We firstly want to ensure that the outer  $\partial_\phi$  axes and the  $\mathbb{Z}_2$  reflection plane are located in the same positions at this interface, which requires that  $\xi = 0 \iff x = 0$ , and  $\xi = 1 \iff y = 1$ . Secondly, given a transformation, one can equate the *Ansätze* at the interface,  $r = r_0$ , and thereby write each of  $\{\mathcal{T}_{in}, \mathcal{C}_{in}, \mathcal{B}_{in}, \mathcal{S}_{in}, \mathcal{F}_{in}, \mathcal{A}_{in}\}$  in terms of  $\{\mathcal{T}_{out}, \mathcal{C}_{out}, \mathcal{B}_{out}, \mathcal{S}_{out}, \mathcal{F}_{out}, \mathcal{A}_{out}\}$ , and *vice versa*. The key is to ensure that none of these relationships diverges at any point on  $r = r_0$ , including at the  $\partial_\phi$  axis and the  $\mathbb{Z}_2$  reflection plane. However, importantly, this need not be the case globally, only in the region in the vicinity of the interface of the two regions. Therefore, for example, the  $r$  and  $\xi$  coordinates need not be well defined at the horizons of the black holes or at the inner axis, both of which lie deep within the inner region.

The coordinate transformation we used is given by

$$x = (1 - r)\xi\sqrt{2 - \xi^2}, \quad y = \sqrt{1 - (1 - r)(1 - \xi^2)}, \quad (6.17)$$

or, inversely,

$$r = 1 - \sqrt{x^2 + (1 - y^2)^2}, \quad \xi = \left(1 - \frac{1 - y^2}{\sqrt{1 + x^2 - y^2(2 - y^2)}}\right)^{1/2}. \quad (6.18)$$

In effect,  $\{r, \xi\}$  can be thought of as a form of polar coordinates about the point  $(x, y) = (0, 1)$ , which recall is the position of infinity for the Israel-Khan spacetime, taken such that  $r = 1$  corresponds to this point.

Having taken this choice of coordinate transformation, it will be the boundary conditions that we set on the boundary between the inner and outer regions at the  $r = r_0$  interface which will ensure that the metric is smooth in the vicinity of the  $r = r_0$ . On the left hand side of Figure 6.3 we give a schematic diagram of the domain of the  $\mathbb{Z}_2$ -symmetric binary solution, with the inner and outer regions in blue and orange, respectively. On the right of the figure, we plot these regions in the  $(x, y)$  plane. The outer region is situated between infinity, at  $(x, y) = (0, 1)$  (or, equivalently, at  $r = 1$ ), and a constant  $r$  slice,  $r = r_0$ .

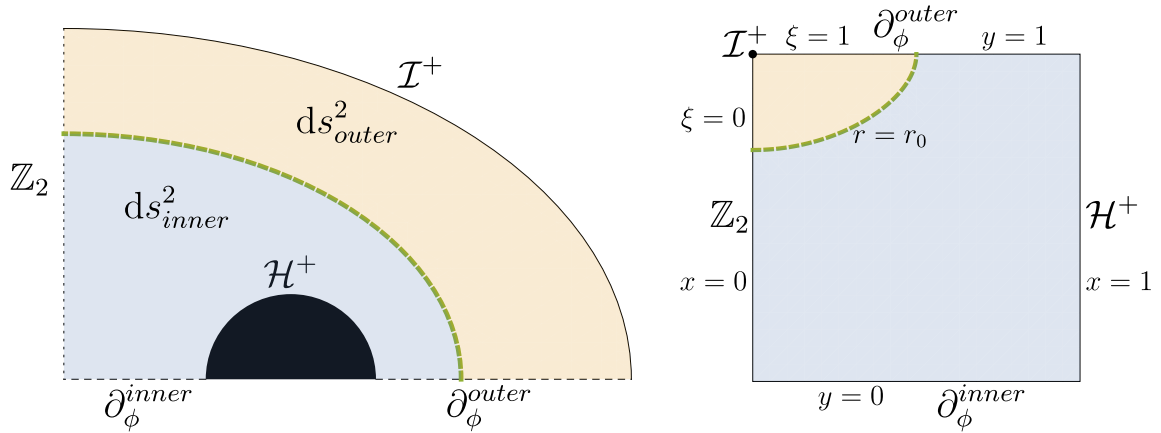


**Fig. 6.3:** On the left we show the schematic drawing of the coordinate domain of the  $\mathbb{Z}_2$ -symmetric solutions. The sketch is split into the inner region, in blue, where the inner *Ansatz* written in  $\{x, y\}$  coordinates is taken and the outer region, in orange, where the outer *Ansatz* in  $\{r, \xi\}$  coordinates is used instead. On the right hand side we plot these region in the  $(x, y)$  plane. Infinity is the point  $(x, y) = (0, 1)$  at which  $r = 1$ . Near infinity, constant  $r$  surfaces are curves from  $x = 0$ , at which  $\xi = 0$ , to  $y = 1$ , at which  $\xi = 1$ . The interface between the inner and outer regions is chosen to be such a constant  $r$  slice, shown as a dashed green curve.

### 6.2.5 Boundary conditions

Let us consider the boundaries of our spacetime, discerning whether each of them lies within the outer or inner regions entirely, or straddles them both. We have the conformal boundary, which lies entirely in the outer region. We have the horizon at  $x = 1$  and the inner axis at  $y = 0$ , which both lie solely in the inner region. And finally we have the  $\mathbb{Z}_2$  reflection plane and the outer axis, which are present in both regions. Let us first deal with the boundary conditions for the inner and outer region before turning our attention to the boundary conditions we must set at the interface of the regions.

**Inner boundary conditions.** In the region near the black holes in which we use the ring-like  $\{x, y\}$  coordinates we have a pentagonal domain. One boundary is the patching boundary which we will deal with momentarily. The remaining boundaries are dealt with as follows:

- *The  $\mathbb{Z}_2$  reflection plane at  $x = 0$ .* Here we want the metric to be even and the gauge potential to be odd. Hence, we enforce at  $x = 0$  that

$$0 = \frac{\partial \mathcal{T}_{in}}{\partial x} = \frac{\partial \mathcal{C}_{in}}{\partial x} = \frac{\partial \mathcal{B}_{in}}{\partial x} = \frac{\partial \mathcal{S}_{in}}{\partial x} = \mathcal{F}_{in} = \mathcal{A}_{in}. \quad (6.19)$$

- *The horizon at  $x = 1$ .* The metric functions must be regular across the horizon. Moreover, since the horizon is a Killing horizon, generated by  $\partial_t$ , the gauge potential must be constant on the horizon. Interestingly though, we find that this gauge potential need not be zero and indeed can take a range of values for a given boundary profile. Hence, we set at  $x = 1$  that

$$0 = \frac{\partial \mathcal{T}_{in}}{\partial x} = \frac{\partial \mathcal{C}_{in}}{\partial x} = \frac{\partial \mathcal{B}_{in}}{\partial x} = \frac{\partial \mathcal{S}_{in}}{\partial x} = \mathcal{F}_{in}, \quad \mathcal{A}_{in} = \nu_R, \quad (6.20)$$

where  $\nu_R$  will be an extra parameter of the solution space, with the subscript  $R$  denoting that it is the value of the vector potential on the right-hand horizon. This parameter is discussed in detail in Section 6.3.2. Due to the fact the gauge potential is odd across  $x = 0$ , the gauge potential at the left-hand horizon, which we denote as  $\nu_L$  will have the opposite sign:  $\nu_L = -\nu_R$ .

- *The inner  $\partial_\phi$  axis at  $y = 0$  and the outer  $\partial_\phi$  axis at  $y = 1$ .* At both of these boundaries, we take the boundary conditions

$$0 = \frac{\partial \mathcal{T}_{in}}{\partial y} = \frac{\partial \mathcal{C}_{in}}{\partial y} = \frac{\partial \mathcal{B}_{in}}{\partial y} = \frac{\partial \mathcal{S}_{in}}{\partial y} = \mathcal{F}_{in} = \frac{\partial \mathcal{A}_{in}}{\partial y}. \quad (6.21)$$

Moreover, in order for there to be no conical singularity along this axis, we require that  $\mathcal{B}_{in} = \mathcal{S}_{in}$  at these boundaries. This can be set as a boundary condition in place of one of the above, but even without doing this it will be enforced by the bulk equations of motion so long as the reference metric also has no conical singularities.

**Outer boundary conditions.** In the asymptotic region we use the  $\{r, \xi\}$  coordinates, and the integration domain is rectangular. Once again, one boundary is the patching boundary to the inner region, and the other three are given by:

- *The  $\mathbb{Z}_2$  reflection plane at  $\xi = 0$ .* Across this plane, the metric is even and the gauge field is odd. We set

$$0 = \frac{\partial \mathcal{T}_{out}}{\partial \xi} = \frac{\partial \mathcal{C}_{out}}{\partial \xi} = \frac{\partial \mathcal{B}_{out}}{\partial \xi} = \frac{\partial \mathcal{S}_{out}}{\partial \xi} = \mathcal{F}_{out} = \mathcal{A}_{out}. \quad (6.22)$$

- *The outer  $\partial_\phi$  axis at  $\xi = 1$ .* Here, we set

$$0 = \frac{\partial \mathcal{T}_{out}}{\partial \xi} = \frac{\partial \mathcal{C}_{out}}{\partial \xi} = \frac{\partial \mathcal{B}_{out}}{\partial \xi} = \frac{\partial \mathcal{S}_{out}}{\partial \xi} = \mathcal{F}_{out} = \frac{\partial \mathcal{A}_{out}}{\partial \xi}. \quad (6.23)$$

Likewise to the discussion above regarding the  $\partial_\phi$  axis of rotation in the inner coordinates, the absence of a conical singularity requires that  $\mathcal{B}_{out} = \mathcal{S}_{out}$  at this boundary, though this again will be enforced by the equations of motion.

- *The conformal boundary at  $r = 1$ .* Here we set Dirichlet boundary conditions. Holographically these boundary conditions correspond to the choice of metric on which the CFT will live and the choice of the background chemical potential with which we are deforming the CFT. In this case, we take

$$\mathcal{T}_{out} = \mathcal{C}_{out} = \mathcal{B}_{out} = \mathcal{S}_{out} = 1, \quad \mathcal{F}_{out} = 0, \quad \mathcal{A}_{out} = \mu_1 \xi \sqrt{2 - \xi^2}. \quad (6.24)$$

These enforce that the spacetime is asymptotically AdS, having the same asymptotic structure as (6.11). Meanwhile the boundary condition for the Maxwell field means that in the boundary theory we are exciting an  $\ell = 1$  mode of the background electric field (note that  $\xi \sqrt{2 - \xi^2} = \cos \theta$  if we transform back to our familiar angular variable,  $\theta$ ). The parameter,  $\mu_1$ , determines the magnitude of the enforced chemical potential.

**Patching boundary conditions.** Now we come to the tricky issue of the patching boundary conditions. In essence we require that the metric is *continuous* and *differentiable* at this interface, which is chosen to be a constant  $r$  slice,  $r = r_0$ .

In order to do this we can write the metric in either of the patches locally near the interface in the coordinates of the other patch by using the coordinate transformations given by (6.17) and (6.18). Equating the two metrics at  $r = r_0$  gives expressions for  $\{\mathcal{T}_{in}, \mathcal{C}_{in}, \mathcal{B}_{in}, \mathcal{S}_{in}, \mathcal{F}_{in}, \mathcal{A}_{in}\}$  in terms of  $\{\mathcal{T}_{out}, \mathcal{C}_{out}, \mathcal{B}_{out}, \mathcal{S}_{out}, \mathcal{F}_{out}, \mathcal{A}_{out}\}$ , or *vice versa*.

On the boundary of one patch, we enforce these relationships as Dirichlet boundary conditions. This enforces continuity of the metric. As for the other patch, we take derivatives of the relationships between the inner and outer metric functions in the direction normal to the interface, and set these as boundary conditions. This then enforces that the metric is also differentiable at the interface of the patches.

### 6.2.6 The reference metric

Finally let us consider designing a reference metric, which must satisfy certain requirements in order to be suitable for use when solving the Einstein-DeTurck equation (6.4). We need it to contain two black hole horizons, be regular and satisfy all the symmetry assumptions of the desired solution. Finally, we wish it to have the same

asymptotic structure as the desired solution, that is, it must be asymptotically AdS. Each of these conditions is necessary (though not sufficient) to prevent the DeTurck method yielding a Ricci soliton, *i.e.* a solution to the Einstein-DeTurck equation that is not a solution to the Einstein equation. Importantly, however, we do *not* require the reference metric to satisfy any field equations, though we do need it to be  $C^2$ , since the Einstein-DeTurck equations are second-order PDEs.

The warped Israel-Khan metric, (6.9), satisfies all but the asymptotic condition. Conversely, the empty AdS metric, (6.11), satisfies the asymptotic condition but not the condition regarding the presence of horizons. Thus, if we can design a metric that interpolates from the former to the latter as we move from the inner region to the outer region, we shall have a reference metric satisfying all our desired properties.

In previous examples similar interpolating reference metric have been found in a number of ways. In [162] a suitable reference metric is obtained by interpolating within a compact subregion of the spacetime, whilst in [164] an interpolation function with support across the whole spacetime is used. In our case, we use a method most similar to the former.

In the entire inner region, we take the reference metric to be equal to the warped Israel-Khan metric, (6.9). Then we shall split the outer region, which recall is given by  $r \in (r_0, 1)$ , into two sections with an interface,  $r = r_1$ , that we are free to choose with  $r_0 < r_1 < 1$ . In the asymptotic region  $r \in (r_1, 1)$ , we will take the reference metric to be the global AdS metric, (6.13). In the intermediate region,  $r \in (r_0, r_1)$ , we take an interpolation between the warped Israel-Khan and empty AdS metrics. Specifically, we take

$$\bar{ds}_{inter}^2 = I(r) ds_{IK;\Sigma}^2 + (1 - I(r)) ds_{AdS}^2, \quad (6.25)$$

where  $I(r)$  is an interpolating function which is equal to one at  $r = r_0$  and vanishes at  $r = r_1$  to sufficiently high order such that the reference metric is  $C^2$ . In order to obtain  $ds_{IK;\Sigma}^2$  in the outer  $\{r, \xi\}$  coordinates, we simply apply our coordinate transformations, (6.17), which are regular for  $r < r_1$ . This was one benefit of using an intermediate region rather than interpolating the reference metrics across the whole of the outer region, *i.e.* all the way from  $r = r_0$  to  $r = 1$ ; we never needed to deal with difficulties arising due to the coordinate transformation becoming singular at infinity (though these difficulties are certainly not insurmountable). Moreover, we found that taking the reference metric in the asymptotic region to be exactly empty AdS eased the extraction of holographic quantities.

There is a great amount of choice in taking the interpolating function,  $I(r)$ . One could ensure that at  $r = r_0$  and  $r = r_1$  the function approaches one and zero,

respectively, to all orders by using a non-analytic function based on, for example, a hyperbolic tangent function. However, this introduction of non-analyticities slows down the numerics and also can cause large gradients in the solutions. In fact, in order to obtain a  $C^2$  reference metric, we only need the interpolating function to approach the desired values at the endpoints,  $r_0$  and  $r_1$ , to second order. We choose the following interpolating function:

$$I(r) = \left(\frac{r-r_1}{r_0-r_1}\right)^4 \left(10 - 20\left(\frac{r-r_1}{r_0-r_1}\right)^2 + 15\left(\frac{r-r_1}{r_0-r_1}\right)^4 - 4\left(\frac{r-r_1}{r_0-r_1}\right)^6\right), \quad (6.26)$$

which, respectively, approaches one and zero at  $r_0$  and  $r_1$  up to third order in  $r$ .

Patching together the reference metrics in each of the regions discussed so far leads to a reference metric across the whole coordinate domain which is  $C^2$  and is compatible with all the boundary conditions.

### 6.2.7 Patching and numerics

We have two coordinate domains, the inner and outer regions, with coordinate systems  $\{x, y\}$  and  $\{r, \xi\}$ , respectively. The inner region is also naturally pentagonal, and so to carry out numerics we split it into two separate rectangular patches. Moreover, we split the outer region into two patches, so that we can easily fix the reference metric to be the interpolating reference metric, (6.25), in an intermediate patch and the empty AdS metric in the asymptotic patch.

In Figure 6.4, we have sketched how the four patches are situated in the spacetime. Patch I and II (blue) constitute the inner region, where the ring-like  $\{x, y\}$  coordinates are used and the reference metric is the warped Israel-Khan metric. Meanwhile, the reference metric is global AdS in region IV (orange) and so  $\{r, \xi\}$  coordinates are used. The reference metric interpolates in a continuous and differentiable fashion from the warped Israel-Khan metric to global AdS in patch III (green). In order to define this interpolating reference metric it is necessary that both the  $\{x, y\}$  and  $\{r, \xi\}$  coordinate systems and the transformation between them are well-defined in this intermediate patch. Consequently, either the inner or outer *Ansatz* could be used in this patch, but since its boundaries are constant  $r$  and constant  $\xi$  surfaces, it is most natural to use the outer *Ansatz*.

There is a great deal of freedom when fixing the precise position of the boundaries between patches. We took the boundaries between patch I and II to be  $x = x_0 y \sqrt{2 - y^2}$ , between patch II and III to be  $r = r_0$ , and between patch III and IV to be  $r = r_1$ , for

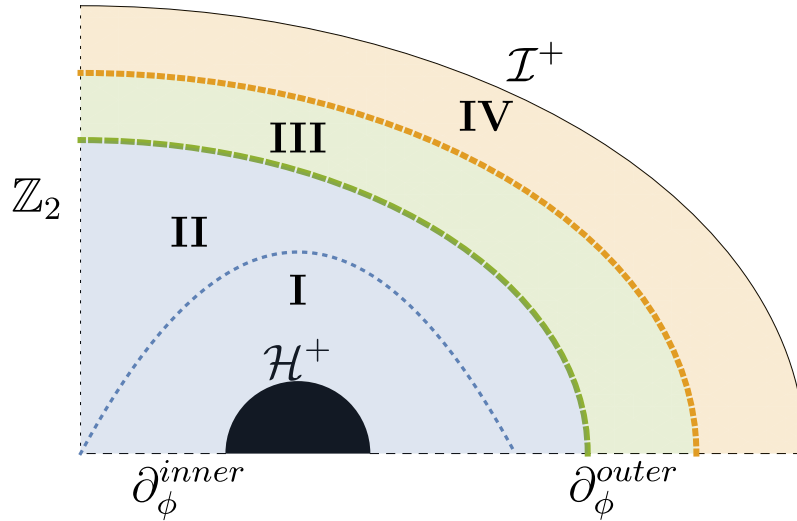


**Fig. 6.4:** A schematic drawing of the coordinate domain, and the four patches used. In the inner region, shaded blue and composed of patches I and II, the ring-like  $\{x, y\}$  coordinates are used, whereas in the outer region, which is shaded orange and made up of patches III and IV, the  $\{r, \xi\}$  coordinates are used. The reference metric is given by the warped Israel-Khan metric in regions I and II and the empty AdS metric in region IV, whilst in region III it interpolates between these two metrics in a continuous and differentiable manner.

fixed constants,  $x_0$ ,  $r_0$  and  $r_1$ . For the most part, we took these patching parameters to have the values  $x_0 = 0.5$ ,  $r_0 = 0.5$ ,  $r_1 = 0.95$ . One can also add extra patches in regions in which the solutions have large derivatives in order to speed up the numerical method and improve the accuracy of the solutions.

We discretize each of the patches with an  $N \times N$  Chebyshev-Gauss-Lobatto grid and use transfinite interpolation and pseudospectral methods to approximate the PDEs by a large set of non-linear algebraic equations, which can then be solved iteratively with the Newton-Raphson method, as described in Section 2.3.

The main difficulty with this approach is to find a good seed which will converge to a solution. To alleviate this we use the so-called  $\delta$ -trick, which is described in Section 2.4.2. This allows one to artificially begin with equations that necessarily have a certain solution and from there slowly adapt the equations of motion towards those which we really are aiming to solve, *i.e.* the Einstein-DeTurck and Maxwell equations, at each step solving intermediate equations. We also found it useful to vary  $\alpha$ , the parameter of the family of the warped Israel Khan metric, given in (6.9), during this process, ensuring that at the end we land on the value of  $\alpha$  given in (6.10) which ensures there are no conical singularities. In our case, we begin with equations that are automatically solved by the reference metric with  $\alpha = 0$  and a vanishing Maxwell field.

### 6.2.8 Removing the $\mathbb{Z}_2$ symmetry

In the above, we assumed that the bulk solution was  $\mathbb{Z}_2$  symmetric. Now let us drop this assumption to find more general solutions.

Without this symmetry, we cannot no longer use the  $\xi = x = 0$  plane as a boundary of the coordinate domain, and instead have to solve for the full range of the angular coordinates, *i.e.* for  $x \in (-1, +1)$  in the inner coordinate system and for  $\xi \in (-1, +1)$  in the outer coordinate system. We can find a system of patches for this domain simply by doubling the patches from the symmetric case. Hence we have eight patches, as shown in Figure 6.5, which we have labelled with the Roman numerals, **I-IV**, and the subscripts  $L$  and  $R$  (denoting left and right, respectively) in order to keep touch with the patches in the symmetric case.

Note, that we need to set boundary conditions at both the right horizon,  $\mathcal{H}_R^+$ , at  $x = +1$  and the left horizon,  $\mathcal{H}_L^+$ , at  $x = -1$ . These will both be of the form described in (6.20). With the boundary potential taken (in the usual polar coordinate,  $\theta$ ) to be  $\mu(\theta) = \mu_1 \cos \theta$ , we assumed in the method described above that the vector potential inherited the odd symmetry of this boundary potential about  $\theta = \pi/2$  in the bulk. Hence, we were implicitly setting  $\nu_L = -\nu_R$ . In general, though, we can set the value

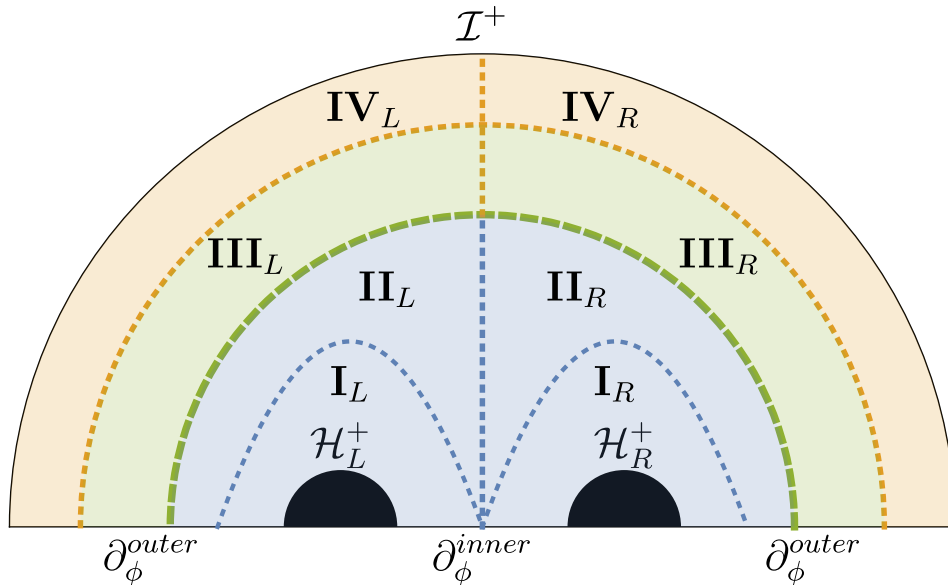


**Fig. 6.5:** The coordinate domain for the non-symmetric solutions, split now into eight different patches. Similarly to the symmetric case, the reference metric is warped Israel-Khan near the black holes (blue), global AdS in the asymptotic region (orange) and interpolates between the two in the intermediate region (green).

of the gauge potential to be two unrelated values at the two horizons:

$$\mathcal{A}_{in}(-1, y) = \nu_L \quad \text{and} \quad \mathcal{A}_{in}(+1, y) = \nu_R. \quad (6.27)$$

and break the boundary symmetry in the bulk by enforcing that  $\nu_L \neq -\nu_R$ . We were able to find such solutions by perturbing away from the symmetric solutions.

We can also explicitly break the  $\mathbb{Z}_2$  symmetry of the boundary profile. For example, we were able to obtain solutions arising from a boundary profile in which an  $\ell = 2$  mode was added to the  $\ell = 1$  mode, given by

$$\mu(\theta) = \mu_1 \cos \theta + \mu_2 \cos 2\theta. \quad (6.28)$$

### 6.2.9 Changing the number of dimensions

The method to obtain solutions in five dimensions is almost identical to that described above for axisymmetric four-dimensional solutions. In each metric described, one need only replace the  $d\phi^2$  by the metric of a two-sphere,  $d\Omega^2 = d\psi^2 + \sin^2 \psi d\phi^2$ . Hence rather than axisymmetry, the five-dimensional binaries possess an  $SO(3)$  symmetry, with a two-sphere being preserved.

The key difficulty is finding a first solution in five dimensions. To do so, we used the  $\delta$ -trick once again, this time beginning with the equations of motion of the four dimensional problem. Specifically, if we let  $E_{4d}$  and  $E_{5d}$  denote the equations of motion of the four- and five-dimensional problems, respectively, we considered

$$E(\delta) = \delta E_{4d} + (1 - \delta) E_{5d}. \quad (6.29)$$

Thus, a four-dimensional binary solution solves  $E(1) = 0$ . We then slowly decreased  $\delta$  to zero, solving  $E(\delta) = 0$  at each intermediate stage, using the previous solution as a seed, to obtain a five-dimensional binary solution, satisfying  $E(0) = 0$ . We found it necessary to move around the parameter space (specifically increasing  $\nu_R$  or decreasing  $\mu_1$ ) during the process as  $\delta$  decreased in order for the equation,  $E(\delta) = 0$ , to continue having a solution at each intermediate value of  $\delta$ . Once an initial five-dimensional binary solution is found, it is fairly easy to perturb from this starting point to find other solutions nearby in the parameter space.

### 6.2.10 Extracting the holographic quantities

Let us review how the holographic stress tensor and conserved current of the boundary CFT can be extracted from the bulk solutions, using the procedure of holographic renormalization [120], reviewed in general in Section 1.3.3. We will focus on the case of the four-dimensional solutions, and we will set  $\ell_4 = 1$ . The holographic quantities of the five-dimensional bulk solutions can also be extracted using (1.36a) and (1.36b), though in this case the procedure is much more complicated due to the presence of the conformal anomaly in odd bulk dimensions.

We consider the metric locally near the conformal boundary. This is defined in terms of the  $\{r, \xi\}$  coordinates of the outer *Ansatz*, given by (6.16a), and the boundary is the  $r = 1$  surface. We first expand the equations of motion and the requirement that the DeTurck vector vanishes order-by-order in  $r$  around  $r = 1$ , whilst also assuming the asymptotic boundary conditions. This local analysis restricts the form of the unknown metric functions near the boundary to a large degree:

$$\begin{aligned} \mathcal{T}_{out}(r, \xi) = & 1 + \alpha_1(\xi) (1 - r)^3 \\ & + \left( \frac{3}{2} \alpha_1(\xi) + 4\alpha_6(\xi)^2 \right) (1 - r)^4 + \gamma_1(\xi) (1 - r)^{\frac{1}{2}(3+\sqrt{33})} + \dots \end{aligned} \quad (6.30a)$$

$$\begin{aligned} \mathcal{C}_{out}(r, \xi) = & 1 + 4 \left( (2 - \xi^2) \mu'(\xi) - \alpha_6(\xi)^2 \right) (1 - r)^4 \\ & + \gamma_2(\xi) (1 - r)^{\frac{1}{2}(3+\sqrt{33})} + \dots \end{aligned} \quad (6.30b)$$

$$\mathcal{B}_{out}(r, \xi) = 1 + \alpha_3(\xi) (1 - r)^3 + \frac{3}{2} \alpha_3(\xi) (1 - r)^4 + \gamma_1(\xi) (1 - r)^{\frac{1}{2}(3+\sqrt{33})} + \dots \quad (6.30c)$$

$$\begin{aligned} \mathcal{S}_{out}(r, \xi) = & 1 - (\alpha_1(\xi) + \alpha_3(\xi)) (1 - r)^3 \\ & - \left( 4(2 - \xi^2) \mu'(\xi)^2 + \frac{3}{2} (\alpha_1(\xi) + \alpha_3(\xi)) \right) (1 - r)^4 \\ & + \gamma_1(\xi) (1 - r)^{\frac{1}{2}(3+\sqrt{33})} + \dots \end{aligned} \quad (6.30d)$$

$$\mathcal{F}_{out}(r, \xi) = \beta_5(\xi) (1 - r)^4 + \frac{16}{3} (2 - \xi^2) \mu'(\xi) \alpha_6(\xi) (1 - r)^4 \log(1 - r) + \dots \quad (6.30e)$$

$$\mathcal{A}_{out}(r, \xi) = \mu(\xi) + \alpha_6(\xi) (1 - r) + \dots \quad (6.30f)$$

where all terms in the expansion (including the higher order terms denoted by  $\dots$ ) are determined in terms of the six unknown functions,  $\{\alpha_1, \alpha_3, \alpha_6, \beta_5, \gamma_1, \gamma_2\}$ . In order to determine these six functions though, one must solve the equations in the full spacetime, whilst requiring regularity deep within the bulk. Fortunately, we will see only the  $\{\alpha_1, \alpha_3, \alpha_6\}$  functions arise in the holographic stress tensor and conserved current, and so, in particular, the coefficients of the non-analytic terms,  $\gamma_1$  and  $\gamma_2$ , do not need to

be calculated in the analysis. Moreover the asymptotic analysis also enforces that the  $\alpha$  functions are related by

$$\alpha_3'(\xi) = \frac{2 \left( 3\xi (\alpha_1(\xi) + 2\alpha_3(\xi)) - 8 (1 - \xi^2) \alpha_6(\xi) \mu'(\xi) \right)}{3 (1 - \xi^2)}. \quad (6.31)$$

Next we can transform to Fefferman-Graham gauge [121] near the conformal boundary, *i.e.* we seek a coordinate transformation which locally near the boundary brings the metric and gauge potential into the form

$$ds^2 = \frac{1}{z^2} \left[ dz^2 + \left( g_{\mu\nu}^{(0)} + g_{\mu\nu}^{(2)} z^2 + g_{\mu\nu}^{(3)} z^3 \right) dx^\mu dx^\nu + \mathcal{O}(z^4) \right] \quad (6.32a)$$

$$A = \left( A_\mu^{(0)} + A_\mu^{(1)} z + \mathcal{O}(z^2) \right) dx^\mu \quad (6.32b)$$

where  $g^{(0)}$  is metric of the Einstein static Universe and  $A^{(0)}$  is the boundary chemical potential, and the Greek indices run over the coordinates which span the boundary. This can be achieved simply by taking

$$r = 1 - \frac{1}{2}z + \frac{1}{8}z^2 - \frac{1}{8}z^3 + \frac{7}{128}z^4. \quad (6.33)$$

Once the metric is in this gauge, the vacuum expectation values of the holographic stress tensor and the conserved current can be, respectively, read off using (1.34) and the expansion of the metric functions near the conformal boundary, given in (6.30). One finds that these holographic quantities are given in  $\{t, \xi, \phi\}$  coordinates of the boundary metric by

$$\langle T^\mu{}_\nu \rangle = \frac{3}{128\pi G_N} \text{diag} (\alpha_1, \alpha_3, -\alpha_1 - \alpha_3) \quad (6.34a)$$

$$\langle J^\mu \rangle = \frac{1}{8\pi G_N} (\alpha_6, 0, 0). \quad (6.34b)$$

Note that the stress tensor is traceless and the current is conserved,  $D_\mu \langle J^\mu \rangle = 0$ , where  $D_\mu$  is the covariant derivative arising from the boundary metric. Moreover, due to the relation given in (6.31), the stress tensor and conserved current satisfy a Ward identity, given by

$$D_\mu \langle T^\mu{}_\nu \rangle = F_{\mu\nu}^{(0)} \langle J^\mu \rangle, \quad (6.35)$$

where  $F^{(0)}$  is the field strength tensor associated to the boundary potential,  $A^{(0)}$ .

## 6.3 Results

We were able to obtain a very large family of binary solutions. Let us focus on the case in which the boundary profile for the chemical potential is given by an  $\ell = 1$  mode, so that we have

$$\mu(\theta) = \mu_1 \cos \theta, \quad (6.36)$$

and for the remainder of the chapter, let us set  $\ell_d = 1$ . We will use  $L$  and  $R$  subscripts to differentiate between quantities associated to the left (on the  $\theta = \pi$  side) and right (on the  $\theta = 0$  side) horizons, respectively. The horizons have temperatures,  $T_L$  and  $T_R$ . We assumed that the two temperatures were equal, with  $T_L = T_R =: T$ , though it seems likely that they could take different values.

### 6.3.1 Charges

Of particular interest will be the charge density,  $\rho := \langle J^t \rangle$ , and the total energy,

$$E := - \int_{\Sigma} d\mathbf{x} \sqrt{h} n^\mu k^\nu \langle T_{\mu\nu} \rangle, \quad (6.37)$$

where  $\Sigma$  is a Cauchy slice of the boundary geometry, which in our case is a  $(d - 2)$ -dimensional sphere, with  $h$  denoting the determinant of its induced metric. Meanwhile,  $k^\mu$  is the stationary Killing vector field of the boundary geometry and  $n^\mu$  the unit normal to  $\Sigma$ .

The total charge is given by

$$Q := \int_{\Sigma} \sqrt{h} \rho(\theta) = \frac{1}{4\pi} \int_{\Sigma} \star F, \quad (6.38)$$

where the second equality follows from the definition of the charge density,  $\rho$ . We shall also consider the integral of the charge density over the left and right hemispheres, respectively denoted by  $Q_L^{(inf)}$  and  $Q_R^{(inf)}$ .

The charge of each horizon can be defined by a surface integral over a spatial cross-section of the horizon:

$$Q_R^{(hor)} := \frac{1}{4\pi} \int_{\mathcal{H}_R^+} \star F. \quad (6.39)$$

Gauss' law implies that  $Q_L^{(hor)} + Q_R^{(hor)} = Q$ . As usual, the Bekenstein-Hawking entropy of each horizon is proportional to their areas:

$$S_R = \frac{1}{4G_N} \mathcal{A}_{\mathcal{H}_R^+}. \quad (6.40)$$

### 6.3.2 The parameter space of solutions

Interestingly, we saw in Section 6.2.5 that even for a given choice of  $\mu_1$  and  $T$ , there are still further parameters which must be fixed to specify a particular binary solution. Due to the fact each horizon is a Killing horizon with Killing vector field,  $\partial_t$ , the vector potential is constant on each horizon:

$$A \Big|_{\mathcal{H}_R^+} = \nu_R dt, \quad (6.41)$$

where  $\nu_L$  and  $\nu_R$  are two constants, which we dub the *local chemical potential* at the respective horizons. It turns out  $\nu_L$  and  $\nu_R$  need not be zero. Indeed, for fixed values of  $\mu_1$  and  $T$  there is a continuous range of values of  $\nu_L$  and  $\nu_R$  for which we were able to find binary solutions.

Note that there is no gauge transformation which can alter  $\nu_L$  and  $\nu_R$  whilst remaining in the static gauge (with  $A \propto dt$  and  $A_t$  time-independent) except shifting the vector potential by a constant everywhere. Hence fixing that the  $\ell = 0$  mode of the boundary profile is zero fixes the gauge of the vector potential completely.

From the perspective of AdS/CFT, the presence of the  $\nu_L$  and  $\nu_R$  parameters is extremely surprising. By the addition of the chemical potential, we are deforming the field theory, and the extra parameters suggest that under this deformation there is a whole family of stationary states parameterised by these continuous parameters, even for a fixed value of the temperature. Since the parameters  $\nu_L$  and  $\nu_R$  are defined by the behaviour of the solution on the horizons, which lie very deep within the bulk, it is not at all clear what these quantities correspond to in the field theory.

For a general choice of these parameters, the  $\mathbb{Z}_2$  symmetry, about  $\theta = \pi/2$ , of the boundary data is broken in the bulk, and so the equations will need to be solved across the whole coordinate domain, as depicted in Figure 6.5. However, one can force the bulk solution to inherit this symmetry by setting  $\nu_L = -\nu_R$ .

In Figure 6.6, we plot the value of the proper distance between the horizons on the left and the value of the charges on the right for each of the  $\mathbb{Z}_2$ -symmetric solutions with  $\mu = 1.5$  and  $T = 1$ . These necessarily satisfy  $S_L = S_R$  and  $Q_L^{(\text{hor})} = -Q_R^{(\text{hor})}$ , thus, though the charge of each horizon depends on  $\nu_R$ , the *net charge* is always zero. Therefore, the existence of this one-dimensional family of  $\mathbb{Z}_2$ -symmetric solutions represent continuous non-uniqueness of the bulk solution for given boundary data.

There is a turning point for  $\nu_R$ , at  $\nu_R \simeq -0.2861$ . We have coloured in blue and orange the two branches either side of this turning point. Along either branch, solutions cease to exist as you increase the parameter beyond  $\nu_R \simeq -0.2861$ , however, since no

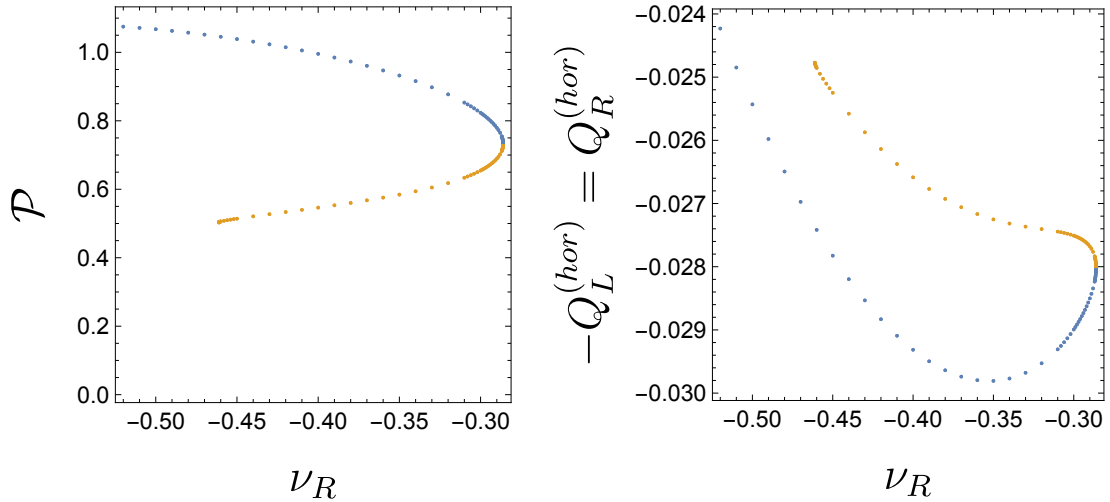


**Fig. 6.6:** The proper distance (left) between and the electric charges (right) of the horizons for each of the  $\mathbb{Z}_2$ -symmetric solutions with  $T = 1$  and  $\mu_1 = 1.5$  in four dimensions. There is a turning point at  $\nu_R \simeq -0.2861$ , either side of which we use different colours to indicate the two branches of solutions.

singularities arise and some physical quantities begin to have large derivatives with respect to  $\nu_R$ , it is highly suggestive that new solutions (the other branch) will be able to be found by instead decreasing  $\nu_R$  once again. We used the method described in Section 2.4.4 to perturb from a solution on one branch to a solution on the other.

In Figure 6.7, we plot how the entropy, energy, charge of the horizon and charge of the boundary hemispheres of the solutions (again with  $T = 1$  and  $\mu_1 = 1.5$ ) depend on the proper distance between the horizons. This plot helps to elucidate the necessity of the extra continuous parameter,  $\nu_R$ . One can alter the charges of the black holes, whilst in a counteracting fashion changing the distance between them, thereby maintaining a static configuration. From the bottom-left panel, we see that the balancing act between charge and proper distance does not occur in a simple monotonic fashion, due to the complicated balancing of multiple forces.

We see in the top-right panel of Figure 6.7 that the energy takes a maximum value, at  $\mathcal{P} \simeq 0.85$ . At this point, to leading order, the distance between the horizons is changing, but the energy is unaltered. This suggests there is a zero-mode, and thus a change of stability. Since the entropy is decreasing at this value of  $\mathcal{P}$ , it suggests that the solutions with  $\mathcal{P} < 0.85$  are more stable than those with  $\mathcal{P} > 0.85$  within this subfamily of solutions. We similarly find evidence of a turning point for the energy among subfamilies of the five-dimensional solutions with fixed temperature and boundary chemical potential.

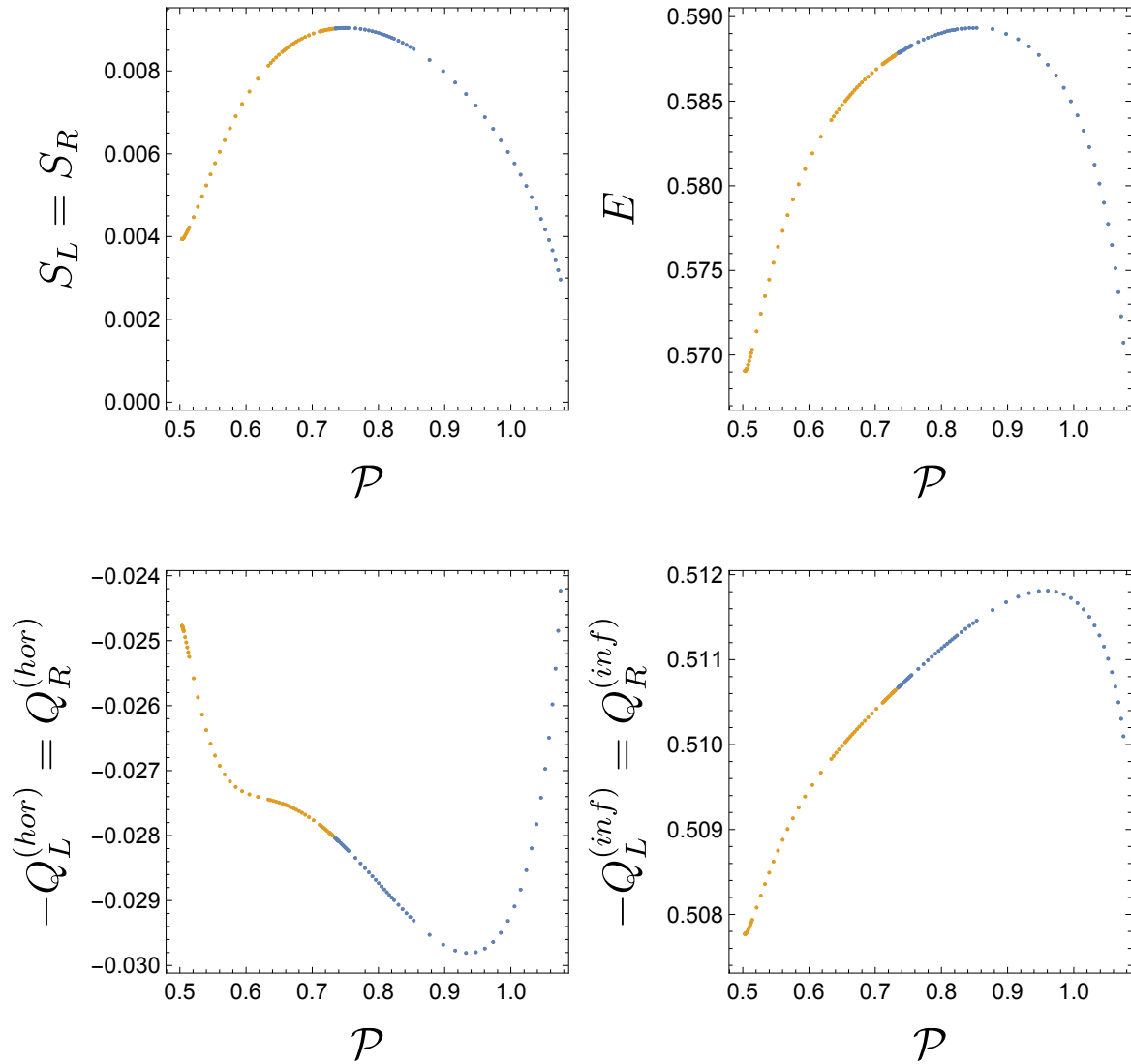


**Fig. 6.7:** A plot of various thermodynamic quantities (clockwise from bottom-left: charges of the horizons, entropy, energy, charges of the asymptotic hemispheres) against the proper distance between the horizons for four-dimensional  $\mathbb{Z}_2$ -symmetric solutions with the same temperature and boundary potential,  $T = 1$  and  $\mu = 1.5$ . The differently coloured points correspond to different branches, with a turning point at  $\nu_R \simeq -0.2861$ .

As seen in Figure 6.6,  $\nu_R$  can only be decreased to certain values on either branch before solutions cease to exist. The Kretschmann scalar at the horizons increases as  $\nu_R$  is decreased towards these values, hence it is possible that singularities are arising at these points in the parameter space. However, the evidence for this is inconclusive and solutions could cease to exist without the presence of singularities (perhaps in a similar manner to [233]) or there could be further turning points.

### 6.3.3 Thermodynamics

The binary solutions satisfy a first law of black hole mechanics, or thermodynamics, relationship, given by

$$\delta E = \sum_{i \in \{L, R\}} \left( T_i \delta S_i + \nu_i \delta Q_i^{(\text{hor})} \right) + \int_{\Sigma} d\mathbf{x} \sqrt{h} \mu(\theta) \delta \rho(\theta). \quad (6.42)$$

The final term must be calculated as an integral due to the fact that the boundary chemical potential,  $\mu(\theta)$ , is not constant. However, if one is only interested in variations which keep  $\mu(\theta)$  fixed, one can instead consider

$$G = E - \sum_{i \in \{L, R\}} \left( T_i S_i + \nu_i Q_i^{(\text{hor})} \right) - \int_{\Sigma} d\mathbf{x} \sqrt{h} \mu(\theta) \rho(\theta), \quad (6.43)$$

which will consequently satisfy a first law relationship,

$$\delta G = - \sum_{i \in \{L, R\}} \left( S_i \delta T_i + Q_i^{(\text{hor})} \delta \nu_i \right), \quad (6.44)$$

under such variations. The fact that only variations of the charges, rather than any quantities within an integral, are involved in (6.44) makes it easier to verify on the numerical solutions, and we were able to do so for the binary solutions in both four and five dimensions.

Under the AdS/CFT duality, the first law described in (6.42) will also relate variations of charges of the field theory which should be possible to be defined without reference to a gravitational bulk. However, whilst  $\nu_i$  and  $Q_i^{(\text{hor})}$  have clear physical meanings in the bulk as quantities defined on the horizon, their meaning in terms of the boundary theory is not at all clear. Therefore the presence of the terms in the first law concerning these quantities is perplexing from the perspective of the field theory. The situation is somewhat analogous to the thermodynamics of the asymptotically flat five-dimensional black rings discovered in [234], where dipole charges do appear in the first law of black hole mechanics [235], and yet cannot be measured at spatial infinity.

Furthermore, it is not clear that  $G$  is the value one would derive as the free energy by computing directly from the action, and indeed it seems unlikely that there even is a meaningful definition of the free energy at all. This is because Wick rotating the bulk solutions yields a Euclidean solution that is singular at the horizons unless the vector potential vanishes there, *i.e.*  $\nu_R = \nu_L = 0$ . No gauge transformation can be

taken to ensure these conditions unless  $\nu_R = \nu_L$ , which is generically not the case. The binary solutions are static, but intrinsically Lorentzian in nature.

## 6.4 Discussion

In this chapter we have presented the first examples of binary black hole solutions in Einstein-Maxwell theory with a negative cosmological constant in both four and five dimensions<sup>1</sup>. We have obtained a large family of such solutions, and in particular we showed that there are unexpected, extra parameters which are given by the value of the gauge potential at each of the horizons but do not have clear meanings from the boundary.

One source for future research would be to extend the solution space. It would be particularly interesting to ascertain whether the magnitude of the chemical potential can be taken to be arbitrarily small whilst still allowing for the existence of binary solutions. Moreover, if multi-black hole solutions exist near extremality in  $d \geq 5$ , they could provide a metastable phase in the RG flow, as conjectured in [237], possibly establishing a connection with the fragmentation scenario described in [238].

One could also allow for rotation. This could be done in a way still respecting axisymmetry, by having the black holes both rotate on their shared axis, à la [104]. This would introduce another degree of non-uniqueness, since the net angular momentum would still be zero if the black holes were spinning in opposite directions at the same speed. Moreover, rotation could induce spin-spin interactions between the two black holes, which may affect their stability properties.

Furthermore, the existence of the binary solutions suggests strongly that configurations with more than two disconnected black holes will also exist. Indeed, even with the same  $\ell = 1$  boundary profile, one could envisage a static configuration comprised of many black holes with alternating charges situated in a line along the  $\partial_\phi$  axis of symmetry.

The solutions described in this chapter can be S-dualized into magnetically charged binaries. These binaries, in turn, could serve as the starting point for constructing a traversable wormhole, as demonstrated in [239]. The advantage of this approach is that the initial binary configuration exists as a static solution and may indeed prove to be stable. We leave this construction for future work.

---

<sup>1</sup>We note though that multi-black hole solutions with anti-de Sitter boundary conditions have been *conjectured* to exist in [236] within the context of the bosonic sector of Fayet-Iliopoulos  $\mathcal{N} = 2$  gauged supergravity with a cubic prepotential. Indeed, the same reference discusses some of the properties of these intriguing multi-black hole solutions using the probe approximation.

Finally, although the solutions presented in this chapter possess no supersymmetry and are found at finite temperature, one might wonder whether supersymmetric solutions could exist. Given that the boundary chemical potential is necessarily nontrivial, one would need to search for possible supersymmetric solutions with spatially modulated deformations, perhaps using the approach pioneered in [240].

It would also be of great interest to understand if the binary solutions ever dominate over the soliton or polarised black hole solutions of [231]. However, as discussed above, a thermodynamic investigation is difficult, since it is not clear there is a well-defined notion of free energy. If the horizons have non-equal local chemical potential, then the solutions are *not* in thermoelectric equilibrium, and so it seems there is no good choice of ensemble in which to compare with the soliton and single horizon solutions.

The solutions we have found with  $\nu_L \neq \nu_R$  will become unstable under  $\mathcal{O}(N^{-2})$  corrections. The reason is that the two black holes can exchange via Hawking radiation Planckian-sized black holes of different electric charges and eventually reach global chemical equilibrium. However, this process occurs over very long time scales. This is perhaps akin to many-body localization, where systems undergo phases that exhibit local equilibrium but on much longer time scales eventually reach global equilibrium. Local equilibrium is usually associated with the existence of almost conserved quantities that make the system almost integrable, and that are responsible for delaying global thermalisation. In our case, one can conjecture that these local conserved quantities are the electric charges of each individual black hole.<sup>2</sup>

The solutions found in this work, let alone any of these further conjectured solutions, constitute a plethora of multi-black hole solutions in AdS. It would be extremely desirable to better understand the states of the CFT dual to these configurations correspond to, and in particular the meaning of the extra parameters on the field theory side.

---

<sup>2</sup>I would like to thank Sean Hartnoll for the discussions pertaining to this paragraph.

# Chapter 7

## Discussion

This thesis has exhibited a number of stationary solutions to the Einstein-Maxwell equations with a negative cosmological constant. Much of the interest in such solutions is due to the AdS/CFT correspondence which maps them to stationary, thermal states of a strongly coupled CFT. The desire to study such a CFT under the influence of gravitational and electromagnetic sources leads to the necessity of solving the bulk equations numerically using the methods described in Chapter 2.

The rotating RSII black hole solutions of Chapter 3 in many regards stand apart from the other solutions of this thesis. The Randall-Sundrum brane acts as an IR cut-off in the bulk, meaning that the dual theory is a CFT with a UV cut-off which is coupled to dynamical gravity. Hence, by studying a rotating black hole in the RSII model, one can hope to gain insight into how a strongly coupled QFT behaves around a rotating black hole, including the backreaction of the QFT with the geometry. The establishment of the bulk geometry stands as a first step towards such efforts. Furthermore, since the gravitational theory on the brane is given by four-dimensional GR with corrections from the CFT, the RSII model provides a genuine candidate for extra dimensions in our Universe, so long as the coupling between the CFT and gravity is not too strong. Indeed, in order to maintain this model as a feasible mechanism to include extra dimensions, it is vital that it exhibits rotating black holes which very closely resemble Kerr black holes at large scales. This fact is verified in Chapter 3, and the deviation of small braneworld black holes from the Kerr metric is quantified. It would be desirable to investigate more finely-grained features of these black holes, since these may give tests to falsify the RSII model, particularly if microscopic black holes were to be found to be created in particle colliders.

One key way in which the rotating RSII black holes differ from the other black hole solutions presented in this thesis is that they are in thermodynamic equilibrium.

---

For the other, out-of-equilibrium solutions of this thesis, one cannot Wick rotate the solutions to give regular Euclidean solutions. This means there is not a well-defined notion of free energy for these solutions. Thus, despite being stationary, these solutions are intrinsically Lorentzian.

The black tunnels and hammocks of Chapter 4 are the gravitational duals to a strongly coupled CFT residing on a fixed de Sitter-Schwarzschild background which possesses an event and a cosmological horizon. The two solutions correspond to two different phases of the CFT on this background; the tunnels correspond to a confined phase with suppressed flow between the two horizons, whereas the hammocks correspond to a deconfined phase with a large amount of flow. In the bulk the key difference between the solutions is the structure of the horizon, with the deconfined phase manifesting itself in the bulk by the presence of a flowing horizon in the hammock which is non-Killing. Neither of the solutions are in thermal equilibrium. This makes any thermodynamic argument of dominance of one state over the other extremely difficult. It seems likely one would need to study the dynamical stability of the solutions under perturbations in order to argue for dominance.

The holographic batteries of Chapter 5 show that this failure of the solutions to be in thermodynamic equilibrium can occur even if the two boundary horizons have exactly the same temperature. In this case though, a chemical potential is added to the boundary theory as a source, with a potential difference between the two horizons. This generates a conserved current in the boundary theory, and via bulk calculations one can measure the conductivity of the CFT in the non-linear regime. The fact that flow is generated by Joule heating, rather than an enforced difference of temperatures between the two boundary horizons means that the structure of the bulk horizon is subtly different to other previously found funnel solutions found, this time with the past boundary of the future horizon lying deep within the bulk.

Finally in Chapter 6, we showed that the addition of a background electric field can support static, charged binary solutions in AdS. One of the great intrigues of these spacetimes is that for given boundary charges, there is a continuous space of solutions in the bulk. This means that these solutions represent continuous non-uniqueness of the bulk solution for given boundary data. Furthermore, the parameters spanning this space have natural definitions in terms of the horizons of the two black holes, but the meaning of them from the perspective of the boundary theory is extremely mysterious. The dual family of CFT states also run over this parameter space but it is not clear at all what the meaning of these extra parameters is in terms of the CFT without making reference to the bulk theory. This issue is highlighted in particular since the

first law of thermodynamics relationship that the binaries (and hence the dual CFT states) satisfy contain terms relating to these parameters. Furthermore, except for specific values of the parameters, the binary solutions are also not in thermodynamic equilibrium, since the gauge potential on the horizons is non-equal in general. Wick rotating a binary solution into the Euclidean sector will cause the Maxwell field to be singular at the horizons unless the gauge potential vanishes at each of them — but cannot be made to be the case for a general binary solution. Hence, again there is no well-defined notion of the free energy. This problem is extremely striking in this case, since the binary solutions are static with horizons with equal temperature and an overall net zero charge, and yet still they do not yield regular Euclidean solutions.

By studying these black hole solutions, we have obtained insights into the behaviour of large  $N$ , strongly coupled quantum field theories under the influence of complicated sources, a task that would be impossible without the aid of holography. These out-of-equilibrium black hole solutions suggest that there are profound differences between how such large  $N$ , strongly coupled fields behave to one's intuitive expectation from free or weakly coupled fields. Studying stationary black holes in AdS remains our best, and often only, method to study the behaviour of these strongly coupled fields in many situations.

Personally though, I believe the study of these black hole solutions would still be interesting in its own right even if gauge/gravity duality were still a twinkle in Juan Maldacena's eye. General relativity is a beautiful and elegant theory, and it is fascinating to discover the space of stationary black hole solutions, once thought to be almost completely featureless, is really rather rich, varied and intricate.

# References

- [1] William D. Biggs and Jorge E. Santos. Rotating Black Holes in Randall-Sundrum II Braneworlds. *Phys. Rev. Lett.*, 128(2):021601, 2022. doi: 10.1103/PhysRevLett.128.021601.
- [2] William D. Biggs and Jorge E. Santos. Black tunnels and hammocks. *JHEP*, 11:021, 2022. doi: 10.1007/JHEP11(2022)021.
- [3] William D. Biggs and Jorge E. Santos. Holographic batteries. *Phys. Rev. D*, 109(10):L101904, 2024. doi: 10.1103/PhysRevD.109.L101904.
- [4] William D. Biggs and Jorge E. Santos. Charged Static AdS Black Hole Binaries. arXiv:1703.06476, 6 2024.
- [5] A. Einstein. Zur allgemeinen Relativitätstheorie. *Sitzungsberichte der Königlich Preussischen Akademie der Wissenschaften*, page 778, 1915.
- [6] David Hilbert. Die Grundlagen der Physik (Erste Mitteilung). *Nachrichten von der Gesellschaft der Wissenschaften zu Göttingen. Mathematisch-physikalische Klasse*, pages 395–407, 1915.
- [7] Albert Einstein. On the electrodynamics of moving bodies. *Annalen Phys.*, 17:891–921, 1905. doi: 10.1002/andp.200590006.
- [8] Hermann Minkowski. Raum und Zeit. *Physikalische Zeitschrift*, 10:75–88, 1908.
- [9] Hawking, S. W., and George Francis Rayner Ellis. *The large scale structure of space-time*. Cambridge University Press, 1973.
- [10] Charles W. Misner, K. S. Thorne, and J. A. Wheeler. *Gravitation*. W. H. Freeman, San Francisco, 1973. ISBN 978-0-7167-0344-0, 978-0-691-17779-3.
- [11] Robert M. Wald. *General Relativity*. Chicago Univ. Pr., Chicago, USA, 1984. doi: 10.7208/chicago/9780226870373.001.0001.
- [12] Sean M. Carroll. *Spacetime and Geometry: An Introduction to General Relativity*. Cambridge University Press, 7 2019. ISBN 978-0-8053-8732-2, 978-1-108-48839-6, 978-1-108-77555-7. doi: 10.1017/9781108770385.
- [13] Karl Schwarzschild. Über das Gravitationsfeld eines Massenpunktes nach der Einsteinschen Theorie. *Sitzungsberichte der Königlich Preussischen Akademie der Wissenschaften*, pages vol. I, 189–196, 1916.

- 
- [14] Roger Penrose. Gravitational collapse and space-time singularities. *Phys. Rev. Lett.*, 14:57–59, 1965. doi: 10.1103/PhysRevLett.14.57.
- [15] R. Penrose. Gravitational collapse: The role of general relativity. *Riv. Nuovo Cim.*, 1:252–276, 1969. doi: 10.1023/A:1016578408204.
- [16] S. W. Hawking and R. Penrose. The Singularities of gravitational collapse and cosmology. *Proc. Roy. Soc. Lond. A*, 314:529–548, 1970. doi: 10.1098/rspa.1970.0021.
- [17] Garret Birkhoff. Relativity and modern physics. *Harvard University Press*, 1923.
- [18] Hans Reissner. Über die Eigengravitation des elektrischen Feldes nach der Einsteinschen Theorie. *Annalen der Physik*, 1916.
- [19] Hermann Weyl. Zur Gravitationstheorie. *Annalen der Physik*, 1917.
- [20] Gunnar Nordström. On the energy of the gravitational field in Einstein’s theory. *Verhandl. Koninkl. Ned. Akad. Wetenschap., Afdel. Natuurk., Amsterdam.*, 1918.
- [21] George Barker Jeffery. The field of an electron on Einstein’s theory of gravitation. *Proc. R. Soc. Lond.*, 1921.
- [22] R. Penrose. Singularities and time-asymmetry, in *General Relativity - An Einstein Centenary Survey*, edited by S. W. Hawking and W. Israel. page 581–638, 1979.
- [23] Roy P. Kerr. Gravitational field of a spinning mass as an example of algebraically special metrics. *Phys. Rev. Lett.*, 11:237–238, 1963. doi: 10.1103/PhysRevLett.11.237.
- [24] R. Penrose and R. M. Floyd. Extraction of rotational energy from a black hole. *Nature*, 229:177–179, 1971. doi: 10.1038/physci229177a0.
- [25] R. H. Dicke. Coherence in Spontaneous Radiation Processes. *Phys. Rev.*, 93: 99–110, 1954. doi: 10.1103/PhysRev.93.99.
- [26] Ya. B. Zel’Dovich. Generation of Waves by a Rotating Body. *Soviet Journal of Experimental and Theoretical Physics Letters*, 14:180, August 1971.
- [27] Ya. B. Zel’Dovich. Amplification of Cylindrical Electromagnetic Waves Reflected from a Rotating Body. *Soviet Journal of Experimental and Theoretical Physics*, 35:1085, January 1972.
- [28] E T. Newman, R. Couch, K. Chinnapared, A. Exton, A. Prakash, and R. Torrence. Metric of a Rotating, Charged Mass. *J. Math. Phys.*, 6:918–919, 1965. doi: 10.1063/1.1704351.
- [29] E. T. Newman and A. I. Janis. Note on the Kerr spinning particle metric. *J. Math. Phys.*, 6:915–917, 1965. doi: 10.1063/1.1704350.
- [30] David Robinson. Four decades of black holes uniqueness theorems. In *Kerr Fest: Black Holes in Astrophysics, General Relativity and Quantum Gravity*, 8 2004.

- [31] Piotr T. Chrusciel, Joao Lopes Costa, and Markus Heusler. Stationary Black Holes: Uniqueness and Beyond. *Living Rev. Rel.*, 15:7, 2012. doi: 10.12942/lrr-2012-7.
- [32] Werner Israel. Event horizons in static vacuum space-times. *Phys. Rev.*, 164:1776–1779, 1967. doi: 10.1103/PhysRev.164.1776.
- [33] Gary L. Bunting and A. K. M. Masood-Ul-Alam. Nonexistence of multiple black holes in asymptotically Euclidean static vacuum space-time. *General Relativity and Gravitation*, 19(2):147–154, February 1987. doi: 10.1007/BF00770326.
- [34] R. Schon and Shing-Tung Yau. On the Proof of the positive mass conjecture in general relativity. *Commun. Math. Phys.*, 65:45–76, 1979. doi: 10.1007/BF01940959.
- [35] Richard Schon and Shing-Tung Yau. Proof of the positive mass theorem. 2. *Commun. Math. Phys.*, 79:231–260, 1981. doi: 10.1007/BF01942062.
- [36] Edward Witten. A Simple Proof of the Positive Energy Theorem. *Commun. Math. Phys.*, 80:381, 1981. doi: 10.1007/BF01208277.
- [37] Werner Israel. Event horizons in static electrovac space-times. *Commun. Math. Phys.*, 8:245–260, 1968. doi: 10.1007/BF01645859.
- [38] S. D. Majumdar. A class of exact solutions of Einstein’s field equations. *Phys. Rev.*, 72:390–398, 1947. doi: 10.1103/PhysRev.72.390.
- [39] A. Papaetrou. A Static solution of the equations of the gravitational field for an arbitrary charge distribution. *Proc. Roy. Irish Acad. A*, 51:191–204, 1947.
- [40] Peter Ruback. A New Uniqueness Theorem for Charged Black Holes. *Class. Quant. Grav.*, 5:L155, 1988. doi: 10.1088/0264-9381/5/10/005.
- [41] Piotr T. Chrusciel and Paul Tod. The Classification of static electro-vacuum space-times containing an asymptotically flat spacelike hypersurface with compact interior. *Commun. Math. Phys.*, 271:577–589, 2007. doi: 10.1007/s00220-007-0191-9.
- [42] D. Sudarsky and Robert M. Wald. Extrema of mass, stationarity, and staticity, and solutions to the Einstein Yang-Mills equations. *Phys. Rev. D*, 46:1453–1474, 1992. doi: 10.1103/PhysRevD.46.1453.
- [43] D. Sudarsky and Robert M. Wald. Mass formulas for stationary Einstein Yang-Mills black holes and a simple proof of two staticity theorems. *Phys. Rev. D*, 47:R5209–R5213, 1993. doi: 10.1103/PhysRevD.47.R5209.
- [44] Hawking, S.W. Black holes in general relativity. *Communications in Mathematical Physics* 25, 152–166, 1972. doi: 10.1007/BF01877517.
- [45] Istvan Racz and Robert M. Wald. Extensions of spacetimes with killing horizons. *Classical and Quantum Gravity*, 9(12):2643, dec 1992. doi: 10.1088/0264-9381/9/12/008. URL <https://dx.doi.org/10.1088/0264-9381/9/12/008>.

- [46] Istvan Racz and Robert M. Wald. Global extensions of space-times describing asymptotic final states of black holes. *Class. Quant. Grav.*, 13:539–553, 1996. doi: 10.1088/0264-9381/13/3/017.
- [47] Helmut Friedrich, Istvan Racz, and Robert M. Wald. On the rigidity theorem for space-times with a stationary event horizon or a compact Cauchy horizon. *Commun. Math. Phys.*, 204:691–707, 1999. doi: 10.1007/s002200050662.
- [48] Istvan Racz. On further generalization of the rigidity theorem for space-times with a stationary event horizon or a compact Cauchy horizon. *Class. Quant. Grav.*, 17:153–178, 2000. doi: 10.1088/0264-9381/17/1/311.
- [49] S. Alexakis, A. D. Ionescu, and S. Klainerman. Hawking’s local rigidity theorem without analyticity. 2 2009.
- [50] Piotr T. Chrusciel and Robert M. Wald. On the topology of stationary black holes. *Class. Quant. Grav.*, 11:L147–L152, 1994. doi: 10.1088/0264-9381/11/12/001.
- [51] Gregory J Galloway. On the topology of the domain of outer communication. *Classical and Quantum Gravity*, 12(10):L99, oct 1995. doi: 10.1088/0264-9381/12/10/002. URL <https://dx.doi.org/10.1088/0264-9381/12/10/002>.
- [52] B. Carter. Axisymmetric Black Hole Has Only Two Degrees of Freedom. *Phys. Rev. Lett.*, 26:331–333, 1971. doi: 10.1103/PhysRevLett.26.331.
- [53] D. C. Robinson. Uniqueness of the Kerr black hole. *Phys. Rev. Lett.*, 34:905–906, 1975. doi: 10.1103/PhysRevLett.34.905.
- [54] P O Mazur. Proof of uniqueness of the kerr-newman black hole solution. *Journal of Physics A: Mathematical and General*, 15(10):3173, oct 1982. doi: 10.1088/0305-4470/15/10/021. URL <https://dx.doi.org/10.1088/0305-4470/15/10/021>.
- [55] G.L. Bunting. Proof of the uniqueness conjecture for black holes. (*Ph.D. thesis*, University of New England, Armadale, N.S.W.), 1983.
- [56] R. Penney. Axially symmetric zero-mass meson solutions of einstein equations. *Phys. Rev.*, 174:1578–1579, Oct 1968. doi: 10.1103/PhysRev.174.1578. URL <https://link.aps.org/doi/10.1103/PhysRev.174.1578>.
- [57] J. E. Chase. Event horizons in static scalar-vacuum space-times. *Commun. Math. Phys.*, 19(4):276–288, 1970. doi: 10.1007/BF01646635.
- [58] Jacob D. Bekenstein. Transcendence of the law of baryon-number conservation in black-hole physics. *Phys. Rev. Lett.*, 28:452–455, Feb 1972. doi: 10.1103/PhysRevLett.28.452. URL <https://link.aps.org/doi/10.1103/PhysRevLett.28.452>.
- [59] Jacob D. Bekenstein. Nonexistence of baryon number for static black holes. *Phys. Rev. D*, 5:1239–1246, Mar 1972. doi: 10.1103/PhysRevD.5.1239. URL <https://link.aps.org/doi/10.1103/PhysRevD.5.1239>.
- [60] Jacob D. Bekenstein. Nonexistence of baryon number for black holes. ii. *Phys. Rev. D*, 5:2403–2412, May 1972. doi: 10.1103/PhysRevD.5.2403. URL <https://link.aps.org/doi/10.1103/PhysRevD.5.2403>.

- [61] Claudio Teitelboim. Nonmeasurability of the quantum numbers of a black hole. *Phys. Rev. D*, 5:2941–2954, Jun 1972. doi: 10.1103/PhysRevD.5.2941. URL <https://link.aps.org/doi/10.1103/PhysRevD.5.2941>.
- [62] Markus Heusler. No hair theorems and black holes with hair. *Helv. Phys. Acta*, 69(4):501–528, 1996.
- [63] Jacob D. Bekenstein. Novel “no-scalar-hair” theorem for black holes. *Phys. Rev. D*, 51(12):R6608, 1995. doi: 10.1103/PhysRevD.51.R6608.
- [64] Jacob D. Bekenstein. Black hole hair: 25 - years after. In *2nd International Sakharov Conference on Physics*, pages 216–219, 5 1996.
- [65] D. Sudarsky. A Simple proof of a no hair theorem in Einstein Higgs theory. *Class. Quant. Grav.*, 12:579–584, 1995. doi: 10.1088/0264-9381/12/2/023.
- [66] G. W. Gibbons. Selfgravitating magnetic monopoles, global monopoles and black holes. *Lect. Notes Phys.*, 383:110–138, 1991. doi: 10.1007/3-540-54293-0\_24.
- [67] George V. Lavrelashvili and Dieter Maison. Regular and black hole solutions of Einstein Yang-Mills Dilaton theory. *Nucl. Phys. B*, 410:407–422, 1993. doi: 10.1016/0550-3213(93)90441-Q.
- [68] Brian R. Greene, Samir D. Mathur, and Christopher M. O’Neill. Eluding the no hair conjecture: Black holes in spontaneously broken gauge theories. *Phys. Rev. D*, 47:2242–2259, 1993. doi: 10.1103/PhysRevD.47.2242.
- [69] M. S. Volkov and D. V. Galtsov. NonAbelian Einstein Yang-Mills black holes. *JETP Lett.*, 50:346–350, 1989.
- [70] H. P. Kuenzle and A. K. M. Masood-ul Alam. Spherically symmetric static SU(2) Einstein Yang-Mills fields. *J. Math. Phys.*, 31:928–935, 1990. doi: 10.1063/1.528773.
- [71] P. Bizon. Colored black holes. *Phys. Rev. Lett.*, 64:2844–2847, 1990. doi: 10.1103/PhysRevLett.64.2844.
- [72] Carlos A. R. Herdeiro and Eugen Radu. Kerr black holes with scalar hair. *Phys. Rev. Lett.*, 112:221101, 2014. doi: 10.1103/PhysRevLett.112.221101.
- [73] Carlos Herdeiro, Eugen Radu, and Helgi Rúnarsson. Kerr black holes with Proca hair. *Class. Quant. Grav.*, 33(15):154001, 2016. doi: 10.1088/0264-9381/33/15/154001.
- [74] Jacob D. Bekenstein. Black holes and the second law. *Lettere al Nuovo Cimento*, page 737–740, 1972. doi: 10.1007/BF02757029.
- [75] Jacob D. Bekenstein. Black holes and entropy. *Phys. Rev. D*, 7:2333–2346, Apr 1973. doi: 10.1103/PhysRevD.7.2333. URL <https://link.aps.org/doi/10.1103/PhysRevD.7.2333>.
- [76] James M. Bardeen, B. Carter, and S. W. Hawking. The Four laws of black hole mechanics. *Commun. Math. Phys.*, 31:161–170, 1973. doi: 10.1007/BF01645742.

- [77] Robert M. Wald. The thermodynamics of black holes. *Living Rev. Rel.*, 4:6, 2001. doi: 10.12942/lrr-2001-6.
- [78] S. W. Hawking and J. B. Hartle. Energy and angular momentum flow into a black hole. *Commun. Math. Phys.*, 27:283–290, 1972. doi: 10.1007/BF01645515.
- [79] Vivek Iyer and Robert M. Wald. Some properties of Noether charge and a proposal for dynamical black hole entropy. *Phys. Rev. D*, 50:846–864, 1994. doi: 10.1103/PhysRevD.50.846.
- [80] S. W. Hawking. Black hole explosions. *Nature*, 248:30–31, 1974. doi: 10.1038/248030a0.
- [81] S. W. Hawking. Particle Creation by Black Holes. *Commun. Math. Phys.*, 43: 199–220, 1975. doi: 10.1007/BF02345020. [Erratum: *Commun. Math. Phys.* 46, 206 (1976)].
- [82] Jacob D. Bekenstein. Generalized second law of thermodynamics in black hole physics. *Phys. Rev. D*, 9:3292–3300, 1974. doi: 10.1103/PhysRevD.9.3292.
- [83] S. W. Hawking. Breakdown of Predictability in Gravitational Collapse. *Phys. Rev. D*, 14:2460–2473, 1976. doi: 10.1103/PhysRevD.14.2460.
- [84] Ahmed Almheiri, Donald Marolf, Joseph Polchinski, and James Sully. Black Holes: Complementarity or Firewalls? *JHEP*, 02:062, 2013. doi: 10.1007/JHEP02(2013)062.
- [85] Roberto Emparan and Harvey S. Reall. Black Holes in Higher Dimensions. *Living Rev. Rel.*, 11:6, 2008. doi: 10.12942/lrr-2008-6.
- [86] Gary T. Horowitz, editor. *Black holes in higher dimensions*. Cambridge Univ. Pr., Cambridge, UK, 2012. ISBN 978-1-107-01345-2.
- [87] Steven B. Giddings. Black holes in the lab? *Gen. Rel. Grav.*, 34:1775–1779, 2002. doi: 10.1023/A:1020739305635.
- [88] Marco Cavaglia. Black hole and brane production in TeV gravity: A Review. *Int. J. Mod. Phys. A*, 18:1843–1882, 2003. doi: 10.1142/S0217751X03013569.
- [89] Panagiota Kanti. Black holes in theories with large extra dimensions: A Review. *Int. J. Mod. Phys. A*, 19:4899–4951, 2004. doi: 10.1142/S0217751X04018324.
- [90] Keisuke Fujii et al. Tests of the Standard Model at the International Linear Collider. Technical report, 2019.
- [91] H. Davoudiasl, B. Lillie, and T. G. Rizzo. Probing the universal Randall-Sundrum model at the ILC. In *2005 International Linear Collider Physics and Detector Workshop and 2nd ILC Accelerator Workshop*, 9 2005.
- [92] Philipp Roloff, Ulrike Schnoor, Rosa Simoniello, and Boruo Xu. Double Higgs boson production and Higgs self-coupling extraction at CLIC. *Eur. Phys. J. C*, 80(11):1010, 2020. doi: 10.1140/epjc/s10052-020-08567-7.

- [93] S. Hwang. A rigidity theorem for ricci flat metrics. *Geometriae Dedicata*, 71: 5–17, 1998. doi: 10.1023/A:1005094911005.
- [94] Gary W. Gibbons, Daisuke Ida, and Tetsuya Shiromizu. Uniqueness and nonuniqueness of static black holes in higher dimensions. *Phys. Rev. Lett.*, 89:041101, 2002. doi: 10.1103/PhysRevLett.89.041101.
- [95] Marek Rogatko. Uniqueness theorem of static degenerate and nondegenerate charged black holes in higher dimensions. *Phys. Rev. D*, 67:084025, Apr 2003. doi: 10.1103/PhysRevD.67.084025. URL <https://link.aps.org/doi/10.1103/PhysRevD.67.084025>.
- [96] Robert C. Myers and M. J. Perry. Black Holes in Higher Dimensional Space-Times. *Annals Phys.*, 172:304, 1986. doi: 10.1016/0003-4916(86)90186-7.
- [97] Roberto Emparan and Harvey S. Reall. A Rotating black ring solution in five-dimensions. *Phys. Rev. Lett.*, 88:101101, 2002. doi: 10.1103/PhysRevLett.88.101101.
- [98] Gregory J. Galloway and Richard Schoen. A Generalization of Hawking’s black hole topology theorem to higher dimensions. *Commun. Math. Phys.*, 266:571–576, 2006. doi: 10.1007/s00220-006-0019-z.
- [99] Gregory J. Galloway. Rigidity of outer horizons and the topology of black holes. 8 2006.
- [100] Stefan Hollands, Akihiro Ishibashi, and Robert M. Wald. A Higher dimensional stationary rotating black hole must be axisymmetric. *Commun. Math. Phys.*, 271:699–722, 2007. doi: 10.1007/s00220-007-0216-4.
- [101] Stefan Hollands and Akihiro Ishibashi. On the ‘Stationary Implies Axisymmetric’ Theorem for Extremal Black Holes in Higher Dimensions. *Commun. Math. Phys.*, 291:403–441, 2009. doi: 10.1007/s00220-009-0841-1.
- [102] Vincent Moncrief and James Isenberg. Symmetries of Higher Dimensional Black Holes. *Class. Quant. Grav.*, 25:195015, 2008. doi: 10.1088/0264-9381/25/19/195015.
- [103] Oscar J. C. Dias, Gary W. Gibbons, Jorge E. Santos, and Benson Way. Static Black Binaries in de Sitter Space. *Phys. Rev. Lett.*, 131(13):131401, 2023. doi: 10.1103/PhysRevLett.131.131401.
- [104] Oscar J. C. Dias, Jorge E. Santos, and Benson Way. Spinning Black Binaries in de Sitter space. 6 2024.
- [105] S. Perlmutter et al. Discovery of a supernova explosion at half the age of the Universe and its cosmological implications. *Nature*, 391:51–54, 1998. doi: 10.1038/34124.
- [106] S. Perlmutter et al. Measurements of  $\Omega$  and  $\Lambda$  from 42 High Redshift Supernovae. *Astrophys. J.*, 517:565–586, 1999. doi: 10.1086/307221.

- [107] Brian P. Schmidt et al. The High Z supernova search: Measuring cosmic deceleration and global curvature of the universe using type Ia supernovae. *Astrophys. J.*, 507:46–63, 1998. doi: 10.1086/306308.
- [108] Adam G. Riess et al. Observational evidence from supernovae for an accelerating universe and a cosmological constant. *Astron. J.*, 116:1009–1038, 1998. doi: 10.1086/300499.
- [109] Juan Maldacena. The Large N limit of superconformal field theories and supergravity. *Adv. Theor. Math. Phys.*, 2:231–252, 1998. doi: 10.1023/A:1026654312961.
- [110] Edward Witten. Anti-de Sitter space and holography. *Adv. Theor. Math. Phys.*, 2:253–291, 1998. doi: 10.4310/ATMP.1998.v2.n2.a2.
- [111] Ofer Aharony, Steven S. Gubser, Juan Maldacena, Hiroshi Ooguri, and Yaron Oz. Large N field theories, string theory and gravity. *Phys. Rept.*, 323:183–386, 2000. doi: 10.1016/S0370-1573(99)00083-6.
- [112] A. Zaffaroni. Introduction to the AdS-CFT correspondence. *Class. Quant. Grav.*, 17:3571–3597, 2000. doi: 10.1088/0264-9381/17/17/306.
- [113] Juan Martin Maldacena. TASI 2003 lectures on AdS / CFT. In *Theoretical Advanced Study Institute in Elementary Particle Physics (TASI 2003): Recent Trends in String Theory*, pages 155–203, 9 2003.
- [114] Gary T. Horowitz and Joseph Polchinski. Gauge/gravity duality. pages 169–186, 2 2006.
- [115] Joseph Polchinski. Introduction to Gauge/Gravity Duality. In *Theoretical Advanced Study Institute in Elementary Particle Physics: String theory and its Applications: From meV to the Planck Scale*, pages 3–46, 10 2010. doi: 10.1142/9789814350525\_0001.
- [116] Veronika E. Hubeny. The AdS/CFT Correspondence. *Class. Quant. Grav.*, 32(12):124010, 2015. doi: 10.1088/0264-9381/32/12/124010.
- [117] Makoto Natsuume. *AdS/CFT Duality User Guide*, volume 903. 2015. ISBN 978-4-431-55441-7, 978-4-431-55440-0. doi: 10.1007/978-4-431-55441-7.
- [118] Horațiu Năstase. *Introduction to the AdS/CFT Correspondence*. Cambridge University Press, 2015.
- [119] Martin Ammon and Johanna Erdmenger. *Gauge/Gravity Duality: Foundations and Applications*. Cambridge University Press, 2015.
- [120] Sebastian de Haro, Sergey N. Solodukhin, and Kostas Skenderis. Holographic reconstruction of space-time and renormalization in the AdS / CFT correspondence. *Commun. Math. Phys.*, 217:595–622, 2001. doi: 10.1007/s002200100381.
- [121] Charles Fefferman and C. Robin Graham. Conformal invariants. In *Élie Cartan et les mathématiques d'aujourd'hui - Lyon, 25-29 juin 1984*, number S131 in Astérisque. Société mathématique de France, 1985. URL [http://www.numdam.org/item/AST\\_1985\\_\\_S131\\_\\_95\\_0/](http://www.numdam.org/item/AST_1985__S131__95_0/).

- [122] M. Henningson and K. Skenderis. The Holographic Weyl anomaly. *JHEP*, 07:023, 1998. doi: 10.1088/1126-6708/1998/07/023.
- [123] Oscar J. C. Dias, Prahar Mitra, and Jorge E. Santos. New phases of  $\mathcal{N} = 4$  SYM at finite chemical potential. *JHEP*, 05:053, 2023. doi: 10.1007/JHEP05(2023)053.
- [124] Maximo Banados, Claudio Teitelboim, and Jorge Zanelli. The Black hole in three-dimensional space-time. *Phys. Rev. Lett.*, 69:1849–1851, 1992. doi: 10.1103/PhysRevLett.69.1849.
- [125] S. W. Hawking and Don N. Page. Thermodynamics of Black Holes in anti-De Sitter Space. *Commun. Math. Phys.*, 87:577, 1983. doi: 10.1007/BF01208266.
- [126] Edward Witten. Anti-de Sitter space, thermal phase transition, and confinement in gauge theories. *Adv. Theor. Math. Phys.*, 2:505–532, 1998. doi: 10.4310/ATMP.1998.v2.n3.a3.
- [127] Donald Marolf, Mukund Rangamani, and Toby Wiseman. Holographic thermal field theory on curved spacetimes. *Class. Quant. Grav.*, 31:063001, 2014. doi: 10.1088/0264-9381/31/6/063001.
- [128] A. Liam Fitzpatrick, Lisa Randall, and Toby Wiseman. On the existence and dynamics of braneworld black holes. *JHEP*, 11:033, 2006. doi: 10.1088/1126-6708/2006/11/033.
- [129] Veronika E. Hubeny, Donald Marolf, and Mukund Rangamani. Hawking radiation in large  $N$  strongly-coupled field theories. *Class. Quant. Grav.*, 27:095015, 2010. doi: 10.1088/0264-9381/27/9/095015.
- [130] Veronika E. Hubeny, Donald Marolf, and Mukund Rangamani. Black funnels and droplets from the AdS C-metrics. *Class. Quant. Grav.*, 27:025001, 2010. doi: 10.1088/0264-9381/27/2/025001.
- [131] Veronika E. Hubeny, Donald Marolf, and Mukund Rangamani. Hawking radiation from AdS black holes. *Class. Quant. Grav.*, 27:095018, 2010. doi: 10.1088/0264-9381/27/9/095018.
- [132] Marco M. Caldarelli, Oscar J. C. Dias, Ricardo Monteiro, and Jorge E. Santos. Black funnels and droplets in thermal equilibrium. *JHEP*, 05:116, 2011. doi: 10.1007/JHEP05(2011)116.
- [133] Pau Figueras, James Lucietti, and Toby Wiseman. Ricci solitons, Ricci flow, and strongly coupled CFT in the Schwarzschild Unruh or Boulware vacua. *Class. Quant. Grav.*, 28:215018, 2011. doi: 10.1088/0264-9381/28/21/215018.
- [134] Jorge E. Santos and Benson Way. Black Funnels. *JHEP*, 12:060, 2012. doi: 10.1007/JHEP12(2012)060.
- [135] Jorge E. Santos. To go or not to go with the flow: Hawking radiation at strong coupling. *JHEP*, 06:104, 2020. doi: 10.1007/JHEP06(2020)104.

- [136] Valeri P. Frolov and Don N. Page. Proof of the generalized second law for quasistationary semiclassical black holes. *Phys. Rev. Lett.*, 71:3902–3905, 1993. doi: 10.1103/PhysRevLett.71.3902.
- [137] Sebastian Fischetti, Jorge E. Santos, and Benson Way. Dissonant Black Droplets and Black Funnels. *Class. Quant. Grav.*, 34(15):155001, 2017. doi: 10.1088/1361-6382/aa79ba.
- [138] Sebastian Fischetti and Donald Marolf. Flowing Funnels: Heat sources for field theories and the AdS<sub>3</sub> dual of CFT<sub>2</sub> Hawking radiation. *Class. Quant. Grav.*, 29:105004, 2012. doi: 10.1088/0264-9381/29/10/105004.
- [139] Sebastian Fischetti, Donald Marolf, and Jorge E. Santos. AdS flowing black funnels: Stationary AdS black holes with non-Killing horizons and heat transport in the dual CFT. *Class. Quant. Grav.*, 30:075001, 2013. doi: 10.1088/0264-9381/30/7/075001.
- [140] Donald Marolf and Jorge E. Santos. Phases of Holographic Hawking Radiation on spatially compact spacetimes. *JHEP*, 10:250, 2019. doi: 10.1007/JHEP10(2019)250.
- [141] Lisa Randall and Raman Sundrum. A Large mass hierarchy from a small extra dimension. *Phys. Rev. Lett.*, 83:3370–3373, 1999. doi: 10.1103/PhysRevLett.83.3370.
- [142] Lisa Randall and Raman Sundrum. An Alternative to compactification. *Phys. Rev. Lett.*, 83:4690–4693, 1999. doi: 10.1103/PhysRevLett.83.4690.
- [143] Steven S. Gubser. AdS / CFT and gravity. *Phys. Rev. D*, 63:084017, 2001. doi: 10.1103/PhysRevD.63.084017.
- [144] James W. York, Jr. Role of conformal three geometry in the dynamics of gravitation. *Phys. Rev. Lett.*, 28:1082–1085, 1972. doi: 10.1103/PhysRevLett.28.1082.
- [145] G. W. Gibbons and S. W. Hawking. Action Integrals and Partition Functions in Quantum Gravity. *Phys. Rev. D*, 15:2752–2756, 1977. doi: 10.1103/PhysRevD.15.2752.
- [146] S. W. Hawking, T. Hertog, and H. S. Reall. Brane new world. *Phys. Rev. D*, 62:043501, 2000. doi: 10.1103/PhysRevD.62.043501.
- [147] A. Chamblin, S. W. Hawking, and H. S. Reall. Brane world black holes. *Phys. Rev. D*, 61:065007, 2000. doi: 10.1103/PhysRevD.61.065007.
- [148] Roberto Emparan, Alessandro Fabbri, and Nemanja Kaloper. Quantum black holes as holograms in AdS brane worlds. *JHEP*, 08:043, 2002. doi: 10.1088/1126-6708/2002/08/043.
- [149] Pau Figueras and Toby Wiseman. Gravity and large black holes in Randall-Sundrum II braneworlds. *Phys. Rev. Lett.*, 107:081101, 2011. doi: 10.1103/PhysRevLett.107.081101.

- [150] Shohreh Abdolrahimi, Celine Cattoen, Don N. Page, and Shima Yaghoobpour-Tari. Large Randall-Sundrum II Black Holes. *Phys. Lett. B*, 720:405–409, 2013. doi: 10.1016/j.physletb.2013.02.034.
- [151] Daoyan Wang and Matthew W. Choptuik. Black hole formation in Randall-Sundrum II braneworlds. *Phys. Rev. Lett.*, 117(1):011102, 2016. doi: 10.1103/PhysRevLett.117.011102.
- [152] Toby Wiseman. *Numerical construction of static and stationary black holes*. 2012.
- [153] Óscar J. C. Dias, Jorge E. Santos, and Benson Way. Numerical Methods for Finding Stationary Gravitational Solutions. *Class. Quant. Grav.*, 33(13):133001, 2016. doi: 10.1088/0264-9381/33/13/133001.
- [154] Pau Figueras and Toby Wiseman. On the existence of stationary Ricci solitons. *Class. Quant. Grav.*, 34(14):145007, 2017. doi: 10.1088/1361-6382/aa764a.
- [155] Koushik Balasubramanian and Christopher P. Herzog. Losing Forward Momentum Holographically. *Class. Quant. Grav.*, 31:125010, 2014. doi: 10.1088/0264-9381/31/12/125010.
- [156] Aaron Poole, Kostas Skenderis, and Marika Taylor. (A)dS<sub>4</sub> in Bondi gauge. *Class. Quant. Grav.*, 36(9):095005, 2019. doi: 10.1088/1361-6382/ab117c.
- [157] Geoffrey Compère, Adrien Fiorucci, and Romain Ruzziconi. The  $\Lambda$ -BMS<sub>4</sub> group of dS<sub>4</sub> and new boundary conditions for AdS<sub>4</sub>. *Class. Quant. Grav.*, 36(19):195017, 2019. doi: 10.1088/1361-6382/ab3d4b. [Erratum: *Class. Quant. Grav.* 38, 229501 (2021)].
- [158] Gary T. Horowitz, Maciej Kolanowski, and Jorge E. Santos. Almost all extremal black holes in AdS are singular. *JHEP*, 01:162, 2023. doi: 10.1007/JHEP01(2023)162.
- [159] Charles Fefferman and C. Robin Graham. The ambient metric. *Ann. Math. Stud.*, 178:1–128, 2011.
- [160] Lloyd N. Trefethen. *Spectral Methods in MATLAB*. Society for Industrial and Applied Mathematics, USA, 2000. ISBN 0898714656.
- [161] Gary T. Horowitz, Nabil Iqbal, Jorge E. Santos, and Benson Way. Hovering Black Holes from Charged Defects. *Class. Quant. Grav.*, 32:105001, 2015. doi: 10.1088/0264-9381/32/10/105001.
- [162] Matthew Headrick, Sam Kitchen, and Toby Wiseman. A New approach to static numerical relativity, and its application to Kaluza-Klein black holes. *Class. Quant. Grav.*, 27:035002, 2010. doi: 10.1088/0264-9381/27/3/035002.
- [163] Pau Figueras and Saran Tunyasuvunakool. Localized Plasma Balls. *JHEP*, 06:025, 2014. doi: 10.1007/JHEP06(2014)025.
- [164] Pau Figueras and Saran Tunyasuvunakool. Black rings in global anti-de Sitter space. *JHEP*, 03:149, 2015. doi: 10.1007/JHEP03(2015)149.

- [165] Jorge E. Santos and Benson Way. Black Droplets. *JHEP*, 08:072, 2014. doi: 10.1007/JHEP08(2014)072.
- [166] Óscar J. C. Dias, Jorge E. Santos, and Benson Way. Rings, Ripples, and Rotation: Connecting Black Holes to Black Rings. *JHEP*, 07:045, 2014. doi: 10.1007/JHEP07(2014)045.
- [167] Michael Kalisch, Sebastian Möckel, and Martin Ammon. Critical behavior of the black hole/black string transition. *JHEP*, 08:049, 2017. doi: 10.1007/JHEP08(2017)049.
- [168] Herman L. Verlinde. Holography and compactification. *Nucl. Phys. B*, 580: 264–274, 2000. doi: 10.1016/S0550-3213(00)00224-8.
- [169] W. Israel. Singular hypersurfaces and thin shells in general relativity. *Nuovo Cim. B*, 44S10:1, 1966. doi: 10.1007/BF02710419. [Erratum: *Nuovo Cim. B* 48, 463 (1967)].
- [170] Behnam Pourhassan, Anha Bhat, Hrishikesh Patel, Mir Faizal, and Nicholas Mantella. Proposed experimental test of Randall-Sundrum Models. 7 2019.
- [171] T. J. M. Zouros and D. M. Eardley. Instabilities of massive scalar perturbations of a rotating black hole. *Annals Phys.*, 118:139–155, 1979. doi: 10.1016/0003-4916(79)90237-9.
- [172] Steven L. Detweiler. Klein-Gordon equation and rotating black holes. *Phys. Rev. D*, 22:2323–2326, 1980. doi: 10.1103/PhysRevD.22.2323.
- [173] Gary T. Horowitz, Maciej Kolanowski, Grant N. Remmen, and Jorge E. Santos. Extremal Kerr Black Holes as Amplifiers of New Physics. *Phys. Rev. Lett.*, 131(9):091402, 2023. doi: 10.1103/PhysRevLett.131.091402.
- [174] Gary T. Horowitz, Maciej Kolanowski, Grant N. Remmen, and Jorge E. Santos. Sudden breakdown of effective field theory near cool Kerr-Newman black holes. *JHEP*, 05:122, 2024. doi: 10.1007/JHEP05(2024)122.
- [175] Alexander Kaus and Harvey S. Reall. Charged Randall-Sundrum black holes and  $N=4$  super Yang-Mills in  $AdS(2) \times S^{*2}$ . *JHEP*, 05:032, 2009. doi: 10.1088/1126-6708/2009/05/032.
- [176] Sean A. Hartnoll, Gary T. Horowitz, Jorrit Kruthoff, and Jorge E. Santos. Diving into a holographic superconductor. *SciPost Phys.*, 10(1):009, 2021. doi: 10.21468/SciPostPhys.10.1.009.
- [177] Sean A. Hartnoll, Gary T. Horowitz, Jorrit Kruthoff, and Jorge E. Santos. Gravitational duals to the grand canonical ensemble abhor Cauchy horizons. *JHEP*, 10:102, 2020. doi: 10.1007/JHEP10(2020)102.
- [178] Maxime Van de Moortel. Violent nonlinear collapse in the interior of charged hairy black holes. 9 2021.

- [179] Pau Figueras and Toby Wiseman. Stationary holographic plasma quenches and numerical methods for non-Killing horizons. *Phys. Rev. Lett.*, 110:171602, 2013. doi: 10.1103/PhysRevLett.110.171602.
- [180] Roberto Emparan and Marina Martinez. Black String Flow. *JHEP*, 09:068, 2013. doi: 10.1007/JHEP09(2013)068.
- [181] Meng Sun and Yong-Chang Huang. Kerr Black string flow. *Nucl. Phys. B*, 897:98–110, 2015. doi: 10.1016/j.nuclphysb.2015.05.017.
- [182] Irene Amado and Amos Yarom. Black brane steady states. *JHEP*, 10:015, 2015. doi: 10.1007/JHEP10(2015)015.
- [183] Eugenio Megias. Out-of-equilibrium energy flow and steady state configurations in AdS/CFT. *PoS*, EPS-HEP2015:366, 2015. doi: 10.22323/1.234.0366.
- [184] Christopher P. Herzog, Michael Spillane, and Amos Yarom. The holographic dual of a Riemann problem in a large number of dimensions. *JHEP*, 08:120, 2016. doi: 10.1007/JHEP08(2016)120.
- [185] Eugenio Megias. Far-from-equilibrium energy flow and entanglement entropy. *EPJ Web Conf.*, 164:01010, 2017. doi: 10.1051/epjconf/201716401010.
- [186] Julian Sonner and Benjamin Withers. Universal spatial structure of nonequilibrium steady states. *Phys. Rev. Lett.*, 119(16):161603, 2017. doi: 10.1103/PhysRevLett.119.161603.
- [187] Christian Ecker, Johanna Erdmenger, and Wilke van der Schee. Non-equilibrium steady state formation in 3+1 dimensions. *SciPost Phys.*, 11(3):047, 2021. doi: 10.21468/SciPostPhys.11.3.047.
- [188] Stephen R. Green, Stefan Hollands, Akihiro Ishibashi, and Robert M. Wald. Superradiant instabilities of asymptotically anti-de Sitter black holes. *Class. Quant. Grav.*, 33(12):125022, 2016. doi: 10.1088/0264-9381/33/12/125022.
- [189] Vijay Balasubramanian and Per Kraus. A Stress tensor for Anti-de Sitter gravity. *Commun. Math. Phys.*, 208:413–428, 1999. doi: 10.1007/s002200050764.
- [190] Pau Figueras, Keiju Murata, and Harvey S. Reall. Black hole instabilities and local Penrose inequalities. *Class. Quant. Grav.*, 28:225030, 2011. doi: 10.1088/0264-9381/28/22/225030.
- [191] R. Gregory and R. Laflamme. Black strings and p-branes are unstable. *Phys. Rev. Lett.*, 70:2837–2840, 1993. doi: 10.1103/PhysRevLett.70.2837.
- [192] Luis Lehner and Frans Pretorius. Black Strings, Low Viscosity Fluids, and Violation of Cosmic Censorship. *Phys. Rev. Lett.*, 105:101102, 2010. doi: 10.1103/PhysRevLett.105.101102.
- [193] Benjamin E. Niehoff, Jorge E. Santos, and Benson Way. Towards a violation of cosmic censorship. *Class. Quant. Grav.*, 33(18):185012, 2016. doi: 10.1088/0264-9381/33/18/185012.

- [194] Óscar J. C. Dias, Jorge E. Santos, and Benson Way. Localised  $AdS_5 \times S^5$  Black Holes. *Phys. Rev. Lett.*, 117(15):151101, 2016. doi: 10.1103/PhysRevLett.117.151101.
- [195] Gary T. Horowitz, Jorge E. Santos, and Benson Way. Evidence for an Electrifying Violation of Cosmic Censorship. *Class. Quant. Grav.*, 33(19):195007, 2016. doi: 10.1088/0264-9381/33/19/195007.
- [196] Toby Crisford and Jorge E. Santos. Violating the Weak Cosmic Censorship Conjecture in Four-Dimensional Anti-de Sitter Space. *Phys. Rev. Lett.*, 118(18):181101, 2017. doi: 10.1103/PhysRevLett.118.181101.
- [197] A. G. Green and S. L. Sondhi. Nonlinear quantum critical transport and the schwinger mechanism for a superfluid-mott-insulator transition of bosons. *Phys. Rev. Lett.*, 95:267001, Dec 2005. doi: 10.1103/PhysRevLett.95.267001. URL <https://link.aps.org/doi/10.1103/PhysRevLett.95.267001>.
- [198] Julian Sonner and A. G. Green. Hawking radiation and nonequilibrium quantum critical current noise. *Phys. Rev. Lett.*, 109:091601, Aug 2012. doi: 10.1103/PhysRevLett.109.091601. URL <https://link.aps.org/doi/10.1103/PhysRevLett.109.091601>.
- [199] Sean A. Hartnoll, Andrew Lucas, and Subir Sachdev. *Holographic Quantum Matter*. MIT Press, 2018. ISBN 978-0-262-03843-0.
- [200] Roberto Emparan, David Licht, Ryotaku Suzuki, Marija Tomašević, and Benson Way. Black tsunamis and naked singularities in AdS. *JHEP*, 02:090, 2022. doi: 10.1007/JHEP02(2022)090.
- [201] David Tong. Holographic conductivity. *Acta Physica Polonica B*, 44:2579, 12 2013. doi: 10.5506/APhysPolB.44.2579.
- [202] Gary T. Horowitz, Jorge E. Santos, and David Tong. Optical Conductivity with Holographic Lattices. *JHEP*, 07:168, 2012. doi: 10.1007/JHEP07(2012)168.
- [203] Gary T. Horowitz, Jorge E. Santos, and David Tong. Further Evidence for Lattice-Induced Scaling. *JHEP*, 11:102, 2012. doi: 10.1007/JHEP11(2012)102.
- [204] Mike Blake, David Tong, and David Vegh. Holographic Lattices Give the Graviton an Effective Mass. *Phys. Rev. Lett.*, 112(7):071602, 2014. doi: 10.1103/PhysRevLett.112.071602.
- [205] Tomas Andrade and Benjamin Withers. A simple holographic model of momentum relaxation. *JHEP*, 05:101, 2014. doi: 10.1007/JHEP05(2014)101.
- [206] Aristomenis Donos and Jerome P. Gauntlett. Holographic Q-lattices. *JHEP*, 04:040, 2014. doi: 10.1007/JHEP04(2014)040.
- [207] Aristomenis Donos and Jerome P. Gauntlett. Thermoelectric DC conductivities from black hole horizons. *JHEP*, 11:081, 2014. doi: 10.1007/JHEP11(2014)081.

- [208] Aristomenis Donos and Jerome P. Gauntlett. The thermoelectric properties of inhomogeneous holographic lattices. *JHEP*, 01:035, 2015. doi: 10.1007/JHEP01(2015)035.
- [209] Mukund Rangamani, Moshe Rozali, and Darren Smyth. Spatial Modulation and Conductivities in Effective Holographic Theories. *JHEP*, 07:024, 2015. doi: 10.1007/JHEP07(2015)024.
- [210] Richard A. Davison and Blaise Goutéraux. Dissecting holographic conductivities. *JHEP*, 09:090, 2015. doi: 10.1007/JHEP09(2015)090.
- [211] Gary T. Horowitz, Nabil Iqbal, and Jorge E. Santos. Simple holographic model of nonlinear conductivity. *Phys. Rev. D*, 88(12):126002, 2013. doi: 10.1103/PhysRevD.88.126002.
- [212] Benjamin Withers. Nonlinear conductivity and the ringdown of currents in metallic holography. *JHEP*, 10:008, 2016. doi: 10.1007/JHEP10(2016)008.
- [213] Maxime Gadioux and Harvey S. Reall. Creases, corners, and caustics: Properties of nonsmooth structures on black hole horizons. *Phys. Rev. D*, 108(8):084021, 2023. doi: 10.1103/PhysRevD.108.084021.
- [214] D. C. Robinson. A simple proof of the generalization of Israel’s theorem. *General Relativity and Gravitation* 8, 695–698, 1977.
- [215] Steven S. Gubser. Breaking an Abelian gauge symmetry near a black hole horizon. *Phys. Rev. D*, 78:065034, 2008. doi: 10.1103/PhysRevD.78.065034.
- [216] Sean A. Hartnoll, Christopher P. Herzog, and Gary T. Horowitz. Holographic Superconductors. *JHEP*, 12:015, 2008. doi: 10.1088/1126-6708/2008/12/015.
- [217] Oscar J. C. Dias, Gary T. Horowitz, and Jorge E. Santos. Black holes with only one Killing field. *JHEP*, 07:115, 2011. doi: 10.1007/JHEP07(2011)115.
- [218] Mikhail S. Volkov and Dmitri V. Gal’tsov. Gravitating nonAbelian solitons and black holes with Yang-Mills fields. *Phys. Rept.*, 319:1–83, 1999. doi: 10.1016/S0370-1573(99)00010-1.
- [219] Robert C. Myers. Higher Dimensional Black Holes in Compactified Space-times. *Phys. Rev. D*, 35:455, 1987. doi: 10.1103/PhysRevD.35.455.
- [220] Hideki Ishihara, Masashi Kimura, Ken Matsuno, and Shinya Tomizawa. Kaluza-Klein Multi-Black Holes in Five-Dimensional Einstein-Maxwell Theory. *Class. Quant. Grav.*, 23:6919–6926, 2006. doi: 10.1088/0264-9381/23/23/019.
- [221] Henriette Elvang and Pau Figueras. Black Saturn. *JHEP*, 05:050, 2007. doi: 10.1088/1126-6708/2007/05/050.
- [222] Hideo Iguchi and Takashi Mishima. Black di-ring and infinite nonuniqueness. *Phys. Rev. D*, 75:064018, 2007. doi: 10.1103/PhysRevD.78.069903. [Erratum: Phys.Rev.D 78, 069903 (2008)].

- [223] Keisuke Izumi. Orthogonal black di-ring solution. *Prog. Theor. Phys.*, 119: 757–774, 2008. doi: 10.1143/PTP.119.757.
- [224] Henriette Elvang and Maria J. Rodriguez. Bicycling Black Rings. *JHEP*, 04:045, 2008. doi: 10.1088/1126-6708/2008/04/045.
- [225] Henriette Elvang and Gary T. Horowitz. When black holes meet Kaluza-Klein bubbles. *Phys. Rev. D*, 67:044015, 2003. doi: 10.1103/PhysRevD.67.044015.
- [226] Shinya Tomizawa, Hideo Iguchi, and Takashi Mishima. Rotating Black Holes on Kaluza-Klein Bubbles. *Phys. Rev. D*, 78:084001, 2008. doi: 10.1103/PhysRevD.78.084001.
- [227] Hideo Iguchi, Takashi Mishima, and Shinya Tomizawa. Boosted black holes on Kaluza-Klein bubbles. *Phys. Rev. D*, 76:124019, 2007. doi: 10.1103/PhysRevD.78.109903. [Erratum: Phys.Rev.D 78, 109903 (2008)].
- [228] Marco Astorino, Roberto Emparan, and Adriano Viganò. Bubbles of nothing in binary black holes and black rings, and viceversa. *JHEP*, 07:007, 2022. doi: 10.1007/JHEP07(2022)007.
- [229] Shinya Tomizawa and Ryotaku Suzuki. Static equilibrium of multi-black holes in expanding bubbles in five dimensions. 3 2024.
- [230] Edward Witten. Instability of the Kaluza-Klein Vacuum. *Nucl. Phys. B*, 195: 481–492, 1982. doi: 10.1016/0550-3213(82)90007-4.
- [231] Miguel S. Costa, Lauren Greenspan, Miguel Oliveira, João Penedones, and Jorge E. Santos. Polarised Black Holes in AdS. *Class. Quant. Grav.*, 33(11): 115011, 2016. doi: 10.1088/0264-9381/33/11/115011.
- [232] Israel, W., Khan, K.A. Collinear particles and bondi dipoles in general relativity. *Nuovo Cim*, 33:331–344, 1964. doi: {10.1007/BF02750196}.
- [233] Oscar J. C. Dias, Gary T. Horowitz, and Jorge E. Santos. Extremal black holes that are not extremal: maximal warm holes. *JHEP*, 01:064, 2022. doi: 10.1007/JHEP01(2022)064.
- [234] Roberto Emparan. Rotating circular strings, and infinite nonuniqueness of black rings. *JHEP*, 03:064, 2004. doi: 10.1088/1126-6708/2004/03/064.
- [235] Keith Copsey and Gary T. Horowitz. The Role of dipole charges in black hole thermodynamics. *Phys. Rev. D*, 73:024015, 2006. doi: 10.1103/PhysRevD.73.024015.
- [236] Dionysios Anninos, Tarek Anous, Frederik Denef, and Lucas Peeters. Holographic Vitrification. *JHEP*, 04:027, 2015. doi: 10.1007/JHEP04(2015)027.
- [237] Gary T. Horowitz, Maciej Kolanowski, and Jorge E. Santos. A deformed IR: a new IR fixed point for four-dimensional holographic theories. *JHEP*, 02:152, 2023. doi: 10.1007/JHEP02(2023)152.

- 
- [238] Juan Martin Maldacena, Jeremy Michelson, and Andrew Strominger. Anti-de Sitter fragmentation. *JHEP*, 02:011, 1999. doi: 10.1088/1126-6708/1999/02/011.
- [239] Juan Maldacena, Alexey Milekhin, and Fedor Popov. Traversable wormholes in four dimensions. *Class. Quant. Grav.*, 40(15):155016, 2023. doi: 10.1088/1361-6382/acde30.
- [240] Jerome P. Gauntlett and Christopher Rosen. Susy Q and spatially modulated deformations of ABJM theory. *JHEP*, 10:066, 2018. doi: 10.1007/JHEP10(2018)066.
- [241] Maren Stein. Perturbative Construction of Stationary Randall-Sundrum II Black Holes on a 5-Brane. *JHEP*, 09:067, 2016. doi: 10.1007/JHEP09(2016)067.

# Appendix A

## Convergence tests

### A.1 Convergence properties of the rotating RSII black holes

As explained in Section 2.1, when using the DeTurck trick, one must generally check that the solutions to the Einstein-DeTurck equations obtained numerically are not Ricci solitons. We can check this by monitoring the DeTurck norm, given by  $\xi^a \xi_a$ . We compute its maximum value across the data points, and seek to show that this value is converging to zero in the continuum limit.

In Fig. A.1, we have plotted the maximum value of the DeTurck norm for a couple of solutions against  $n_x$ , the number of lattice points used on the  $x$  axis in our discretization. In each case, we have maintained a ratio of  $n_x : n_y : n_u = 4 : 3 : 3$ , where  $n_i$  is the number of lattice points for the  $i$ -coordinate.

For the majority of our parameter space, the maximum value of the DeTurck norm across the lattice points is very small. Spectral collocation methods should exhibit exponential convergence as the number of data points is increased, and though we do find that the DeTurck norm decreases as the number of lattice points increases, the convergence is extremely slow. However, this is still consistent with exponential convergence, just one with an extremely small coefficient multiplying the exponent. The only solutions which have reasonably large values of DeTurck norm, for our resolution of  $40 \times 30 \times 30$ , are the small black holes with  $\beta$  very small. However, these are far less phenomenologically interesting than the large braneworld black holes that more closely resemble four-dimensional black holes. Similar convergence plots have been obtained in [149] and [241].

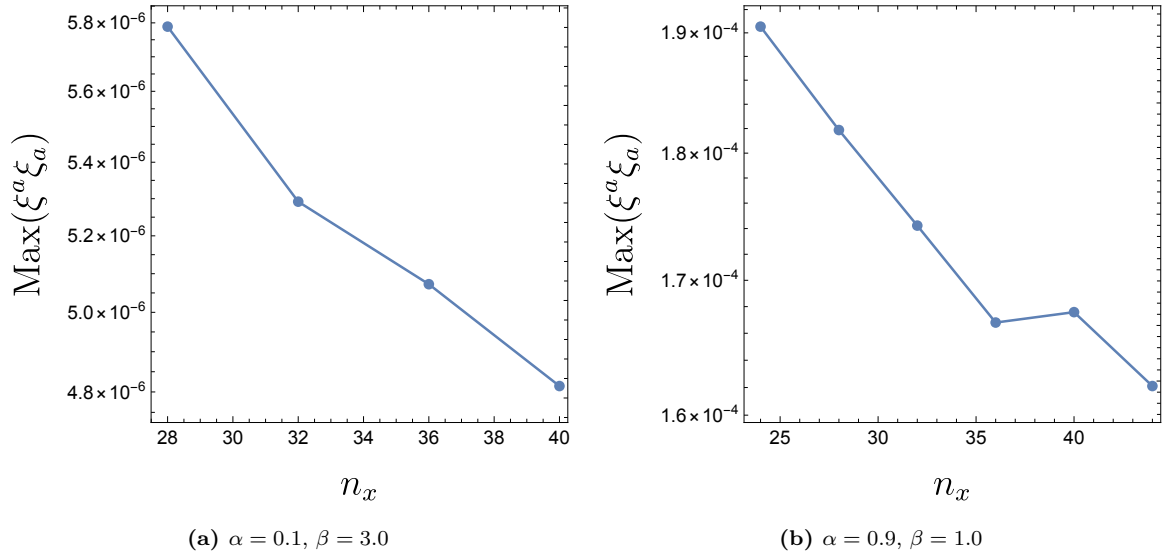


**Fig. A.1:** The maximum value of the norm of the DeTurck vector,  $\xi^a \xi_a$  against the number grid points in the  $x$  direction, denoted by  $n_x$ , for the rotating RSII black holes. In each case we kept the ratio  $n_x : n_y : n_u$  fixed at 4 : 3 : 3.

## A.2 Convergence properties of the black tunnels

In Section 4.2, we argued that due to the staticity of the black tunnels, Ricci solitons could not exist, *i.e.* any solution to the Einstein-DeTurck equation would necessarily also be a solution to the Einstein equation. Despite this, it is worth checking explicitly that the DeTurck vector,  $\xi^a$ , does vanish in the continuum limit, and moreover it provides a good metric of the accuracy of the numerical solutions and the speed of convergence. In Figure A.2, we have plotted the maximum value of the norm of the DeTurck vector, given by  $\xi^2 = \xi^a \xi_a$ , across each of the lattice points. We have varied the number of lattice points used in the numerical method, keeping the ratio between the number of points in the  $x$  and  $y$  directions fixed at 1 : 1.

Clearly the norm of the DeTurck vector becomes smaller and smaller as the number of lattice points is increased, suggesting, as expected, that we are indeed approaching a solution to the Einstein equation. In Figure A.2 we have used a log-log scale in the axes to demonstrate that the convergence follows a power law behaviour. The reason the convergence is slower than exponential is because of the non-analytic behaviour arising in the expansion of the solution near the boundary.

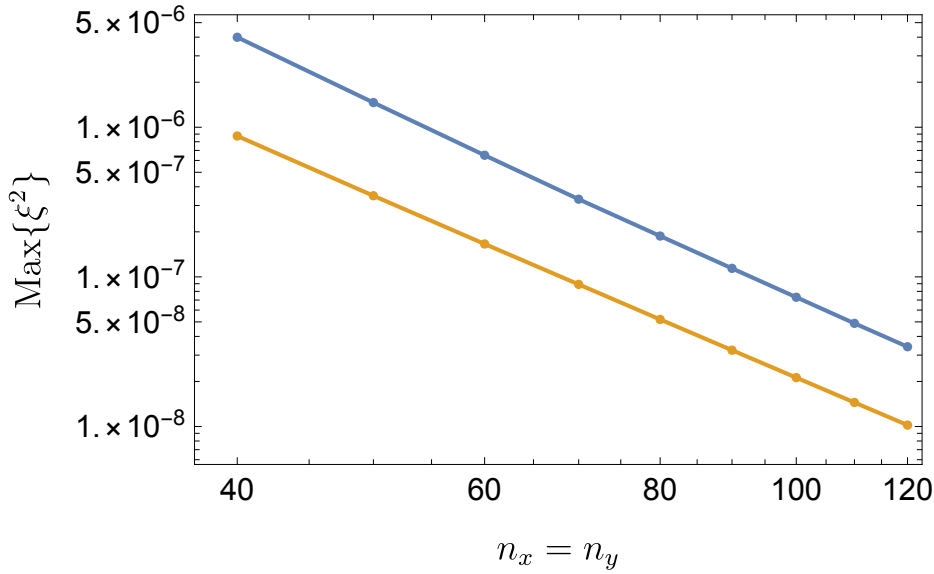


**Fig. A.2:** The maximum value of the norm of the DeTurck vector,  $\xi^2 = \xi^a \xi_a$ , across the black tunnel solutions, plotted in a log-log plot against the number of lattice points in each direction. The blue points correspond to the black tunnel solution with  $\rho_h = 0.3$  and the orange points correspond to the black tunnel solution with  $\rho_h = 0.9$ . In each case  $n_x = n_y$  where  $n_i$  is the number of points used for the  $i$ -coordinate. The straight line in the log-log scale is indicative of power-law convergence.

### A.3 Convergence properties of the black hammocks

As discussed in Section 2.2, the numerical scheme for finding stationary solutions in Bondi-Sachs gauge works by solving only a subset of the Einstein equation, specifically the bulk equations,  $E_{ij} = 0$ , for  $i, j \neq v$ . We set the remaining components of the Einstein equation to zero,  $E_{va} = 0$ , only as a boundary condition at  $y = 1$ . If this is the case then the contracted Bianchi identity should ensure that in fact  $E_{va} = 0$  throughout the whole spacetime on a solution to the bulk equations. However, keeping track of  $E_{va}$  throughout the bulk allows one to check the numerical method and its convergence properties as one increases the number of lattice points used in the discretization.

In Figure A.3 we have plotted the maximum absolute value throughout the whole bulk of the  $E_{va}$  components of the Einstein equation. On the  $x$ -axis is the number of lattice points used in each direction in the discretization process, once again with the ratio of points in the  $x$  and  $y$  directions fixed at 1 : 1.

This plot clearly shows that the maximum error in  $E_{va}$  becomes very small as one increases the number of points, meaning that the numerical method converges very well to a solution to the Einstein equation. Indeed, high precision was used in order to extract the holographic quantities, and this is the reason the DeTurck norm is smaller than usual numerical precision of around  $10^{-12}$  for solutions with more lattice points.

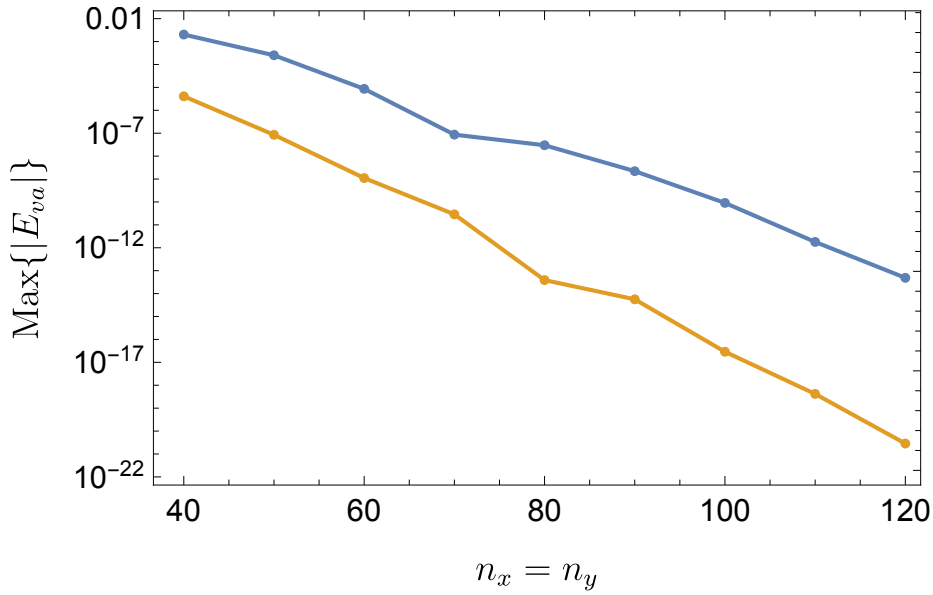


**Fig. A.3:** The maximum value across the numerical black hammock solutions of the components,  $E_{va}$ , of the Einstein equation that are not explicitly solved as bulk equations plotted in a log plot against the number of lattice points in each direction. The blue points correspond to the black hammock solution with  $\rho_h = 0.3$  and the orange points correspond to the black hammock solution with  $\rho_h = 0.9$ . In each case  $n_x = n_y$  where  $n_i$  is the number of points used for the  $i$ -coordinate.

This time the plot is a log plot, that is, there is a log scale on the  $y$ -axis, but not the  $x$ -axis. Therefore, the fact that the plot seems to roughly give a straight line is indicative of exponential convergence, which is expected since no non-analytic terms arise in Bondi-Sachs gauge. The hammocks were also obtained using the DeTurck method, but in this gauge there was only power-law convergence, again due to the presence of non-analytic terms.

## A.4 Convergence properties of the holographic batteries

The holographic batteries were found in both the Bondi-Sachs and DeTurck gauges.

In the former, one can perform a convergence test keeping track of how well the supplementary equations, which are only set as boundary conditions at the horizon, are satisfied in the rest of the spacetime. In Figure A.4, we plot the maximum value of the supplementary equations across the bulk against the number of lattice points used in the numerics in a log-log plot. The roughly linear behaviour of the convergence in the log-log plot suggests power-law convergence.

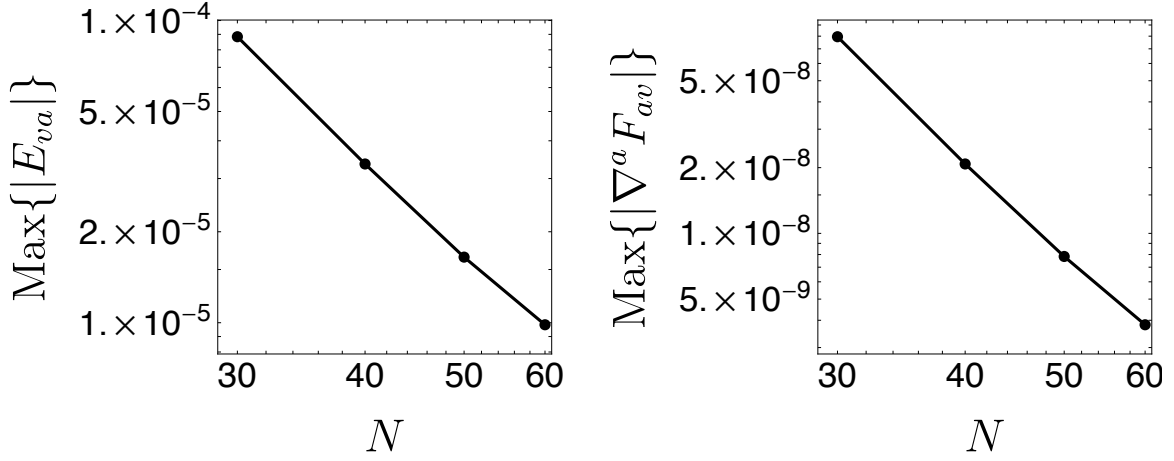


**Fig. A.4:** The maximum value of the supplementary equations,  $E_{va}$  on the left and  $\nabla^a F_{ab}$  on the right, for a holographic battery with  $\mu = 0.36$  obtained numerically on a discrete lattice of size  $2N \times N$  for different values of  $N$ , plotted in a log-log plot.

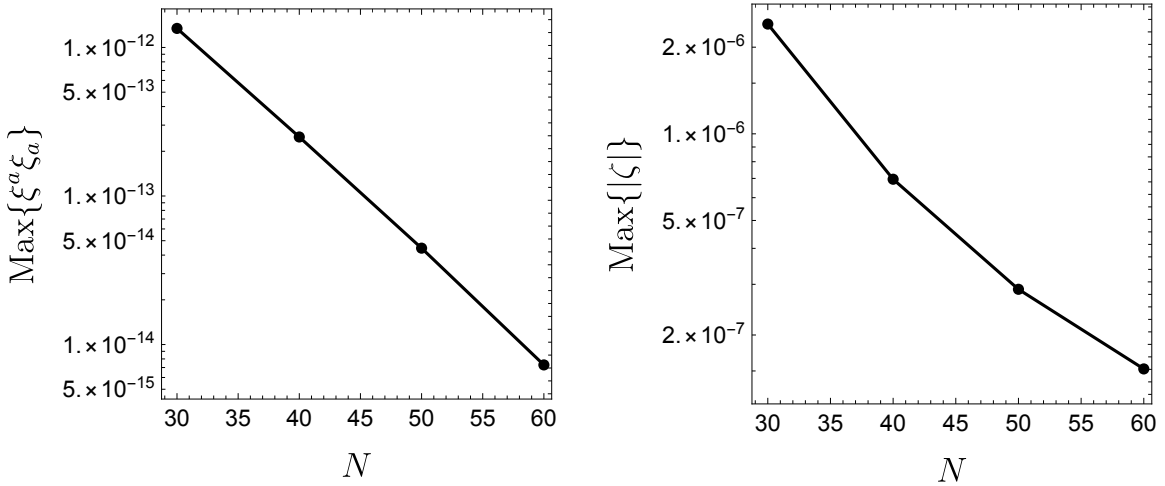


**Fig. A.5:** The maximum norm of the DeTurck vector on the left and of the DeTurck potential  $\zeta$  on the right for a holographic battery with  $\mu = 1$  in DeTurck gauge. The solutions were found numerically on a discrete lattice of size  $2N \times N$  for different values of  $N$ , plotted in a log plot.

For the solutions found in DeTurck gauges, we can track the DeTurck vector  $\xi^a$  and  $\zeta$  in order to study the convergence properties of the numerics in DeTurck gauge. We plot such convergence tests in Figure A.5 for the holographic battery with  $\mu = 1$ . Once again the plots suggest power law convergence. Note that since the batteries are not static solutions, one may be concerned that the DeTurck vector could be a non-zero null vector. However, we also checked explicitly that each component of the DeTurck vector tend towards zero confirming that we really do have convergence to a solution to the Einstein-Maxwell equations.

## A.5 Convergence properties of the charged AdS binary solutions

The binary solutions were found using the DeTurck method, so once again we must check that they are not Ricci solitons. Fig. A.6 shows a log-plot the maximum value of the norm of the DeTurck vector across each lattice point of each patch for the numerical solutions obtained with different values of the resolution,  $N$ . The left panel corresponds to four-dimensional,  $\mathbb{Z}_2$ -symmetric binary solutions with  $T = 1$ ,  $\mu_1 = 1.5$  and  $\nu_R = -0.45$ , whilst the solutions in the right panel are five-dimensional,  $\mathbb{Z}_2$ -symmetric binary solutions with  $T = 1$ ,  $\mu_1 = 1.4$  and  $\nu_R = 0$ .

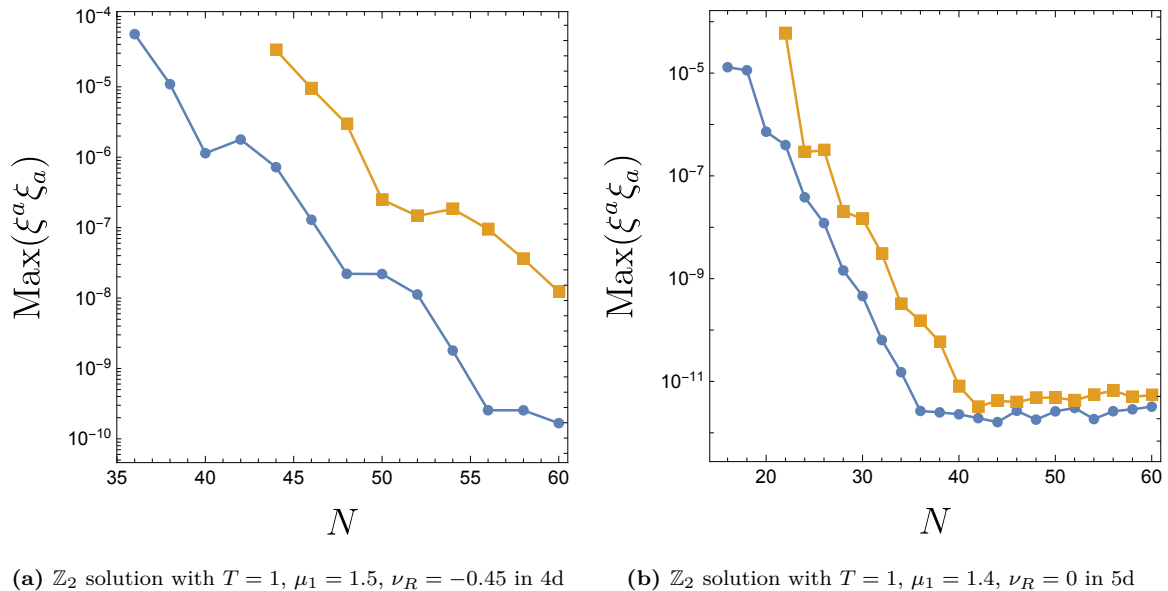


**Fig. A.6:** The maximum value of the DeTurck norm for binary solutions obtained with a resolution in each patch of  $N \times N$ . The left corresponds to a four-dimensional solution and the right to a five-dimensional solution. In each case, two different solutions, differentiated by colour, are found for the values of the input parameters, either side of a turning point.

$\mathbb{Z}_2$ -symmetric binary solutions with  $T = 1$ ,  $\mu_1 = 1.4$  and  $\nu_R = 0$ . In each case we were able to find two different solutions for the given input parameters, either side of a turning point. We have used different colours to differentiate between the solutions from the two different branches. The colours used in the left panel correspond with those used for the two different branches in Fig. 6.6 and Fig. 6.7.

The specific four-dimensional solution chosen has relatively large derivatives, explaining why a large number of points is needed to reduce the DeTurck vector. On the other hand, the chosen five-dimensional solution converges more quickly before hitting numerical precision at around  $10^{-12}$ . Both plots are consistent with power-law convergence, as expected for the DeTurck method.

# Appendix B

## Universal properties of the holographic batteries for small voltage

### B.1 Conductance for other profiles

We also computed holographic batteries for other choices of the chemical potential profile,  $g(x)$ . In each case, we fixed  $g(1) = 1 = -g(-1)$  and  $g'(1) = 0 = g'(-1)$ .

For example, we considered two other profiles, named the *tanh profile* and the *cubic profile* and given, respectively, by

$$g_{\text{tanh}}(x) := \tanh\left(\frac{x\sqrt{2-x^2}}{1-x^2}\right) \quad \text{and} \quad g_{\text{cubic}}(x) := \frac{1}{2}(3x - x^3) \quad (\text{B.1})$$

In Figure B.1 we plot the conductance of the tanh and cubic profiles in black and grey, respectively.

Just as with the sine profile, we find that in each case  $G/\nu \rightarrow 2$  as  $V/T_H \rightarrow 0$ ; we provide a proof in the next section that this is a universal feature of all choices of profile,  $g(x)$ . Moreover, qualitatively, the shape of each of the conductance curves is very similar, with the conductance increasing with voltage. In each case the derivative of the conductance with respect to  $V/T_H$  reaches a maximum, with the gradient of the curve decreasing after this point. The position of this turning point of the derivative depends upon the choice of profile.

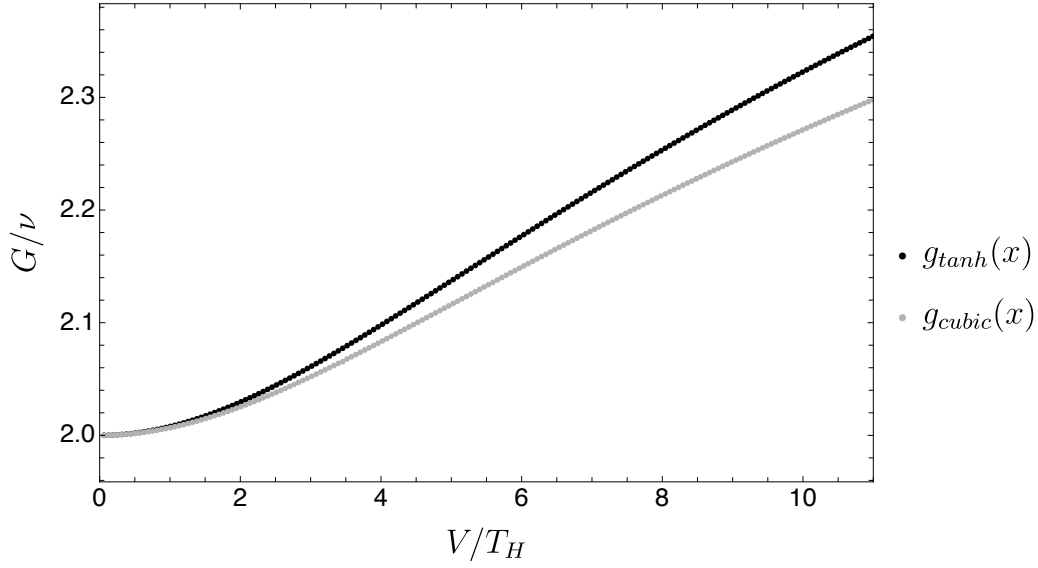


**Fig. B.1:** The conductance against the potential difference for holographic batteries with different profiles used for the source chemical potential. For the dots in black we used the tanh profile, whilst the dots in grey correspond to batteries defined with the cubic profile.

## B.2 A proof of the linear behaviour of the conductance

In Figures 5.3 and B.1 we saw that the ratio  $G/\nu$  tends to two in the limit  $V/T_H \rightarrow 0$  seemingly for whatever profile we use. In this section we provide a proof that this limiting behaviour occurs universally for any choice of the profile,  $g(x)$ , which is odd in  $x$ .

We begin by taking our *Ansatz* (5.11) with

$$q_i = 1 \quad \text{for} \quad i \in \{1, 2, 3, 5\} \quad (\text{B.2a})$$

with

$$q_4 = 0, \quad q_6 = \delta\mu \hat{q}_6(x, y) \quad \text{and} \quad q_7 = \delta\mu \hat{q}_7(x, y) \quad (\text{B.2b})$$

where  $\delta\mu$  is taken to be arbitrarily small. To linear order in  $\delta\mu$ , the equations take the following simple form:

$$4(1-y^2) \frac{\partial^2 \hat{q}_6(x, y)}{\partial y^2} + (1-x^2)^2 \sqrt{2-x^2} \frac{\partial}{\partial x} \left( \sqrt{2-x^2} \frac{\partial \hat{q}_6(x, y)}{\partial x} \right) = 0, \quad (\text{B.3a})$$

$$\frac{\partial \hat{q}_7(x, y)}{\partial y} + \frac{1-x^2}{1-y^2} \left[ \frac{A_2}{\sqrt{2-x^2}} + \frac{\partial \hat{q}_6(x, y)}{\partial x} \right] = 0, \quad (\text{B.3b})$$

where  $A_2$  is a constant to be determined in what follows. We now change to a new set of coordinates with which it is easier to explain our results. Let

$$X = x\sqrt{2-x^2}. \quad (\text{B.4})$$

In terms of  $X$ , the equations (B.3) read

$$(1-y^2)\frac{\partial^2 \hat{q}_6(X,y)}{\partial y^2} + (1-X^2)^{3/2} \frac{\partial}{\partial x} \left( \sqrt{1-X^2} \frac{\partial \hat{q}_6(X,y)}{\partial X} \right) = 0, \quad (\text{B.5a})$$

$$\frac{\partial \hat{q}_7(X,y)}{\partial y} + \frac{1}{1-y^2} \frac{\sqrt{1-X^2}}{\sqrt{1+\sqrt{1-X^2}}} \left[ A_2 + 2\sqrt{1-X^2} \frac{\partial \hat{q}_6(X,y)}{\partial X} \right] = 0. \quad (\text{B.5b})$$

The general solution to (B.5a) can be written as

$$\hat{q}_6(X,y) = (A_0 + A_1 y) \arcsin X + (1-X^2)^{1/4} \int_{-\infty}^{+\infty} dq b(q) S_q(X) K_q(y) \quad (\text{B.6a})$$

with

$$\frac{\partial}{\partial X} \left[ (1-X^2) \frac{\partial S_q(X)}{\partial X} \right] + \left( \frac{q^2}{1-X^2} - \frac{1}{4} \right) S_q(X) = 0 \quad (\text{B.6b})$$

and

$$(1-y^2) \frac{\partial^2 K_q(y)}{\partial y^2} - \frac{1}{4} (1+4q^2) K_q(y) = 0. \quad (\text{B.6c})$$

Meanwhile, for  $\hat{q}_7$ , we find that

$$\begin{aligned} \hat{q}_7(X,y) = Z(X) + \frac{\sqrt{1-X^2}}{2\sqrt{1+\sqrt{1-X^2}}} & \left[ (2A_0 + 2A_1 + A_2) \log(1-y) \right. \\ & \left. - (2A_0 - 2A_1 + A_2) \log(1+y) \right] \\ + \frac{4(1-X^2)^{1/4}}{\sqrt{1+\sqrt{1-X^2}}} & \int_{-\infty}^{+\infty} dq \frac{b(q)}{1+4q^2} \left[ X S_q(X) - 2(1-X^2) \frac{\partial S_q(X)}{\partial X} \right] \frac{\partial K_q(y)}{\partial y} \end{aligned} \quad (\text{B.6d})$$

where  $Z(X)$  is an integration function, and  $A_0$ ,  $A_1$  and  $A_2$  are constants to be determined in what follows.

General complex solutions to (B.6b) can be written as

$$\tilde{S}_q(X) = z_1(q) P_{-1/2}^{iq}(X) + z_2(q) Q_{-1/2}^{iq}(X) \quad (\text{B.7})$$

where  $P_\mu^\nu(X)$  are associated Legendre functions of the first kind of order  $\mu$  and degree  $\nu$ ,  $Q_\mu^\nu(X)$  are associated Legendre functions of the second kind of order  $\mu$  and degree  $\nu$  and  $z_1(q)$  and  $z_2(q)$  are arbitrary integration constants.

On the other hand, general complex solutions to (B.6c) can be written as

$$\tilde{K}_q(y) = p_1(q) {}_2F_1\left(-\frac{1}{4} - \frac{iq}{2}, -\frac{1}{4} + \frac{iq}{2}; \frac{1}{2}; y^2\right) + p_2(q) y {}_2F_1\left(\frac{1}{4} - \frac{iq}{2}, \frac{1}{4} + \frac{iq}{2}; \frac{3}{2}; y^2\right) \quad (\text{B.8})$$

where  $p_1(q)$  and  $p_2(q)$  are arbitrary integration constants, while  ${}_2F_1(a, b; c; z)$  is a Gauss hypergeometric function. Regularity at  $y = 1$  (the future event horizon) demands that

$$p_2(q) = -\frac{2\Gamma\left(\frac{1}{4} - \frac{iq}{2}\right)\Gamma\left(\frac{iq}{2} + \frac{1}{4}\right)}{\Gamma\left(-\frac{iq}{2} - \frac{1}{4}\right)\Gamma\left(\frac{iq}{2} - \frac{1}{4}\right)} p_1(q) \quad (\text{B.9})$$

so that

$$\tilde{K}_q(y) = \frac{\Gamma\left(\frac{5}{4} - \frac{iq}{2}\right)\Gamma\left(\frac{5}{4} + \frac{iq}{2}\right)}{\sqrt{\pi}} (1 - y^2) {}_2F_1\left(\frac{3}{4} - \frac{iq}{2}, \frac{3}{4} + \frac{iq}{2}; 2; 1 - y^2\right) \quad (\text{B.10})$$

and in particular we have chosen  $p_1(q) = 1$  above so that  $\tilde{K}_q(0) = 1$ . Note that we necessarily have  $\tilde{K}_q(1) = 0$ . Note that we want  $q_6$  and  $q_7$  to be *real* functions, and the symmetries of the hypergeometric function are such that

$$K_q(y) = \frac{1}{2}(\tilde{K}_q(y) + \tilde{K}_{-q}(y)) = \tilde{K}_q(y). \quad (\text{B.11})$$

Next we look at the boundary conditions at  $X = \pm 1$  (i.e.  $x = \pm 1$ ). Here we want  $\hat{q}_6(\pm 1, y) = \pm 1$ , so that  $q_6(\pm 1, y) = \pm \delta\mu$ . It is a simple exercise to show that near  $X = \pm 1$  we have  $S_1(X) \sim (1 \pm X)^{\frac{iq}{2}} + \gamma (1 \pm X)^{\frac{-iq}{2}}$ , with  $\gamma$  a constant. This means that the last term in (B.6a) does not contribute near  $X = \pm 1$ , so long as  $b(q)$  does not grow very large as  $q \rightarrow +\infty$ . As such, our boundary conditions demand that  $A_1 = 0$  in (B.6).

Note that regularity at the future event horizon, located at  $y = 1$ , also demands that  $A_2 = -2A_0$ , so that no  $\log(1 - y)$  term appears on the right hand side of (B.6d). Moreover, note that by comparing (B.5b) with (5.17) in the main text, one finds that  $C_1 = -A_2\delta\mu$ . Therefore, at this stage we only need to connect  $A_0$  with  $\mu$  appearing in the main text.

Thus far we have imposed all boundary conditions, except those at the conformal boundary. Firstly, we choose  $Z(X)$  in (B.6d) so that  $\hat{q}_7(X, 0) = 0$ , that is to say

$$Z(X) = \frac{8(1-X^2)^{1/4}}{\sqrt{1+\sqrt{1-X^2}}} \int_{-\infty}^{+\infty} dq \frac{b(q)}{1+4q^2} \left[ X S_q(X) - 2(1-X^2) \frac{\partial S_q(X)}{\partial X} \right] \cdot \frac{\Gamma\left(\frac{1}{4} - \frac{iq}{2}\right) \Gamma\left(\frac{1}{4} + \frac{iq}{2}\right)}{\Gamma\left(-\frac{1}{4} - \frac{iq}{2}\right) \Gamma\left(-\frac{1}{4} + \frac{iq}{2}\right)}. \quad (\text{B.12})$$

We are thus left to determine  $b(q)$  for a given profile. Let the profile be given as in the main text by  $q_6(X, 0) = \delta\mu g(X)$  with  $g(X)$  and odd function of  $X$  satisfying  $g(1) = 1$ . This means we want to choose the  $S_q(X)$  to be real and odd. Demanding that  $S_q(X)$  is odd, implies

$$z_2(q) = -\frac{1}{\pi} \left( 2i + \frac{4}{i + e^{\pi q}} \right) z_1(q). \quad (\text{B.13})$$

while demanding that  $S_q(X)$  is real, imposes

$$S_q(X) = \frac{1}{2} \left( \tilde{S}_q(X) + \overline{\tilde{S}_q(X)} \right) \quad (\text{B.14})$$

where a bar denotes complex conjugation.

Using known properties of the associated Legendre functions and the Dirac delta distributions, one can prove that

$$\int_{-1}^1 dX \frac{S_q(X) S_p(X)}{1-X^2} = \eta(p) [\delta(p-q) + \delta(p+q)] \quad (\text{B.15a})$$

with

$$\eta(p) = \frac{1}{p\pi} \left\{ \frac{2\pi}{\sinh p\pi} + \left[ \frac{1}{\sinh p\pi} - i \right] \Gamma\left(\frac{1}{2} - ip\right)^2 + \left[ \frac{1}{\sinh p\pi} + i \right] \Gamma\left(\frac{1}{2} + ip\right)^2 \right\}, \quad (\text{B.15b})$$

where  $\delta(x)$  is a Dirac delta function.

The procedure to determine  $b(q)$  (and thus the full bulk solution) from a given profile is now clear. First, from (B.6a) with  $A_1 = 0$ , we demand

$$g(X) = A_0 \arcsin X + (1-X^2)^{1/4} \int_{-\infty}^{+\infty} dq b(q) S_q(X) \quad (\text{B.16})$$

Note that  $g(1) = 1$ , so that we must take  $A_0 = \frac{2}{\pi}$  and hence, after rearranging we have

$$\frac{1}{(1-X^2)^{1/4}} \left[ g(X) - \frac{2}{\pi} \arcsin X \right] = \int_{-\infty}^{+\infty} dq b(q) S_q(X)$$

and thus

$$\begin{aligned} \int_{-1}^1 dX \frac{S_p(X)}{(1-X^2)^{5/4}} \left[ g(X) - \frac{2}{\pi} \arcsin X \right] &= \int_{-1}^1 dX \int_{-\infty}^{+\infty} dq b(q) \frac{S_p(X) S_q(X)}{1-X^2} \\ &= \int_{-\infty}^{+\infty} dq b(q) \int_{-1}^1 dX \frac{S_p(X) S_q(X)}{1-X^2} \\ &= \eta(p) [b(p) + b(-p)] . \end{aligned} \quad (\text{B.17})$$

so that

$$b(p) + b(-p) = \frac{1}{\eta(p)} \int_{-1}^1 dX \frac{S_p(X)}{(1-X^2)^{5/4}} \left[ g(x) - \frac{2}{\pi} \arcsin X \right] . \quad (\text{B.18})$$

Finally, because  $S_p(X) = S_{-p}(X)$  and  $K_p(y) = K_{-p}(y)$ , it follows that

$$\hat{q}_6(X, y) = \frac{2}{\pi} \arcsin X + (1-X^2)^{1/4} \int_0^{+\infty} dq [b(q) + b(-q)] S_q(X) K_q(y) \quad (\text{B.19})$$

thus completing the bulk solution for a generic boundary profile  $g(X)$ .

Overall, we have learned that  $A_0 = 2/\pi$ , and hence  $A_2 = -4/\pi$ , which in turn implies that, in the notation of the main text,  $C_1 = 4\delta\mu/\pi$ . Finally applying the definition of the conductance, (5.29), for this small amplitude,  $\delta\mu$ , one finds that  $G/\nu = 2$ , irrespective of the choice of odd profile,  $g(x)$ .